Motion Comfort in the Flying-V

MSc Thesis

Basem Deeb

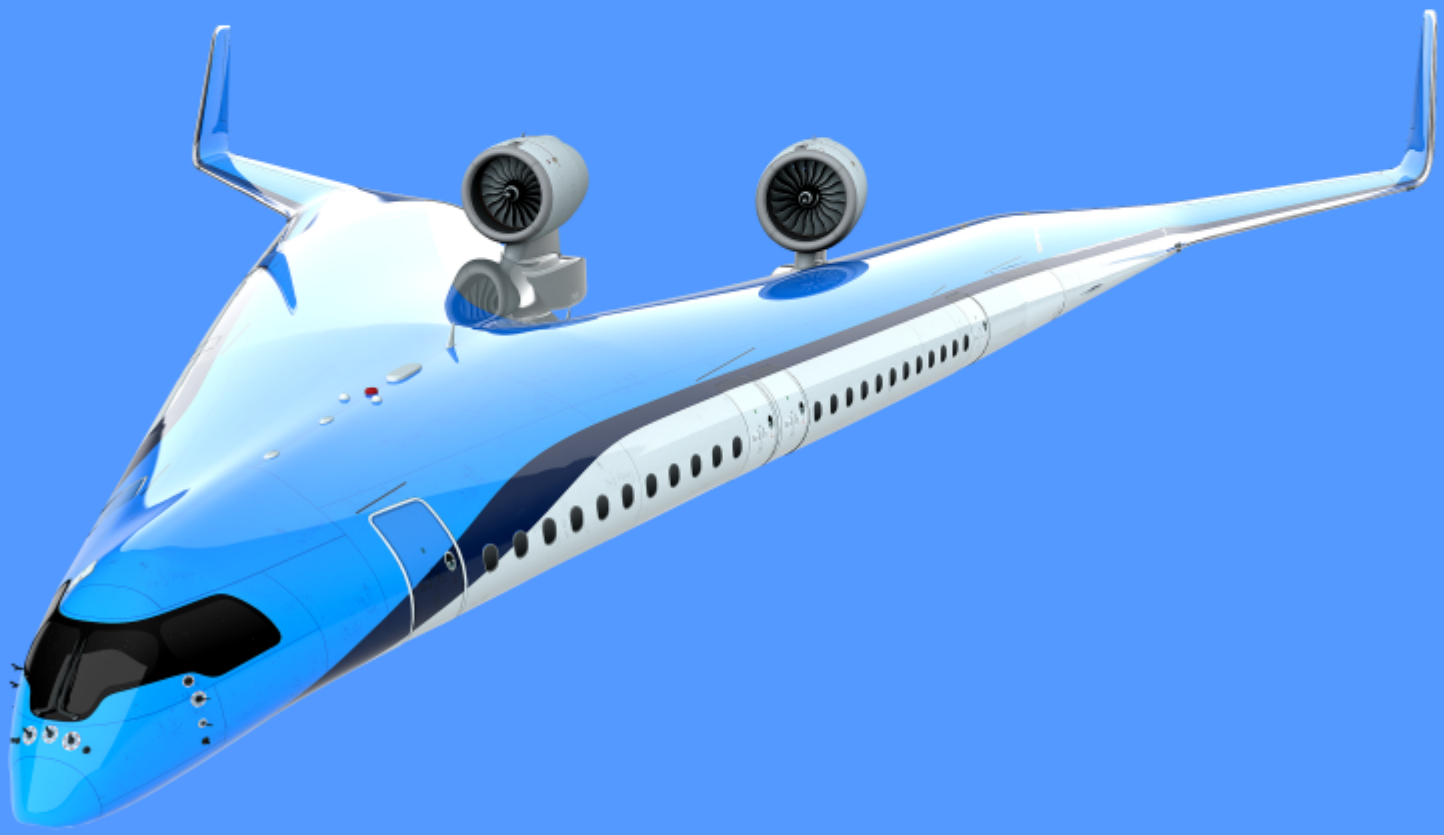

Delft University of Technology

TU Delft

Motion Comfort in the Flying-V

MSc Thesis

by

Basem Deeb

Student Number

5197368

To obtain the degree of Master of Science at the Delft University of Technology, to be defended publicly on Thursday August 24, 2023 at 9:30 AM

Thesis committee: Prof. dr. ir. M. Mulder, C&S, AE, TU Delft, chair
Dr. ir. D. M. Pool, C&S, AE, TU Delft, supervisor
Ir. O. Stroosma, C&S, AE, TU Delft, supervisor
Dr. F. Yin, ANCE, AE, TU Delft, external member

This thesis cannot be made public until August 24, 2025
An electronic version of this thesis is available at http://repository.tudelft.nl/.

TU Delft

Preface

Reflecting on this thesis project, I extend my sincere gratitude to Dr. Ir. Daan Pool, Ir. Olaf Stroosma, and Ir. Rowenna Wijlens for their invaluable feedback, insightful ideas, and enthusiasm for my topic during our meetings. I also wish to express my appreciation to the participants of my experiment, whose commitment and willingness to contribute their time aided in the collection of invaluable data.

Concluding this journey, I am profoundly thankful to my family and friends, who have stood by me as unwavering supporters throughout my master's program and thesis work.

Basem Deeb
Delft, August 2023

Contents

1

Introduction

1.1. Introduction to motion sickness and the Flying-V

In humans, motion sickness is a multi-symptomatic syndrome that is frequently characterized by first symptoms like headache, dizziness, sweating, stomach awareness, and nausea [1]. The severity of these symptoms typically increases next, leading to retching and emesis [2]. Reason and Brand [3] have found out that all people who have a functioning vestibular system can experience motion sickness.

One of TU Delft's current research programs to improve aviation's sustainability is the Flying-V. Due to its aerodynamic form and lower weight, the design is anticipated to consume 20% less fuel than the current most energy-efficient aircraft (Airbus A350) [4]. The primary body of the Flying-V is merged into the wings, eliminating the need for a central body. However, it is still not known if sitting further away from the center of rotation in the Flying-V would increase the susceptibility of a human to get more motion sick, compared to sitting close to the center of rotation.

In this research, the motion sickness in the Flying-V is investigated and researched by simulating maneuvers and estimating the motion sickness for different locations in the Flying-V. This research contains a literature study about the motion sickness theories and models. Moreover, an analysis of specific forces that passengers would experience in the Flying-V and what maneuver would trigger the motion sickness. Thereafter, a motion sickness model will be developed and used to simulate and predict the motion sickness in different locations in the Flying-V. This analysis will help to understand if the motion sickness increase the further the seats are from the center of rotation of the aircraft.

Based on the results of the analysis, an experiment will be designed and performed in SIMONA research simulator. The experiment will have different conditions and participants will be invited to perform all the different conditions in the experiment.

1.2. Research objective and research questions

The design and layout of the Flying-V has promising results, as it showed drag reduction of 10% compared to the conventional design with comparable performance requirements [5]. However, it is suspected that passengers who sit further away from the center of rotation will experience more motion sickness than those who sit closer to the center of rotation of the aircraft. Therefore, there is an increasing need to have a motion sickness model to predict the incidence of motion sickness that the passenger will feel during the flight to ensure the passengers' comfortability and to take it into account in the route path planning and execution of the maneuvers in the Flying-V. Thus, the primary research objective is:

Research Objective

To develop and validate a motion sickness model to predict the motion sickness incidence in the Flying-V

The research questions are defined in a way that combining the answers for all questions will lead to achieve the primary research objective. In this research, there is a main research question and several sub-

questions in order to provide an answer to the main research question and the higher-level questions. The main research question is:

Main research question

What are the flight parameters that contribute to motion sickness in the Flying-V?

The research sub-questions are:

Research question 1

Which motion sickness model is better suited to predict the motion sickness in the Flying-V?

Research question 2

What visual conditions increase the incidence of motion sickness?

Research question 3

Which component of the motion has the biggest influence on the specific forces?

Research question 4

Which Flying-V's maneuver provides a bigger conflict signals and a higher motion sickness incidence value?

Research question 5

Which seat configuration in the Flying-V causes the most motion sickness?

The literature phase will provide the first and second research sub-questions' answers, as well as the seat coordinates with respect to the Flying-V's center of rotation. Moreover, it will provide the seat configuration that has been designed for the Flying-V, which will be used in the fifth question. Thereafter, the analysis phase starts, which will answer the third, fourth, and fifth research sub-questions. The answer to the third question is obtained by using the data from the pilot-in-the-loop experiments that have been done. The specific forces are calculated at the center of gravity (c.g.). These specific forces are transformed into the Design Eye Reference Point (DERP) for various seat positions, and each component is analysed to determine which component is dominant in them. By constructing the selected motion sickness model and running the various scenarios using a simulation program, the fourth and fifth research sub-questions are addressed.

1.3. Outline of the report

The structure of the report can be seen in Figure 1.1. The first part is the scientific paper that has been done after concluding the literature phase. The second part is the preliminary report that includes: the second chapter discusses the motion sickness theories and models, the third chapter on the Flying-V and what research has been done on it, the fourth chapter is an analysis of the specific force of the maneuvers, the fifth chapter is a simulation of the motion sickness model using the maneuvers, the sixth chapter is the experiment proposal, and the conclusion is in the seventh chapter.

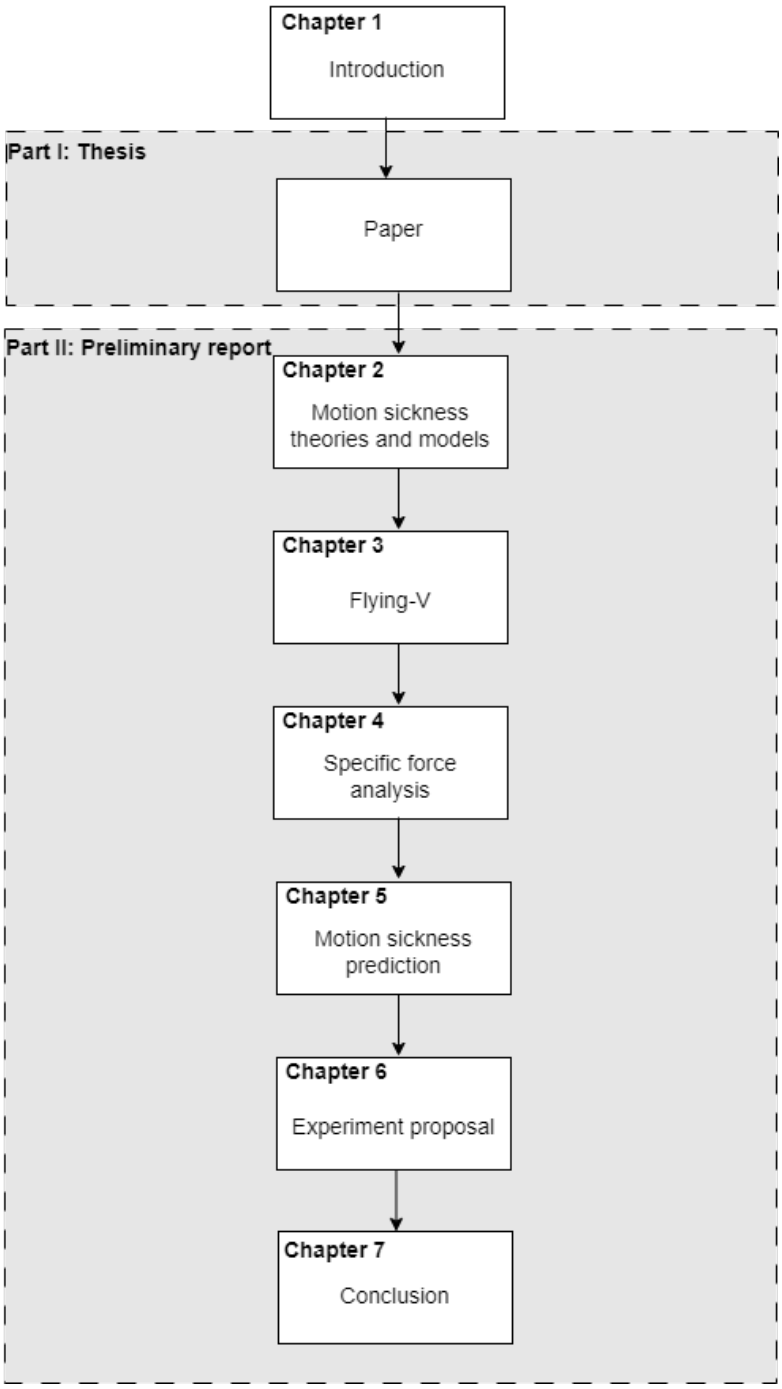

Figure 1.1: Outline of the report

Part I:

Paper: Effect of the Flying-V Configuration on Passenger Motion Comfort: An Experimental Study

Effect of the Flying-V Configuration on Passenger Motion Comfort: An Experimental Study

Basem Deeb *
Delft University of Technology

The Flying-V is an innovative aircraft design developed by Delft University of Technology. Its unique configuration positions passengers laterally farther away from the centre of rotation compared to conventional aircraft. In light of this unique structure, a passenger-in-the-simulator experiment was conducted using the SIMONA Research Simulator to examine to what extent the severity of motion sickness increases with greater lateral distance from the centre of rotation. The experiment was conducted using the Time to Bank manoeuvre. Due to the rolling acceleration, as the lateral distance of the seating position from the centre of rotation increases, passengers experience a higher magnitude of heave motion in addition to the roll motion. The participants were exposed to three different lateral seating positions, including sitting at the centre of rotation; sitting laterally offset at 3.5 m; and sitting laterally offset at 7 m. The motion sickness was predicted using the 6 Degrees of Freedom-Subjective Vertical Conflict model that gives the Motion Sickness Incidence. According to the model's prediction, an increase in the level of heave motion is expected to lead to a higher level of motion sickness severity for passengers. During the experiment, participants' motion sickness severity was assessed using the MIsery SCale (MISC). Although no statistically significant differences were observed among the conditions, sitting laterally offset at 7 m had a higher mean of the participants' maximum MISC score of 3 than sitting laterally offset at 3.5 m, with a mean of the participants' maximum MISC score of 2.4. However, neither of these conditions showed higher scores than sitting at the centre of rotation, with a mean of the participants' maximum MISC score of 3.6. Therefore, the results suggest that sitting laterally farther away from the centre of rotation in the Flying-V did not lead to increased motion sickness severity.

Nomenclature

CG	=	Centre of Gravity
DOF	=	Degree of Freedom
MISC	=	MIsery SCale
MSI	=	Motion Sickness Incidence
MSSQ	=	Motion Sickness Susceptibility Questionnaire
OTO	=	Otolith
RMS	=	Root Mean Square
SCC	=	Semicircular Canal
SP	=	Seating Position
SRS	=	SIMONA Research Simulator
SVC	=	Subjective Vertical Conflict
TTB	=	Time to Bank
a	=	inertial acceleration
A	=	inertial-to-body transformation
b	=	the indifferent point of the hill function
f_x, f_y, f_z	=	specific force components in x, y, and z directions
F_x, F_y, F_z	=	force components in x, y, and z directions
g	=	gravitational acceleration
G	=	slope parameter of the sigmoid function

*MSc student, Aerospace Engineering, Control and Simulation profile

k	=	gain of the motion filter
K_{wc}, K_{vc}, K_{ac}	=	feedback gains of the 6DOF-SVC model
K_1, K_2	=	desired final roll angles for the sigmoid function
M	=	aircraft mass
p, q, r	=	roll, pitch, and yaw rates
$\dot{p}, \dot{q}, \dot{r}$	=	time derivatives of roll, pitch, yaw rates
P	=	maximum percentage of motion sick people under the given circumstances
t_1, t_2, t_3	=	time vectors of the sigmoid function
u, v, w	=	velocity component along the aircraft's x, y, and z axes
$\dot{u}, \dot{v}, \dot{w}$	=	time derivatives of u, v, w
x, y, z	=	longitudinal, lateral, and vertical axis
v_s, a_s, ω_s	=	sensed subjective vertical, acceleration, and angular velocity
$\hat{v}, \hat{a}, \hat{\omega}$	=	expected subjective vertical, acceleration, and angular velocity
$\Delta v, \Delta a, \Delta\omega$	=	subjective vertical, acceleration, and angular velocity conflict
ζ	=	damping of the motion filter
μ	=	mean
σ	=	standard deviation
τ_d, τ_I	=	time constants of the 6DOF-SVC model
ϕ, θ, ψ	=	Euler roll, pitch, and yaw angles
ω_n, ω_b	=	natural break-frequency and third order pole of the third-order high-pass motion filter

I. Introduction

A current research program at Delft University of Technology (TU Delft) is to improve the sustainability of aviation through the possible employment of the 'Flying-V' aircraft concept. The Flying-V's unique design integrates the primary body into the wings, eliminating the need for a central fuselage. Therefore, due to its aerodynamic form and lower weight, the design is anticipated to consume 20% less fuel than the current most energy-efficient aircraft (i.e. Airbus A350) [1], [2]. Despite the resulting aerodynamic benefits, it is still unknown to what extent sitting laterally farther away from the centre of rotation in the Flying-V and being seated rotated with respect to the direction of flight will increase the severity of motion sickness for passengers, as compared to conventional aircraft. Therefore, researching motion comfort in the Flying-V is crucial for its overall success and passenger satisfaction. The comfort and well-being of passengers are directly impacted by the level of motion sickness experienced during flight. By focusing on researching and understanding motion sickness in the Flying-V, a better understanding can be gained regarding the effect of the Flying-V's configuration on passengers' comfort. This knowledge can then be utilised to improve motion comfort in the Flying-V, which would create a more positive flying experience and potentially attract a wider range of passengers.

Motion sickness in humans is a syndrome characterised by various symptoms such as dizziness, headache, stomach awareness, sweating, and nausea [3]. These symptoms can also progress to more severe stages, including retching and vomiting [4]. Reason and Brand [5] have found that everyone who has a functioning vestibular system can experience motion sickness. Several motion sickness models have been developed to predict the occurrence of motion sickness in response to specific stimuli. These models include Oman's model [6], Lawther and Griffin's model [7], the 6 Degrees of Freedom (DOF)-Subjective Vertical Conflict (SVC) model [8], the Multi-Sensory Observer Model [9], the UNIPG Model [10], and the Particle Filter Model [11]. The 6DOF-SVC model includes 6 DOFs in three-dimensional space. This model has been validated and used widely in motion sickness studies such as Irmak et al. [12], Kamiji et al. [8], Wada et al. [13], Turan et al. [14], and Wada [15]. Hence, the 6DOF-SVC model has an advantage in terms of reliability and validity, compared to the other motion sickness models. Therefore, in the current research, the 6DOF-SVC model is utilised to predict motion sickness in the context of the Flying-V. The preliminary analysis suggested that motion sickness severity for passengers is primarily affected by the roll acceleration and the additional vertical acceleration experienced by passengers seated laterally offset from the centre of rotation. Thus, this research focused specifically on the impact of roll motion and the combination of roll and heave motion on motion sickness severity due to sitting laterally farther away from the centre of rotation. By studying the effect of the combination of the roll and vertical motions, the research aims to gain insights into how these motions contribute to the overall motion comfort experienced by passengers in the Flying-V. Moreover, to compare the effect of vertical motion combined with roll motion on humans using different stimuli, the results of this study are compared to previous studies that explored the effects of various DOF motions on motion sickness severity. For instance, Irmak et al. [16] examined the influence of increasing amplitude of fore-aft

motion, Beard et al. [17] investigated the combination of lateral and roll motions with different frequencies, Joseph et al. [18] explored the effects of increasing magnitude in the combination of lateral and roll motions, and Wertheim et al. [19] studied the effect of heave, pitch, and roll motions individually and in combination. The comparison is based on data collected on the motion sickness severity caused by the fore-aft motion in a previous study, to the motion sickness severity caused by the combination of the roll and vertical motion of the current study. Moreover, it aims to determine if the combination of translational and rotational motion led to increased motion sickness severity in previous studies compared to the current study.

The seats that are used in this research are the 26° staggered seats designed by Liu et al. [20], which are parallel to the centre-line of the Flying-V. Joosten et al. [21] have evaluated the Flying-V's lateral directional handling qualities, performing manoeuvres such as the Dutch Roll; Coordinated Turn Capability; Time to Bank (TTB); One Engine Inoperative Trim; and Steady Heading Sideslip. This research will primarily focus on the TTB manoeuvre, as preliminary analysis revealed that passengers that sit laterally farther away from the centre of rotation are affected by these fast manoeuvres, and these fast manoeuvres exhibit distinct specific force due to the geometry of the Flying-V, in comparison to conventional aircraft.

The first step of the research is the specific force analysis, which aims to identify the specific force component most influenced by the Flying-V's configuration. The second step of the research is the motion sickness prediction using the 6DOF-SVC model that evaluates the extent to which motion sickness increases with increasing lateral distance from the centre of rotation. Finally, in the third step of the research, a passenger-in-the-simulator experiment was designed and conducted using the SIMONA Research Simulator (SRS) to carry out the study. Twelve participants were exposed to three different conditions corresponding to different lateral positions in the Flying-V: sitting at the centre of rotation; sitting 3.5m laterally offset from the centre of rotation; and sitting 7m laterally offset from the centre of rotation. The experimental results were then compared to the predictions generated by the 6DOF-SVC model [12], to assess the model's ability to predict motion sickness severity in the Flying-V.

This paper is structured as follows: Section II provides the specific force analysis and motion sickness prediction; Section III outlines the experimental method employed in the study; Section IV presents the experiment results; Section V encompasses a discussion of the findings; and Section VI presents the conclusion of the paper.

II. Analysis

A. Specific Force

The gravitational acceleration (g) and inertial acceleration (a) work on the otolith at the same time, which gives the specific force (f) [8]. In this case, it is used in the aircraft body reference frame and the initial feeling of upright is upward ($f = a - g$). Due to the unique design of the Flying-V, passengers will be exposed to different motions and specific force than those experienced in conventional "tube-and-wing" aircraft. Figure 1 shows a comparison between the geometry of the Airbus A350 and the Flying-V.

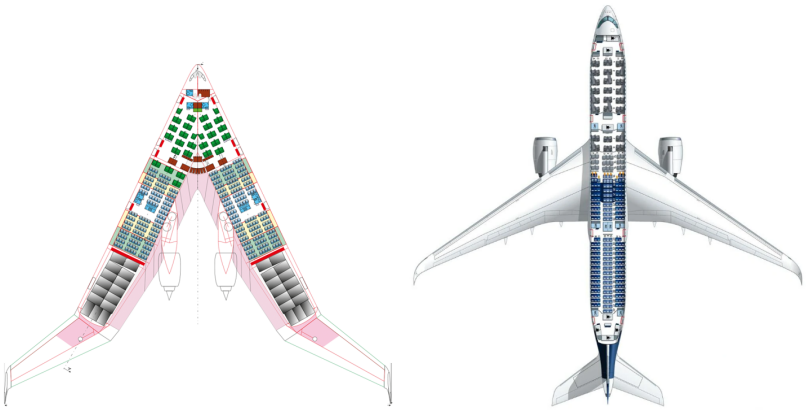

(a) Top view of the Flying-V [22] (b) Top view of the Airbus A350*

Fig. 1 Comparison between the Flying-V and the A350

The specific force components are calculated at the Centre of Gravity (CG). Then a coordinate transformation of the specific force components from the CG to various locations within the Flying-V is done. This allows for identifying which specific force component changes when passengers are seated laterally farther away from the centre of rotation. Equation 1 is employed to compute the specific force at the CG, in the aircraft body reference frame.

$$\begin{pmatrix} \dot{u} \\ \dot{v} \\ \dot{w} \end{pmatrix} = \frac{1}{M} \begin{pmatrix} F_{x(\mathrm{CG})} \\ F_{y(\mathrm{CG})} \\ F_{z(\mathrm{CG})} \end{pmatrix} - \begin{pmatrix} p \\ q \\ r \end{pmatrix} \times \begin{pmatrix} u \\ v \\ w \end{pmatrix} + A\overrightarrow{g} \tag{1}$$

where A is the inertial-to-body frame transformation:

$$A = \begin{pmatrix} \cos\theta\cos\psi & \cos\theta\sin\psi & \text{-}\sin\theta \\ \sin\phi\sin\theta\cos\psi - \cos\phi\sin\psi & \sin\phi\sin\theta\sin\psi + \cos\phi\cos\psi & \sin\phi\cos\theta \\ \cos\phi\sin\theta\cos\psi + \sin\phi\sin\psi & \cos\phi\sin\theta\sin\psi - \sin\phi\cos\psi & \cos\phi\cos\theta \end{pmatrix} \tag{2}$$

where (u, v, w) represent the velocity components along the aircraft's x, y, and z axes, respectively. Similarly, $(\dot{u}, \dot{v}, \dot{w})$ represent the time derivatives of (u, v, w). (ϕ, θ, ψ) correspond to the Euler roll, pitch, and yaw angles. (p, q, r) represent the roll, pitch, and yaw rates, respectively. $\overrightarrow{g}$ denotes the gravity vector. $(F_{x(\mathrm{CG})}, F_{y(\mathrm{CG})}, F_{z(\mathrm{CG})})$ are the longitudinal, lateral, and vertical forces, respectively, at the CG. M is the aircraft mass. The combination of force components $(F_{x(\mathrm{CG})}, F_{y(\mathrm{CG})}, F_{z(\mathrm{CG})})$ with $(1/M)$ gives the specific force components at the CG $(f_{x(\mathrm{CG})}, f_{y(\mathrm{CG})}, f_{z(\mathrm{CG})})$.

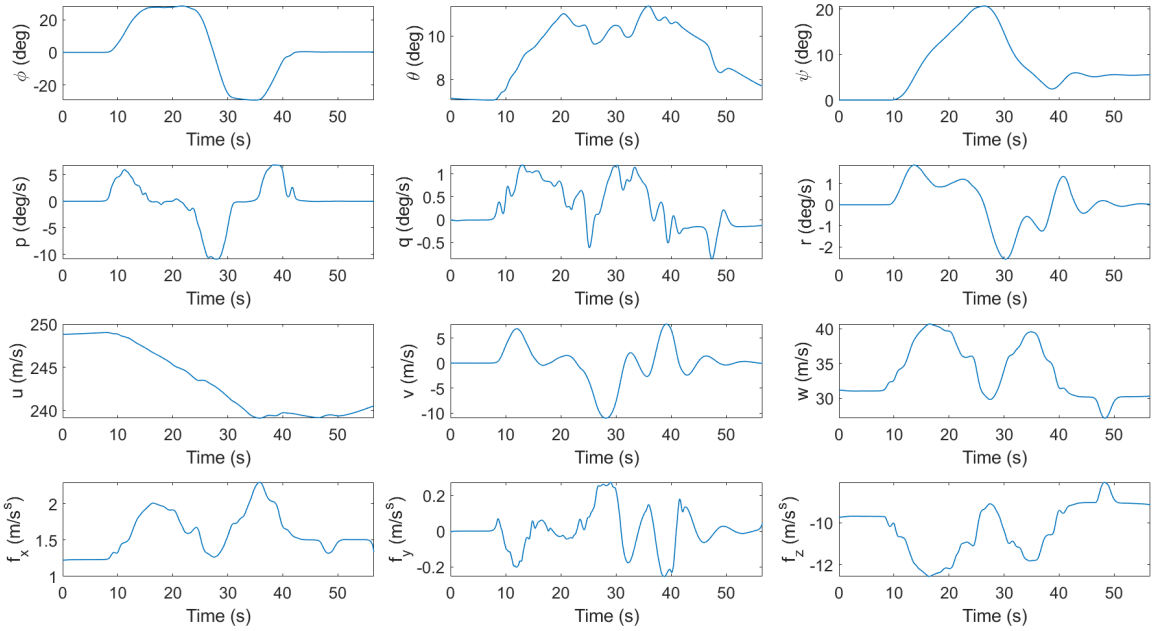

Fig. 2 TTB flight data and the calculated specific force components [21]

Figure 2 presents the Euler angles, Euler rates, the velocity components along the Flying-V's x, y, and z axes, and the calculated f_x, f_y, and f_z specific force components during the TTB simulator flight data [21]. The TTB manoeuvre involves rolling the aircraft by +/-30° around the centre of rotation, pitching from an initial angle of 7° up to 11° and then back down, and yawing to the right by 20° and then back to the left. During pitch-up of the aircraft, passengers feel a longitudinal specific force in the forward direction. f_x starts at around 1.2 m/s^2 due to the pitch trim angle, which is around 7°. During a turn, passengers would experience a centrifugal force that pushes the passengers away from the centre of the turn and towards the side of the aircraft. The lateral gravity component of the passenger cancels this force, leaving a small lateral force that would be felt by the passengers. By comparing f_y and f_z, it is evident that the vertical

*https://www.onceinalifetimejourney.com/reviews/airlines/review-of-lufthansa-business-class-a350/, Date: 29/07/2023

specific force component experienced by passengers is stronger than the lateral specific force component. The f_z felt by the passengers in the aircraft increases as the centrifugal force increases during the TTB manoeuvre. Therefore, passengers would feel heavier than they truly are. A coordinate transformation of the specific force components from the CG to different Seating Positions (SP) is done by [23]:

$$f_{x(\mathrm{SP})} = (-r^2 - q^2)x_{\mathrm{SP}} + (pq - \dot{r})y_{\mathrm{SP}} + (\dot{q} + pr)z_{\mathrm{SP}} + f_{x(\mathrm{CG})} \tag{3}$$

$$f_{y(\mathrm{SP})} = (\dot{r} + pq)x_{\mathrm{SP}} + (-r^2 - p^2)y_{\mathrm{SP}} + (qr - \dot{p})z_{\mathrm{SP}} + f_{y(\mathrm{CG})} \tag{4}$$

$$f_{z(\mathrm{SP})} = (pr - \dot{q})x_{\mathrm{SP}} + (qr + \dot{p})y_{\mathrm{SP}} + (-q^2 - p^2)z_{\mathrm{SP}} + f_{z(\mathrm{CG})} \tag{5}$$

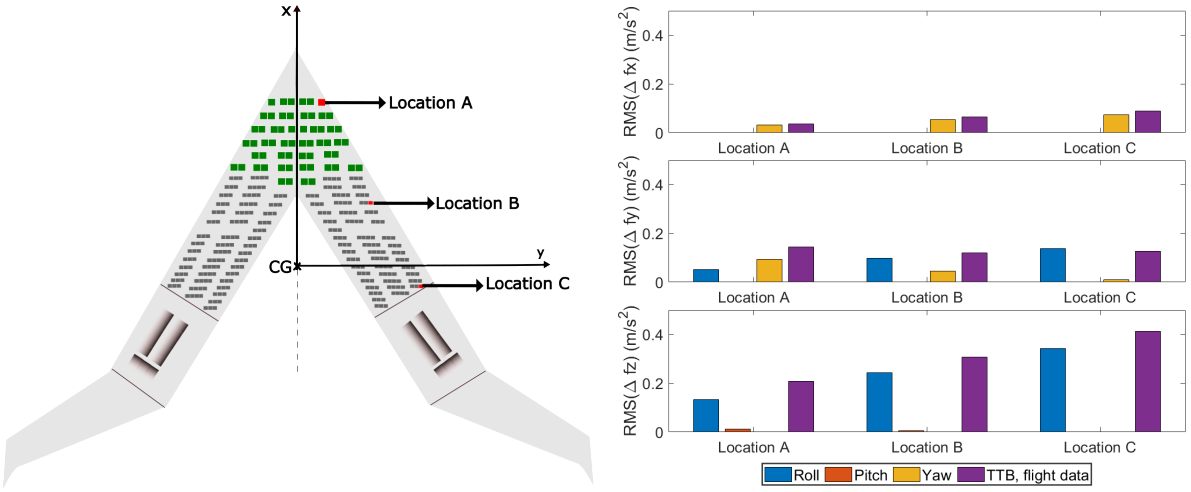

(a) 26° rotated seat configuration and different locations used

(b) RMS of the specific forces differences between the outboard seats and the CG

Fig. 3 Flying-V's seats and RMS of the difference in specific force components between the outboard seats and the CG

Figure 3(a) shows the different locations (Location A, Location B, and Location C) that are used to calculate the RMS of the difference in specific force components between these locations and the CG, using the 26° rotated seat configuration, which is parallel to the centre line of the Flying-V. These locations are used because they represent the most-front, middle, and most-aft outboard locations in the Flying-V. Figure 3(b) shows the Root Mean Square (RMS) difference in the specific force components between the CG and different locations in the Flying-V, denoted as A, B, and C. To identify the dominant component (roll, pitch, or yaw) at the CG in the TTB manoeuvre within the context of the Flying-V aircraft and whether the results are influenced by the artefact of the model that produced the simulator flight data, simplified manoeuvres of roll, pitch, and yaw were done in the analysis as well. The simplified manoeuvres were adjusted to match the key characteristics of the TTB simulator flight data, such as the roll angle range from +30° to −30°. A sigmoid function was used to fit the simulator flight data, allowing for fine-tuning of its parameters to accurately capture the essential features of the simulator flight data. The analysis of the data indicates that the vertical specific force component f_z is the most influenced by the seating locations of passengers, particularly when they are seated laterally farther away from the centre of rotation. The disparity between the CG and the respective locations becomes more pronounced as the distance from the centre of rotation increases. The RMS difference in f_z between the CG and location A is approximately 0.2 m/s^2, which increases to approximately 0.4 m/s^2 at location C, the farthest from the centre of rotation. This difference is primarily attributed to the roll motion. The specific force components f_x and f_y exhibit relatively small variations across different locations compared to the effects observed in f_z. The RMS result of f_y remains relatively constant across all locations, around 0.1 m/s^2. f_x shows a minimal increase, reaching up to 0.1 m/s^2 at the farthest location C. Hence, for further analysis in this paper, the focus will primarily be on the vertical component of the specific force and the roll motion.

Figure 4 shows the f_z at Locations A, B, C, and the CG in the Flying-V using Equation 5. The distinction between Locations A, B, C, and the CG in f_z only happens when the aircraft's rolling acceleration is changed. To have equivalent results for both wings in the Flying-V, the asymmetrical original simulator flight data from Joosten et al. [21] have been made symmetrical. When rolling right, the seats on the right wing have a downward vertical acceleration compared to the seats on the left wing, which will have an upward vertical acceleration, and the opposite is true when rolling left. Passengers that are sitting farther away from centre of rotation will experience higher extra vertical acceleration due to the roll acceleration, compared to the passengers sitting closer to the centre of rotation.

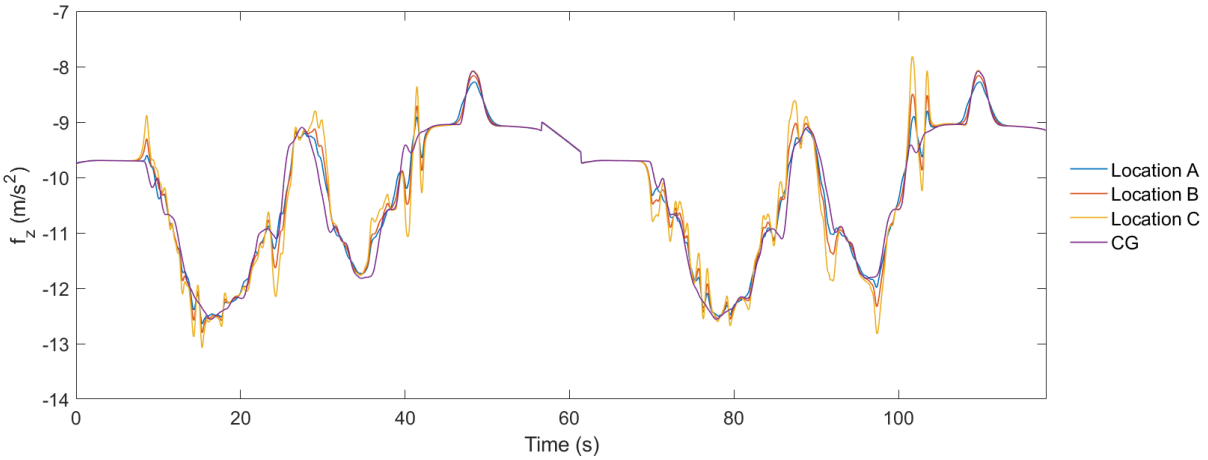

Fig. 4 Vertical specific force at different locations in the Flying-V using the symmetrical TTB data

B. Motion Sickness Modelling

The 6DOF-SVC model [12] was employed to predict motion sickness in the Flying-V. The specific force components calculated from the symmetrical TTB data that were based on the simulator flight data [21], along with the angular velocity obtained from the same data, were utilised in the model.

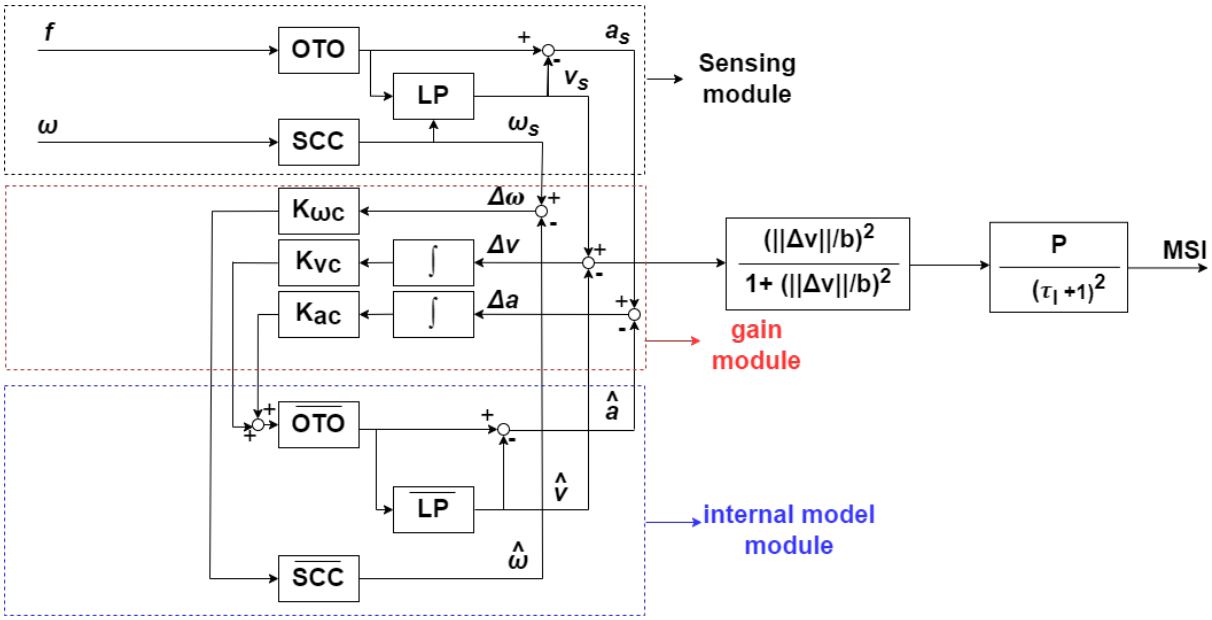

Fig. 5 6DOF-SVC model [12] [8]

Figure 5 illustrates the 6DOF-SVC model. The model consists of three modules: (i) the sensing module; (ii) the gain module; and (iii) the internal model module. The sensing module receives inputs of specific force components and angular velocity. These inputs are then used to generate sensed values for acceleration (a_s), subjective vertical (v_s), and angular velocity (ω_s). The internal model module, on the other hand, generates estimates for the states of acceleration ($\hat{a}$), subjective vertical ($\hat{v}$), and angular velocity ($\hat{\omega}$). The model is parameterised by several feedback gains and filters. In the gain module, the subjective vertical and acceleration conflicts are passed through the integral gains (K_{vc}/s and K_{ac}/s), while the angular velocity is passed through a proportional gain ($K_{\omega c}$). This is passed to the internal model module, which has subsequent estimates ($\hat{a}$, $\hat{v}$, and $\hat{\omega}$). The Semicircular Canals (SCC) are represented by first-order high-pass (SCC = $(\tau_d s)/(\tau_d s + 1)$. The Otolith (OTO) is assumed as a unit matrix. LP and $\overline{\text{LP}}$ represent first-order low-pass filters used to estimate the subjective vertical [12]. The estimates ($\hat{a}$, $\hat{v}$, and $\hat{\omega}$) are then compared to the corresponding sensed states (v_s, a_s, and ω_s). The sensory conflict is the discrepancy between the sensed and internal state estimates. The model has three conflict terms: (i) acceleration conflict (Δa); (ii) subjective vertical conflict (Δv); and (iii) angular velocity conflict ($\Delta\omega$). The three conflict terms are then fed into the internal model through the gain module. Thereafter, using a second-order Hill function and second-order integration, only the subjective vertical conflict (Δv) is used to predict a Motion Sickness Incidence (MSI), representing the percentage of individuals who would experience emesis as a result of the motion. The MSI is the model's output. The three modules in the model are based on Irmak et al. study [12], however, Irmak et al. have not incorporated the part to calculate the MSI. Therefore, the part to calculate the MSI is based on Kamiji et al. [8]. Table 1 lists the model's parameters.

Table 1 6DOF-SVC parameters [8]

Parameter	$K_{\omega c}$	K_{vc}	K_{ac}	τ_d (s)	b (m/s^2)	τ_I (min)	P (%)
Value	5	5	1	7	0.5	12	85

Three assumptions are used to conduct the simulations:

1) The passengers were seated in the right wing of the Flying-V, which corresponded to the seat where the motion cues were presented in the simulator. This is a design choice that has been made since the manoeuvre has been made symmetrical, therefore, equivalent results will be obtained for both wings;
2) The passengers' head orientation would be aligned with the orientation of the aircraft, therefore, aligned with the aircraft's x-axis; and
3) The visual system has not been implemented in the 6DOF-SVC model, therefore, it is assumed that there is no vision (i.e. eyes closed). However, in the experiment, participants were asked to keep their eyes open, but there were no outside visuals. Hence, it was a non-moving vision situation. This approach ensures that the experiment replicates what participants experience in real flight, rather than instructing them to keep their eyes closed.

1. Simulator Flight Data

First, the symmetrical TTB manoeuvre that has been based on the simulator flight data of Joosten et al. [21] is used to predict the MSI in the Flying-V. The model's conflict terms revealed that the vertical conflict is the most prominent component of the motion sickness experienced in the Flying-V, as has been seen in the preliminary analysis. Figure 6 presents a heatmap depicting the relative increase/decrease in MSI at different locations in the Flying-V compared to the CG position, after running the symmetrical TTB manoeuvre for 1-hour. The heatmap demonstrates that the MSI intensifies as the locations move farther away from the centre of rotation. Notably, the relative increase in MSI gets up to 13.9% compared to the reference location at the CG, due to the lateral offset seating positions relative to the aircraft's centre of rotation.

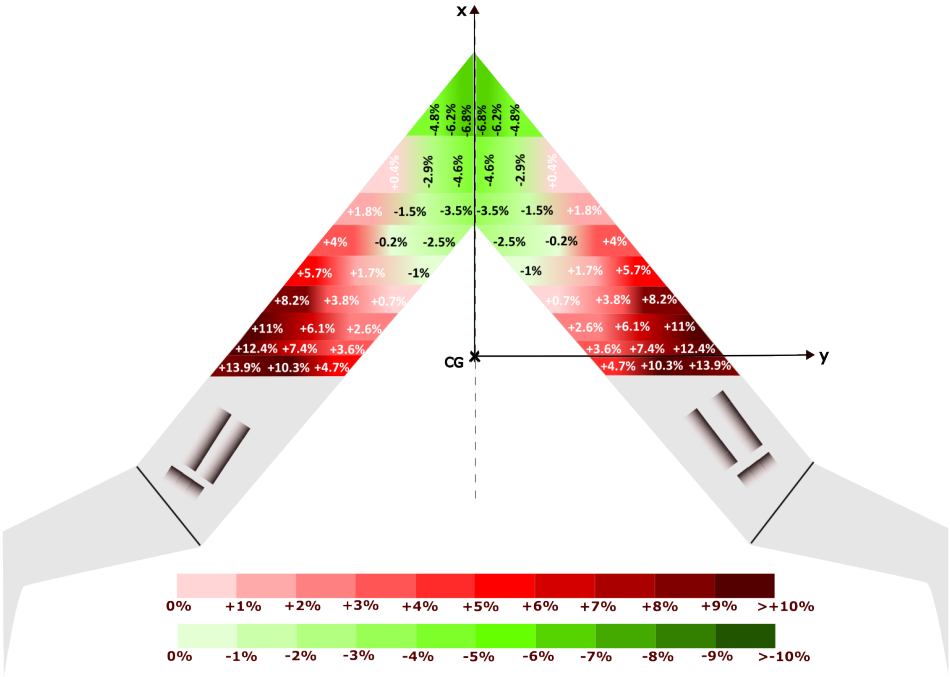

Fig. 6 MSI heatmap for the Flying-V based on the symmetrical flight data [21]

2. Simplified Manoeuvre

The symmetrical TTB manoeuvre has a low frequency. The manoeuvre's low frequency will cause an excessive motion filtering of the original manoeuvre due to the small motion space of the SRS. Thus, to avoid excessive motion filtering and to make the manoeuvre feasible in the SRS, it is chosen to simplify the TTB manoeuvre by neglecting the aerodynamics and the movement of the CG for this experiment. This simplification allows for a focus on the high-frequency components of the manoeuvre and reduces the amount of motion filtering required, compared to including the aerodynamics and CG movement. Therefore, the focus instead will be on the roll motion and the extra vertical acceleration it causes to the passengers that are sitting laterally farther away from the centre of rotation. This will enable the investigation of the impact of sitting laterally farther away from the centre of rotation on motion sickness. A motion filter is used to make sure that the simplified manoeuvre is feasible in the SRS. Therefore, this section shows the simplified manoeuvre before (unfiltered) and after (filtered) using the motion filter.

Unfiltered Manoeuvre To replicate the symmetrical TTB manoeuvre that is based on the simulator flight data, the experiment utilises the roll flight data derived from the TTB manoeuvre conducted by Joosten et al. [21]. This manoeuvre involves a symmetrical roll motion of +/-30° around the centre of rotation. Figure 7(a) presents a comparison between the roll data obtained from the simulator flight data and the simplified unfiltered manoeuvre data, which was generated using the sigmoid function. The sigmoid function for ϕ consists of three parts representing different phases of rolling motion:

1) The first part corresponds to rolling from 0° to +30° and is defined as $\phi = K_1 + (K_2 - K_1)/(1 + \exp(-G(t_1 - M_1)))$, where K_1 and K_2 are the desired roll angles (0° and 30° respectively), t_1 is the time vector ranging from 0 to 12 seconds, and M_1 is the midpoint of this sigmoid function at 6 seconds
2) The second part corresponds to rolling from +30° to −30° and is defined as $\phi = K_2 + (-2K_2)/(1 + \exp(-G(t_2 - M_2)))$, where t_2 is the time vector ranging from 12 to 24 seconds, and M_2 is the midpoint of this sigmoid function at 18 seconds
3) The third part corresponds to rolling from −30° to 0° and is defined as $\phi = -K_2 + (K_1 + K_2)/(1 + \exp(-G(t_3 - M_3)))$, where t_3 is the time vector ranging from 24 to 36 seconds, and M_3 is the midpoint of this sigmoid function at 30 seconds.

The parameter G is the slope parameter and is set to 1 s^{-1}. After defining the three sigmoid functions, they are

concatenated together to form the complete roll motion trajectory from +30° to −30°. Additionally, the symmetry of the data is added by including the rolling motion from −30° to +30° after the initial roll. Figure 7(a) shows that the simulator flight data exhibit approximately 10 seconds of unmoving period at the beginning and 20 seconds of unmoving period at the end of the manoeuvre. To ensure that the experiment does not include prolonged periods of inactivity, the sigmoid function has been designed to not include these stationary periods. The sigmoid function captures important characteristics of the manoeuvre, such as the time to bank and the transition from positive to negative banking angle. In both cases, a ϕ of +/-30° is achieved, with a peak p of approximately 13 deg/s and a peak $\dot{p}$ of 4.5 deg/s^2. It can be seen that the simulator flight data contain fast oscillations, which might be an artefact of the dynamics model used to calculate the simulator flight data. Figure 7(b) depicts the f_z, excluding the movement of the CG, for two locations: the centre of rotation and the most outboard lateral seating position at 13 m away from the centre of rotation. It is seen that the location at the centre of rotation maintains a constant f_z of -9.8 m/s^2 throughout the motion because it only includes roll motion and there is no heave motion. However, for the most outboard location, f_z reaches a magnitude of -10.8 m/s^2 during the left roll and -8.8 m/s^2 during the right roll, due to the extra vertical acceleration of the roll acceleration. Only the acceleration due to the roll acceleration and the lateral offset from the centre of rotation is used ($a_z = \dot{p}y$). During the rolling motion, the gravity component is assumed to remain constant to match what passengers would feel in an actual flight scenario. f_z is given by the equation $f_z = \dot{p}y - g$. Additionally, there is no lateral specific force component f_y experienced during the rolling motion, as it would not be felt in an actual coordinated flight scenario, resulting in f_y = 0 m/s^2.

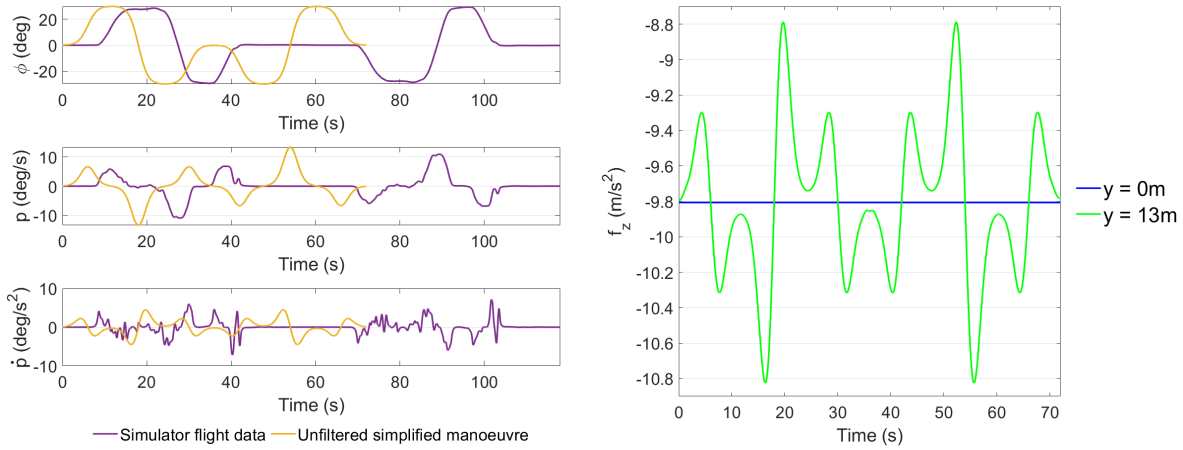

(a) Roll motion comparison between simulator flight data and unfiltered simplified manoeuvre

(b) f_z at the CG and the most outboard seating position during the simplified TTB manoeuvre

Fig. 7 Roll comparison between simulator flight data and unfiltered simplified manoeuvre and vertical specific force for the unfiltered simplified manoeuvre

The specific force components and the angular velocity are used as input in the 6DOF-SVC model to predict the MSI at different locations in the Flying-V, for a simulation of 1-hour. Figure 8 shows the heatmap of the relative increase in MSI using unfiltered simplified manoeuvre, exhibiting that the relative increase in MSI can get up to 52.2% for the most outboard seating position (y = 13 m) in the Flying-V, compared to the CG position. The relative difference in MSI between the CG and different seating positions in the Flying-V is more prominent in this case compared to using the symmetrical TTB that is based on the simulator flight data, due to ignoring the aerodynamic and CG effects.

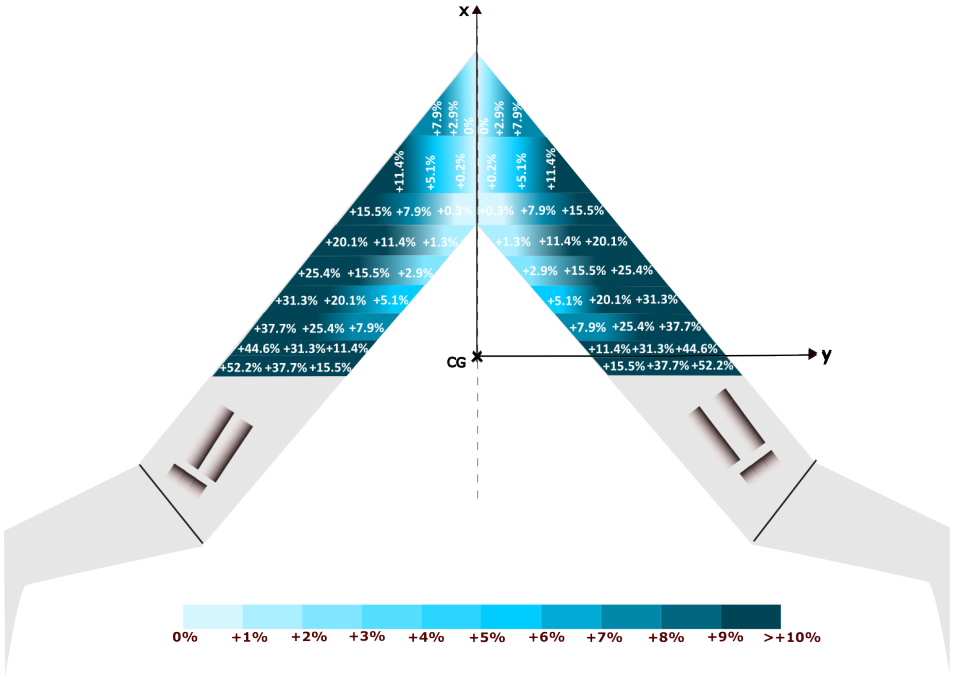

Fig. 8 MSI heatmap for the Flying-V based on the TTB unfiltered simplified manoeuvre

Filtered Manoeuvre To ensure that the designed simulator movement remains within the limited motion space of the SRS, motion filtering of the simplified TTB manoeuvre is necessary to ensure that the experiment can be conducted within the simulator's limitations. The full range of motion in the Flying-V can not be fully replicated in the SRS due to its constrained motion capabilities. In addition, not all locations within the Flying-V can be accurately replicated in the SRS, due to the same reason. This may result in some limitations in terms of the specific locations that can be studied and simulated within the experimental setup. In Section III.C, the filtering of the simplified TTB manoeuvre is discussed in more detail, including the specific parameters used for the motion filter. With the current set of motion filter parameters (the gain, the natural break-frequency of the second order filter, the third order pole, and the damping of the motion filter), the SRS is capable of replicating motion up to a lateral location of y = 7 m. Figure 9(a) provides a comparison between the unfiltered and filtered data of the roll motion. The unfiltered simplified TTB manoeuvre exhibited a peak ϕ of 30°, peak p of 13.2°/s, and peak $\dot{p}$ of 4.5°/s^2. However, after applying the motion filter, the peaks in ϕ, p, and $\dot{p}$ were reduced to 4°, 2.9°/s, and 2.3°/s^2, respectively. Moreover, Figure 9(a) demonstrates a phase shift between the filtered and unfiltered simplified TTB manoeuvre. However, this should not present any issues, as no other stimuli are being presented during the experiment. Figure 9(b) shows the f_z felt by passengers using the filtered simplified manoeuvre for the seating positions at the centre of rotation and the most outboard lateral seat (y = 7 m) the SRS can simulate with the current motion filter parameters. In the most outboard lateral seating position in the SRS, f_z reaches -10.1 m/s^2 during the left roll and -9.5 m/s^2 during the right roll, indicating the additional vertical acceleration caused by rolling. A comparison between Figures 7(b) and 9(b) shows that in the filtered case, the f_z for the location at y = 7 m is reduced compared to the unfiltered case, due to the application of motion filtering on the manoeuvre. The small oscillations in the filtered f_z are due to the transformation from the body to the inertial reference frame and the translation from the filter reference to the upper gimbal point of the SRS in the motion filter. However, the f_z for the location at y = 0 m remains approximately the same for both the filtered and unfiltered simplified manoeuvre.

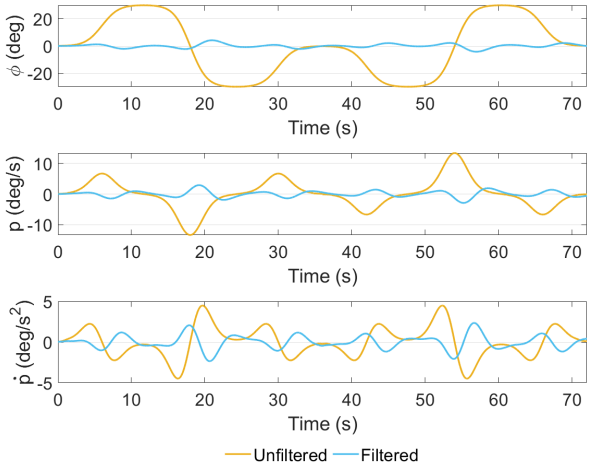

(a) Roll motion comparison

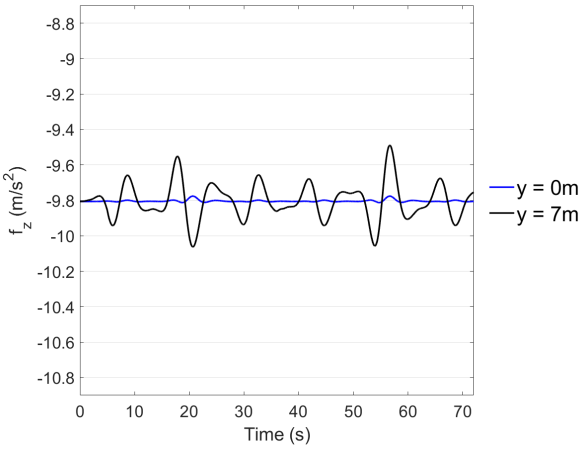

(b) f_z at the CG and the most outboard seating position the simulator can simulate using the current motion filter paramteres

Fig. 9 Roll comparison between the unfiltered and filtered simplified manoeuvre and vertical specific force for the filtered simplified manoeuvre

Figure 10 illustrates the heatmap of the MSI for the filtered simplified TTB manoeuvre. The black areas in the heatmap indicate locations that are not feasible to replicate within the SRS with the current motion filter parameters; namely, beyond 7m. Despite the reduction in the MSI as a result of the filtering process, a comparison between Figures 8 and 10 reveals that the relative differences in MSI have remained approximately the same in the comparable locations. The difference in MSI between the CG and y = 7m in the unfiltered simplified manoeuvre is approximately 15.5% and in the filtered simplified manoeuvre is approximately 12.7%. Therefore, despite motion filtering resulting in a reduction in MSI, it is expected that sitting laterally farther away from the centre of rotation will increase the motion sickness severity, compared to sitting at the centre of rotation.

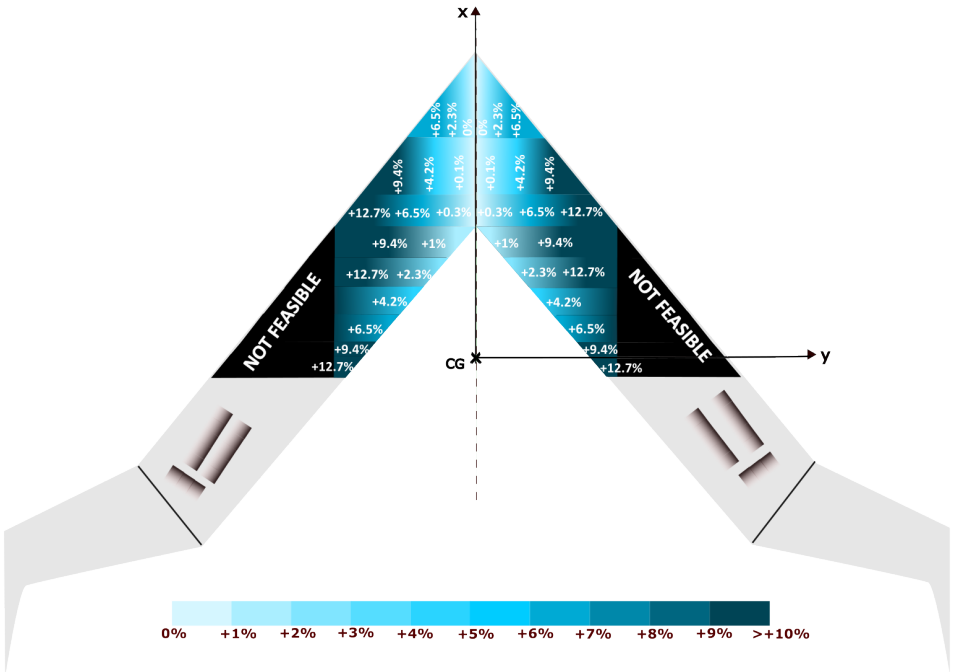

Fig. 10 MSI heatmap for the Flying-V based on the TTB filtered simplified manoeuvre

Figure 11 shows the relationship between sitting laterally away from the centre of rotation and the MSI. Applying the motion filter resulted in a reduction in MSI of approximately 62.6% for y = 0 m, 62.9% for y = 3.5 m, and 63.5% for y = 7 m. Prior to the implementation of the motion filter, there was a difference of approximately 15.5% in MSI between a lateral offset of y = 0m and y = 7 m, a difference of about 3.9% between y = 0 m and the middle location y = 3.5 m, and a difference of around 11.1% between y = 3.5 m and y = 7 m. Notably, the difference in MSI between y = 3.5 m and y = 7m is nearly three times greater than the difference between y = 0 m and y = 3.5 m. The relative differences in percentage have remained approximately the same. Therefore, the model predicts an exponential increase in MSI with increasing lateral distance from the centre of rotation.

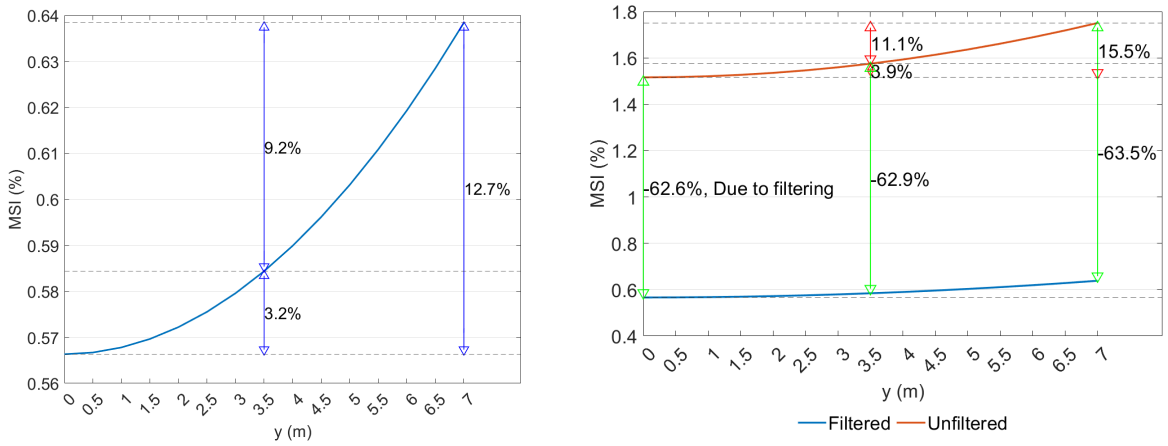

(a) MSI of the filtered simplified manoeuvre

(b) MSI comparison between the filtered and unfiltered simplified manoeuvre

Fig. 11 Percentage differences in MSI between three locations

Figure 12 shows the time development of MSI for three lateral locations: 0 m, 3.5 m, and 7 m, using the simplified symmetrical TTB manoeuvre. The MSI exhibits an exponential increase over time, eventually reaching values of 0.566%, 0.584%, and 0.638% for 0 m, 3.5 m, and 7 m, respectively.

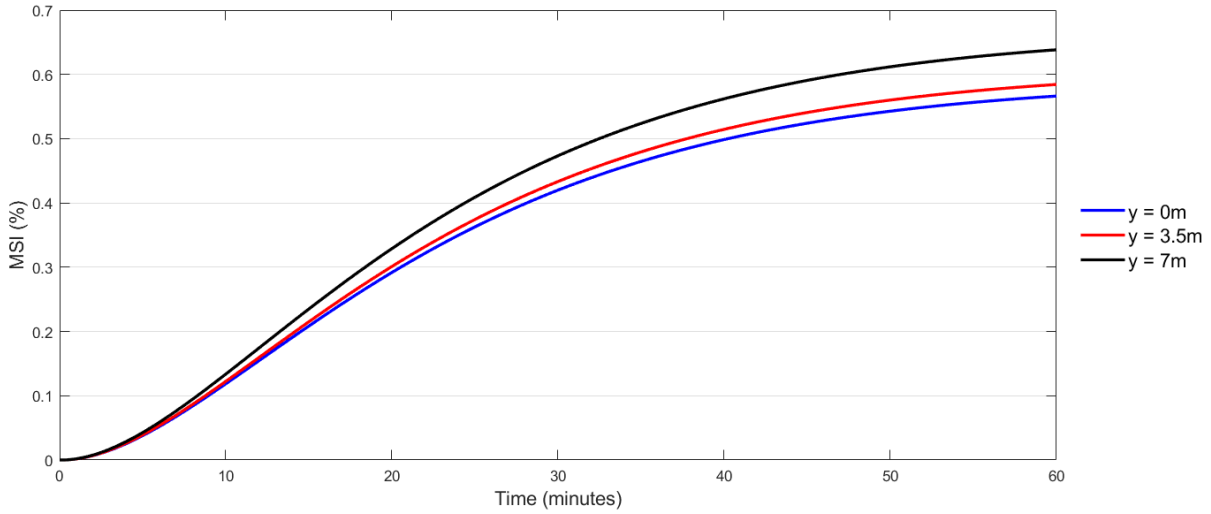

Fig. 12 MSI development according to the 6DOF-SVC model for the simplified symmetrical TTB manoeuvre

III. Experiment

To explore the potential correlation between passengers' lateral seating positions in the Flying-V and the severity of motion sickness, a passenger-in-the-simulator experiment was conducted. The objectives of the experiment were to assess whether the severity of motion sickness increased as participants were seated laterally farther away from the centre of rotation, and to gather subjective motion comfort data for comparison with the predictions of the 6DOF-SVC model. During the experiment, participants were exposed to three distinct conditions, and each condition has a different lateral distance from the Flying-V's centre of rotation.

A. Independent Variables

The experiment focused on a single independent variable, which is the lateral distance from the centre of rotation, to examine its influence on passengers' motion sickness severity. The conditions are:

1) Condition 1: y = 0 m, roll motion only. Figure 13(b) shows the simulator position during the rolling to the right
2) Condition 2: y = 3.5 m, roll motion combined with heave motion. Figure 13(c) shows the simulator position during the combined rolling and heave motion, where the motion utilises half of the actuators' motion space, compared to the SRS's neutral position seen in Figure 13(a)
3) Condition 3: y = 7 m, roll motion combined with heave motion. Figure 13(d) depicts the simulator position during the combined rolling and heave motion, where the motion utilises the maximum available range of the actuators' motion space, compared to the SRS's neutral position seen in Figure 13(a)

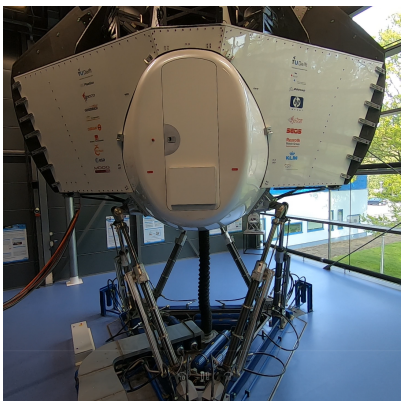

(a) The neutral position of the SRS

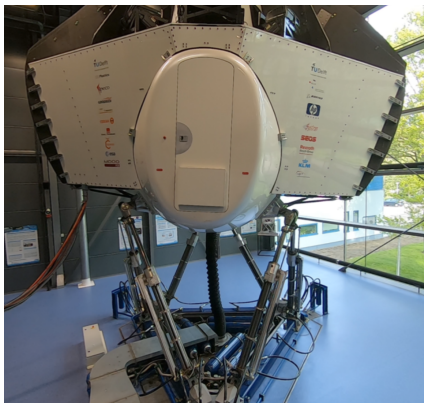

(b) The maximum SRS position for y = 0 m

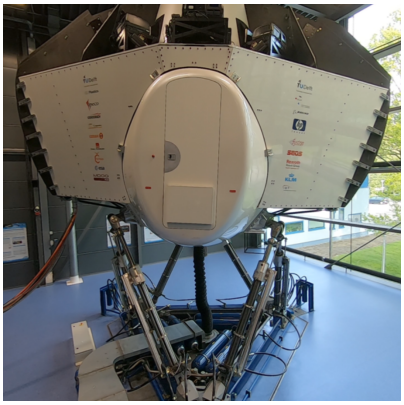

(c) The maximum SRS position for y = 3.5 m

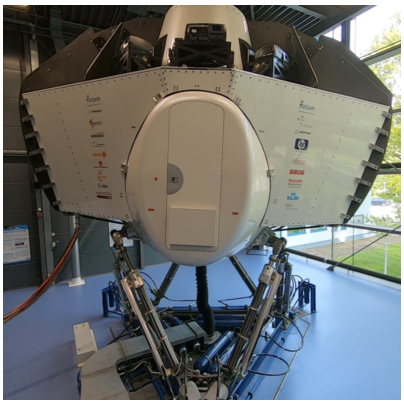

(d) The maximum SRS position for y = 7 m

Fig. 13 Simulator motion for the three conditions during a roll to the right

Three conditions were used to investigate the correlation between motion sickness and lateral seating positions relative to the centre of rotation. The lateral distance between Condition 1 and 2 was equal to the lateral distance

between Condition 2 and 3. Using three conditions allows for an examination of whether motion sickness severity follows the pattern predicted by the 6DOF-SVC model, as shown in Figure 11(a). Furthermore, the choice of three conditions also took into consideration the time constraints associated with using the SRS, as it was available for a limited period. The roll motion was identical across all three conditions, allowing for a focused investigation of the effects of varying heave motion on motion sickness severity.

B. Apparatus

The experiment was conducted in the SRS at TU Delft (see Figure 14(a)). The simulator's hydraulic 6-DOF hexapod motion system has a maximum actuator displacement of 1.12 m, a maximum speed of 0.9 m/s, and a maximum acceleration of 13 m/s^2 [24], [25]. The participants were seated inside a closed cabin and fastened with a five-point harness, and no visual cues were presented to the participants, see Figure 14(b). An intercom system was used to enable two-way communication between the experimenter and the participants. Over their headset, participants heard an aircraft's jet engine, to cover the sound of the moving actuators of the SRS. During the experiment, participants verbally reported their MIsc SCores (MISC), which were then recorded by the experimenter. Participants had a screen in front of them to display the MISC scores.

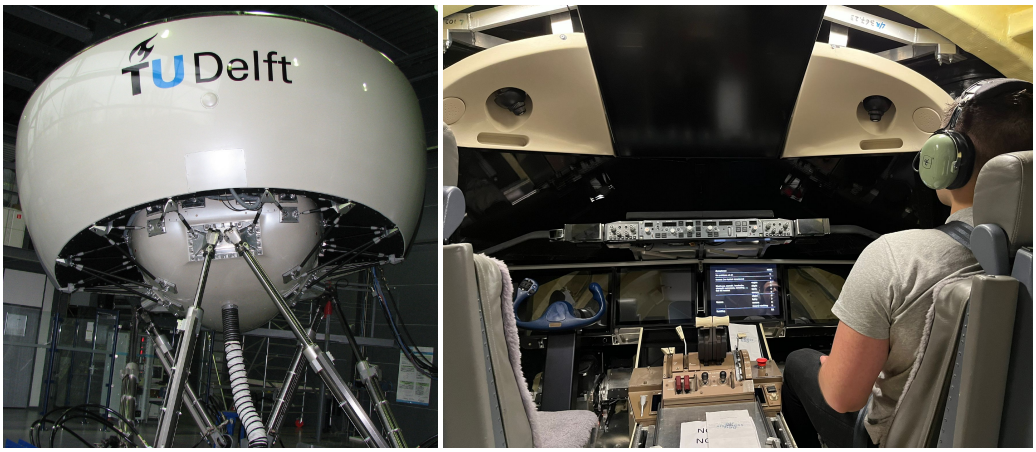

(a) SIMONA Research Simulator (b) Setup inside SIMONA Research Simulator

Fig. 14 Experiment setup

C. Experiment Condition Design

In order to make the simplified symmetrical TTB manoeuvre shown in Section II.B.2 feasible in the simulator, filtering was applied to the simplified TTB unfiltered manoeuvre, see Section II.B.2. A third-order high-pass filter was utilised, as the third-order filter has a return-to-neutral effect, which allows for a faster return of the cab to its neutral position during steady-state accelerations, compared to a second-order high-pass filter [26]. The third-order filter is given by [26]:

$$H(s) = \frac{ks^2}{s^2 + \omega_n^2 s + 2\zeta\omega_n} \cdot \frac{s}{s + \omega_b} \tag{6}$$

where k is the gain, ω_n is the natural break-frequency of the second-order filter, ω_b sets the third-order pole and ζ is the damping of the filter. The optimisation of the motion cues is done based on the Sinacori fidelity criteria, following the approach by Gouverneur [26]. A low break-frequency is used in order to allow for a wide variety of lateral positions to be performed in the simulator, without excessively filtering the original manoeuvre.

Table 2 shows the filter parameters and Figure 15 shows the Gouverneur analysis plot [26] for the lateral location of y = 7 m, which is the most outboard seat location the SRS can simulate with the current motion filter parameters. In this figure, the dots represent the different combinations of k and ω_n for the simplified TTB manoeuvre, ensuring that the required motion space remains within its limits of the SRS. A square symbol indicates that the length limit of one of the

actuators has been exceeded, and a plus symbol indicates that both the actuator length and velocity limits have been exceeded [26]. The blue dot represents the design choice of k and ω_n. Hence, the selection of k as 1 and ω_n as 1 rad/s is made to ensure that the SRS stays within the operational limits. The motion filter parameters are applied for both the roll and heave motion, resulting in the preservation of the kinematic relationships, making the simulator rotate around a point offset to the left for Conditions 2 and 3, and around the centre of rotation for Condition 1.

Table 2 Motion filter parameters

Parameter	ω_b (rad/s)	ω_n (rad/s)	ζ	k
Value	0.3	1	0.7	1

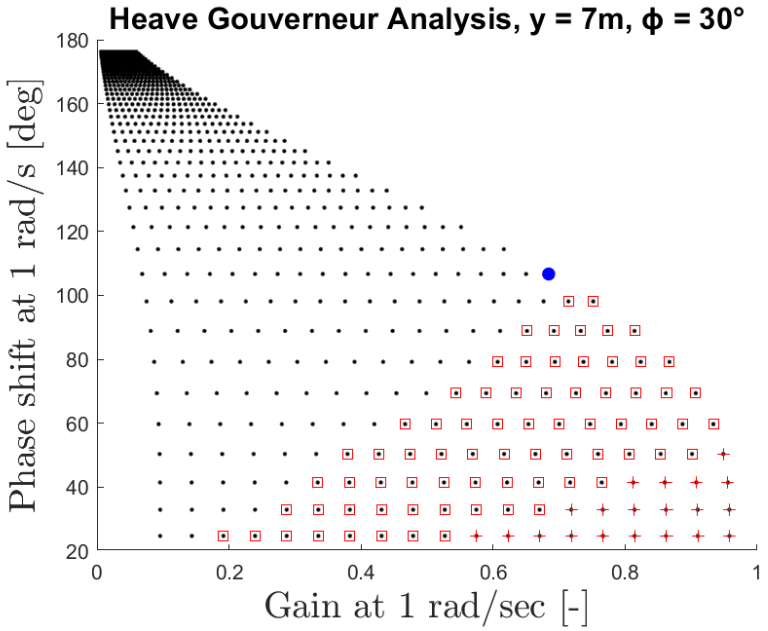

Fig. 15 Gouverneur analysis plot [26]

The heave motion data of the simulator for the conditions is shown in Figure 16(a). The simulator's maximum vertical acceleration (a_z) is around 0.3 m/s^2 for Condition 3. Figure 16(b) shows the roll motion data of the simulator. The simulator is rolling around 4°, which is consistent for all conditions. The peak frequency of the simplified TTB symmetrical manoeuvre is around 0.16 Hz. Figure 15 shows that the phase shift is approximately 110°.

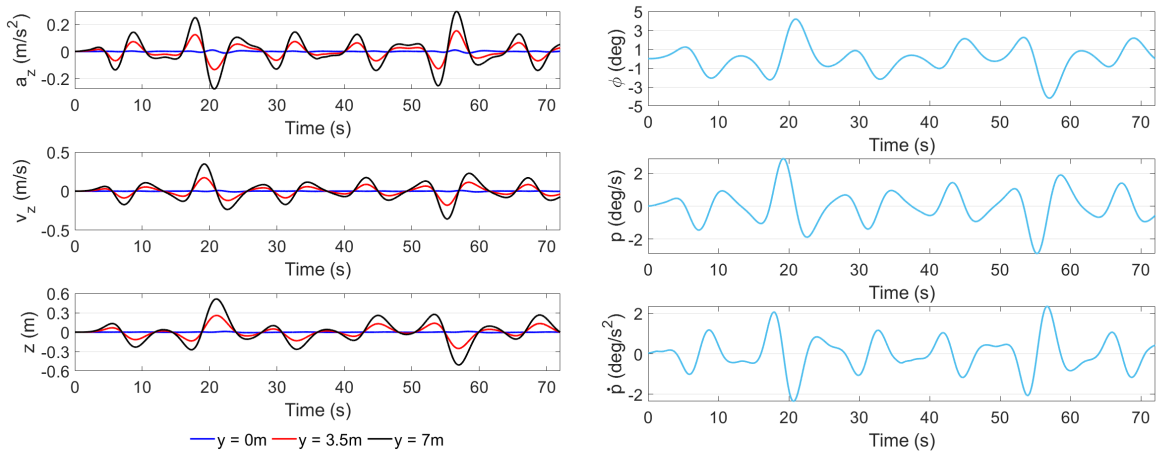

(a) Vertical acceleration, velocity, and displacement of the simulator

(b) Roll angle, rate, and acceleration of the simulator

Fig. 16 Heave and roll motion data of the simulator

Figure 9(a) provided a comparison between the unfiltered and filtered data of the roll motion, and Section II.B.2 provided an explanation for the filtered and unfiltered roll motion. Figures 17(a) and 17(b) show a comparison of the unfiltered and filtered data for the heave motion in both Conditions 2 and 3, respectively. In Condition 3, prior to the motion filtering, the peak a_z was recorded at 0.5 m/s^2, the peak vertical velocity (v_z) reached 1.6 m/s, and the peak vertical displacement (z) measured 3.5 m. Following the motion filtering, heave motion has been reduced to not exceed the simulator capabilities. The peak a_z reduced to 0.3 m/s^2, indicating a decrease in the vertical acceleration. Similarly, the peak v_z decreased to 0.3 m/s, indicating a reduced vertical velocity. Additionally, the peak z decreased to 0.5 m, reflecting a smaller magnitude of vertical displacement, compared to the unfiltered heave motion. Condition 2 has been reduced in the same order, as can be seen in Figure 17(a). Furthermore, Figure 17 also shows the phase shift between the filtered and unfiltered simplified TTB manoeuvre. However, as previously mentioned, this should not introduce any issues, given that no additional stimuli are presented during the experiment.

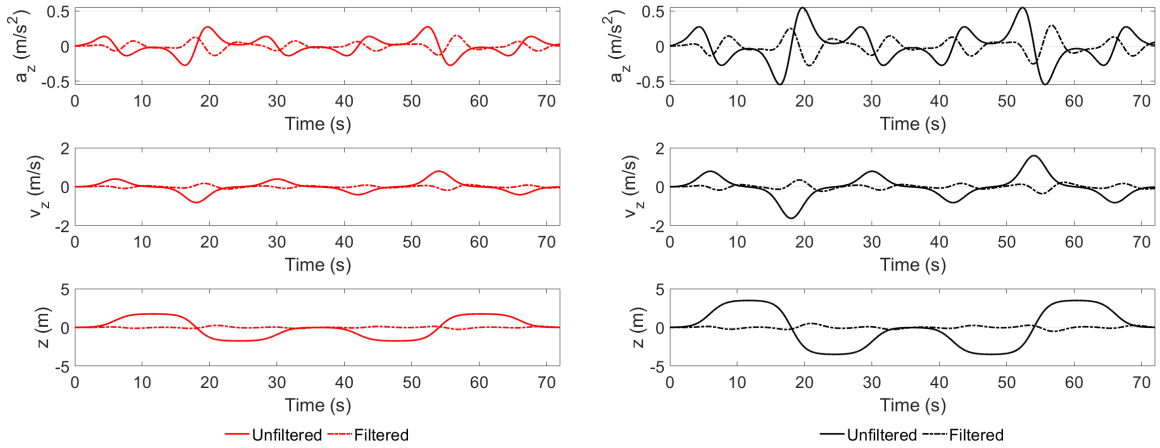

(a) Condition 2 comparison

(b) Condition 3 comparison

Fig. 17 Comparison between the filtered and unfiltered symmetrical TTB manoeuvre data, for Conditions 2 and 3

D. Participants

Eight male and four female participants (μ = 23.8 yr, σ = 1.7 yr) completed the experiment. With the exception of one participant that attends Breda University of Applied Sciences, all participants were TU Delft students. None of the participants had prior knowledge of the study. Their motion sickness susceptibility was assessed using the Motion Sickness Susceptibility Questionnaire (MSSQ), with a median score of 12 (μ = 15.3, σ = 7.6), indicating an average motion sickness susceptibility at the 52nd percentile [27]. None of the participants reported having any vestibular disorders and all reported normal or corrected-to-normal vision. Prior to their participation, written informed consent was obtained from each participant. The protocol and experimental design were approved by the Human Research Ethics Committee at TU Delft.

E. Experiment Procedures

On different days, all participants were put through the experiment's three different conditions, with at least 24 hours in between each session. To reduce the order effect on the dependent measures, participants were counterbalanced in the order of the three conditions. At the beginning of the first session, participants received instructions on how to use the MISC to evaluate their motion sickness (see Table 3). Additionally, participants were informed that if they reported a MISC score of 6, the session would be terminated.

Table 3 MIsery SCale symptoms and ratings [28]

Symptom		**Rating**
No problems		0
Slight discomfort but no specific symptoms		1
Dizziness, warm, headache, stomach awareness, sweating etc.	Vague Some Medium Severe	2 3 4 5
Nausea	Some Medium Severe Retching	6 7 8 9
Vomiting		10

Participants were instructed to maintain a relaxed and upright posture during the experiment while being seated in the right-hand simulator seat. Participants were instructed to maintain a straight back and a relaxed posture while looking straightforward throughout the sessions. Visual cues were not used during the experiment. Participants reported their MISC score every 30 seconds, in response to a 'ping' sound that they heard using the headset they were wearing throughout the duration of the 1-hour exposure to the motion in the SRS. The researcher wrote down their reply. To aid participants in providing accurate scores, an image of the MISC scale was displayed in the simulator, positioned on the left side of the participants' seat, see Figure 14(b). Participants were allowed to freely turn their heads and refer to the scale whenever necessary to accurately assess their level of motion sickness.

F. Dependent Measures

Three subjective measures were collected for each participant in the experiment:

1) Motion Sickness Susceptibility Questionnaire: the participants' susceptibility to motion sickness was assessed prior to the experiment itself, using the MSSQ short version, which compared their individual susceptibility to that of the general population [27];
2) Motion sickness scores: throughout the 1-hour motion exposure, the time-course development of motion sickness was monitored using the participants' MISC ratings. This is consistent to what has been done in Irmak et al [16], [29], and Wijlens et al. [30]. The MISC ratings are taken at 30-second intervals. Mean and maximum MISC scores are used to compare the motion sickness severity in the conditions; and
3) Motion sickness symptoms checklist: at the end of each experiment session, symptoms encountered during the motion exposure were evaluated using a specific motion sickness symptoms checklist that included 24 typically observed symptoms. A 4-point ordinal scale (none, some, medium, and severe) was used to rate the severity of

the symptoms. This symptoms' checklist has been used in Wijlens et al. [30].

G. Hypotheses

Based on the simulations conducted with the 6DOF-SVC model (see Section II.B), two hypotheses were formulated, proposing that:

1) Participants exposed to both roll and heave motion will experience higher levels of motion sickness compared to being exposed to roll motion only, as measured by the MISC scores; and
2) As the lateral distance from the centre of rotation increases, the MISC values reported by participants will exhibit a non-linear increase. Specifically, the MISC values are expected to increase exponentially with the linearly increasing lateral distance.

IV. Results

A. Mean MISC

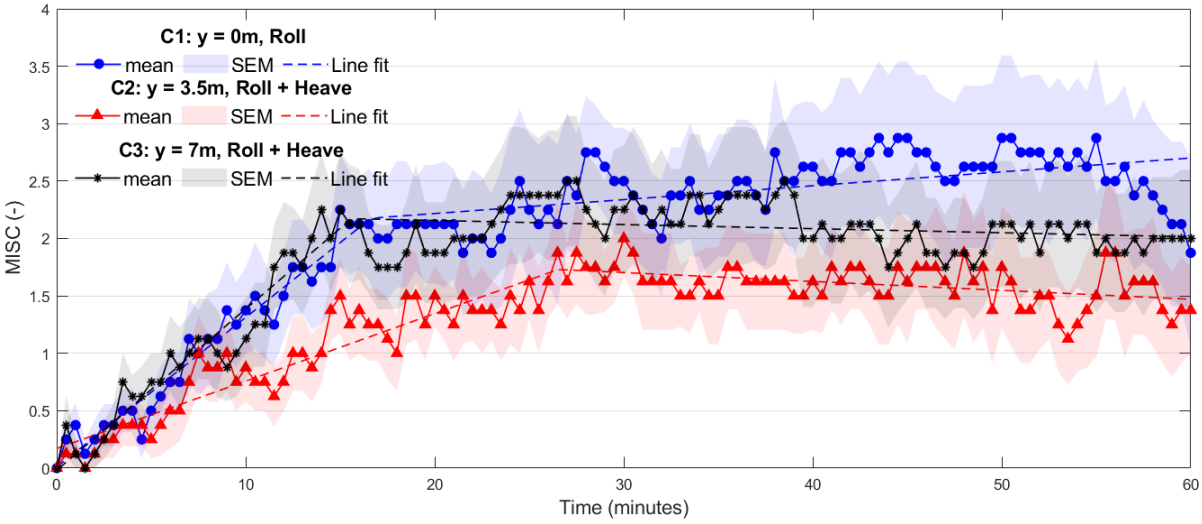

Fig. 18 Average temporal progression of MISC scores across experimental conditions

Figure 18 displays the average time development of MISC scores along with the corresponding Standard Error of the Mean (SEM) in the shaded areas. The first session of Participant 1 was terminated due to technical issues in the SRS, and a replacement was found to maintain 12 participants in the experiment. Participant 2 reported a MISC score of 6 in Condition 1, with 20 minutes to finish the session. Therefore, the session was aborted prematurely and a score of 6 has been assumed for the rest of the session. The padding technique could introduce a potential bias for the average MISC scores in Condition 1 for the last 20 minutes. However, this padding technique has been utilised in previous motion sickness studies such as Webb et al. [31], Griffin et al. [32], and Irmak et al. [29], Turan et al. [14], and Wada [15]. Four participants (Participants 8, 11, 12, and 13) have not shown susceptibility to the motion and their scores have been excluded, their MISC scores were mostly 0 during the sessions (see Appendix VII.B for the individual MISC scores of the participants). Excluding non-susceptible participants can result in a more valid representation of the average motion sickness temporal progresssion. In Figure 18, the trends of the three conditions show an initial increasing pattern, followed by a stabilisation of the MISC scores. To better visualise the point at which the scores begin to stabilise, two lines have been fitted to the data for each of the three conditions. By fitting two lines to the average MISC scores of all conditions, the transition from an increasing phase to a stabilisation phase becomes more apparent, providing insights into the time periods when the motion sickness scores begin to stabilise for each condition. For Conditions 1 and 3, the increase in MISC is similar up to approximately 16 minutes, after which Condition 1 continues to increase but with a reduced steepness, while Condition 3 reaches a point of stability without further changes. In the case of Condition 2, the scores continue to increase until around 26.5 minutes, at which point they start to stabilise. However, the slope for

Condition 2 is lower compared to that of Conditions 1 and 3. This implies that the motion sickness severity in roll motion only of Condition 1 may have an upward trend, but the symptoms do not escalate as rapidly as in the initial increasing phase. While participants in the roll and heave motions of Conditions 2 and 3 have reached a level of motion sickness severity where the symptoms stabilise and no further changes in the MISC scores. The time development of MISC, as observed in the experiment data, exhibits a stabilising phase, which contrasts with the predictions of the 6DOF-SVC model, see Figure 12. The model predicted an exponential increase in motion sickness over time without capturing the stabilising phase that was observed in the experiment. At the end of the motion exposure, the mean MISC scores for Conditions 1, 2, and 3 were 1.8, 2, and 1.3, respectively.

To gain a more comprehensive understanding of the temporal dynamics of motion sickness and the differences between the conditions in the experiment, the increasing and stabilising phases will be analysed separately. As a result, the first 30-minute period will be examined separately from the second 30-minute period. The choice of a 30-minute period is due to the fact that for all conditions, the MISC data no longer shows an increasing trend within this timeframe. This approach allows for a nuanced analysis of both the increasing phase and the subsequent stabilisation phase. By distinguishing these two distinct phases, meaningful conclusions can be drawn regarding the impact of sitting farther away from the centre of rotation on the motion sickness scores of the participants.

B. MISC 0–30 minutes (increasing phase)

To compare the conditions, the maximum MISC was used. The maximum MISC captures the peak intensity of motion sickness experienced by participants.

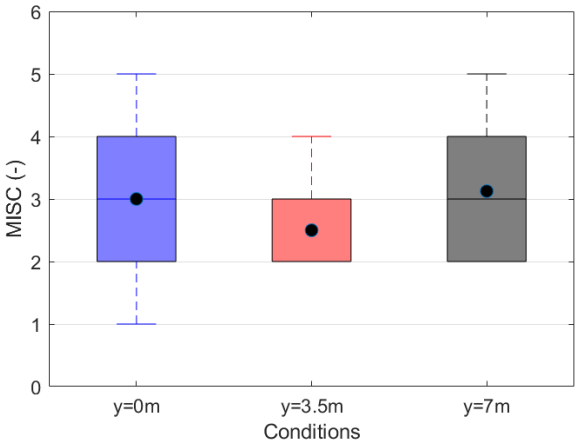

Fig. 19 Maximum MISC scores for the first 30-minute time period

Figure 19 shows the maximum MISC score in the first 30-minute period of the motion for participants, and the dots indicate the mean of the individual participants' maximum MISC scores. A statistical analysis using Friedman's test was performed to examine the maximum MISC scores across the three conditions. The experiment data revealed no statistically significant difference among the maximum MISC scores of the three conditions (p = 0.3035).

The experimental data have yielded results that differ from the predictions made by the 6DOF-SVC model. According to the 6DOF-SVC predictions, Condition 1 was expected to have the lowest motion sickness severity, while motion sickness severity was anticipated to increase exponentially with increasing distance from the centre of rotation, as seen in Figure 11. However, the experimental data shows that the mean of the individual participants' maximum MISC scores in Condition 1 was 3, with only a slight increase to an average of 3.1 in Condition 3. Condition 2 exhibited the lowest mean of the individual participants' maximum MISC scores of 2.5. Although these variations were observed, it is important to note that no statistically significant differences were found among the conditions.

These findings indicate that the experimental data did not align with the expected exponential increase in MSI as the distance from the centre of rotation increased, as was predicted by the 6DOF-SVC model.

C. MISC 30-60 minutes (stabilising phase)

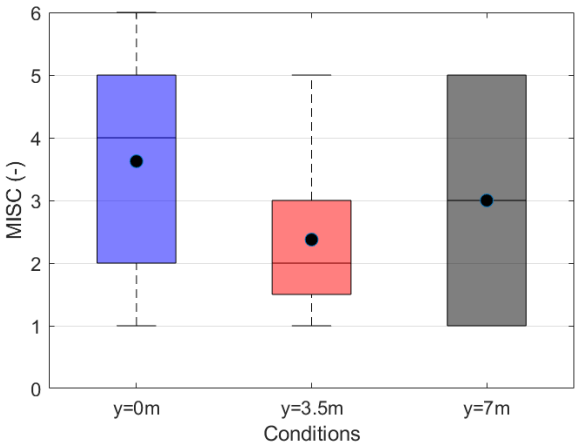

Fig. 20 Maximum MISC scores for the second 30-minute time period

Figure 20 shows the maximum MISC scores by participants in the second 30-minute period and the mean of the individual participants' maximum MISC scores. A Friedman's test was performed on the maximum MISC scores, which showed that there is no statistically significant difference (p = 0.0930). Comparing Figures 19 and 20 shows that the mean of the individual participants' maximum MISC scores for Condition 1 has increased in the second 30-minute period, while Condition 2 and 3 are approximately the same.

Similarly to the increasing phase, the experimental data in the stabilising phase revealed contrasting results compared to the predictions made by the 6DOF-SVC model. Condition 1 exhibited a mean of the individual participants' maximum MISC scores of 3.6. Condition 3 had a mean of the individual participants' maximum MISC scores of 3. Condition 2 displayed the lowest mean of the individual participants' maximum MISC scores of 2.3. These findings suggest that the addition of heave motion to roll motion did not result in an increase in the severity of motion sickness, contrary to the predictions of the 6DOF-SVC model.

D. Comparison between the Model's Output and MISC Data

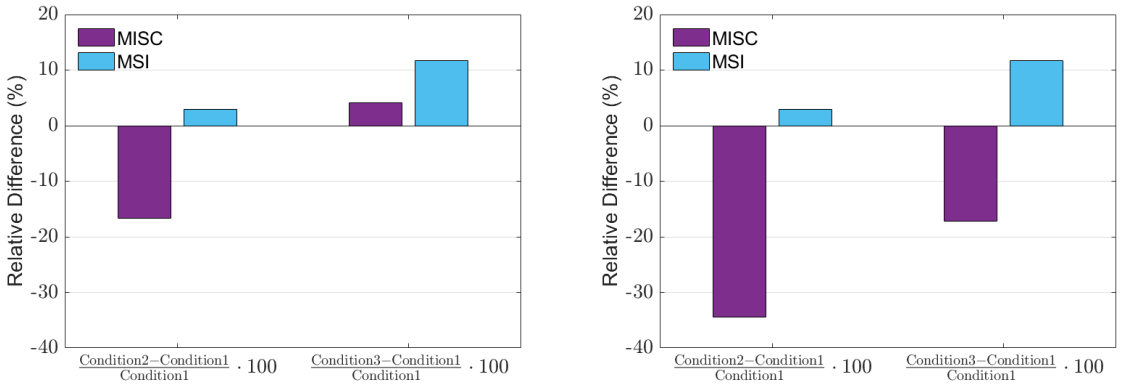

(a) First 30-minute period

(b) Second 30-minute period

Fig. 21 Relative difference in MISC and MISC of Conditions 2 and 3 compared to Condition 1

Figure 21(a) shows a comparison of Conditions 2 and 3 with Condition 1 in terms of the predicted MSI and the mean of the individual participants' maximum MISC scores. For the first 30-minute period, comparing Condition 2 to

Condition 1, the model predicts an increase in MSI for Condition 2 indicated by an approximate 3% increase, while the MISC data demonstrate a contrasting decrease in motion sickness severity of approximately 16.5% in Condition 2. Similarly, when comparing Condition 3 to Condition 1, the model predicted an estimated 11.5% increase in MSI for Condition 3, while the MISC data showed a relatively smaller increase of approximately 4% for Condition 3. Comparing Condition 3 to Condition 1 in the second 30-minute period (see Figure 21(b)), the MISC scores showed a decrease in motion sickness severity for Condition 3 compared to Condition 1 of approximately 17%. Additionally, the increase in maximum MISC scores in Condition 1 compared to Condition 2 becomes more pronounced during this phase, which means that there is greater discomfort in the roll motion only of Condition 1 compared to the combination of roll and heave motion in Condition 2.

The comparison between the predicted MSI of the 6DOF-SVC model and the experiment's MISC scores is challenging due to differences in the data type and the inability to directly compare their magnitudes. However, despite this limitation, the comparison aims to assess whether the MISC scores followed the same trend of increasing motion sickness severity exponentially with distance as the predicted MSI. The experimental results did not support the prediction that the addition of the heave motion due to being seated laterally farther away from the centre of rotation to the roll motions would increase motion sickness severity, see Figure 18.

E. Motion Sickness Symptoms

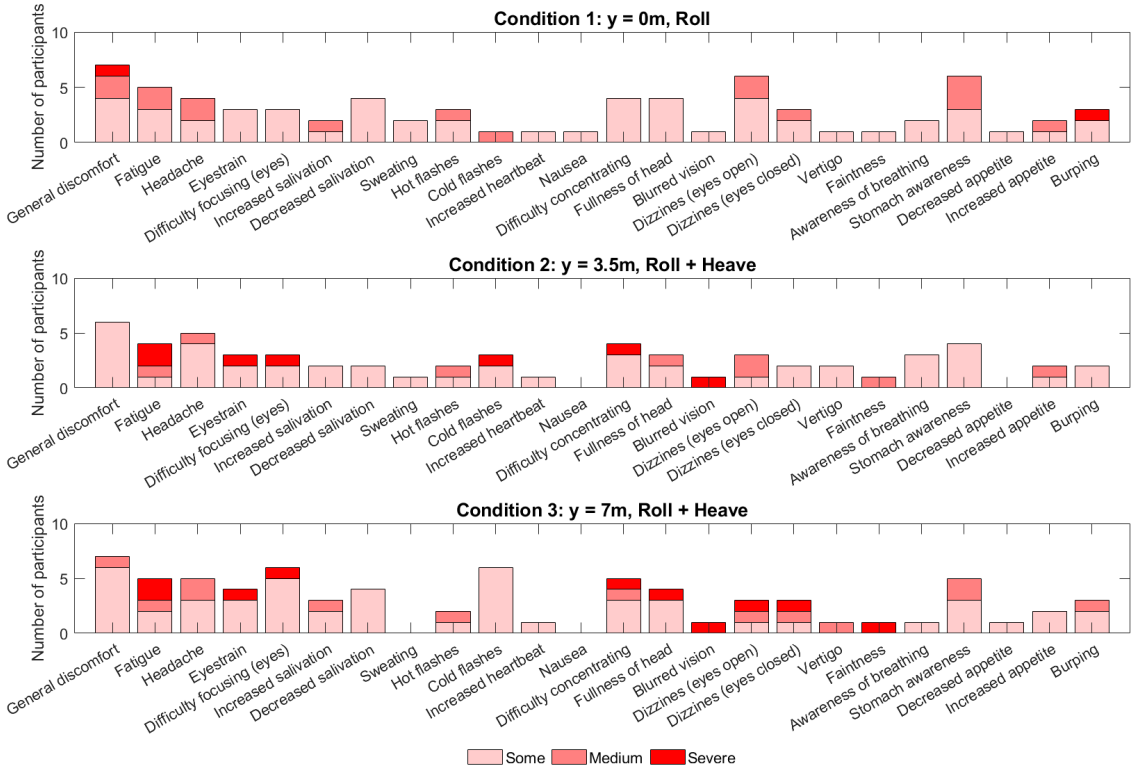

Fig. 22 Common motion sickness symptoms occurring throughout the three conditions

Figure 22 presents the occurrence of common motion sickness symptoms across all conditions. This analysis focused only on participants who reported experiencing specific symptoms to some extent. Therefore, participants who had chosen "none" for a specific symptom in the checklist are not shown in this figure, only for this specific symptom. Moreover, it also excluded the four participants (Participants 8, 11, 12, and 13) who did not show susceptibility to motion sickness in their MISC scores. In Condition 1, a higher or equal number of participants reported the presence of 7 symptoms with higher severity, compared to Conditions 2 and 3. These symptoms include general discomfort, sweating, hot flashes, nausea, fullness of head, dizziness (eyes open), and stomach awareness. Similarly, in Condition 3,

a higher or equal number of participants reported the presence of 6 symptoms with higher severity. These symptoms include fatigue, eyestrain, difficulty focusing, increased salivation, cold flashes, and difficulty concentrating. For the remaining 11 symptoms, the number of participants experiencing them was either equal across conditions or Condition 2 recorded a higher number of participants. These findings align with the MISC data obtained from the experiment, which indicated that Condition 2 resulted in the least motion sickness, while Conditions 1 and 3 showed similar levels of motion sickness.

F. Sessions Order Effect

This analysis aimed to assess whether the collected data from participants had been influenced by habituation or order effect, and to determine if there is any decrease in motion sickness severity due to habituation and adaptation over successive exposures to motion stimuli. To investigate the presence of habituation or adaptation effects throughout the experiment, the mean MISC scores were calculated across all three sessions, irrespective of the conditions. Examining these factors ensures that the experimental results remain unbiased and allow for an accurate interpretation of the findings.

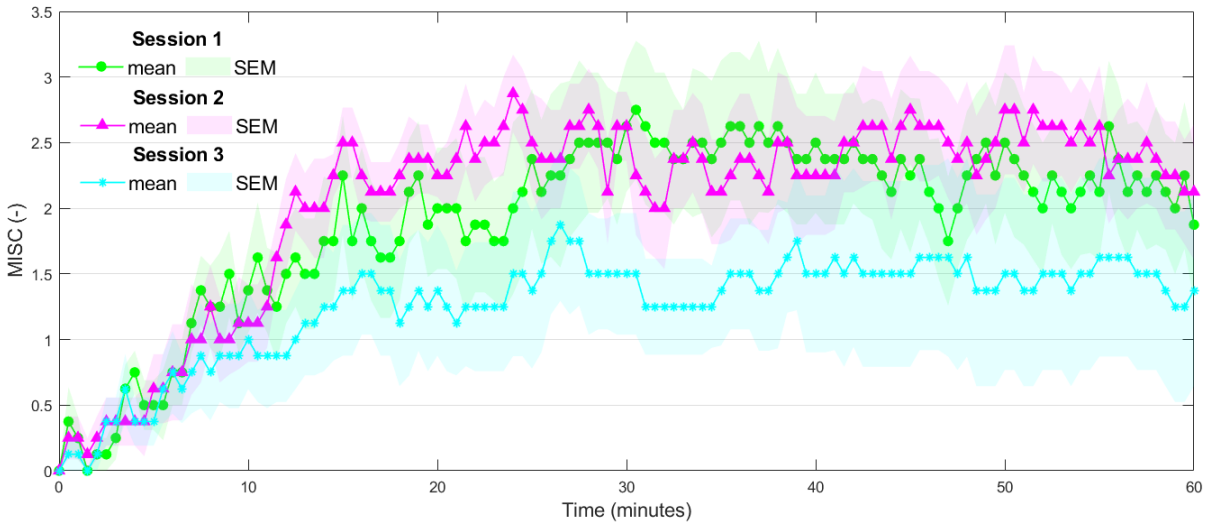

Fig. 23 Average temporal progression of MISC scores across experimental sessions

Figure 23 displays the mean MISC scores across the sessions and its SEM; namely, averaged across the different conditions. Sessions 1 and 2 exhibit similar scores, with Session 1 showing a maximum mean MISC score of 2.75 and Session 2 with a maximum of 2.87. In Session 3, lower scores are recorded compared to Sessions 1 and 2, with a maximum mean MISC score of 1.87. Moreover, the scores stabilise earlier in Session 3 compared to the previous sessions. Since Sessions 1 and 2 demonstrated similar scores, with Session 2 occasionally even showing higher scores, it can be considered that factors other than habituation may have influenced the decreased motion sickness severity in Session 3. Moreover, due to the exclusion of four participants who did not show susceptibility to motion sickness, the experimental design became unbalanced. Table 4 shows the order of the conditions that have been performed by the participants, excluding the participants who have not shown susceptibility to motion sickness. It can be seen that in Session 3, Condition 2 was performed more than Conditions 1 and 3. Due to the unbalanced experiment design after excluding 4 participants, it is difficult to draw definite conclusions about habituation.

Table 4 Experiment's conditions order for participants

Participant no.	Session 1	Session 2	Session 3
Participant 2	Condition 2	Condition 3	Condition 1
Participant 3	Condition 3	Condition 1	Condition 2
Participant 4	Condition 1	Condition 3	Condition 2
Participant 5	Condition 2	Condition 1	Condition 3
Participant 6	Condition 3	Condition 2	Condition 1
Participant 7	Condition 1	Condition 2	Condition 3
Participant 9	Condition 3	Condition 1	Condition 2
Participant 10	Condition 1	Condition 3	Condition 2

V. Discussion

A. Hypotheses

The MISC data have shown two phases: an increasing phase and stabilising phase. In the increasing phase, Condition 3 had a slightly higher mean of the individual participants' maximum MISC scores compared to Condition 1 (3.1 vs. 3), while Condition 2 had a lower average mean of the individual participants' maximum MISC scores compared to Condition 1 (2.5 vs. 3). While the stabilising phase showed that Condition 3 had a lower mean of the individual participants' maximum MISC scores compared to Condition 1 (3 vs. 3.6), Condition 2 still exhibited a lower mean of the individual participants' maximum MISC scores compared to Condition 1 (2.3 vs. 3.6). Therefore, the MISC data did not provide sufficient evidence to support Hypothesis 1, which suggested that participants exposed to both roll and heave motion would experience a higher level of motion sickness compared to roll motion only. No statistically significant differences were found among the conditions. The data suggest that the addition of heave motion to the roll motion has not increased the motion sickness severity, compared to the roll motion only. Thus, Hypothesis 1 is inconclusive. Given the lack of statistically significant differences between the conditions, it can be concluded that the MISC scores do not exhibit an exponential increase with lateral distance, making Hypothesis 2 rejected, which suggested that the MISC values are expected to increase exponentially with increasing lateral distance from the centre of rotation. Additionally, the severity of motion sickness symptoms does not show a consistently increasing pattern in relation to the lateral distance from the centre of rotation. Conditions 1 and 3 exhibit an equal number of symptoms displaying the highest occurrences, while the remaining symptoms show equal occurrences across conditions or are more pronounced in Condition 2, indicating no clear relationship between symptoms severity and the distance from the centre of rotation. The relatively small differences in motion sickness observed between the conditions can be attributed to the space limitations of the SRS. The differences in the motion between the conditions were small because of the small motion space that the SRS has, compared to what is expected to have in the Flying-V. It is anticipated that in the real Flying-V, the differences in motion sickness severity between the conditions would likely be greater due to the bigger magnitude of the heave motion experienced by passengers sitting laterally offset from the centre of rotation.

B. Individual Differences

In this experiment, a notable difference was observed among the participants regarding their susceptibility to motion sickness. Out of the 12 participants, 4 did not exhibit susceptibility to motion sickness based on their responses to the stimuli. Their MISC scores remained consistently low (0 or 1) throughout the conditions. Interestingly, this contrasted with the MSSQ scores collected prior to the experiment, which indicated an average or higher susceptibility to motion sickness compared to the general population. This discrepancy can be attributed to the possibility that these participants may have overestimated their susceptibility to motion sickness when initially selected to participate in the experiment, in order to join the experiment. Alternatively, it is also plausible that these participants are simply not susceptible to the specific vertical motion experienced in the experiment. This has been observed in the study of Wertheim et al. [19], which involved heave motion. In Wertheim et al. study, out of 22 participants, only one exceeded a MISC score of 2, while the remaining participants recorded MISC scores below 2. Additionally, in the current research among the participants who did show susceptibility to motion sickness, there were variations in the time course development of motion sickness. Some participants exhibited a continuous change in their MISC scores over time, while others reached a plateau and maintained relatively stable scores. When comparing the individual responses observed in this experiment

to the findings of Irmak et al. [29] on motion sickness in a car slalom manoeuvre with external and internal vision, notable differences can be observed. In the study by Irmak et al., a considerable number of participants reached a MISC score of 7 within 30 minutes, which contrasts with the findings of this experiment. Similarly, another study by Irmak et al. [16] focusing on amplitude dynamics of motion sickness also demonstrated a trend of increasing MISC scores until reaching a score of 7. However, this experiment investigating the effects of vertical motion in the Flying-V with a peak frequency of around 0.16 Hz revealed distinct effects on individuals where the motion sickness development stabilised after 30 minutes, and with larger variability in MISC scores among participants compared to previous experiments, which can be attributed to the fact that Irmak et al. have different motion direction than the one used in the current research and slightly different peak frequency of 0.2 Hz.

C. Model and Experiment Results

To evaluate the accuracy of the 6DOF-SVC model, a comparison was made between the predicted MSI and the observed MISC scores obtained from the experiment. However, it is important to note that this comparison should be interpreted cautiously since MISC scores are ordinal data and MSI is ratio data, which are completely different. A comparison can be made between the trend predicted by the 6DOF-SVC model when sitting laterally farther away from the centre of rotation and the trend observed in the MISC data. Based on the model, Condition 1 was expected to have the lowest motion sickness severity among the conditions and there would be an exponential increase in the motion sickness severity the farther laterally the seats are from the centre of rotation, but this was not observed in the MISC scores. The MISC data indicated that the addition of heave motion to the roll motion did not result in an increase in the severity of motion sickness for passengers positioned laterally farther away from the centre of rotation.

The MISC data revealed distinct increasing and stabilising phases of motion sickness, but the stabilising phase was not captured by the 6DOF-SVC model, which predicts an exponential increase of the MSI with time. Consequently, further modifications to the accumulation model that calculates the MSI are required to enhance the model's ability to accurately predict these temporal dynamics of motion sickness. It is recommended to fit the development of motion sickness using Oman's model [6], because it is a model that can capture the individual motion sickness responses and how motion sickness develops over time. Previous studies, such as the one conducted by Irmak et al. [16], have successfully captured the motion sickness development of participants by using the original Oman's model and doing modifications of it. The results were promising and demonstrated the ability to predict MISC scores using fore-aft motion experiments. However, it remains unknown whether this approach can be applied to other directions, such as the vertical direction in the Flying-V. Further research is needed to determine the applicability and predictive capabilities of Oman's model for different motion directions in the context of the Flying-V. Moreover, Irmak [12] noted that the 6DOF-SVC model performs less accurately when it comes to rotational acceleration motion. This limitation stems from the fact that the model is a partial observer, in that it observes head angular velocity but lacks observation of acceleration and gravity [12]. The specific force is first low-pass and then high-pass filtered, and that has the most pronounced influence on the model's output, and the resulting tracking error directly leads to the conflict terms [12]. This mechanism is deviating from the general observer framework explained by Oman [33].

Moreover, the 6DOF-SVC model that was used does not include the visual system (i.e. eyes closed). However, the participants in the experiment were instructed to keep their eyes open, even though no visual stimuli were presented. Consequently, they received conflicting and non-moving visual cues. This discrepancy may also contribute to the difference observed between the output of the 6DOF-SVC model and the experimental data. Despite the existence of extensions to the 6DOF-SVC models that incorporate angular velocity visualisation, as demonstrated by Wada et al. [34], or include visual vertical aspects, as presented by Liu et al. [35], these models lack validation and verification using large datasets. Additionally, they do not include the entirety of the visual system. Consequently, applying these models raises uncertainty regarding the reliability of their outcomes.

D. Results' Relevance and Recommendation

The MISC scores across the three sessions (see Figure 23) demonstrated that the scores in the third session are lower compared to Sessions 1 and 2. This trend is also observed in the symptoms' severity checklist over sessions (see Appendix VII.C), where Session 3 indicates a lower number of participants experiencing symptoms or experiencing them with reduced severity. One possible explanation for this is the unbalanced design of the experiment, after excluding the data from the 4 participants who did not show susceptibility to motion sickness. In Session 3, there was a higher number of participants who performed Condition 2 compared to Conditions 1 and 3. It is unknown if Session 3 showed lower scores compared to Sessions 1 and 3 because Condition 2 is the least provocative due to its motion, or because

Session 3 exhibited the lowest scores due to habituation and that participants had habituated to similar movement. To effectively confirm habituation, a balanced design with equal participant allocation to each condition is preferable.

To gain insights into the effects of different types of motion on motion sickness severity, the results of this experiment were compared to the findings of Irmak et al. [16], who conducted a study involving fore-aft motion with different acceleration amplitudes. As mentioned before, an observation from Irmak et al.'s experiment is that the motion sickness scores continued to increase until participants reached a MISC score of 7. In contrast, the current experiment demonstrated a different pattern, with participants' scores stabilising after approximately 26 minutes of exposure in Condition 2 and after approximately 16 minutes for Conditions 1 and 3. Furthermore, only one participant recorded a score of 6 in one of the sessions. The mean MISC scores in this experiment were observed to be lower compared to Irmak et al.'s study. Specifically, Irmak et al. reported mean MISC scores between 4 and 6 for the different conditions, while this experiment yielded mean MISC scores of 2, 1.8, and 1.3. These findings indicate that fore-aft motion, as investigated by Irmak et al., is at least twice as sickening compared to vertical acceleration motion in this experiment. One possible explanation for this discrepancy is the increased demand for postural control in horizontal motion [36]. Additionally, Golding et al. suggested that the motion along the X head-body axis may be more provocative in inducing motion sickness compared to motion along the Z-axis [37]. In the context of the Flying-V, in which passengers predominantly experience vertical motion due to its design, this finding implies that the Flying-V's vertical motion may be less provocative in inducing motion sickness, compared to the fore-aft motion that have been used in Irmak et al. as an example.

In this experiment, it was observed that the combination of translational (vertical) and rotational (roll) motion in Conditions 2 and 3 did not result in an increased level of motion sickness compared to the rotational (roll) motion only in Condition 1. This finding aligns with the study conducted by Beard et al. [17], where they investigated the combination of translational (lateral) and rotational (roll) motion. Beard et al. found that participants experienced less discomfort when exposed to the combined motion compared to cases involving either the lateral component or the roll component of the motion, specifically within the frequency range of 0.2 to 0.5 Hz. The discomfort levels increased as the frequency of the motion increased from 0.2 to 0.5 Hz, which is slightly higher than the peak frequency of 0.16 Hz of this experiment. These findings highlight the complex relationship between different types of motion and their impact on motion sickness. The specific combination of translational and rotational motion, as well as the frequency at which the motion occurs, can influence the level of discomfort experienced by individuals. The current experiment provides further support for the notion that the combination of translational and rotational motion does not necessarily amplify motion sickness symptoms compared to motion involving only one of these components. The particular combination of the acceleration and frequency content of the two stimuli determines the level of provocation associated with the combination of rotational and translational oscillations [4].

Although the experiment did not demonstrate an increase in the severity of motion sickness as participants moved farther away in the lateral direction from the centre of rotation, it remains inconclusive if this would hold true in a real-world scenario. Figures 9(a) and 17 show that the magnitudes of heave and roll motion were reduced to ensure feasibility within the simulator. Additionally, the experiment did not explore the effects of sitting at even greater distances from the centre of rotation as the maximum distance that had been tested was y = 7 m; and the most outboard seat in the Flying-V is planned to be around y = 13 m, which would result in higher magnitudes of heave motion due to sitting laterally farther away from the centre of rotation. Joseph et al. [18] found that the combination of translational and rotational oscillation led to a higher rate of motion sickness during periods of high-magnitude motion, in contrast to low-magnitude motion. This indicates that as the magnitude of motion increases, the probability of experiencing a higher severity of motion sickness also increases. Therefore, it is important to consider that the findings of the current experiment may not fully reflect the potential motion sickness effects associated with sitting at farther distances from the centre of rotation in real-world scenarios. To better understand the relationship between motion sickness severity and sitting laterally offset from the centre of rotation, larger simulators or real aircraft can be utilised. These larger platforms would allow for the incorporation of increased magnitudes of heave motion and seating positions farther away from the centre of rotation. By expanding the experimental setup in this manner, it would be possible to capture a wider range of motion conditions and investigate the impact on motion sickness severity more comprehensively.

Furthermore, it is important to consider that in the conducted experiment, the roll and vertical motion were isolated from other flight parameters typically experienced by passengers during a flight in the Flying-V, such as aerodynamics, pitch and yaw. In an actual aircraft, passengers would likely be exposed to a combination of these flight parameters simultaneously. The combination of multiple motion cues could potentially amplify the motion sickness experienced by passengers, compared to the findings of this experiment. A study conducted by Wertheim et al. [19] found that when heave motion was presented in isolation, it had minimal motion sickness-inducing potential. Similarly, pitch and roll

motions, whether used alone or in combination, had a small potential to induce motion sickness. However, when the heave, pitch, and roll motions were combined, nearly 50% of the participants experienced high levels of motion sickness. These findings suggest that the combination of multiple flight parameters, including roll, vertical, pitch, and yaw, may have an effect on the severity of motion sickness. Therefore, it is plausible that in a real-world scenario where passengers are exposed to the full range of flight parameters in the Flying-V, the motion sickness experienced by individuals sitting laterally farther away from the centre of rotation could be more pronounced than what was observed in this isolated experimental setting.

The seat configuration that has been used in the analysis and the experiment is the 26° rotated seat configuration that is aligned with the centre line of the Flying-V. Another seating configuration that can be used in the Flying-V is the 0° seat configuration, which is aligned with the longitudinal axis of the fuselage. However, there would be difficulty using this seating configuration because the Federal Aviation Administration regulations state that it would offer an adequate level of safety and additional safety requirements are required [20]. The impact of using this seating configuration on motion comfort in the Flying-V remains unknown. Therefore, it is recommended to conduct further research experiments to compare the comfort experienced by passengers using the 0° rotated seat configuration with that of the 26° rotated seat configuration, as these two seating configurations represent the extreme cases of seating configuration in the Flying-V. By studying the motion comfort using these extreme seating positions, there would be an understanding of the boundaries within which seating arrangements should be adjusted to ensure a comfortable experience in the Flying-V.

Further research considering the combined effects of various flight parameters on motion sickness is warranted to provide a more comprehensive understanding of passenger comfort in aircraft configurations like the Flying-V. Moreover, incorporating a wider range of seating positions and magnitudes of motion in the simulator would provide a more understanding of the relationship between seating position and motion sickness in such contexts. Developing an accurate motion sickness model can greatly contribute to the optimisation of its design. This model would enable to optimise seating arrangements and minimise motion sickness experienced by passengers. By enhancing the motion comfort in the Flying-V, it would provide a competitive advantage over other aircraft models, in addition to its superior aerodynamic performance. Such advancements in design and passenger comfort would further establish the Flying-V as a desirable choice in the aviation industry.

VI. Conclusion

This study aimed to investigate to what extent sitting laterally farther away from the centre of rotation would increase the severity of motion sickness in the Flying-V. The manoeuvre that was conducted in this research was the TTB manoeuvre. A passenger-in-the-simulator experiment was conducted, where participants experienced three different conditions: Condition 1 was sitting at the centre of rotation, which involved only roll motion, while Condition 2 was sitting laterally offset from the centre of rotation by 3.5 m and Condition 3 was sitting laterally offset from the centre of rotation by 7 m. Conditions 2 and 3 included a combination of heave and roll motion. As opposed to the 6DOF-SVC model predictions, the MISC data collected during the experiment revealed two distinct phases: an increasing and stabilising phase, under a continuous motion stimulus. During the increasing phase, the mean of the individual participants' maximum MISC scores for Condition 1 was 3, for Condition 2 it was 2.5, and for Condition 3 it was 3.1. In the stabilising phase, the mean of the individual participants' maximum MISC scores for Condition 1 was 3.6, for Condition 2 it was 2.3, and for Condition 3 it was 3. Therefore, the addition of the heave motion along with the roll motion did not lead to an increase in the severity of motion sickness. No statistically significant difference was observed among the three conditions. The experimental findings did not align with the predictions made by the 6DOF-SVC model, which predicted a higher severity of motion sickness with the addition of heave motion.

This research has focused on investigating motion comfort in the Flying-V in the TTB manoeuvre. While the experimental data shows promising results for the motion comfort of the future passengers of the Flying-V, further analysis and experiments to incorporate a larger range of motion magnitudes and combinations of different flight parameters are necessary to gain a comprehensive understanding of the topic. This will optimise the design to improve the passengers' comfort in the Flying-V, and will contribute to the realisation of a more comfortable and passenger-friendly aircraft.

VII. Appendix

A. MSI data

Table 5 shows the MSI values using the symmetrical TTB manoeuvre that is based on the simulator flight data, in different locations in the Flying-V and repeated for 1-hour.

Table 5 MSI using the flight data

		MSI (%)
CG	**-**	3.88
x **= 17m**	**In-board** (y **= 0m)**	3.61
	Middle (y **= 2.5m)**	3.64
	Out-board (y **= 5m)**	3.69
x **= 11m**	**In-board** (y **= 0.5m)**	3.70
	Middle (y **= 3m)**	3.76
	Out-board (y **= 6m)**	3.89
x **= 9m**	**In-board** (y **= 1m)**	3.73
	Middle (y **= 4m)**	3.82
	Out-board (y **= 7m)**	3.95
x **= 7m**	**In-board** (y **= 2m)**	3.78
	Middle (y **= 5m)**	3.87
	Out-board (y **= 8m)**	4.03
x **= 5m**	**In-board** (y **= 3m)**	3.84
	Middle (y **= 6m)**	3.94
	Out-board (y **= 9m)**	4.10
x **= 3m**	**In-board** (y **= 4m)**	3.90
	Middle (y **= 7m)**	4.02
	Out-board (y **= 10m)**	4.20
x **= 1m**	**In-board** (y **= 5m)**	3.98
	Middle (y **= 8m)**	4.11
	Out-board (y **= 11m)**	4.30
x **= 0m**	**In-board** (y**= 6m)**	4.02
	Middle (y **= 9m)**	4.16
	Out-board (y **= 12m)**	4.36
x **= -1m**	**In-board** (y **= 7m)**	4.06
	Middle (y **= 10m)**	4.28
	Out-board (y **= 13m)**	4.42

B. Individual MISC scores

Figure 24 shows the individual MISC scores with different conditions order, for all participants. The dots in the figures indicate the maximum MISC score in the first and second 30 minutes.

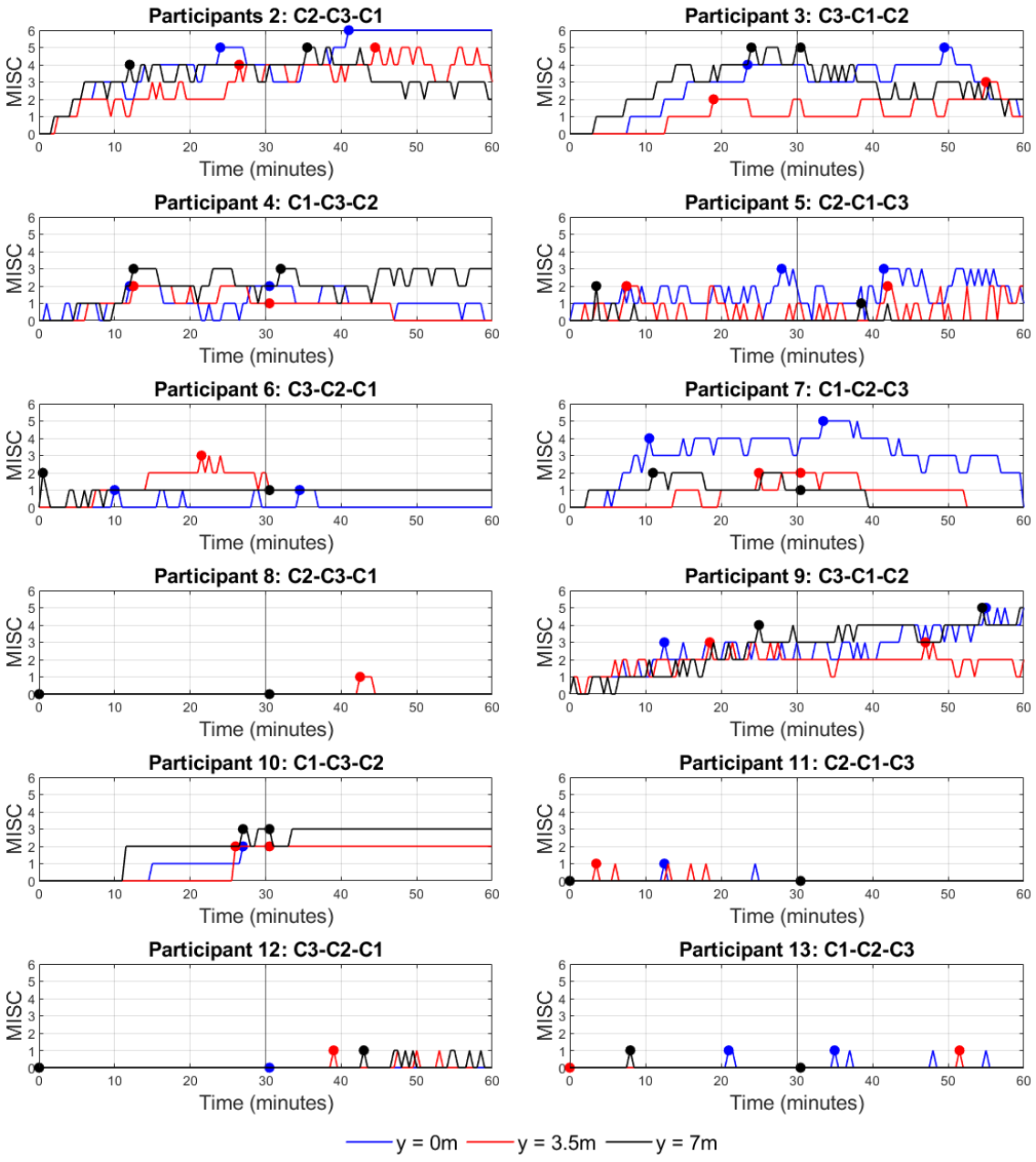

Fig. 24 Individual MISC scores for all 12 participants

C. Symptoms severity across sessions

Figure 25 presents the occurrence of common motion sickness symptoms across all sessions.

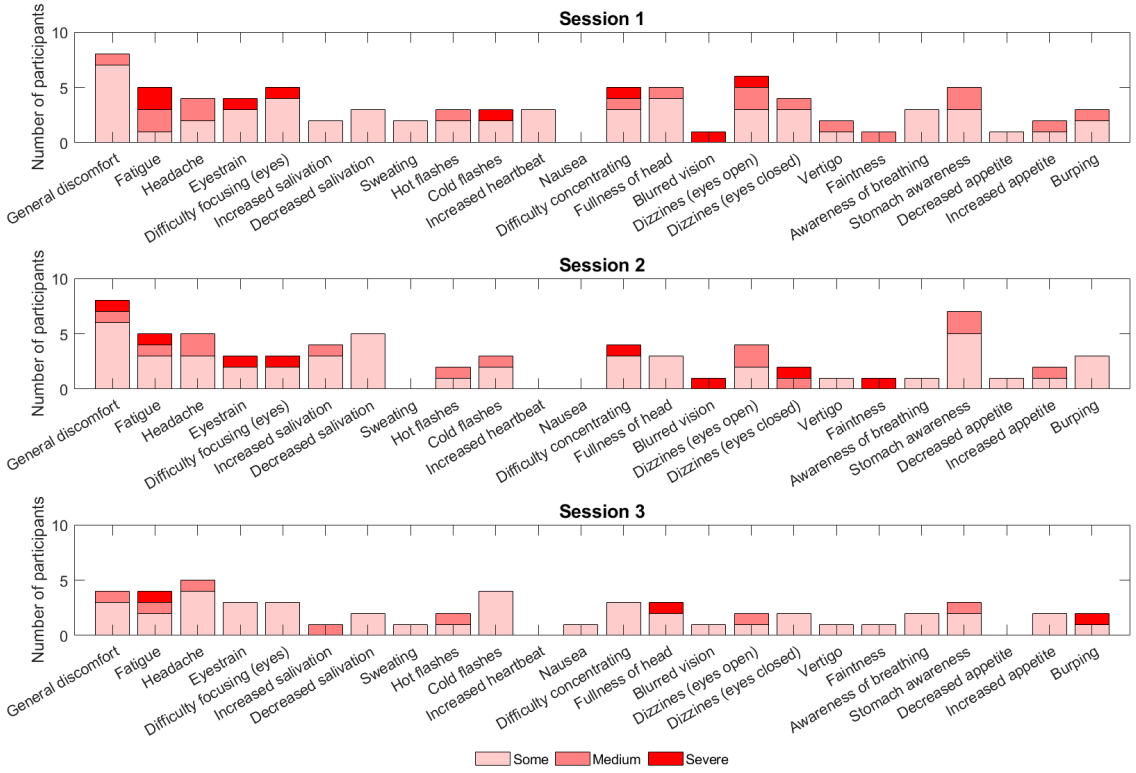

Fig. 25 Common motion sickness symptoms occurring throughout the three sessions

References

[1] Benad, J., "The Flying V - A New Aircraft Configuration for Commercial Passenger Transport," *Deutscher Luft- und Raumfahrtkongress*, 2015, pp. 1–8. https://doi.org/10.25967/370094.

[2] Faggiano, F., Vos, R., Baan, M., and Dijk, R., "Aerodynamic Design of a Flying V Aircraft," *17th AIAA Aviation Technology, Integration, and Operations Conference*, 2017. https://doi.org/10.2514/6.2017-3589.

[3] Bos, J. E., MacKinnon, S. N., and Patterson, A., "Motion sickness symptoms in a ship motion simulator: Effects of inside, outside, and no view," *Aviation, Space, and Environmental Medicine*, Vol. 76, No. 12, 2005, pp. 1111–1118.

[4] Bertolini, G., and Straumann, D., "Moving in a Moving World: A Review on Vestibular Motion Sickness," *Frontiers in Neurology*, Vol. 7, 2016. https://doi.org/10.3389/fneur.2016.00014.

[5] Reason, J. T., and Brand, J. J., *Motion sickness*, Academic Press London ; New York, 1975.

[6] Oman, C. M., "Motion Sickness: a Synthesis and Evaluation of the Sensory Conflict Theory," *Canadian Journal of Physiology and Pharmacology*, Vol. 68, No. 2, 1990, pp. 294–303. https://doi.org/10.1139/y90-044.

[7] Lawther, A., and Griffin, M. J., "Prediction of the Incidence of Motion Sickness from the Magnitude, Frequency, and Duration of Vertical Oscillation," *The Journal of the Acoustical Society of America*, Vol. 82, No. 3, 1987, pp. 957–966. https://doi.org/10.1121/1.395295.

[8] Kamiji, N., Kurata, Y., Wada, T., and Doi, S., "Modeling and Validation of Carsickness Mechanism," *SICE Annual Conference*, 2007, pp. 1138–1143. https://doi.org/10.1109/SICE.2007.4421156.

[9] Newman, M., *A Multisensory Observer Model for Human Spatial Orientation Perception*, MSc. thesis, Massachusetts Institute Of Technology, 2009. URL https://core.ac.uk/download/pdf/4416187.pdf.

[10] Braccesi, C., and Cianetti, F., "Motion sickness. Part I: Development of a Model for Predicting Motion Sickness Incidence," *International Journal of Human Factors Modelling and Simulation*, Vol. 2, No. 3, 2011, pp. 163–187. https://doi.org/10.1504/IJHFMS.2011.044492.

[11] Laurens, J., and Droulez, J., *Probabilistic Reasoning and Decision Making in Sensory-Motor Systems*, 1st ed., Springer Berlin, Heidelberg, 2008. https://doi.org/10.1007/978-3-540-79007-5.

[12] Irmak, T., Pool, D. M., de Winkel, K. N., and Happee, R., "Validating Models of Sensory Conflict and Perception for Motion Sickness Prediction," *Biological Cybernetics*, Vol. 117, 2023, p. 185–209. https://doi.org/10.1007/s00422-023-00959-8.

[13] Wada, T., Kamiji, N., and Doi, S., "A Mathematical Model of Motion Sickness in 6DOF Motion and Its Application to Vehicle Passengers," 2013.

[14] Turan, O., Verveniotis, C., and Khalid, H., "Motion Sickness IOnboard Ships: Subjective Vertical Theory and Its Application to Full-Scale Trials," *Journal of Marine Science and Technology*, Vol. 14, 2009, pp. 409–416. https://doi.org/10.1007/s00773-009-0064-3.

[15] Wada, T., "Computational Model of Motion Sickness Describing the Effects of Learning Exogenous Motion Dynamics," *Frontiers in Systems Neuroscience*, Vol. 15, 2021. https://doi.org/10.3389/fnsys.2021.634604.

[16] Irmak, T., Kotian, V., Happee, R., de Winkel, K. N., and Pool, D. M., "Amplitude and Temporal Dynamics of Motion Sickness," *Frontiers in Systems Neuroscience*, Vol. 16, 2022. https://doi.org/10.3389/fnsys.2022.866503.

[17] Beard, G. F., and Griffin, M. J., "Discomfort Caused by Low-Frequency Lateral Oscillation, Roll Oscillation and Roll-Compensated Lateral Oscillation," *Ergonomics*, Vol. 56, 2013, pp. 103 – 114. https://doi.org/10.1080/00140139.2012.729613.

[18] Joseph, J., and Griffin, M. J., "Motion Sickness from Combined Lateral and Roll Oscillation: Effect of Varying Phase Relationships," *Aviation, Space, and Environmental Medicine*, Vol. 78, 2007, pp. 944–950. https://doi.org/10.3357/ASEM.2043.2007.

[19] Wertheim, A. H., Bos, J. E., and Bles, W., "Contributions of Roll and Pitch to Sea Sickness," *Brain Research Bulletin*, Vol. 47, No. 5, 1998, pp. 517–524. https://doi.org/https://doi.org/10.1016/S0361-9230(98)00098-7.

[20] Liu, Z., Rotte, T., Anjani, S., and Vink, P., "Seat Pitch and Comfort of a Staggered Seat Configuration," *Work*, Vol. 68, 2021, pp. 151–159. https://doi.org/10.3233/WOR-208014.

[21] Joosten, S. K. B., Stroosma, O., Vos, R., and Mulder, M., "Simulator Assessment of the Lateral-Directional Handling Qualities of the Flying-V," *AIAA SciTech Forum 2023*, 2023. https://doi.org/10.2514/6.2023-0906.

[22] Oosterom, W., and Vos, R., "Conceptual Design of a Flying-V Aircraft Family," *AIAA AVIATION 2022 Forum*, 2022. https://doi.org/10.2514/6.2022-3200.

[23] Laban, M., and Mulder, J., "On-Line Identification of Aircraft Aerodynamic Model Parameters," *IFAC Proceedings Volumes*, Vol. 25, No. 15, 1992, pp. 199–204. https://doi.org/https://doi.org/10.1016/S1474-6670(17)50633-3.

[24] Berkouwer, W., Stroosma, O., van Paassen, R., Mulder, M., and Mulder, J. A., "Measuring the Performance of the SIMONA Research Simulator's Motion System," *AIAA Modeling and Simulation Technologies Conference and Exhibit*, 2005. https://doi.org/10.2514/6.2005-6504.

[25] Stroosma, O., van Paassen, M., and Mulder, M., "Using the SIMONA Research Simulator for Human-machine Interaction Research," *AIAA Modeling and Simulation Technologies Conference and Exhibit*, 2003. https://doi.org/10.2514/6.2003-5525.

[26] Gouverneur, B., Mulder, J., van Paassen, M., Stroosma, O., and Field, E., "Optimisation of the SIMONA Research Simulator's Motion Filter Settings for Handling Qualities Experiments," *AIAA Modeling and Simulation Technologies Conference and Exhibit*, 2003. https://doi.org/10.2514/6.2003-5679.

[27] Golding, J. F., "Predicting Individual Differences in Motion Sickness Susceptibility by Questionnaire," *Personality and Individual Differences*, Vol. 41, No. 2, 2006, pp. 237–248. https://doi.org/https://doi.org/10.1016/j.paid.2006.01.012.

[28] Bos, J. E., De Vries, S. C., van Emmerik, M. L., and Groen, E. L., "The Effect of Internal and External Fields of View on Visually Induced Motion Sickness," *Applied ergonomics*, Vol. 41, 2010, pp. 516–521. https://doi.org/10.1016/j.apergo.2009.11.007.

[29] Irmak, T., Pool, D. M., and Happee, R., "Objective and Subjective Responses to Motion Sickness: the Group and the Individual," *Experimental Brain Research*, Vol. 239, No. 2, 2020, pp. 515–531. https://doi.org/10.1007/s00221-020-05986-6.

[30] Wijlens, R., van Paassen, M. M., Mulder, M., Takamatsu, A., Makita, M., and Wada, T., "Reducing Motion Sickness by Manipulating an Autonomous Vehicle's Accelerations," *IFAC-PapersOnLine*, Vol. 55, No. 29, 2022, pp. 132–137. https://doi.org/https://doi.org/10.1016/j.ifacol.2022.10.244.

[31] Webb, N., and Griffin, M., "Eye movement, Vection, and Motion Sickness with Foveal and Peripheral Vision," *Aviation, space, and environmental medicine*, Vol. 74, 2003, pp. 622–5.

[32] Griffin, M., and Newman, M., "Visual Field Effects on Motion Sickness in Cars," *Aviation, space, and environmental medicine*, Vol. 75, 2004, pp. 739–48.

[33] Oman, C. M., "A Heuristic Mathematical Model for the Dynamics of Sensory Conflict and Motion Sickness," *Acta Oto-Laryngologica*, Vol. 94, No. sup392, 1982, pp. 4–44. https://doi.org/10.3109/00016488209108197.

[34] Wada, T., Kawano, J., Okafuji, Y., Takamatsu, A., and Makita, M., "A Computational Model of Motion Sickness Considering Visual and Vestibular Information," *IEEE International Conference on Systems, Man, and Cybernetics (SMC)*, 2020, pp. 1758–1763. https://doi.org/10.1109/SMC42975.2020.9283350.

[35] Liu, H., Inoue, S., and Wada, T., "Motion Sickness Modeling with Visual Vertical Estimation and Its Application to Autonomous Personal Mobility Vehicles," *2022 IEEE Intelligent Vehicles Symposium (IV)*, 2022, pp. 1415–1422. https://doi.org/10.1109/IV51971.2022.9827161.

[36] Lackner, J. R., Graybiel, A., and DiZio, P., "Altered Sensorimotor Control of the Body as an Etiological Factor in Space Motion Sickness," *Aviation, Space, and Environmental Medicine*, Vol. 62, No. 8, 1991, pp. 765–771.

[37] Golding, J. F., Markey, H. M., and Stott, J. R. R., "The Effects of Motion Direction, Body Axis, and Posture on Motion Sickness Induced by Low Frequency Linear Oscillation," *Aviation, Space, and Environmental Medicine*, Vol. 66, 1995, pp. 1046–1051.

Part II:

Preliminary Report

NOTE:

This part has already been graded under AE4020

2

Motion Sickness Theories and Models

Models of motion sickness aim to explain the causes and the reasons behind motion sickness. Three of these theories are: Sensory Conflict Theory (SC), Subjective Vertical Conflict Theory (SVC), and Postural instability theory. SC and SVC theories have been chosen since they explain the development of the motion sickness models, which enable to predict the motion sickness in different movements.

In this chapter, SC and SVC are explained extensively. Thereafter, the most commonly used motion sickness models are presented and compared to each other through a trade-off table to make a decision on which models to work with in this research.

2.1. Theories on Motion Sickness

2.1.1. Sensory Conflict Theory

Sensory conflict theory has provided a broader understanding of the perspective of motion sickness and has been widely accepted to explain the different kinds of motion sickness, such as car sickness, air sickness, and simulator sickness. Claremont [6] has first described motion sickness as the result of a discrepancy between two different sets of sensations. While on a ship, one's eyes may see a stationary environment, but other sensations tell that they are actually moving. Therefore, this may lead to a motion sickness on the ship as a result of this conflict.

Reason [7] has explained the SC theory to be a "neural mismatch". Reason has argued that the brain has an internal model called "neural store" that retains memory traces of paired sensory input and motor commands. The "neural store" keeps updating continuously based on the interaction between the experience and the physical environment [8]. The actual sensory input is then compared with the retrieved sensory memory traces; the difference is the sensory conflict signal. Then Oman [8] has formulated a mathematical model of the SC theory. This model is an extension of the Kalman filter developed by Young and Borah [9].

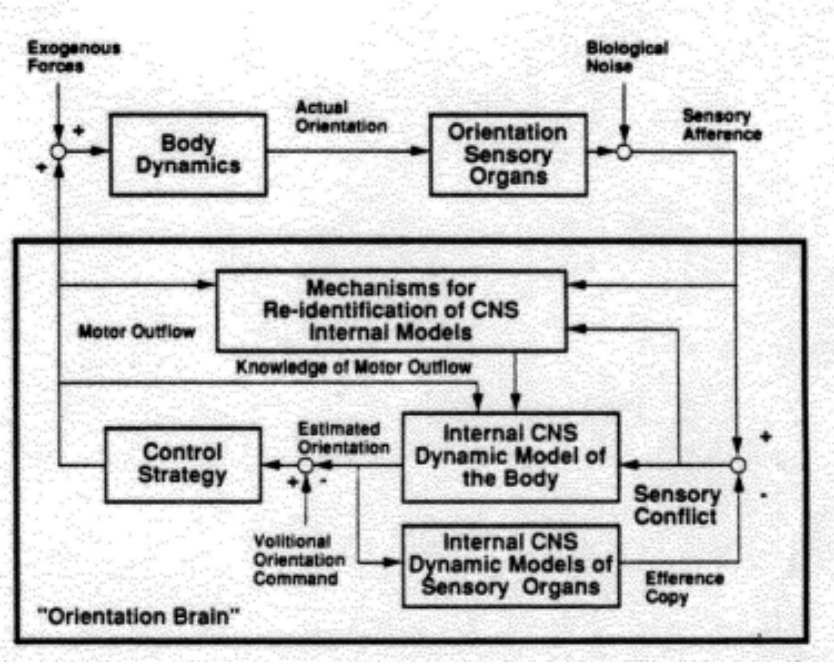

Figure 2.1: Mathematical model for sensory conflict and movement control based on observer theory [8]

Figure 2.1 shows the mathematical model that has been developed by Oman [8]. The internal Central Nervous System (CNS) models are used to calculate the estimated orientation, which then gives an updated muscle command. The estimated orientation is then used by the internal CNS to create an efference copy vector. An efferent signal is the signal that carries information away from the CNS to the muscles, and an afferent signal carries the information from the sensory receptors to the CNS. In a normal situation, the sensory afference and the efference copy should cancel each other. If not, then the difference (and thus the sensory conflict) will trigger corrective muscle commands.

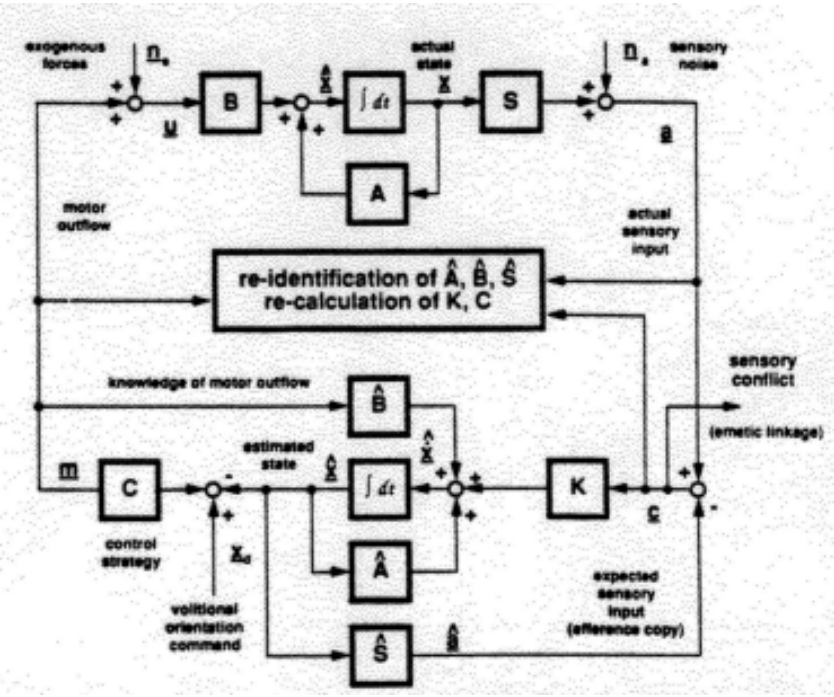

Figure 2.2: Mathematical formulation of sensory conflict model [8]

Figure 2.2 shows the mathematical formulation of the sensory conflict theory developed by Oman [8]. The observer keeps updating the body orientation, while the body and sense organ dynamics are represented by the matrices A, B, and S. The neural store is referred to as $\hat{A}, \hat{B}$, and $\hat{S}$. The conflict vector c is obtained from the difference between the actual sensory input a and the expected sensory input $\hat{a}$.

2.1.2. Subjective Vertical Conflict Theory

Bos and Bles [10] postulate that motion sickness mainly happens because of a conflict between the sensed vertical and the subjective vertical that is based on past experiences. The sensed and Subjective Vertical (SV) refer to the magnitude and direction of the human's estimate of gravity. The gravity component is determined from the gravito-inertial acceleration (GIA). Humans face an impossible physical task in determining verticality: distinguishing between gravity acceleration and linear acceleration due to body movement. Mayne [11] argues that in normal daily life, accelerations only occur for a short amount of time. Therefore, the gravitational acceleration can be separated with a low-pass filter of the GIA. The sensed vertical (v) for all three orthogonal components ($i = x$, y or z) can be written as:

$$v_i = \frac{1}{\tau s + 1} a_i \tag{2.1}$$

The sensed vertical, visual information, muscular commands, non-vestibular proprioceptive information, and ultimately cognitive inputs are then used to estimate the subjective vertical using an internal model based on prior experience. The discrepancy between the sensed vertical and the predicted vertical is fed back to the internal model, so it can best agree with the inputs that are being applied to the system. There are many ways to provide a mathematical formulation for the internal model, and one way is to use a look-up table or neural store [12]. However, in this research, it is assumed that the internal model is just a copy of the transfer functions of the mechanism that is used to calculate the perceived output. The sensed, and subjective vertical can be represented in a vector form that has a magnitude and direction. The conflict is the vector difference between those two vectors. Both vectors can be parallel, but differ in magnitude. They can also have the same magnitude but in the opposite direction, as in the case of the Coriolis effect. The conflict term (c) has no linear relationship with the Motion Sickness Incidence (MSI), which is the percentage of vomiting subjects. A Hill function is used for this because it meets two requirements: larger conflicts are transformed by a logarithmic function, and smaller conflicts can be transformed exponentially. The reason for these two requirements is that people cannot get sicker than sick, resulting in a maximum that is reached asymptotically. Hill function is [10]:

$$h = \frac{(\frac{c}{b})^n}{1 + (\frac{c}{b})^n} \tag{2.2}$$

Where n is the steepness of the function and b is an indifferent point.
Finally, the accumulation of h overtime is calculated to determine the severity of motion sickness. Vomiting is considered to be the maximum manifestation of sickness; thus, MSI does not exceed 100% and it returns to zero after the conflict in the signal is finished. The formula to calculate the MSI is [10]:

$$\text{MSI} = \frac{P}{(\mu s + 1)^2} h \tag{2.3}$$

P is the maximum percentage of people that get sick under given circumstances.

2.2. Motion Sickness Models

2.2.1. Oman's Model

Model definition

This model is based on SC theory.The model that was presented in Section 2.1.1 has been altered in some important details. This can be seen in Figure 2.3. The model allowed for the estimation of a person's subjective motion sickness or discomfort. Figure 2.3 shows the mathematical model of Oman's model. The neural mismatch is processed through the fast and slow paths, then they are added together. These fast and slow paths represent a neural or hormonal processes that are used to continuously to rectify and accumulate the conflict signal [13]. Then signals from both paths are added together and passed through a threshold. According to Oman [13], conflict signals appear to be continuously functionally averaged in the subliminal mind. Finally, the magnitude of the nausea is estimated. The sensitivity to motion sickness then does not only depend on the degree of the conflict signal; it also depends on the adopted amplitude of the signal from both paths, the threshold of nausea, and the time constants. Some limitations of this model are that it assumes that the conflict signal is already known, that the model is linear, and that it determines the states in the CNS using the state observer even though some sensory information might be estimated in a nonlinear manner [14].

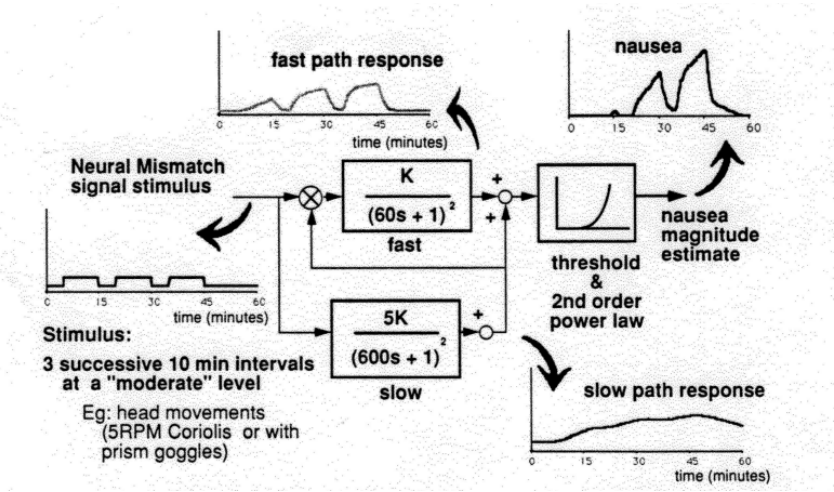

Figure 2.3: Oman's model [13]

Model validation

The model has not been widely used because, in order to use it, the conflict term needs to be known, which is not possible in most cases. Moreover, the model does not predict the MSI, it predicts the individual motion sickness responses. Irmak [15], on the other hand, used the model in the context of motion sickness caused by slalom maneuvers performed by a car at 0.2 Hz and 25 km/h for up to 30 minutes. Sinusoidal motion would therefore lead to a sinusoidal conflict. Irmak [15] has used the lateral conflict as an input to the system. The Oman model has provided a good fit to the subjective sickness scores that were measured by MIsery SCale (MISC), for the initial motion exposure and the hypersensitivity trials. Furthermore, Kotian [16] has used the Oman model in his study about the relation between amplitude of motion stimulus and motion sickness.

2.2.2. Lawther and Griffin's model

Model definition

This model has not been based on the SC or the SVC theories. Lawther and Griffin [17] have developed a model that predicts the Vomiting Incidence (VI) and Illness Rating (IR). It is described in the British Standard BS 6841 [18]. This standard establishes the upper limits for severe discomfort in the presence of a narrowband vertical acceleration of the body at frequencies ranging from 0.1 to 0.63 Hz [14]. Moreover, it defines the frequency filters that are used to determine the frequencies that cause discomfort for a person [14]. The model is based on observations from McCauley et al. [19] and data from Alexander et al. [20]. The model has two parts: the first part uses weighted vertical acceleration filtering, and the second part uses

the Root Mean Square (RMS) of the exposure time. The motion sickness in the model is measured by the Motion Sickness Dose Value (MSDV):

$$\mathrm{MSDV_Z} = \sqrt{\int_0^T a_v^2(t)\,dt} = a_{\mathrm{RMS},v} \cdot \sqrt{T} \tag{2.4}$$

Where T is the exposure time, which is between 20 minutes and 6 hours, a_v is the vertical acceleration that have been filtered for a given frequency [21], $a_{RMS,v}$ is the effective acceleration, which is defined as:

$$a_{RMS,v} = [\frac{1}{N}\sum_{n=0}^{N-1} a_v(n)^2]^{\frac{1}{2}} \tag{2.5}$$

$a_v(n)$ is the acceleration value of the n-th sample after accounting for the weight that varies with acceleration direction. N is the number of data samples.

Moreover, the model predicts the percentage of people who may vomit by VI:

$$\mathrm{VI} = K_m \cdot \mathrm{MSDV_z} \qquad K_m = 0.333 \tag{2.6}$$

K_m is chosen as that because it appeared to be the suitable fit for the data they have collected, and the line with this gradient is almost identical to the linear regression line [17]. However, this result only concerns the people who did not have any adaptation to the stimuli [22].

Additionally, the IR can be calculated in case of prediction of sickness symptoms [23]:

$$\mathrm{IR} = \frac{1}{50} \cdot \mathrm{MSDV_z} \tag{2.7}$$

Lawther et al. [17] did not provide a rationale for their choice of (1/50) in the IR equation.

Model validation

The model has used a wide range of data that has been based on Wesleyan University studies that have been performed by Alexander et al. [20]. The experiment contained exposing 450 participants to an oscillating vertical motion device, and the exposure lasted for 20 minutes or was terminated prematurely by the participant, [17]. Furthermore, the model was validated using data from the Human Factors Research conducted by O'Hanlon and McCauley [21]. Around 1000 subjects were exposed to a vertical motion. The experiment lasts for 2 hours or until the participant vomits or quits. Therefore, the model is best suited for motion that is either a pure vertical motion or a motion where the vertical motion is the most dominant. It does not predict any perception conflict. The model has not been validated against any roll/yaw/pitch motions or horizontal and lateral acceleration.

2.2.3. 6DOF-Subjective Vertical Conflict model

Model definition

This model has been based on the SVC theory. Subjective Vertical Model (SVM) is a model that has been developed by Bos and Bles at TNO Human Factors Research Institute. This model is building on the model that has been developed by Reason and Brand [3]. The output of this model is the MSI.

Figure 2.4 shows the principle of how the SV is determined according to SVM. The linear acceleration, which is assumed to be vertical, is an input for the otoliths (OTO). The input for the models should be in head-fixed reference frame. However, all three orthogonal components ($i = x$, y or z) should be in an earth-fixed reference frame to get a proper three-dimensional result [10]. Then, if the head is being rotated, the rotational acceleration is given for the Semicircular Canal (SCC), with transformation U and the inverse U^{-1} to account for the change in coordinates and to get it back to the main coordinate system, in which the low-pass filter is being executed. The mathematical interpretation to determine the sensed vertical is based on Mayne [11].

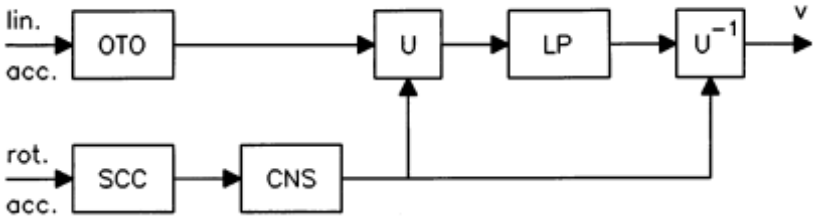

Figure 2.4: Determination of the sensed vertical [10]

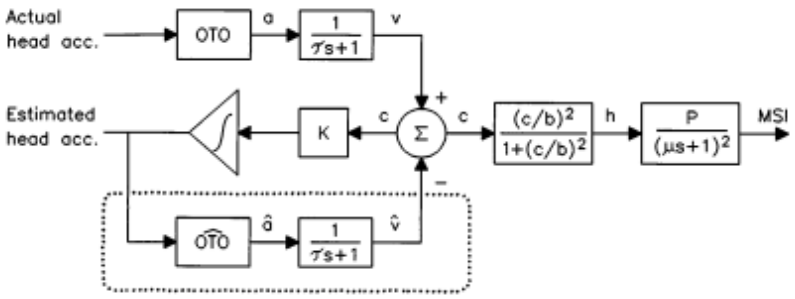

Figure 2.5: Subjective vertical conflict model for passive vertical motion [10]

Figure 2.5 shows the block diagram of SVM. It only takes the vestibular part into account to generate the SV. In this model, the OTO is represented by a unity gain, so it is not essential if a represents the vertical acceleration (in m/s^2) or the OTO organ afferent response (in spikes/s) [10]. Thereafter, the sensed vertical (v) and the subjective vertical ($\hat{v}$) are resolved by a low-pass filter. The integration in the internal model is applied because if the conflict is zero, then the SV remains unchanged rather than becoming zero as well. This model has only 1 Degree Of Freedom (DOF).

Many extended models have been built based on this one. One of these models is the one that was developed by Wada et al. [24]. They have expanded Bos and Bles's model to 6DOF motion in three-dimensional space, which includes the head rotation (roll, pitch, and yaw) as an input [24].

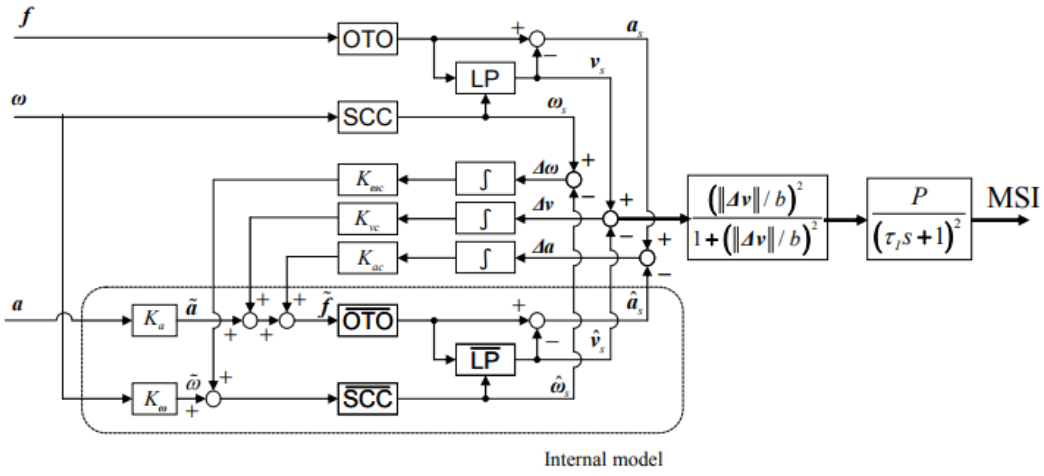

Figure 2.6: 6DOF-SVC model [24]

Figure 2.6 shows the block diagram of the 6DOF-SVC. The inputs are the gravito-inertial acceleration $\vec{f}$ (expressed as $\vec{f} = \vec{a} + \vec{g}$), angular velocity vector $\vec{\omega}$ and the inertial acceleration $\vec{a}$. The vector $\vec{f}$ is provided

to the OTO, and the OTO's transfer function is given as a unit matrix. A vector of ω is provided to the SCC. Linear acceleration $\vec{a}$ is an input for the internal model. Then errors between the sensed and expected signals (such as Δa, Δv and $\Delta\omega$) are calculated, then integrated and multiplied by the gains $K_{\omega c}$, K_{vc} and K_{ac}. The conflict terms that the model provides are: angular velocity conflict $\vec{c}_\omega$ (= $\Delta\omega$), gravity conflict $\vec{c}_g$ (= Δv), and acceleration conflict $\vec{c}_a$ (= Δa). Finally, the MSI is being calculated using the Hill function and a second-order lag with a large time constant.

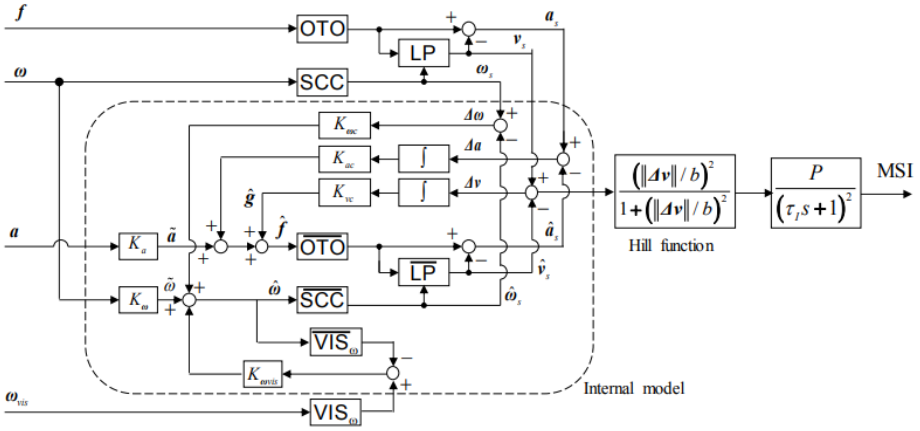

Figure 2.7: 6DOF-SVC model with visual input [25]

Wada [25] has proposed an extension of the 6DOF-SVC model that has visual inputs in it. The visual input of the model is the visual angular velocity (ω_{vis}). The proposed model can be seen in figure 2.7. It is similar to the model shown in Figure 2.6, the only addition is the visual part. Input ω_{vis} denotes the vector of the perceived visual angular velocity visually, which is aimed to be obtained by circular optic flow on the retina and eye movement [25]. The visual system, denoted by VIS_ω is assumed to be a unit matrix. Then the output of the visual part is compared with the predicted visual angular velocity and multiplied by the visual angular velocity gain, which is then added to the estimated angular velocity coming from the SCC part.

Model Validation

The model shown in Figure 2.6 has been validated against five motion paradigms: Cross-Coupled Coriolis Perturbation (CCCP) [26], Pure Roll Perturbation (PRP) [27], Lateral Translational Acceleration (LTA) [28], Vertical Translational Acceleration (VTA) [29] and Off Vertical Axis Rotation (OVAR) [30] [31]. Irmak [15] has investigated the sickness validation of the model using these paradigms. 6DOF-SVC model has provided the best match between the collected data and the motion sickness prediction for VTA and LTA. The model has given remarkably good results in predicting the sickness of VTA, and the main reason for this is that 6DOF-SVC allows the magnitude of the gravity to vary. However, 6DOF-SVC showed worse results for PRP. The model showed a consistent over-estimation of the sickness. Irmak [15] reasons this consistent over-estimation of the sickness for the angular velocity feedback; a weak angular velocity feedback will result in a greater difference between the sensed gravity and the internally estimated gravity. 6DOF-SVC has under-estimated the sickness of OVAR. To validate the model with the visual input shown in Figure 2.7, Wada et al [25] have predicted MSI under different amplitudes and frequencies for horizontal and vertical motion, as well as roll and pitch motions. Firstly, it was validated under the condition that the visual angular velocity and vestibular angular velocity are identical.

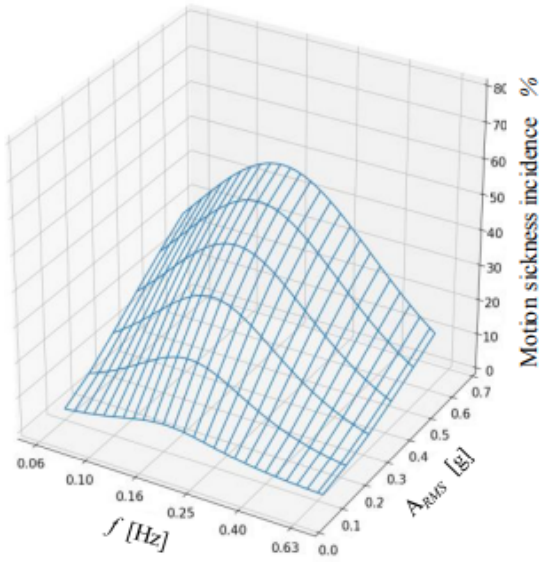

Figure 2.8: Horizontal and vertical motions [25]

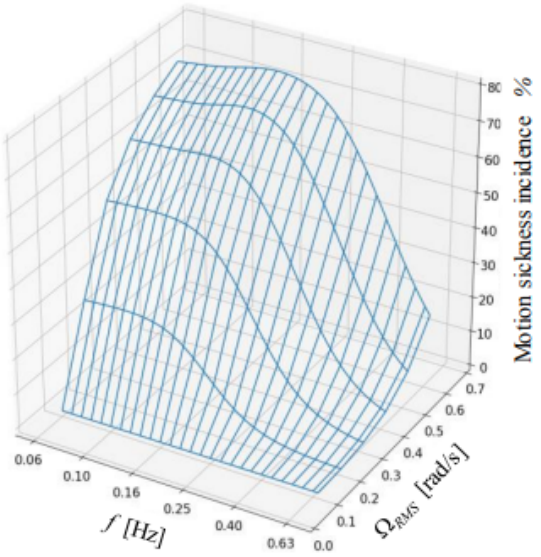

Figure 2.9: Roll and pitch motions [25]

The predicted MSI has been calculated using simple rotation and translation for 1-hour, using the proposed model in Figure 2.7. The model inputs are: (a) translation motion:

$$a = [0, \sqrt{2}A_{RMS}\sin 2\pi f t, 0]^T, \omega = 0, \omega_{VIS} = \omega \tag{2.8}$$

A Translation motion:

$$a = [0, \sqrt{2}A_{\mathrm{RMS}}\sin 2\pi f t, 0]^T, \omega = 0, \omega_{\mathrm{VIS}} = \omega \tag{2.9}$$

B Rotational motion:

$$a = 0, \omega = [0, \sqrt{2}\Omega_{\mathrm{RMS}}\sin 2\pi f t, 0]^T, \omega_{\mathrm{VIS}} = \omega \tag{2.10}$$

Figures 2.8 and 2.9 show the results of the simulation, which are in accordance with the simulations that have been in the model without the visual input [24]. Both show an MSI peak at 0.2Hz.

After that, simulation under three situations is done on a pitch motion:

$$\omega = [\omega_x, \omega_y, \omega_z]^T = [0, \Omega\sin 2\pi f t, 0]^T \tag{2.11}$$

Where $f = 0.2$Hz and $\Omega = \pi/9$ rad/s The three visual conditions are:

- Consistent: Congruence between the visual system and the vestibular system.
- Conflicting: In-congruence between the visual system and the vestibular system.
- Eyes-closed: No visual input.

Figure 2.10 shows the results of the predicted MSI. It can be seen that the conflicting condition has the higher MSI percentage, followed by the eyes closed and consistent conditions. That is in accordance with [32] and [33].

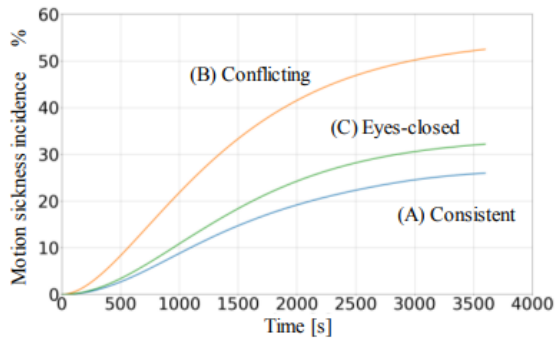

Figure 2.10: Predicted MSI under different visual conditions [25]

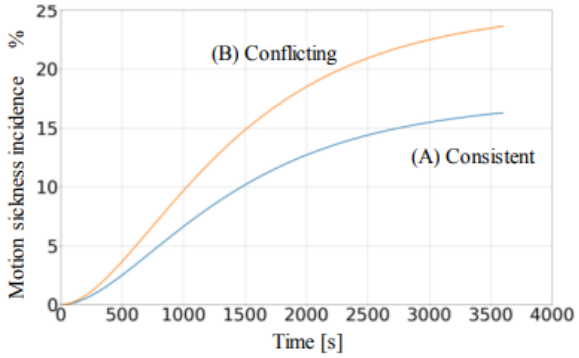

Figure 2.11: Predicted MSI under different visual conditions with experimental data [25]

The experimental data was then gathered by estimating visual perception from camera images. The camera's frame rate was 60Hz, and the IMU's sampling frequency was 1kHz. The motion was pitching by hand for 1 hour with an amplitude of 45° and a frequency of 0.2Hz [25]. Figure 2.11 shows the results of the experiment. It can be seen that the conflicting condition shows a higher predicted MSI than the consistent condition, which is in accordance to what have been shown in Figure 2.10.

2.2.4. Multi-Sensory Observer Model

Model definition

The Multi-Sensory Observer Model (MSOM) is a classical observer model where the afferent signal can be directly used by the internal model, and it has a more integrated structure than the 6DOF-SVC. It contains an internal representation of the sensor dynamics coupled with the physical relationship between different signals. The inputs of the model are the inertial acceleration $\vec{a}$ and the angular velocity $\vec{\omega}$, both in the head reference frame.

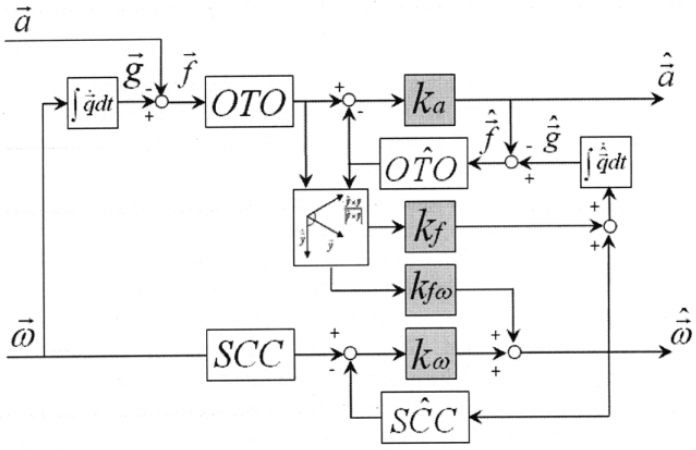

Figure 2.12: The Multi-Sensory Observer Model [34]

The block diagram of the MSOM can be seen in Figure 2.12. The conflict terms in MSOM are: OTO magnitude conflict $\vec{c}_o$, angular velocity conflict $\vec{c}_\omega$, and OTO magnitude angle conflict $\vec{c}_{oa}$. In the MSOM, the gravity vector is fixed to be a constant of -9.81m/s^2, unlike the 6DOF-SVC model. The only conflict that occurs during vertical acceleration, for example, is the OTO magnitude conflict, which is unaffected by acceleration frequency [15]. Therefore, it is inappropriate for sickness prediction.

The model predicts the afferent signals of OTO and SCC. The difference between the expected and actual OTO signals is weighted by k_a to derive the acceleration estimate. This difference is also weighted by k_f and used to rotate the gravity's direction of the observer towards reality. Moreover, the gravireceptor cue is

weighted by $k_{f\omega}$ to estimate the observer's angular velocity, in addition to the weighted error of SCC using k_{ω} [34].

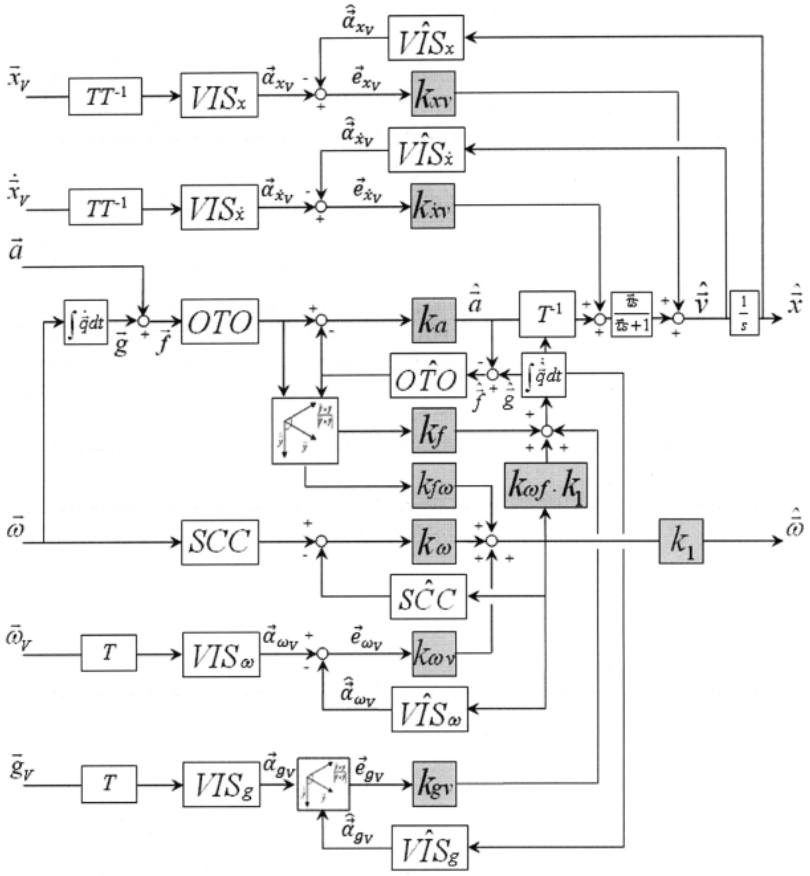

Figure 2.13: The extended MSOM [34]

The MSOM has been extended to include the static and dynamic visual cues inputs, see Figure 2.13. The vestibular system is extended based on the model of Merfeld and Zupan [35]. Newman [34] assumes that the visual system can extract four visual cues, which are: position ($\overrightarrow{x_v}$), velocity ($\overrightarrow{\dot{x}_v}$), angular velocity ($\overrightarrow{\omega_v}$) and gravity ($\overrightarrow{g_v}$). The model assumes that the visual system's sensory dynamics are approximated as a unity for the static and dynamic visual inputs. This is due to the model's not distinguishing between the focal and ambient vision or take into account the limits of visual saturation for both linear and circular vection cues [34]. The visual sensor is represented as a 3x3 identity matrix, and the dynamic sensors are represented as a negative 3x3 identity matrix, because dynamic inputs illicit a sensation of motion in the opposite direction of the visual field [34]. The parameters of the vestibular model's match the ones that have been calculated by Vingerhoets et al. [36].

Model validation

Similar to the 6DOF-SVC model, Irmak [15] has validated the model for the selected paradigms: CCCP, PRP, LTA, VTA, OVAR. Irmak has proposed to use $\overrightarrow{c_o}$ as the conflict for sickness. The MSOM showed a big difference and contradiction between the predicted sickness magnitude for VTA and LTA from the model and the experimental data. This is because of the flat nature of the frequency response of VTA. However, MSOM showed a very close results to the experimental findings regarding PRP. This is because MSOM is capable of distinguishing between the roll signal from acceleration. MSOM has performed poorly for OVAR as well; the prediction of sickness from the model was not similar to the experimental findings. To validate the visual model of MSOM, the model has been validated and showed results for basic visual-vestibular motions that have been simulated by Borah [9] and some visual-vestibular illusions such as: Coriolis, pseudo Coriolis, tilt-gain, and tilt-translation illusions. All of this can be found in Newman's MSc thesis, [34]. All in all, the

MSOM was successful in predicting responses for the visual and visual-vestibular motion paradigms.

2.2.5. UNIPG Model

Model definition

Bracessi and Cianetti [37] have built this model, which is based on the theory of SVC. It computes the perceived vertical, V_p, using a first-order low-pass filter. They use a different time constant for each component of acceleration. The internal model is a copy of the transfer functions of the vestibular system. However, the only inputs for the model are the linear accelerations, as measured by the otoliths. The model disregards the angular velocities measured by the SCC. Figure 2.14 shows the general model of the UNIPG with i linear acceleration.

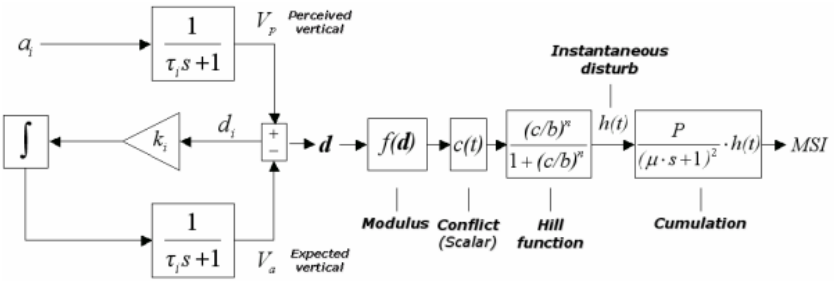

Figure 2.14: UNIPG model [37]

Bracessi and Cianetti have incorporated the visual system in the model and introduced a new version of it called "UNIPG$_{\text{SeMo}}$", which includes the visual acceleration as an input for the model. The internal vestibular dynamic model processes the visual information, resulting in the predicted vestibular signal, which is subsequently subtracted from the perceived vestibular signal. This model is different from the one designed by Wada el al. [25], since this model takes the visual rotational velocity as an input, while the "UNIPG$_{\text{SeMo}}$" takes the visual linear acceleration as an input. Therefore, both of them are not realistic because they do not consider all the visual inputs.

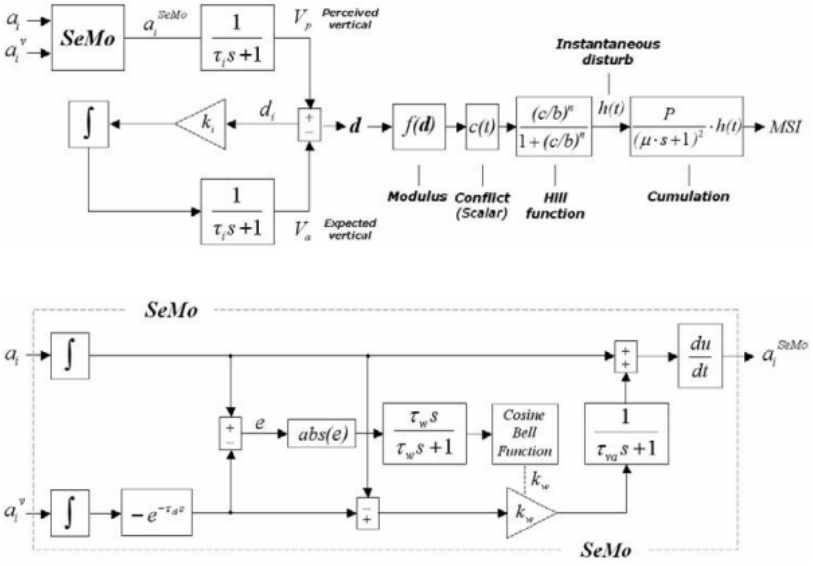

Figure 2.15: UNIPG visual model [37]

Figure 2.15 shows the visual model of UNIPG. The first modification of the model, compared to the model in Figure 2.14, is that the linear acceleration a_i is the input to the vestibular system rather than the

specific force. The vestibular system transfer function is in accordance to Bos and Bles model [10] [37]. The second input of the model is the acceleration related to the peripheral field of vision a_i^v.

Model Validation

The UNIPG is only valid for translational accelerations. It has been validated for vertical and lateral acceleration [37]. The vertical acceleration was validated against the data that has been collected by Bos and Bles [10] and O'Hanlon and McCauley [29]. A comparison [37] has been done between the MSI for sinusoidal vertical motion from O'Hanlon/McCauley and the results obtained from the UNIPG, in addition to the MSI development with time for 2 hours of exposure for a vertical motion. The UNIPG has shown a good fit for the data that it has been compared to. Moreover, the model with the visual input has been validated against data from O'Hanlon/McCauley. The results were in accordance with what has been previously confirmed, which is that the vestibular sense is dominant at high frequencies, with a maximum of 0.2Hz [37], and visual sensation is dominant at low frequencies. Nevertheless, the model has not been validated for a broader set of data and has not been widely used in the industry. The model has not been validated for roll, pitch, and yaw motions.

2.2.6. Particle Filter Model

Model definition

The Particle Filter Model (PFM) has been developed by Laurens and Droulez [38]. It does not depend on the typical theories of motion sickness that have been discussed in Section 2.1. It introduces the idea of probabilistic modeling into motion sickness estimation. Unlike the previous models, the PFM has a probabilistic internal model. It mainly has two parts: forward propagation and likelihood weighting. Figure 2.16 shows the PFM. It uses the notation that Laurens and Droulez have used here [39]. The Gaussian noise ω_t^i for any given particle i is added to the average sensed canal signal from the previous time step $\overrightarrow{V_{t-1}}$, therefore, creating $\vec{C}_t^i$. Thereafter, the angular velocity of the particle can be calculated and integrated over time to give the rotation ($R(\Omega_t^i\ \delta t)$) of the particle from t-1 to t, this when it is multiplied by the particle's orientation gives the orientation of each particle at t Θ_t^i. Each particle is then weighted with respect to the state transition probabilities. The brain is assumed to assign the greatest possibility to stationary states [15]. In PFM, there is no conflict term that is being defined. However, angular velocity conflicts can be calculated. Moreover, PFM does not include any OTO, acceleration, and gravity conflict terms.

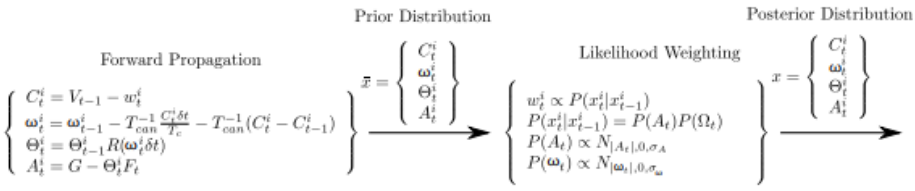

Figure 2.16: Particle Filter Model [15]

Model validation

Laurens and Droulez [38] have validated the model by doing simulations of a rotation at a constant velocity, visual stimulation, lateral oscillation, and roll oscillation using data from Angelaki et al. [40], OVAR data that have been obtained by Angelaki et al. [41] as well. However, they have not validated the model against vertical acceleration data. Similar to SVM and MSOM, Irmak [15] have validated the model against CCCP, PRP, LTA, VTA and OVAR. Due to the lack of OTO and SCC interactions and the lack of estimation for gravito-inertial force, PFM does not predict any motion sickness regarding VTA. In terms of PRP and OVAR, PFM has shown promising results and accurately predicted sickness incidence. The model has not been used extensively in predicting motion sickness and has not been used widely in papers.

2.3. Discussion

In this section, a discussion and a comparison of the different models that have been presented in Section 2.2 will be done. The models are compared based on a number of considerations:

- Vestibular System: The model has a physical representation of the vestibular system (OTO and SCC).

- Visual System: The model takes the visual system into consideration.
- Validation: Data for roll, yaw, pitch, vertical acceleration, lateral acceleration, and forward acceleration were used to validate the model.
- Reliability: Model have been used widely in motion sickness studies.

Oman's model can be directly disregarded from the consideration to use to predict the motion sickness in the Flying-V, since it is a model that gives the individual motion sickness responses, and it assumes that the conflict is already known. However, in the motion sickness in the Flying-V study, it is not possible yet. As a result, it will not be used to forecast motion sickness in the Flying-V.

6DOF-SVC has a physical representation of the OTO and SCC, despite considering the OTO as a unit transfer function; it also lacks any physical coupling between the OTO and SCC (Figure 2.7). Similarly, MSOM has a physical representation of the OTO and SCC and considers the OTO to be a unit transfer function. However, it has a coupling relationship with the SCC and OTO. PFM represents the vestibular system in a probabilistic way and does not have a physical relationship. UNIPG has a physical representation only for the OTO and does not consider the SCC, as it only has the linear acceleration as an input. Lawther and Griffin's model does not have any physical representation of the OTO and SCC. Therefore, MSOM and 6DOF-SVC meet this criteria, while UNIPG, PFM, and Lawther and Griffin's model lack behind.

For the visual system, an updated version of 6DOF-SVC [25] has been done to include the vision part in it, as can be seen in Figure 2.7. However, it only includes the visual angular velocity, which is not realistic because it does not include all the visual inputs. MSOM [34] also takes the vision part into consideration, but in a more detailed way. MSOM includes the visual position, velocity, angular velocity, and gravity (see Figure 2.13). UNIPG [37] also included the vision part, but it only has the visual linear acceleration as an input. PFM does not have any representation for the visual system in the model. Lawther and Griffin's do not include the visual system in their model. Thus, MSOM meets the criteria, while 6DOF-SVC and UNIPG meet these criteria partially, but PFM and Lawther and Griffin's model do not.

Considering the validation, all motions are considered important (thus, lateral, vertical, forward accelerations, and roll, pitch, and yaw). This is because it is not known at this stage of the research of motion sickness in the Flying-V which is the dominant motion in the Flying-V. MSOM and SVM have been validated against wide variety of data and motion, MSOM performed better in rolling and showed promising results for OVAR, while 6DOF-SVC performed better in lateral/vertical/forward accelerations. PFM did not predict any motion sickness due to the lack of OTO and other acceleration conflict, but it has performed better in rolling motion. UNIPG has been validated against vertical acceleration. For rolling, it does not detect any conflict due to the lack of SCC representation and angular velocity input. Lawther and Griffin's model has been only validated for vertical acceleration motion. Therefore, MSOM and 6DOF-SVC performed the best in this category.

For the last point, which is reliability, 6DOF-SVC has been used widely and extensively in a number of motion sickness studies in cars and ships ([42], [24], [43], [44], [25]). MSOM has not been used in motion sickness applications, but it has been used mainly in the aerospace application and operation regarding the spatial orientation perception ([34], [45]). PFM, UNIPG, and Lawther and Griffin's models miss this reliability since it has not been used as extensively as MSOM and 6DOF-SVC.

Table 2.1 shows a trade-off table between all the models and if they meet a certain criterion or not. It can be seen that 6DOF-SVC and MSOM met three criteria and partially one criterion, which is the reliability for MSOM, and visual system for 6DOF-SVC. Therefore, for the next chapters, these two models will be considered and one of them will be used to simulate and predict the motion sickness, depending on the specific forces' analysis.

Table 2.1: Trade-off table between models

Criteria / Models	Vestibular system	Visual system	Validation	Reliability
Oman's model	Does not include mathematical model for OTO and SCC	Does not include any mathematical model for the visual system	Only in terms of individual sickness rating	Showed good results in terms of fitting MISC
Lawther & Griffin's model	Does not include mathematical model for OTO and SCC	Does not include any mathematical model for the visual system	**Lateral/vertical /forward accel.**: vertical acceleration has been validated and showed good results. Lateral and forward acceleration have not been validated **Roll/pitch/yaw**: have not been validated	Has not been used extensively in motion sickness studies
MSOM	It includes mathematical model for OTO and SCC. However, it assumes OTO is a unit transfer function	It includes the position, velocity, angular velocity and gravity visuals	**Lateral/vertical /forward accel.**: model does not perform well because of the conflict's transfer function is independent of acceleration frequency and the peak frequency is at 0.02 Hz [15]. **Roll/pitch/yaw**: model showed good results for rolling. performed poorly for OVAR. Pitch was not validated	Has not been used in motion sickness application but has been used in aerospace spatial orientation application

Table 2.1: Trade-off table between models

Criteria / Models	Vestibular system	Vision system	Validation	Reliability
6DOF-SVC	It includes mathematical model for OTO and SCC. Assumes OTO is a unit transfer function	Wada's model [25] only includes the angular velocity visual information	**Lateral/vertical /forward accel.**: have been validated and the model performs the best compared to other models. **Roll/pitch/yaw**: Irmak [15] found that the model perform worse in this regard	Used widely in motion sickness studies
PFM	Does not include any mathematical model for OTO and SCC	Does not include any mathematical model for the visual system	**Lateral/vertical /forward accel.:** is not applicable due to the lack of interaction between OTO and SCC and the absence of gravito-inertial force estimation **Roll/pitch/yaw:** showed promising results in predicting sickness with rolling motion	Has not been used widely in motion sickness studies
UNIPG	Only has mathematical representation of OTO and not SCC	Only includes the visual acceleration, which is not realistic because it does not include all the visual inputs	**Lateral/vertical /forward accel:** Has only been validated against vertical acceleration and showed good results **Roll/pitch/yaw:** Have not been validated and not applicable due to the absence of SCC consideration	Has not been used widely in motion sickness studies

3
Flying-V

In this chapter, the Flying-V is introduced, along with the studies that have been done so far on it. This chapter contains general information regarding the Flying-V, its handling qualities, its interior layout, and its seating configuration.

3.1. General Information

For over 50 years, wing-body-tail conventional aircraft have been dominant in the commercial aviation industry [46]. However, this configuration is converging to its asymptote of maximum performance and efficiency [47]. Thus, an unconventional aircraft layout has emerged, which is the flying wing.

TU Delft has made a design of this blended-wing-body, which is called the Flying-V, based on a design from Benad [48] and then a design made by Faggiano [49]. Figure 3.1 shows the general view and design of Flying-V. This design and layout produced promising results, as it reduced drag by 10% compared to a conventional design with comparable performance requirements [5]. However, it is suspected that passengers who sit further away from the center of rotation will experience more motion sickness than those who sit closer to the center of rotation.

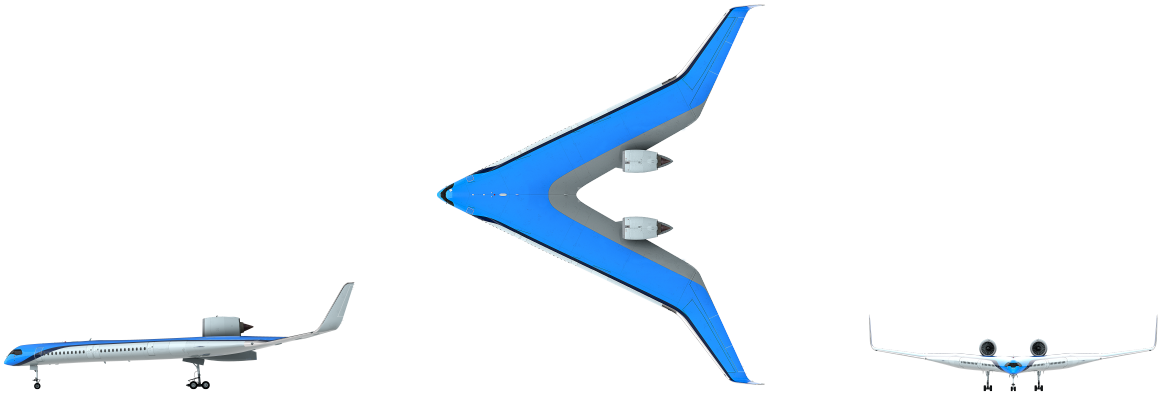

(a) Flying-V side view [4] **(b)** Flying-V top view [4] **(c)** Flying-V front view [4]

Figure 3.1: Flying-V geometry

3.2. Geometry of the Flying-V

The Flying-V does not have a separate horizontal plane. Therefore, it is stabilized by the aerodynamic center that is located behind the most aft c.g. [50]. The pitch and roll are provided by the elevons, which combine the functions of the ailerons and the elevators. The elevons are located at the trailing edge of the outboard wings [50]. The rudders, which are located and integrated with the winglets, provide the yaw. The engines are located behind and above the wings, in such a way that the engine intake is kept behind the trailing edge of the wing. This location comes after considering the inter-engine clearance, center-of-gravity, one-

engine-out yawing moment, and aerodynamic interaction with the wings [50]. More information about the geometry of the Flying-V can be found in the publication of TU Delft [50].

3.3. Interior Design

The interior volume of the Flying-V contains the passenger cabin, the fuel tanks, and the cargo hold. Passengers will be seated in both wings. The proposed interior has a two-class configuration: business class seats and economy class seats.

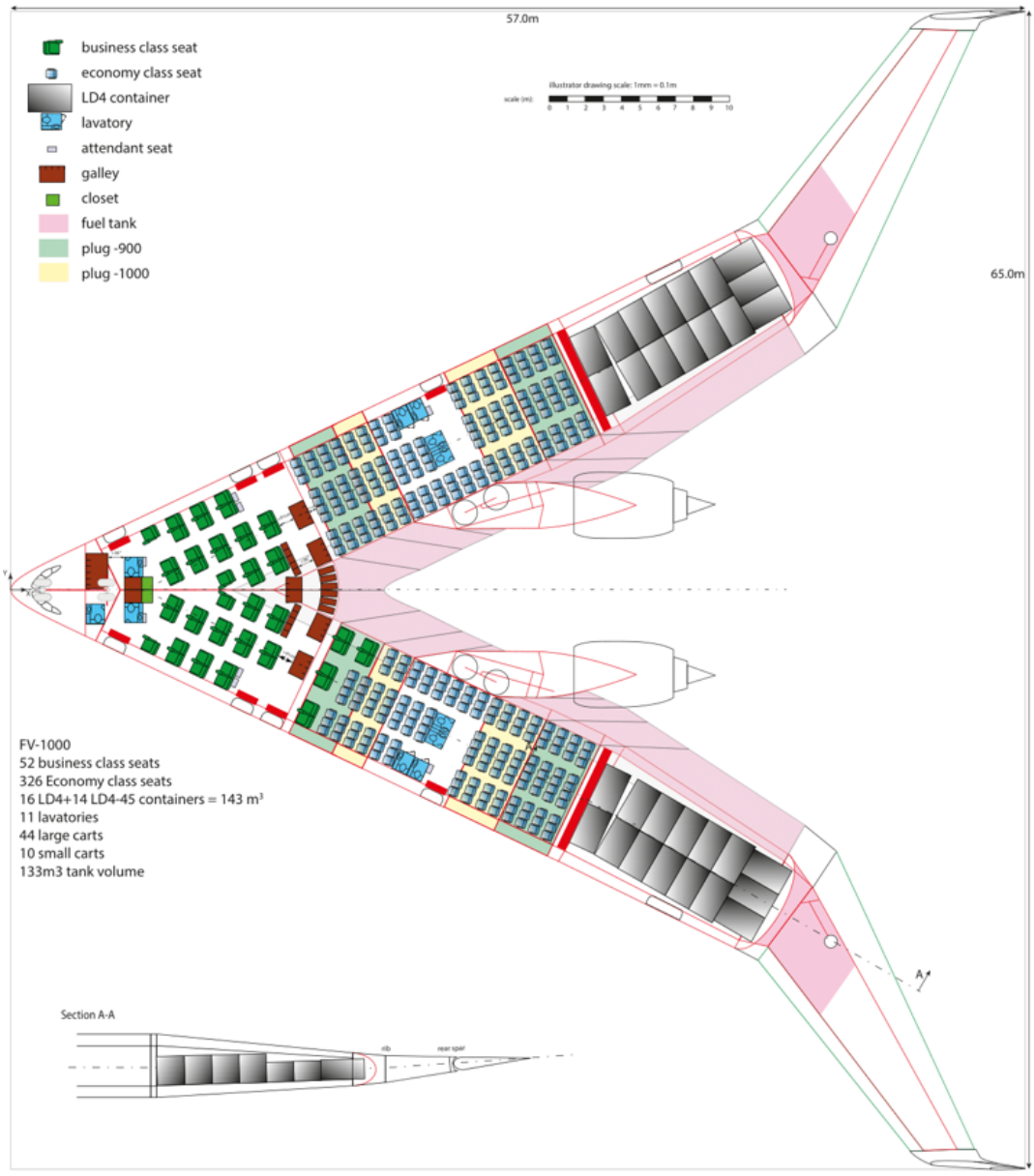

Figure 3.2: Interior design of the Flying-V [51]

Figure 3.2 shows the interior design of the Flying-V and the locations of the business class seat, the economy class seat, the container, the lavatory, the attendant seat, the galley, and the closet. It can be seen that the people who will sit in the aft locations of the wing will be further away from the center of rotation of the aircraft.

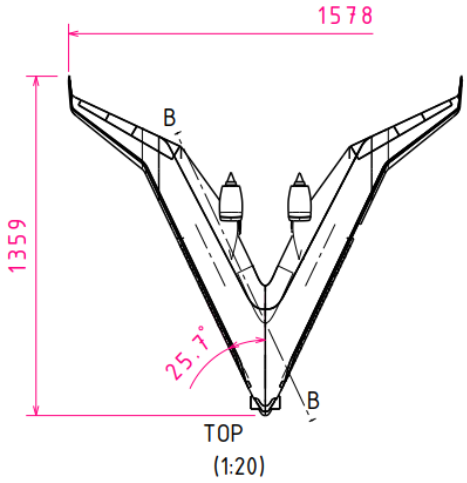

Figure 3.3: Flying-V top view [52]

The angle between the longitudinal axis of the cabin and the center-line of the aircraft is 26°, as can be seen in Figure 3.3. Liu et al. [53] have designed the seat configuration for the current Flying-V design. Each seat is positioned facing the center-line of the aircraft but still in rows perpendicular to the cabin's longitudinal axis, which results in a 26° staggered configuration [53].

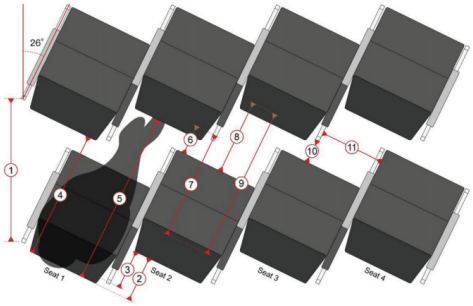

Figure 3.4: 26° staggered seat setup [53]

Figure 3.4 shows the 26° staggered seat setup that Liu et al. [53] have designed. Liu et al. [53] have researched passenger comfortability by doing an experiment using two rows of staggered seats that are positioned at three different pitches. However, this is outside the scope of the motion sickness study.

3.4. Flying-V Handling Qualities

Torelli et al. [54] evaluated the Flying-V's low speed handling characteristics. Vugts et al. [55] evaluated Flying-V's flightpath-oriented control allocation. Joosten et al. [5] evaluated the Flying-V's lateral-directional handling characteristics. Joosten et al. have performed maneuvers such as Dutch Roll Stability (DR), Coordinated Turn Capability (CTC), Time to Bank (TTB), One Engine Inoperative Trim (OEI-T), and Steady Heading Sideslip (SHS) to analyze the lateral-directional handling qualities of the Flying-V. The quantitative benchmarks that have been used are the EASA aircraft regulations of CS-25 [56]. These experiments have been done in the SIMONA Research Simulator. For the current motion sickness study, the flight data that have been obtained from the performed maneuvers for fast (TTB) and slow (CTC) maneuvers will be used to calculate the specific forces at different locations in the Flying-V. These maneuvers are relevant for motion sickness studies because they can potentially induce motion sickness in passengers.

3.5. Conclusion

For the next chapters in the report, realistic seating coordinates with respect to the c.g. of the aircraft that can be obtained from Figure 3.4, will be used to calculate the specific force and the conflict in different seat

locations in the Flying-V. Moreover, the 26° staggered seat setup that was designed by Liu et al. [53] will be used and compared with seats that are parallel to the longitudinal axis of the Flying-V's cabin. The CTC and TTB maneuvers data that have been collected from the pilot-in-the-loop experiments by Joosten et al. [5] are found to be interesting to look at since the aircraft experiences changes in acceleration and movement, that can lead to simulate the vestibular system. The longitudinal, lateral, and vertical specific forces will be calculated at different locations in the Flying-V and checked to see which of the rotational components (roll, pitch, and yaw rates) is dominant. Thereafter, the longitudinal, lateral, and vertical conflicts are calculated by the motion sickness model to see which phase of the maneuver causes the highest conflict in the Flying-V.

4

Specific Force Analysis

In this chapter, the longitudinal, lateral, and vertical specific forces are calculated and analyzed since these are the forces that passengers would feel and experience in the Flying-V. Furthermore, the specific forces are used as inputs to the 6DOF-SVC motion sickness model. Therefore, it is important to understand what might cause the motion sickness during the flight by analyzing the specific forces first.

The outline for this chapter is to first analyze the longitudinal, lateral, and vertical specific forces for TTB maneuver and then analyze CTC maneuver. The specific forces of the maneuvers are calculated for the 26° and 0° rotated seat configuration. Additionally, the specific force calculation of the TTB are verified against simple cases of roll, pitch, and yaw. The conclusion, which is the last part, discusses the findings of the specific forces analysis and what will be used for the motion sickness analysis. The coordinate system that is being used in this analysis is the aircraft body reference frame.

4.1. Time to Bank Maneuver

TTB maneuver performed in [5] involved changing the roll angle ϕ from positive angle to negative angle within a short amount of time. In this case, going from around +30° to −30° within approximately 7 seconds. The data has been obtained from the pilot-in-the-loop experiments [5]. The flight control system that has been used in the experiment is Stability Augmentation System with roll damping (SAS-2) [5]. Figure 4.1 shows the angular velocities and the Euler angles, and the aircraft body velocities of the TTB maneuver.

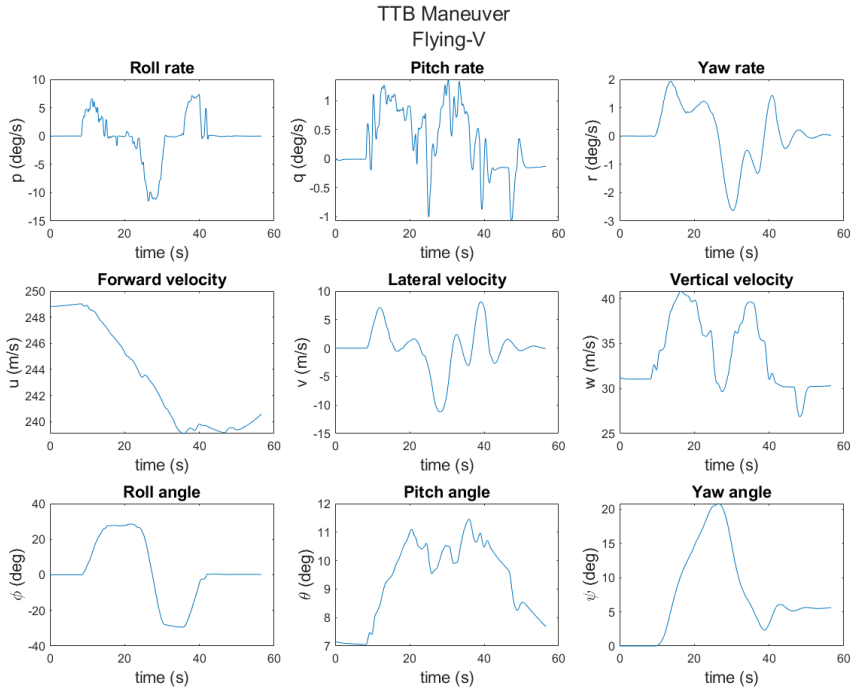

Figure 4.1: TTB maneuver's angular rates, Euler angles, and body velocities

4.1.1. Specific forces at the c.g.

To calculate the specific forces that are related to the motions of the c.g.:

$$\begin{pmatrix} \dot{u} \\ \dot{v} \\ \dot{w} \end{pmatrix} = \frac{1}{M} \begin{pmatrix} F_{x(c.g.)} \\ F_{y(c.g.)} \\ F_{z(c.g.)} \end{pmatrix} - \begin{pmatrix} p \\ q \\ r \end{pmatrix} \times \begin{pmatrix} u \\ v \\ w \end{pmatrix} + A\vec{g} \tag{4.1}$$

(u, v, w) and (p, q, r) represent real-time data from pilot-in-the-loop experiments. $(\dot{u}, \dot{v}, \dot{w})$ are calculated by numerical differentiation. $\vec{g}$ is the gravity vector. The inertial-to-body transformation matrix A is as follows:

$$A = \begin{pmatrix} \cos\theta \cdot \cos\psi & \cos\theta \cdot \sin\psi & \text{-}\sin\theta \\ \sin\theta \cdot \sin\phi \cdot \cos\psi - \cos\phi \cdot \sin\psi & \sin\phi \cdot \sin\theta \cdot \sin\psi + \cos\phi \cdot \cos\psi & \cos\theta \cdot \sin\phi \\ \sin\theta \cdot \cos\phi \cdot \cos\psi + \sin\phi \cdot \sin\psi & \cos\phi \cdot \sin\theta \cdot \sin\psi - \sin\phi \cdot \cos\psi & \cos\theta \cdot \cos\phi \end{pmatrix} \tag{4.2}$$

Thereafter, the specific forces need to be transformed from the c.g. to the passenger's seat with respect to the longitudinal axis. That can be done by transforming from the c.g. to DERP:

$$F_{x(\text{DERP})} = (-r^2 - q^2) \cdot x_{\text{DERP}} + (p \cdot q - \dot{r}) \cdot y_{\text{DERP}} + (\dot{q} + p \cdot r) \cdot z_{\text{DERP}} + F_{x(\text{c.g.})} \tag{4.3}$$

$$F_{y(\text{DERP})} = (\dot{r} + p \cdot q) \cdot x_{\text{DERP}} + (-r^2 - p^2) \cdot y_{\text{DERP}} + (q \cdot r - \dot{p}) \cdot z_{\text{DERP}} + F_{y(\text{c.g.})} \tag{4.4}$$

$$F_{z(\text{DERP})} = (p \cdot r - \dot{q}) \cdot x_{\text{DERP}} + (q \cdot r + \dot{p}) \cdot y_{\text{DERP}} + (-q^2 - p^2) \cdot z_{\text{DERP}} + F_{z(\text{c.g.})} \tag{4.5}$$

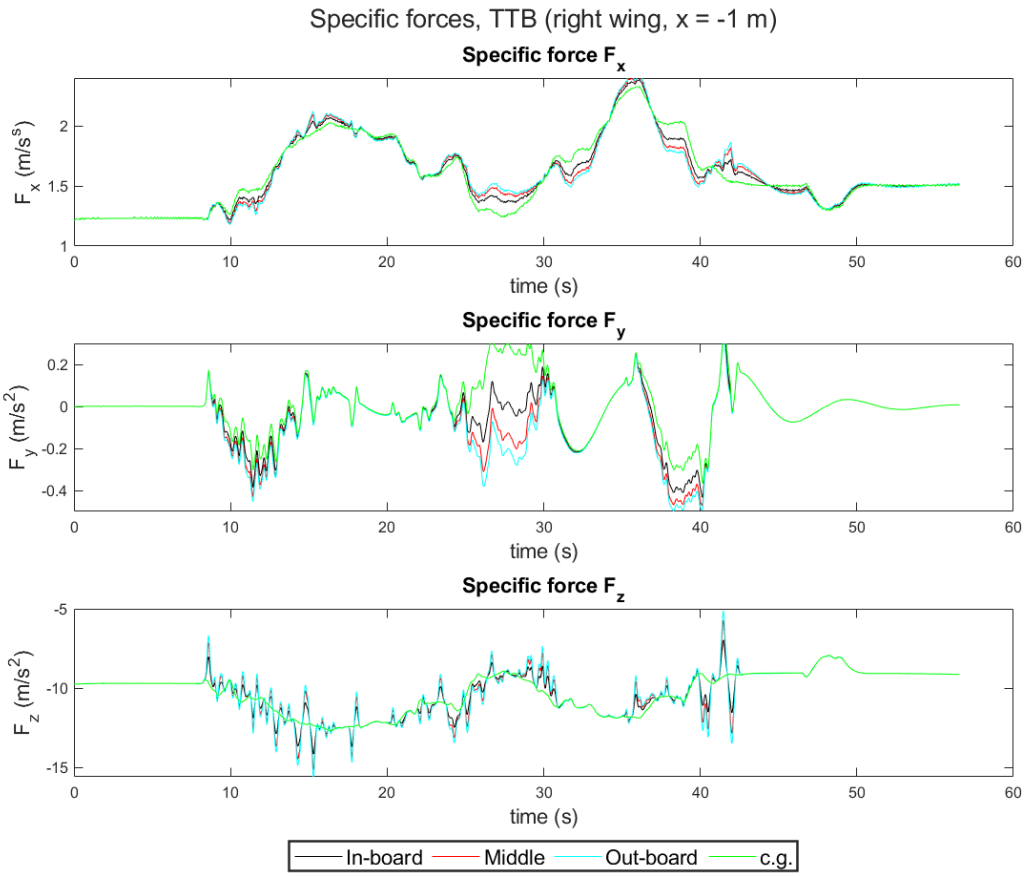

Figure 4.2: Specific forces for the aft seats using the Flying-V's dynamics module

Figure 4.2 shows the specific forces calculated at the c.g. and for the three different lateral y locations that are at x = -1m from the c.g. Cappuyns [57] has developed a full-scale aerodynamic simulation-model of the Flying-V. The aerodynamic model obtained from the Vortex Lattice Method (VLM), and it consists of several limitations. The aerodynamic data is linear, that means this model does not accurately display the corners of the flight envelope [58]. Moreover, frictional drag, ground effect, compressibility, and aeroelasticity effects are not taken into account. Also, the atmospheric model does not include wind, wind shear, nor turbulence [58]. The specific force calculated in Figure 4.2 have been calculated using the flight data that has been measured from the Flying-V's dynamics module. As can be observed, the high-frequency components of the specific forces exhibit prominent peaks that may not accurately reflect reality. The lack of damping in the computation of aerodynamic forces is thought to be the cause of these peaks. The model includes look-up tables that would relate the elevon deflection to the roll moment, for example. Thereafter, elevon deflection will generate the corresponding forces and moments. However, in reality, there would be damping due to the airflow needing some time to adapt itself to the new situation, which would reduce these strong peaks.

In order to remove these prominent peaks from the high-frequency components, the data must be filtered, in order to reflect reality more. Appendix C.1 shows filtering the data across a range of break frequencies. A break frequency of 0.5Hz is chosen since it filters out the strong peaks of the high-frequency components and keeps the peaks of the low-frequency components.

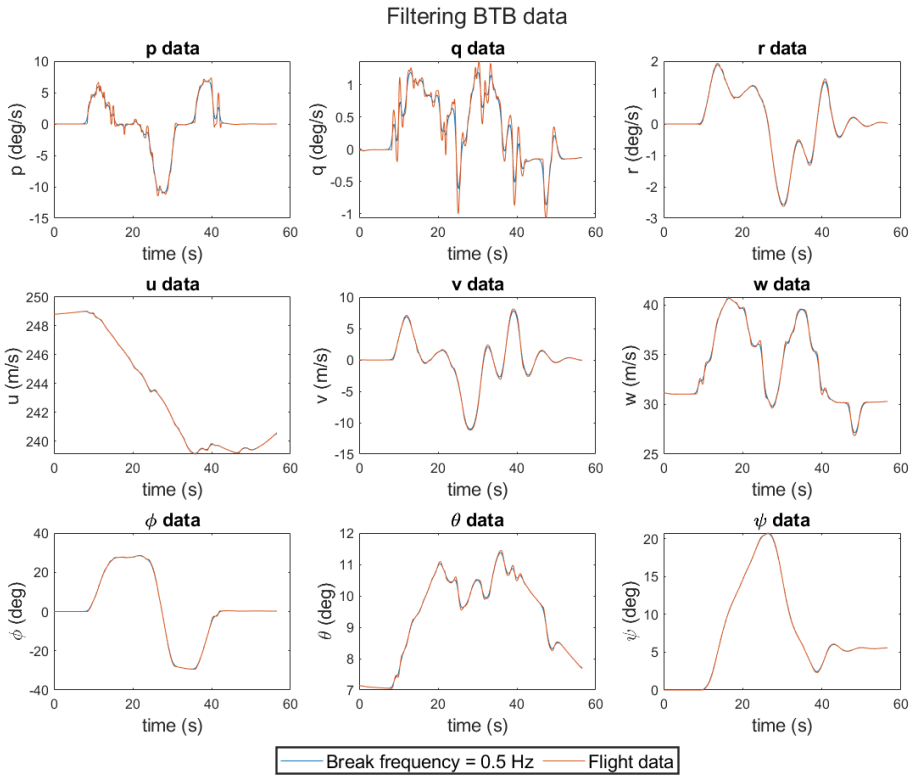

Figure 4.3: Filtering TTB data

Figure 4.3 shows the filtered data with a break frequency of 0.5Hz. In the next sections, the specific forces will be calculated using the filtered data.

The specific forces at the c.g. are calculated using Equation (4.1). Each term of the equation is plotted, and the total specific force is shown.

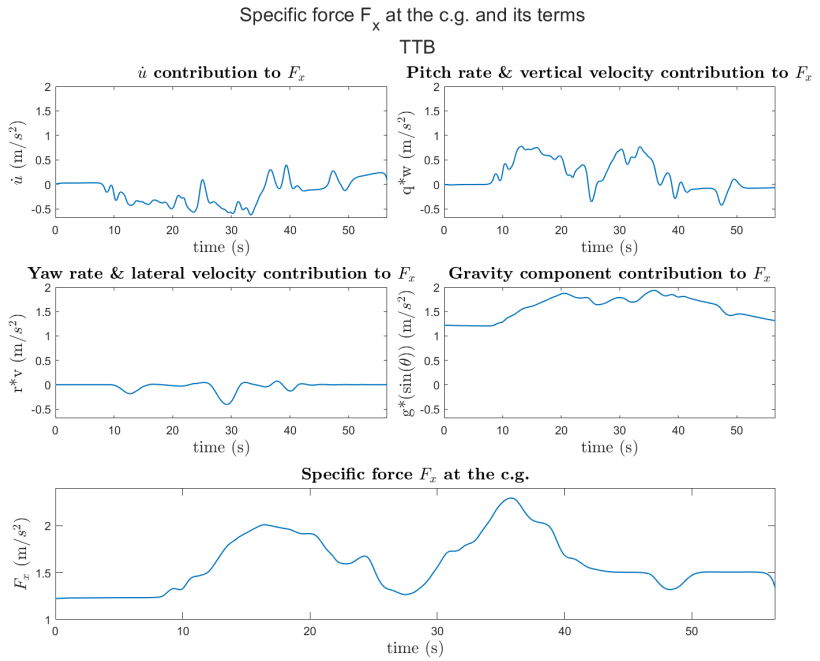

Figure 4.4: Specific force in the longitudinal direction at the c.g.

The longitudinal specific force is the force that acts along the longitudinal axis of the aircraft. During pitch up of the aircraft, passengers would feel a longitudinal specific force in the forward direction. The specific force F_x and its terms are depicted in Figure 4.4. It can be seen that the gravity component is the dominant component. F_x starts at around 1.2 m/s^2 because of the pitch trim angle, which is around 7°. Therefore, passengers would feel a longitudinal specific force due to the pitching of the aircraft. The magnitude of the longitudinal specific force is proportional to the pitch angle and the acceleration of the aircraft. The greater the pitch angle, the greater the longitudinal specific force.

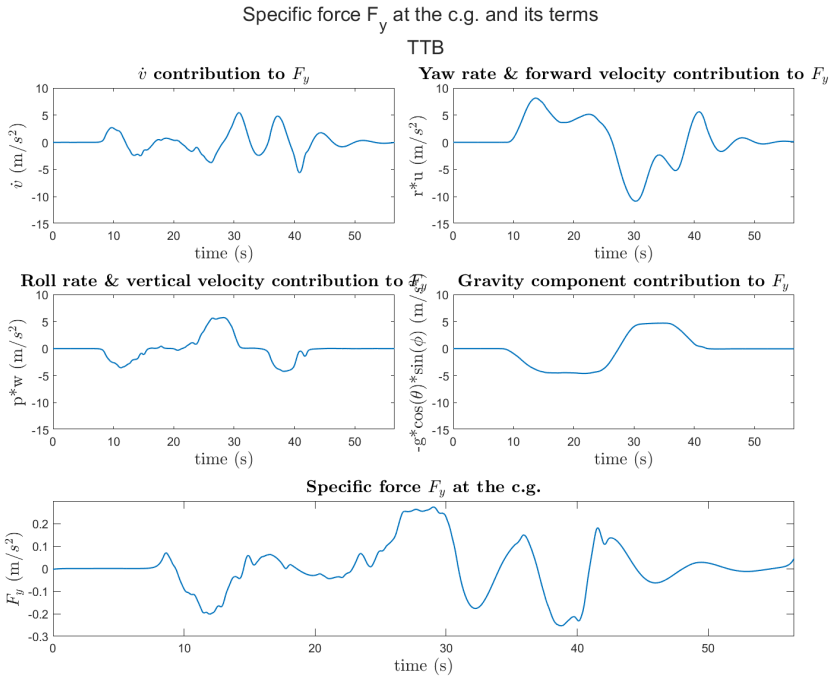

Figure 4.5: Specific force in the lateral direction at the c.g.

The lateral specific force acts along the lateral axis of the aircraft. Figure 4.5 shows the specific force F_y. It can be seen all the components are relatively large, but have opposite signs, therefore, they cancel each other. This leave only a small lateral specific force that will be felt at the c.g. of the aircraft. This lateral specific force is typically small because it is balanced by the vertical specific force. During a turn, passengers would experience a force that pushes the passengers away from the center of the turn and towards the side of the aircraft. The lateral and vertical specific forces would tend to balance each other out, because these two forces are perpendicular to each other, therefore, both contribute to the overall experience of the passengers. The vertical specific force experienced by passengers is much stronger than the lateral specific force, by comparing Figures 4.5 and 4.6.

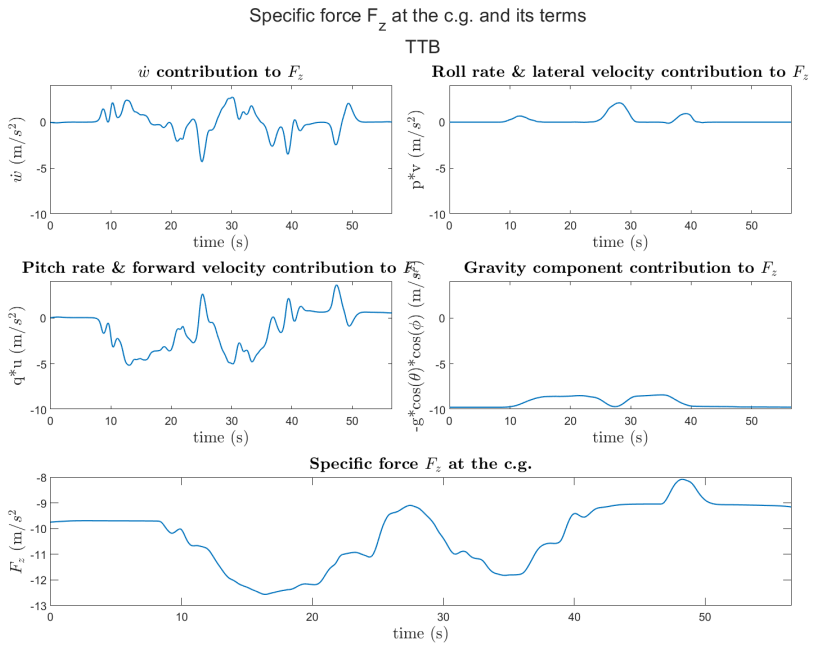

Figure 4.6: Specific force in the vertical direction at the c.g.

The vertical specific force acts along the vertical axis of the aircraft and is created by the centrifugal force that results from the aircraft's rapid change in the bank angle. Figure 4.6 shows the specific force F_z. The vertical acceleration, pitch rate, and forward velocity are the dominant components of the vertical specific force. Moreover, the initial sense of upright is 9.81m/s^2, thus, the vertical specific force is initially at -9.81m/s^2 since this is in aircraft body reference frame. In the case of the aircraft turn, passengers are in motion and continue moving in a straight line, however, the aircraft is turning, which creates a force that acts on the passengers that push them away from the center of the turn and towards the side of the aircraft.

The specific forces will be transformed to different locations in the Flying-V. The analysis will be done on two seating configuration, the first one is the 26° rotated seat configuration with respect to the cabin's longitudinal axis, which is based on the study of Liu et al. [53]. The second seating configuration is the 0° rotated seat configuration with respect to the cabin's longitudinal axis. An analysis of the seating arrangement is conducted to see whether seating orientation has an impact on the specific forces and the motion sickness experienced by the Flying-V's passengers.

4.1.2. 26° rotated seats

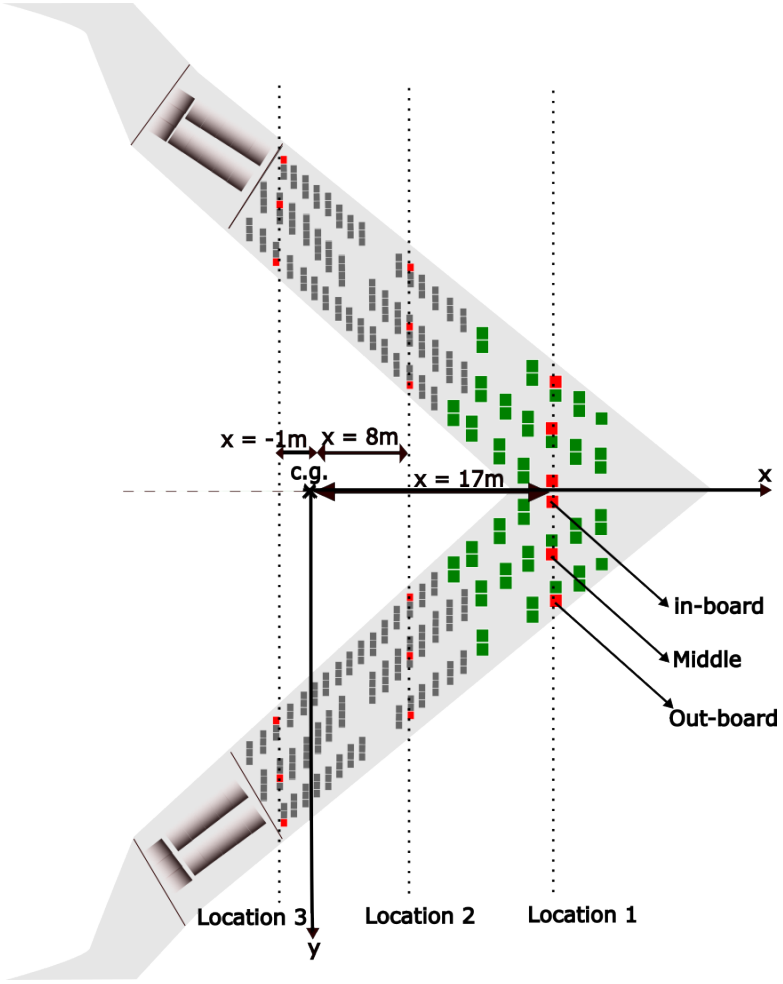

Figure 4.7: 26° rotated seats in the Flying-V

In this section, the seats of the Flying-V are rotated 26° with respect to the longitudinal axis of the cabin, which is in-line with Liu et al. [53] study, as can be seen in Figure 4.7. They are assumed to be parallel to the center-line of the aircraft. No rotation matrix is applied here since the reference frame is the same as the one that has been used in the calculated data of the maneuver. There are three locations that are being shown in Figure 4.7: location 1 is the closest to the center-line, location 3 is the furthest from the center-line, and location 2 is in the middle. In this report, the figures of the most front and most aft locations are shown. The figures for the location in-between (location 2) will be provided in a separate document.

	Location 1	**Location 2**	**Location 3**
	y **(m)**	y **(m)**	y **(m)**
In-board	0	3.3	7.5
Middle	3	6.7	11.5
Out-board	5.2	9.6	13.5

Table 4.1: Locations coordinates in the right wing

To study the specific forces across different seats in the Flying-V, 3 fixed x offsets with respect to the c.g. of the Flying-V are chosen. These fixed x offsets give 3 different locations with varying y distances with respect to the center of rotation of the Flying-V. These three locations to compare with each other are to be called: in-board, middle, and out-board, see Figure 4.7. Table 4.1 shows the coordinates of the different y locations in the three different x offsets. x is the longitudinal distance between the seat and the aircraft's

c.g., which is located at 29.3m from the nose of the aircraft. y is the lateral distance between the seat and the center of rotation.

Specific force F_x In this section, the longitudinal specific forces will be calculated and analyzed for different locations in the Flying-V for the 26° rotated seat configuration. Firstly, the specific force at the c.g. needs to be calculated. This can be done by:

$$(\frac{1}{M})F_{x(\text{c.g.})} = \dot{u} + q \cdot w - r \cdot v + g \cdot \sin(\theta) \tag{4.6}$$

In order to further analyze the components of the longitudinal specific force, Equation (4.3) needs to be arranged:

$$F_{x(\text{DERP})} = (q \cdot y_{\text{DERP}} + r \cdot z_{\text{DERP}}) \cdot p + (-x_{\text{DERP}}) \cdot q^2 + (-x_{\text{DERP}}) \cdot r^2 + (z_{\text{DERP}}) \cdot \dot{q} + (-y_{\text{DERP}}) \cdot \dot{r} + F_{x(\text{c.g.})} \tag{4.7}$$

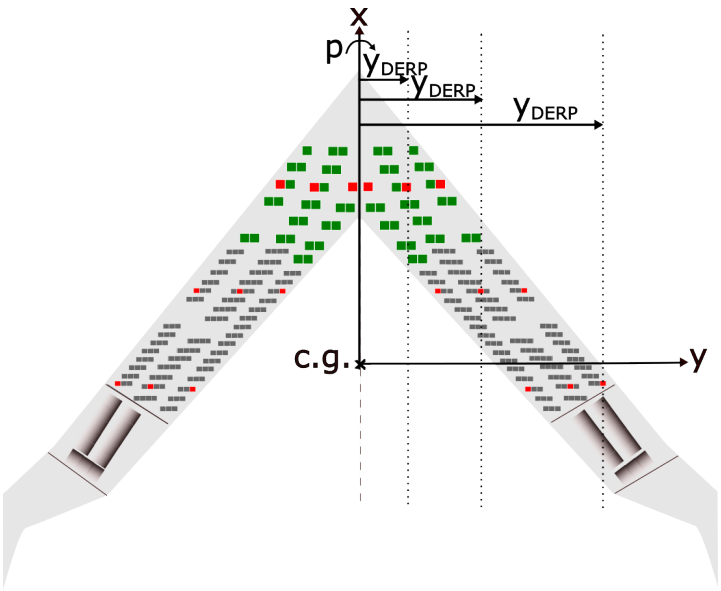

Figure 4.8: Roll rate's arm and contribution to F_x

From Figure 4.8, the contribution of the roll rate for F_x increases linearly with the lateral distance from the center-line of the aircraft, because the arm gets bigger. Thus, the roll rate contribution to F_x increases the more outboard the seats are, because they are further away from the center-line of the aircraft, and they have bigger arm for the moment. Moreover, the roll rate contribution to F_x increases for the seats in the aft locations of the aircraft, compared to the front seats, because they are further away from the center-line of the aircraft.

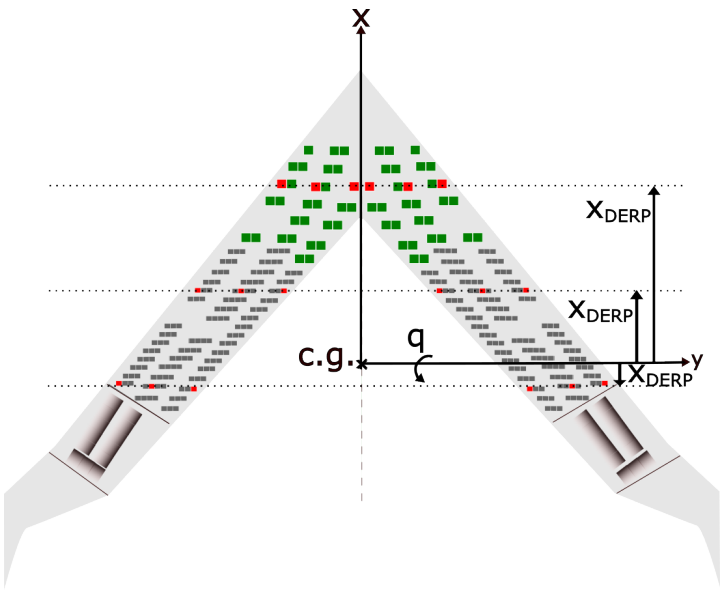

Figure 4.9: Pitch rate's arm and contribution to F_x

Figure 4.9 shows the pitch rate and how the arm of the moment changes depending on the location in the aircraft. Pitch rate contribution to F_x is the biggest for the seats in the front locations of the aircraft because the arm between the c.g. and the seats is the biggest, compared to the other seats in the aft locations in the aircraft. The pitch rate contribution to F_x will be the same for all seats with the same longitudinal position. As a result, passengers will experience the same pitch rate contribution to F_x as they would in a conventional aircraft. The pitch rate contribution to F_x will be smaller for the seats in the aft locations in the aircraft because the arm between the c.g. and the seats gets smaller.

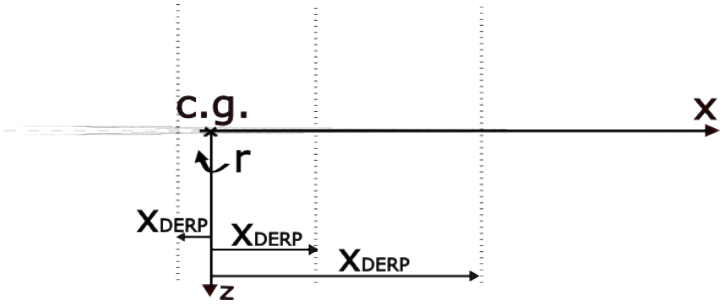

Figure 4.10: Yaw rate's arm and contribution to F_x

Figure 4.10 shows the yaw rate's arm and its contribution to the longitudinal specific force. The yaw rate contribution to F_x increases with the longitudinal position of the seats. As a result, relative to the seats in the aft locations of the aircraft, the yaw rate contribution to F_x for the front locations is greater. This is due to the front seat's larger arm than the aft seats between the c.g. and the seats. Moreover, the yaw rate contribution to F_x will be the same for all seats with the same longitudinal position with respect to the c.g. of the aircraft, therefore, the yaw rate contribution to F_x should not be any different from what passengers would experience in a conventional aircraft.

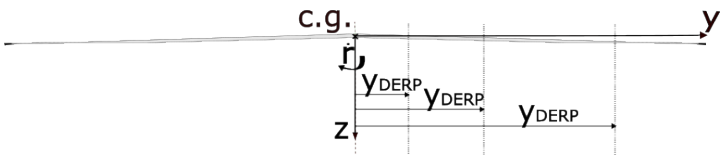

Figure 4.11: $\dot{r}$'s arm and contribution to F_x

Figure 4.11 shows the $\dot{r}$ arm and how its contribution to the longitudinal specific force is dependent on the lateral position of the seats. Thus, for seats of the same longitudinal location, the outboard seats will have higher $\dot{r}$ contribution for F_x because they are further away from the center-line of the aircraft, compared to the inboard and middle seats. Moreover, $\dot{r}$ will increase further for the seats in the aft locations because they are further away from the center-line of the aircraft (thus, have a bigger arm) compared to the front seats in the aircraft.

The specific forces analysis will is done on the collected data from the pilot-in-the-loop experiment for TTB to check which component is the dominant component in the longitudinal specific force. Moreover, the results will be compared to the specific force at the c.g. to see the effect of sitting at a certain offset from it.

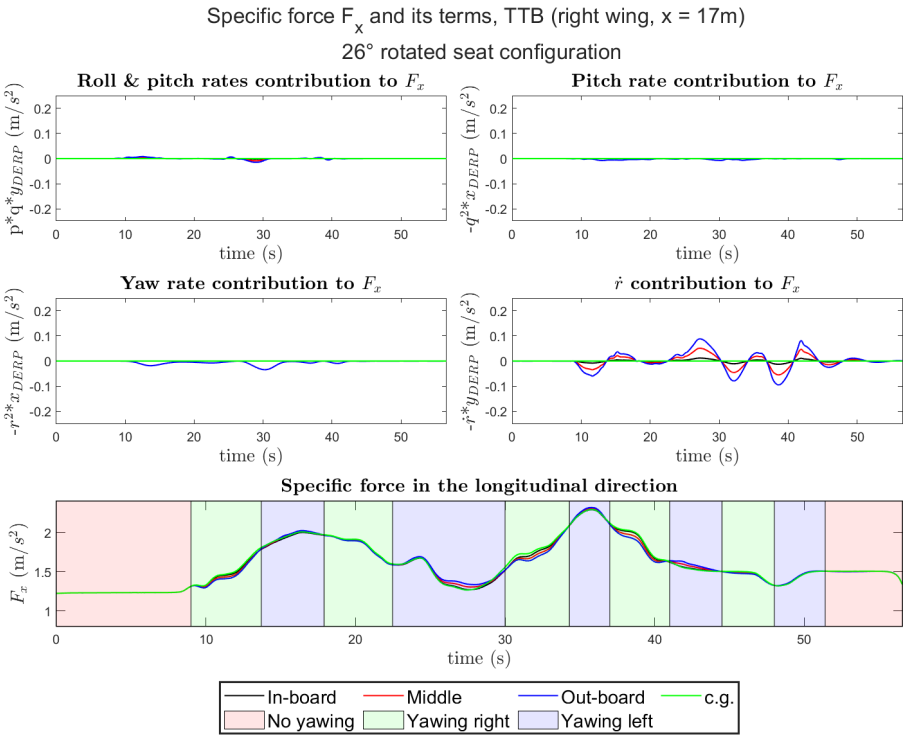

Figure 4.12: Specific force F_x at x = 17m, right wing, 26° rotated seat configuration

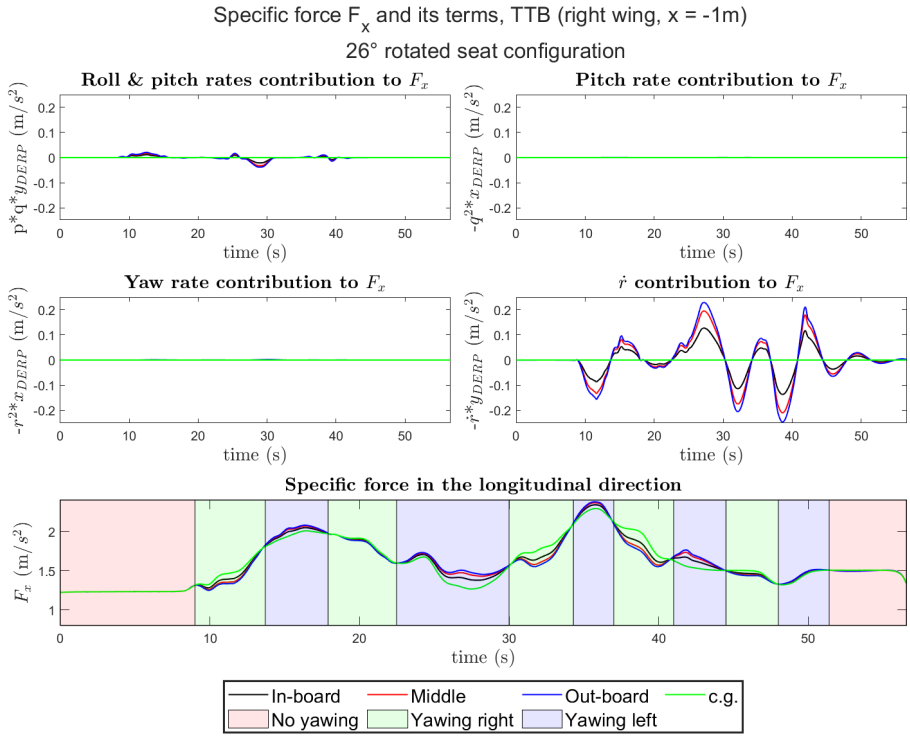

Figure 4.13: Specific force F_y at x = -1m, right wing, 26° rotated seat configuration

Figures 4.12 and 4.13 show F_x for the most front and most aft locations of the right wing in the Flying-V, for the fixed positions that have been determined in Table 4.1. It is clear that the longitudinal specific force's dominant element is $\dot{r}$. The roll, pitch, and yaw rates contribution to F_x are small compared to $\dot{r}$. The $\dot{r}$ contribution to F_x increases linearly with the lateral position of the seats. Therefore, out-board locations have higher $\dot{r}$ contribution to F_x compared to the in-board and middle locations of the same longitudinal location. Moreover, it can be seen that the contribution of $\dot{r}$ to F_x gets bigger for the seats in the aft location because they are further away from the center-line of the aircraft, compared to the seats in the front location. Both wings have the same contribution of $\dot{r}$ to F_x, however, in the opposite direction because the moment arm has a different sign. Since $\dot{r}$ is the dominant component of F_x, the different phases of the maneuver (when yawing right and left, or no yawing) are indicated in the total F_x graph. It can be seen that when the aircraft is yawing right, the outboard location have a lower F_x compared to the c.g., middle, and in-board locations. When yawing left, the outboard location have a higher F_x compared to the c.g., middle, and in-board locations.

Specific force F_y In this section, the lateral specific forces are calculated for the 26° rotated seat configuration. The lateral specific force at the c.g. can be calculated by:

$$(\frac{1}{M})F_{y(\text{c.g.})} = \dot{v} + r \cdot u - p \cdot w - g \cdot \cos(\theta) \cdot \sin(\phi) \tag{4.8}$$

Further analysing F_y, roll, pitch, yaw rates, and $\dot{r}$ can be investigated. Equation (4.4) becomes:

$$F_{y(\text{DERP})} = (q \cdot x_{\text{DERP}}) \cdot p - (y_{\text{DERP}}) \cdot p^2 + (r \cdot z_{\text{DERP}}) \cdot q + (-y_{\text{DERP}}) \cdot r^2 + (-z_{\text{DERP}}) \cdot \dot{p} + (x_{\text{DERP}}) \cdot \dot{r} + F_{y(\text{c.g.})} \tag{4.9}$$

Pitch rate's arm can be seen in Figure 4.9. Thus, the pitch rate contribution to F_y should get smaller for the aft seats because the moment arm gets smaller. However, the pitch rate is coupled with the roll rate. Similarly to F_x, roll rate contribution to F_y increases for the outboard locations compared to the in-board locations, because they are further away from the center-line of the aircraft, thus, have a bigger arm, see Figure 4.8. Moreover, the roll rate contribution to F_y increases more for the seats in the aft locations compared to the seats in the front locations because they are further away from the center-line.

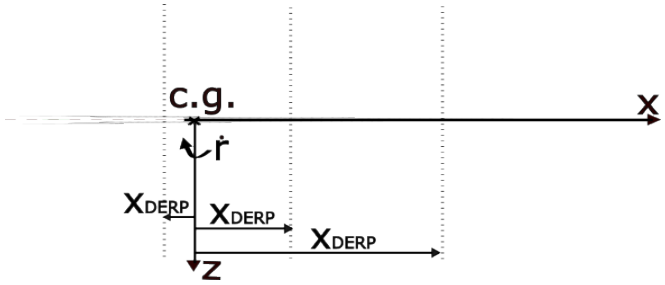

Figure 4.14: $\dot{r}$'s arm and contribution to F_y

The arm of $\dot{r}$ and its contribution to F_y are shown in Figure 4.14, $\dot{r}$ contribution to F_y is the biggest for the seats in the front locations because the arm is the biggest, compared to the seats in the aft locations. This contribution gets smaller the closer the location is to the c.g..

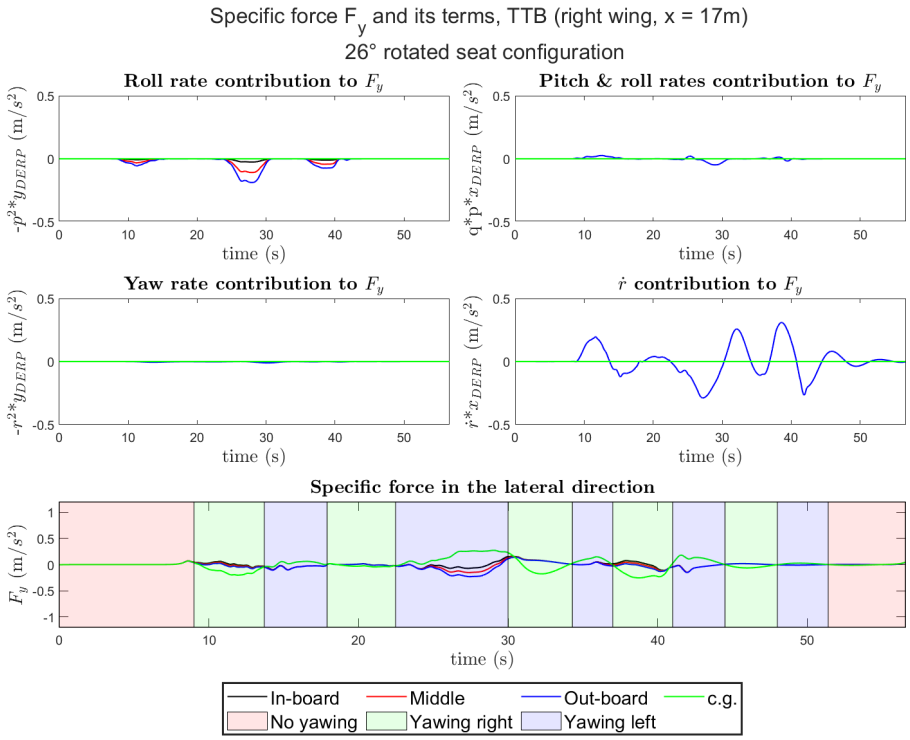

Figure 4.15: Specific force F_y at x = 17m, right wing, 26° rotated seat configuration

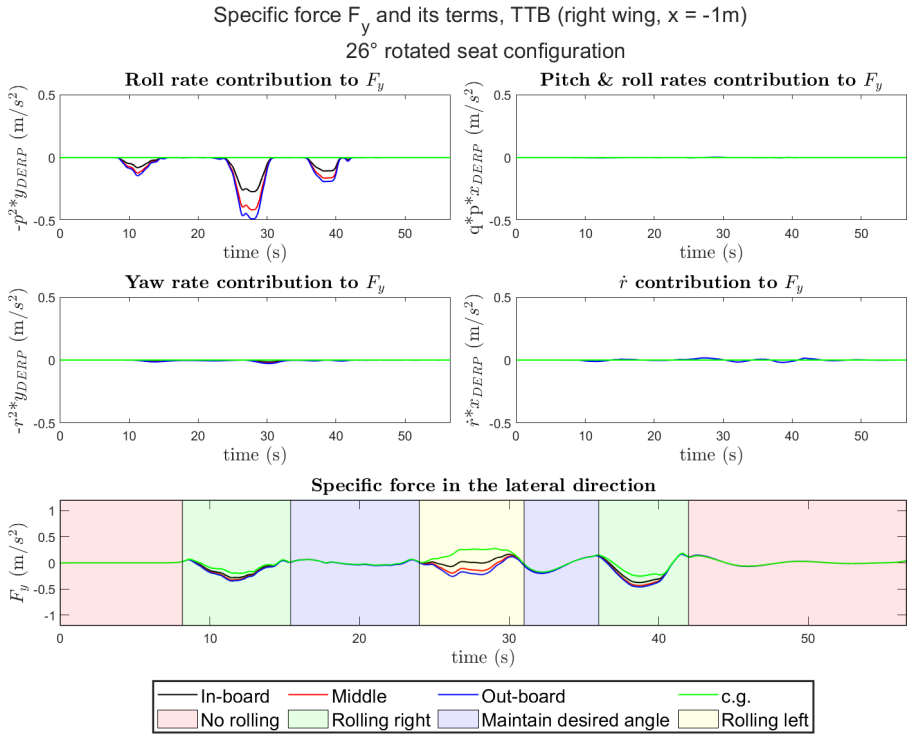

Figure 4.16: Specific force F_y at x = -1m, right wing, 26° rotated seat configuration

Figures 4.15, and 4.16 show the lateral specific force F_y for the most front and most aft locations in the Flying-V (x = 17m, and -1m). The main contributor to the lateral specific force for the front seats is $\dot{r}$. All seats in the same longitudinal position have the same $\dot{r}$ contribution to F_y and this contribution to F_y decreases for the seats in the aft locations. The roll rate contribution to F_y gets bigger for the aft locations because the seats are further away from the center-line. The roll rate contribution to F_y increases linearly for the outboard locations compared to the inboard and middle locations, $\dot{r}$ contribution to F_y is the same for both wings. Both wings have the same roll rate contribution to F_y; however, they have a different sign for the moment arm. The total F_y for the front seats (thus, x = 17m) is colored based on the different yaw phases in the maneuver. It can be seen from Figure 4.15 that for the inboard locations, the lateral specific force is similar to what the passenger would experience in a conventional aircraft seat. The biggest difference between the seats is when yawing left, where the outboard locations have more negative lateral specific force compared to the inboard locations. For the seats in the aft location (thus, x = -1m), the total F_y is colored based on the different roll phases in the maneuver, see Figure 4.16. It can still be seen that the biggest difference between the seats is when rolling left, when changing from the positive bank angle to the negative bank angle. Thus, the outboard locations will have more negative lateral specific force compared to the inboard and middle locations.

Specific force F_z In this section, the vertical specific force is calculated and analyzed for the most aft and most front of the Flying-V. firstly, to calculate the vertical specific force at the c.g.:

$$(\frac{1}{M})F_{z(\text{c.g.})} = \dot{w} + p \cdot v - q \cdot u - g \cdot \cos(\theta) \cdot \cos(\phi) \tag{4.10}$$

Further, analyzing F_z to transform to different locations in the Flying-V, equation (4.5) can be re-written to:

$$F_{z(\text{DERP})} = (r \cdot x_{\text{DERP}} - p \cdot z_{\text{DERP}}) \cdot p + (y_{\text{DERP}}) \cdot \dot{p} + (-x_{\text{DERP}}) \cdot \dot{q} + (r \cdot y_{\text{DERP}} - q \cdot z_{\text{DERP}}) \cdot q + F_{z(\text{c.g.})} \tag{4.11}$$

In addition to the roll and yaw rates, that have been explained in Section 4.1.2, F_z have an additional $\dot{p}$ and $\dot{q}$ components.

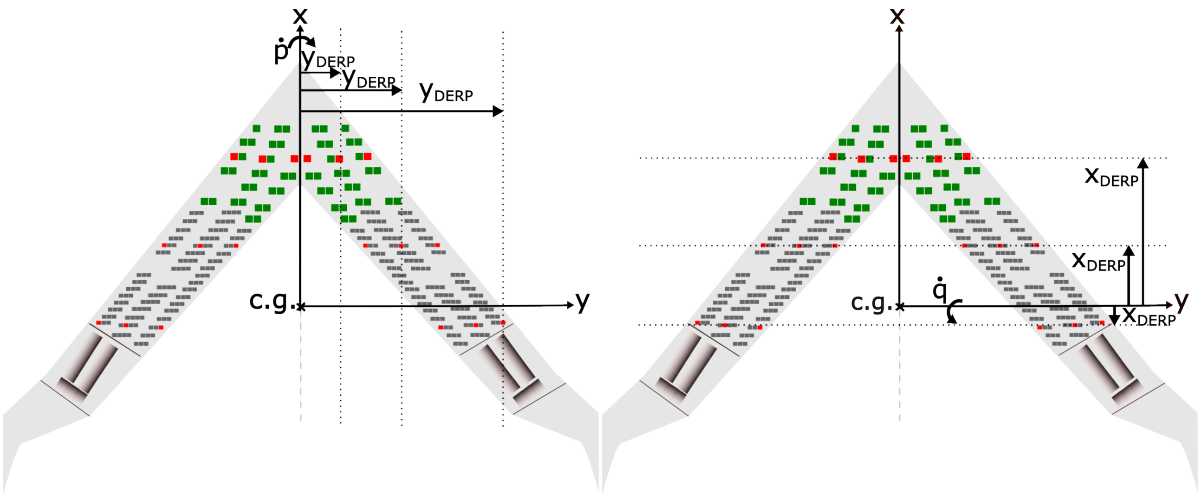

(a) $\dot{p}$'s arm and contribution to F_z

(b) $\dot{q}$'s arm and contribution to F_z

Figure 4.17: $\dot{p}$ and $\dot{q}$'s arms and contribution to F_z

Figure 4.17 shows $\dot{p}$'s and $\dot{q}$'s arms depending on the locations of the seats. $\dot{p}$ contribution to F_z increases linearly with the lateral position of the seats. $\dot{q}$ contribution to F_z is higher for the seats in the front location compared to the seats in the aft location.

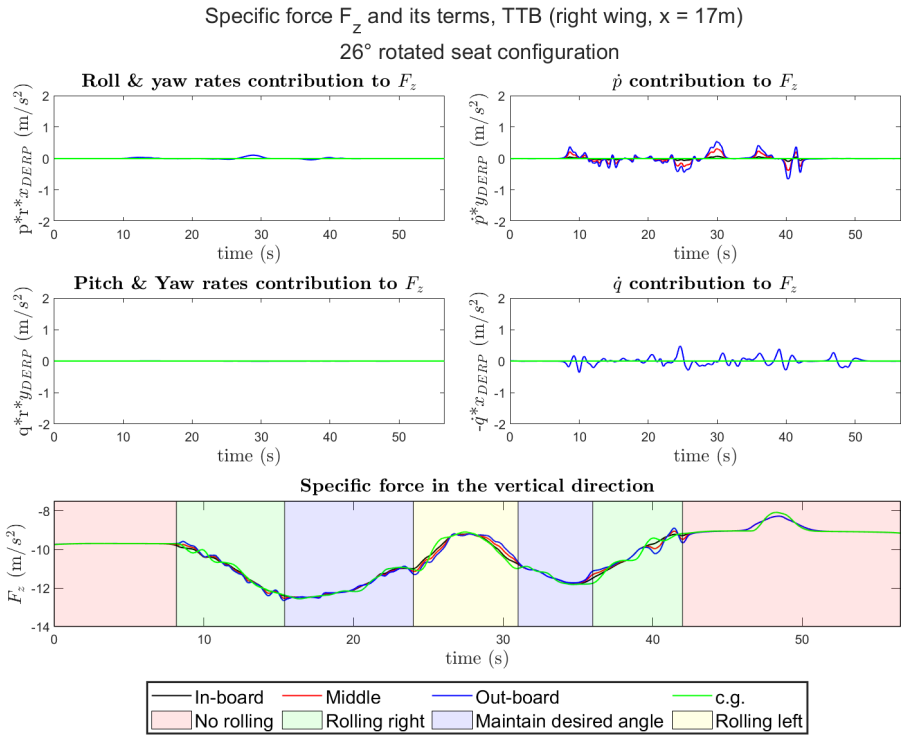

Figure 4.18: Specific force F_z at x = 17m, right wing, 26° rotated seat configuration

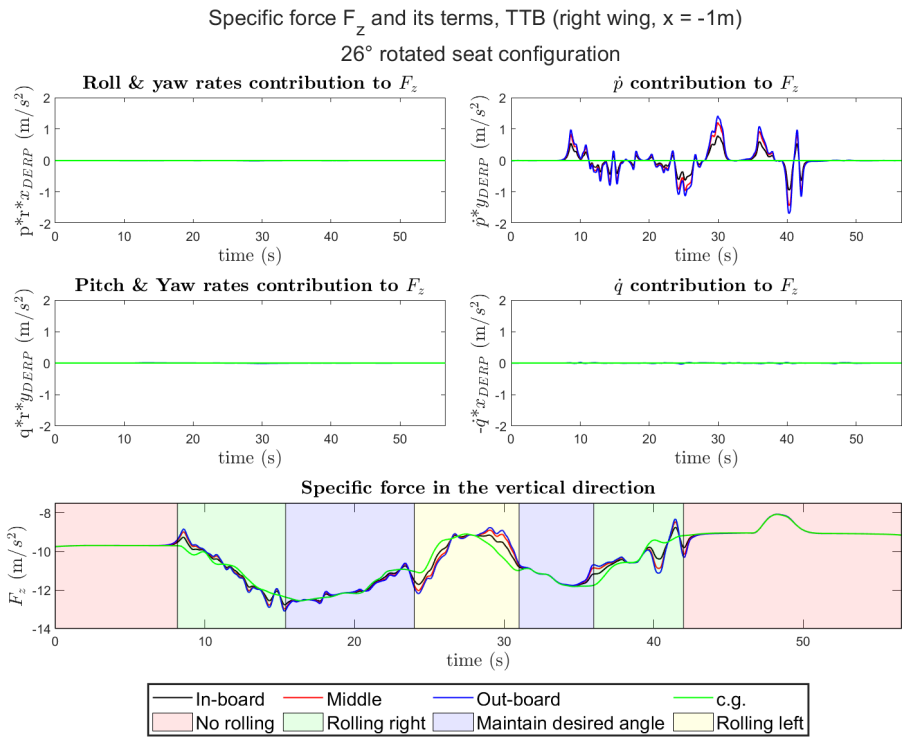

Figure 4.19: Specific force F_z at x = -1m, right wing, 26° rotated seat configuration

The terms for the vertical specific force and the total F_z are shown in Figures 4.18 and 4.19 for the most aft and most front of the Flying-V, for the right wing. It is clear that the $\dot{p}$ contribution to F_z increases for the aft locations (x = -1m) since they are further away from the center-line compared to the front locations, $\dot{p}$ contribution to F_z is the same for both wings; however, the moment arm has a different sign. Furthermore, outboard locations of the same longitudinal location have a higher $\dot{p}$ contribution to F_z, compared to the in-board and middle locations. Moreover, it can be seen that $\dot{q}$ contribution to F_z gets smaller for the aft locations; however, it is the same of what a passenger would experience in a conventional aircraft seat. Since $\dot{p}$ is the dominant term for the vertical specific force, F_z is colored according to the roll phases of the maneuver. Therefore, when rolling right, the seats on the right wing have a downward vertical acceleration compared to the seats on the left wing, which will have an upward vertical acceleration.

4.1.3. 0° rotated seats

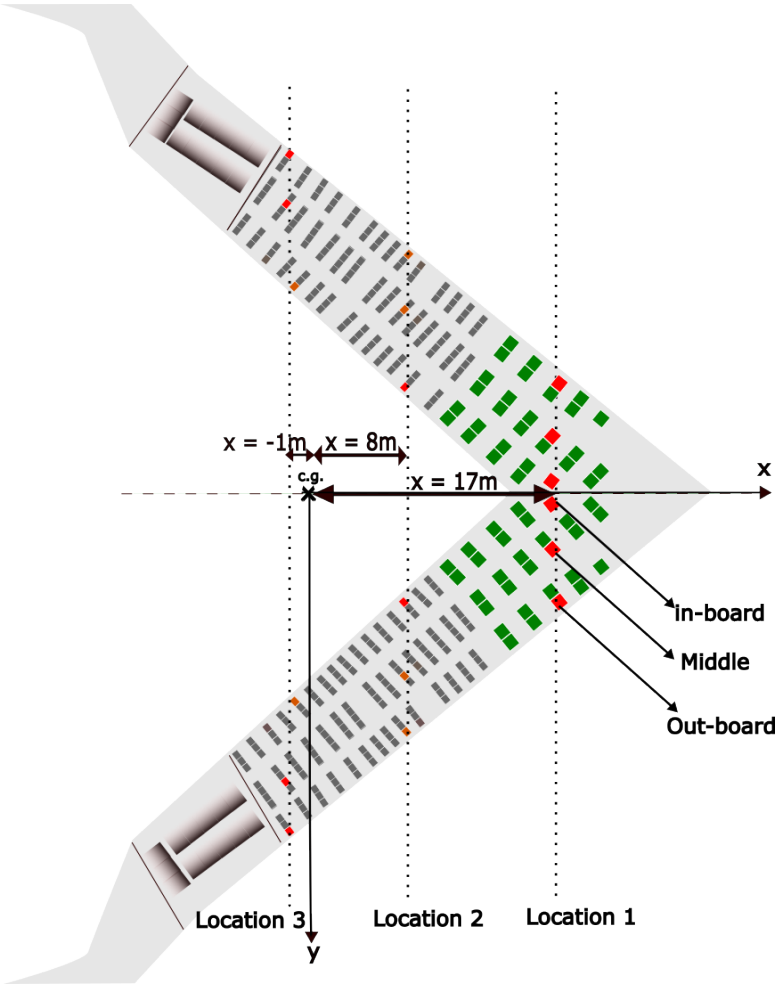

Figure 4.20: 0° rotated seat in the Flying-V

The second seat configuration that will be investigated is the 0° rotated seat configuration, which is parallel to the aisles and the longitudinal axis of the fuselage, as can be seen in Figure 4.20. Therefore, a rotation matrix needs to be applied since the reference frame of the c.g. is different from the reference frame of the seats, it will be rotated around the z-axis by 26°. The seat coordinates are still the same as those shown in table 4.1.

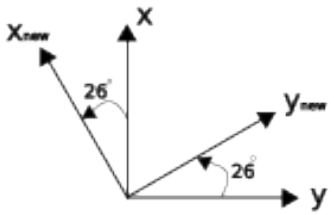

Figure 4.21: Reference frame change

Figure 4.21 shows how the reference frame is rotated and applied to the right wing; the left wing, however, should be a clockwise rotation. The specific forces need to be rotated accordingly. The rotation matrix is:

$$R_z(\psi) = \begin{pmatrix} cos(\psi) & sin(\psi) & 0 \\ -sin(\psi) & cos(\psi) & 0 \\ 0 & 0 & 1 \end{pmatrix} \tag{4.12}$$

Therefore, F_x and F_y should change, and F_z should stay the same for both seat configurations since the rotation is happening around the z-axis.

Specific force F_x In this section, the longitudinal specific force is calculated for the 0° rotated seat configuration.

Similar to Section 4.1.2 and how the specific force terms have been analyzed for the 26° rotated seat configuration, this has been done as well for the 0° rotated seat configuration.

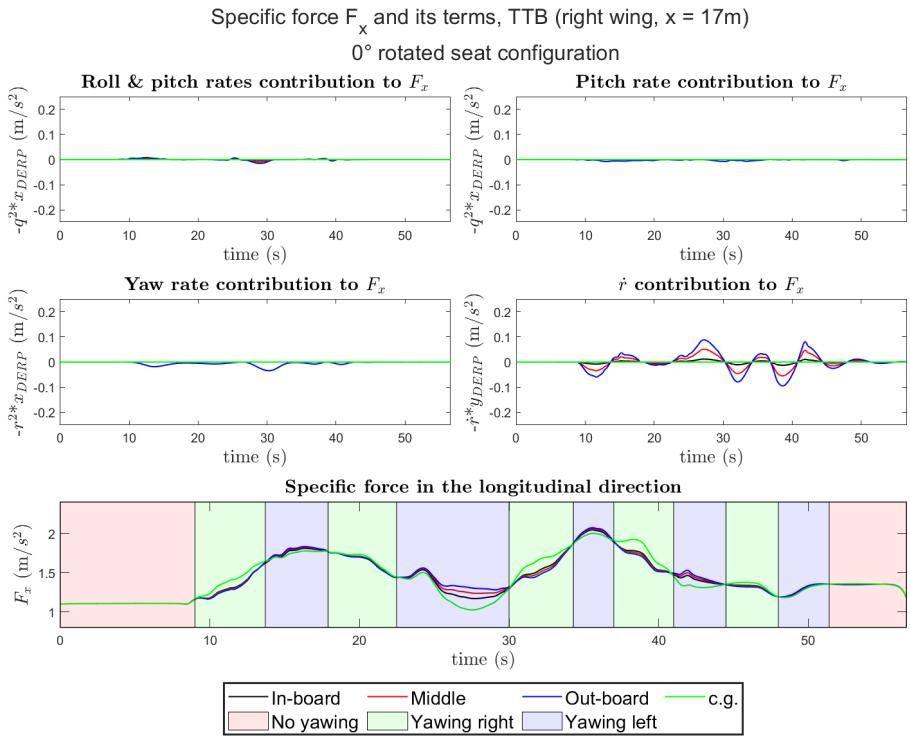

Figure 4.22: Specific force F_x at x = 17m, right wing, 0° rotated seat configuration

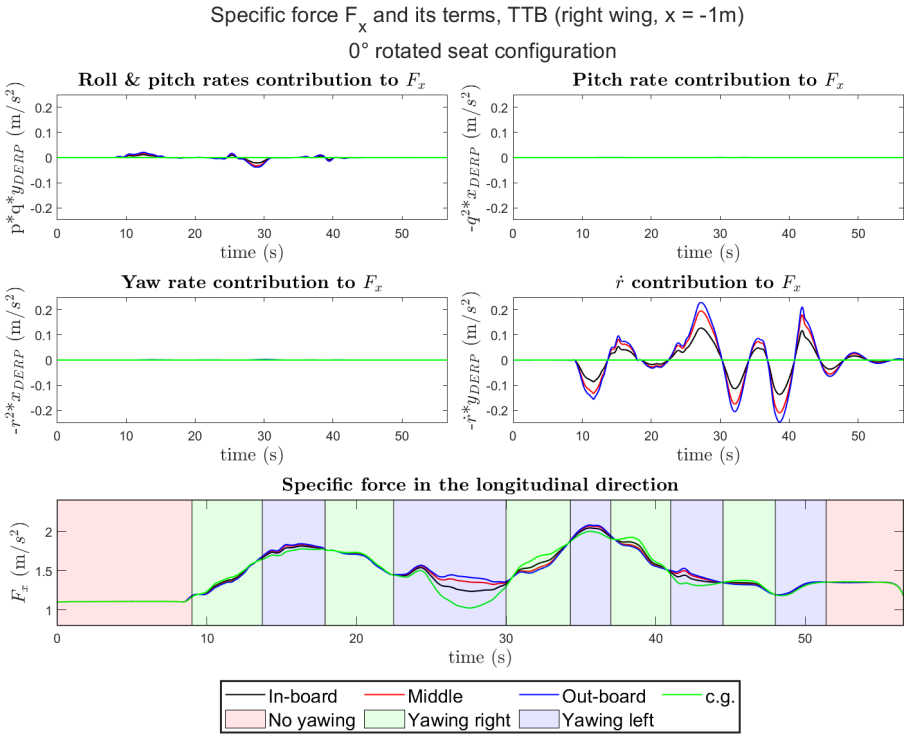

Figure 4.23: Specific force F_x at x = -1m, right wing, 0° rotated seat configuration

Figures 4.22 and 4.23 show the longitudinal specific force and its terms for the most aft and most front of the Flying-V, for the right wing. Similarly to the 26° rotated seat configuration, $\dot{r}$ is the dominant component in F_x. However, because the arm gets shorter, this contribution gets smaller for the aft locations. $\dot{p}$ contribution to F_x increases linearly for the out-board locations, and it gets higher for the aft locations since they are further away from the center-line of the aircraft. The pitch trimmed angle contribution is split between F_x and F_y, which results in a relatively lower longitudinal specific force than the 26° rotated seat configuration. Therefore, some of the longitudinal specific force will be perceived as lateral specific force for the 0° rotated seat configuration.

Specific force F_y The lateral specific force is calculated in this section for the 0° rotated seat configuration.

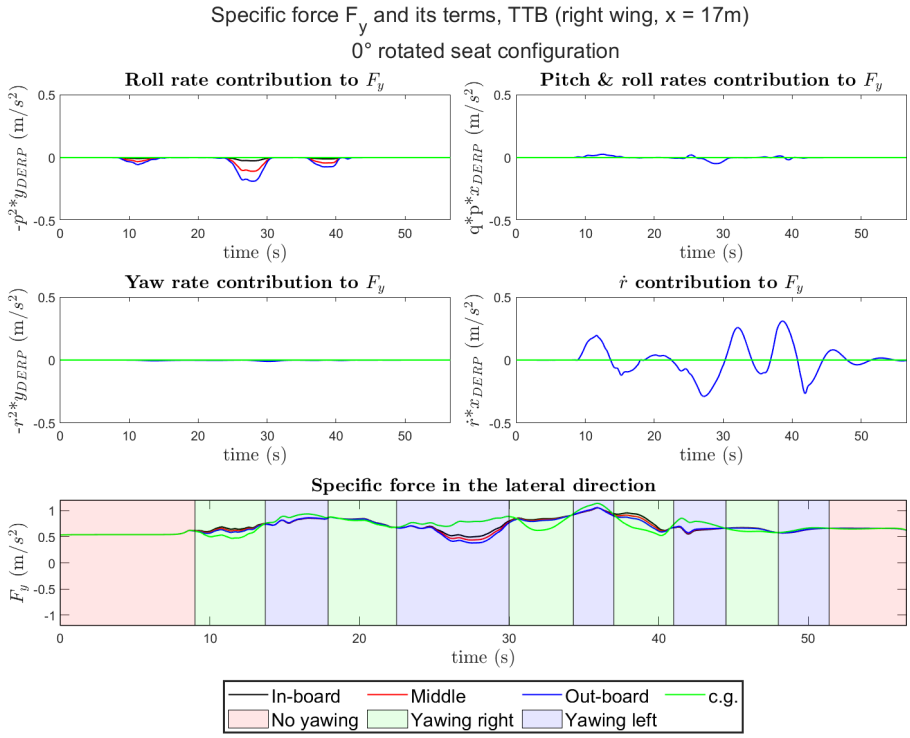

Figure 4.24: Specific force F_y at x = 17m, right wing, 0° rotated seat configuration

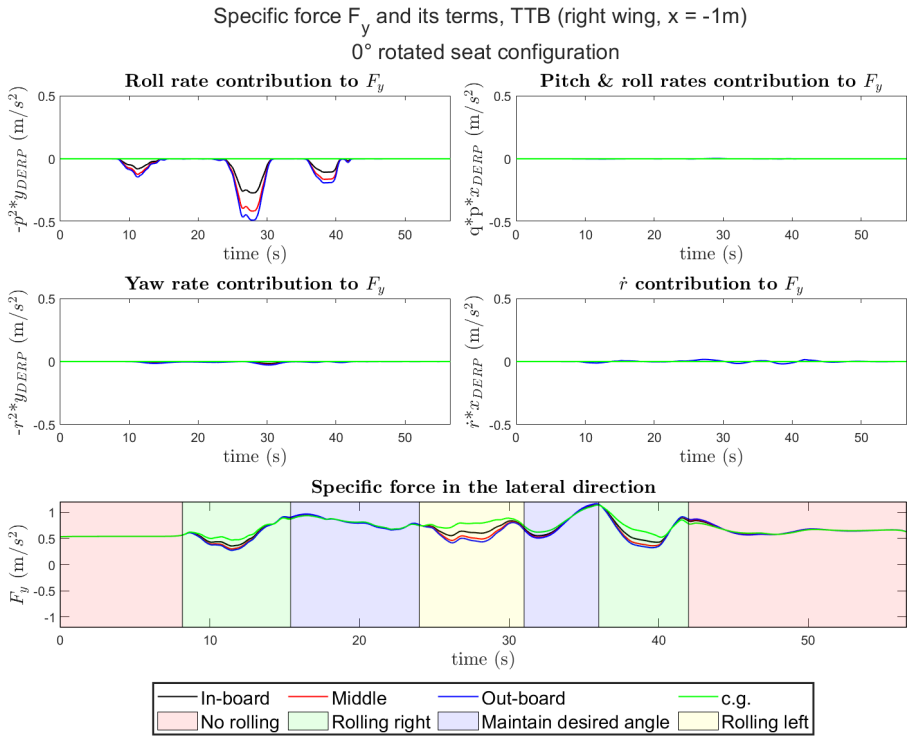

Figure 4.25: Specific force F_y at x = -1m, right wing, 0° rotated seat configuration

Figures 4.24 and 4.25 show the lateral specific force for the right wing. The roll rate contribution to F_y gets bigger for the aft locations. Similarly to the 26° rotated seat configuration, $\dot{r}$ is the dominant component for the front locations, then $\dot{r}$ decreases for the aft locations and the roll rate becomes the dominant component.

It can be seen that the initial value of the lateral specific force is different from the one from the 26° rotated seat configuration since the seats are rotated 26°, and it has a contribution from the pitch trimmed angle. It starts with a positive value for the right wing and a negative value for the left wing.

Specific force F_z The vertical specific force for the 0° rotated seat configuration should be the same as the vertical specific force for the 26° rotated seat configuration, since the z-axis is not rotated.

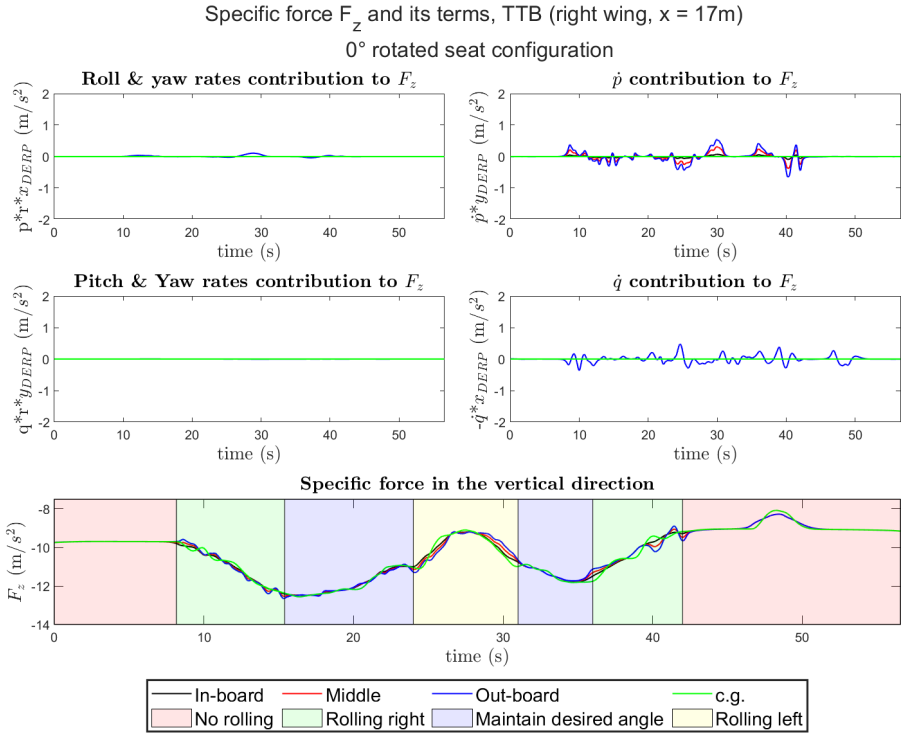

Figure 4.26: Specific force F_z at x = 17m, right wing, 0° seat configuration

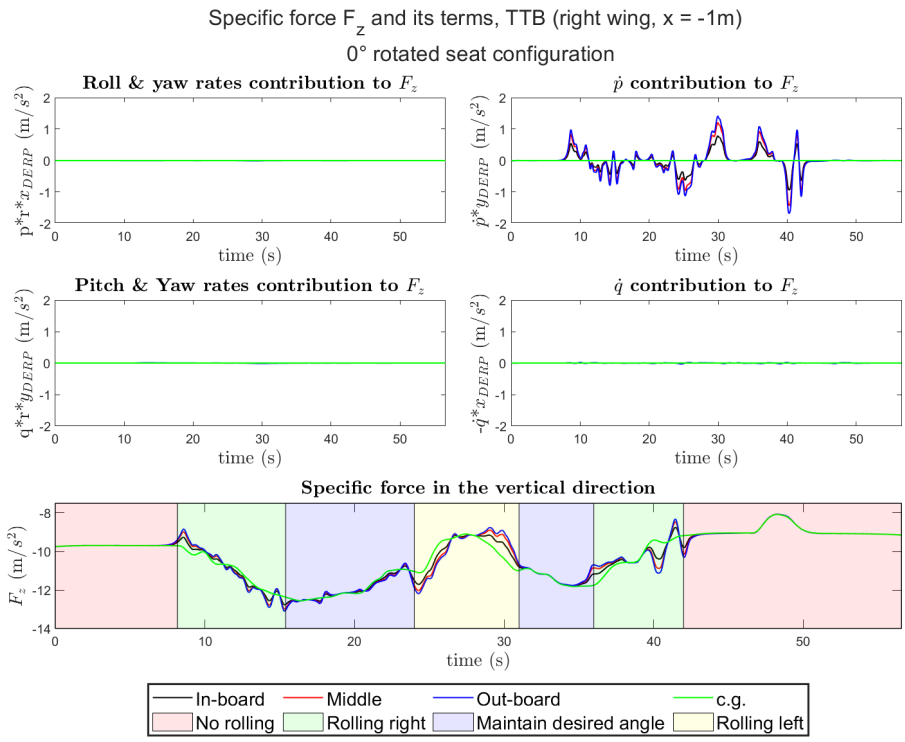

Figure 4.27: Specific force F_z at x = -1m, right wing, 0° seat configuration

4.1.4. Validation

Simple maneuvers of roll, pitch, and yaw have been done to match the phases of the roll, pitch, and yaw phases in the TTB maneuver. The simple cases of roll, pitch, and yaw have been fitted to the flight data of TTB through a sigmoid function. A sigmoid function is used to fit the flight data, so its parameters can be varied to best fit the important characteristics of the flight data, such as the roll rate at which the aircraft needs to go from +30° to -30° in rolling. These simple maneuvers have been done in order to determine which of the roll, pitch, and yaw at c.g. is the dominant maneuver while flying in the Flying-V, and which causes the biggest differences in the specific forces between different locations in the Flying-V and the c.g.. Moreover, doing these simple maneuvers by fitting a sigmoid function will reveal whether the results are still influenced by the artifact of the model that produced the flight data, even after filtering them, or whether the results obtained are correct. The results of these simple maneuvers are provided in a supporting document that is attached with this report. In this section, the final results of performing these simple maneuvers are presented.

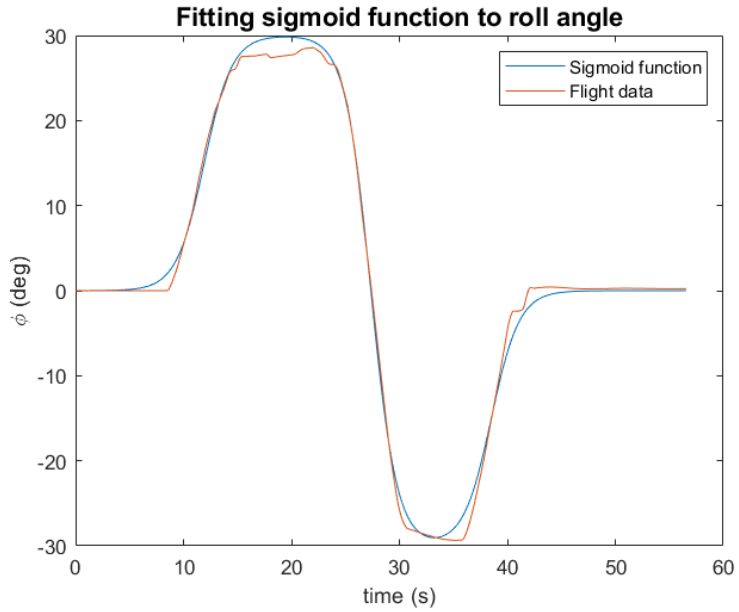

Figure 4.28: Fitting sigmoid function to ϕ flight data

Figure 4.28 shows an example of fitting a sigmoid function to the ϕ data from the flight data. The important characteristics of the maneuver such as the rate at which the aircraft is rolling is kept. The same is applied for yawing and pitching.

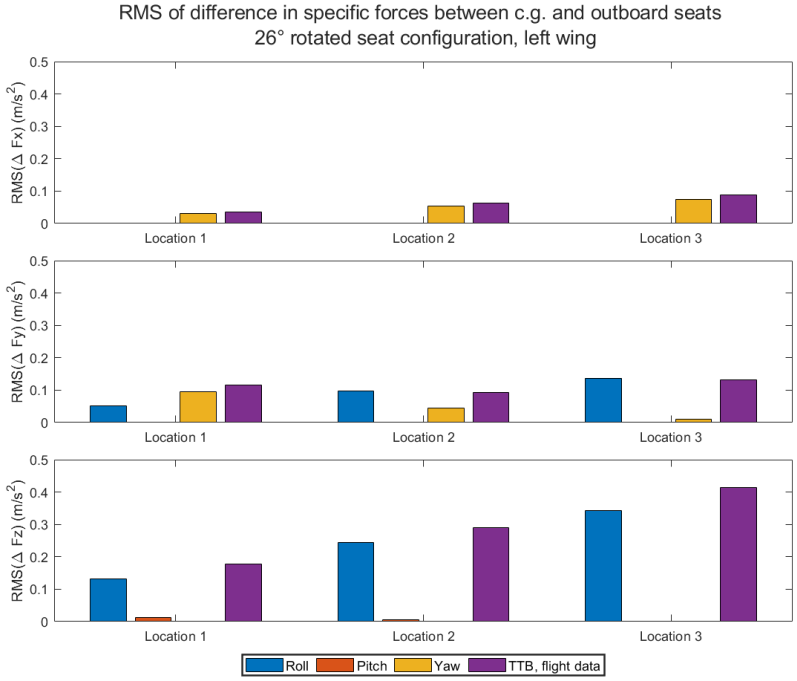

Figure 4.29: RMS Specific forces differences for the left wing, 26° rotated seat configuration

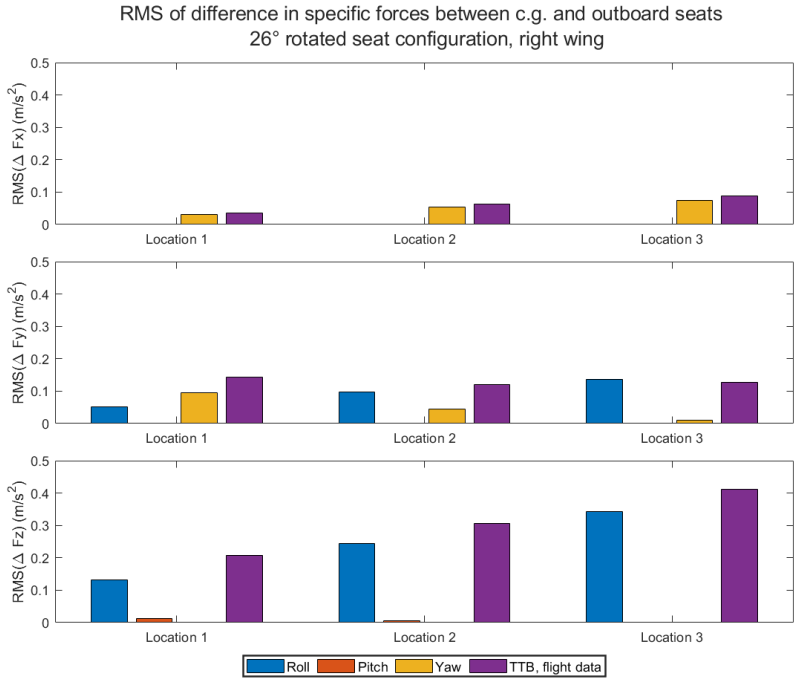

Figure 4.30: RMS Specific forces differences for the right wing, 26° rotated seat configuration

Figures 4.29 and 4.30 show the RMS difference in the specific forces between the c.g. position and the outboard locations, for the right and left wings, due to the asymmetry of the recorded maneuver. In comparison to the longitudinal specific force F_x and the lateral specific force F_y, the difference in the vertical specific force F_z shows the greatest difference between the seat positions and the c.g.. Furthermore, it can be seen that the roll is the primary contributor to the TTB maneuver's F_z. Additionally, in F_x and F_y, the difference between seats that are farther away from the center-line and seats that are closer to the center-line is small compared to the difference in F_z.

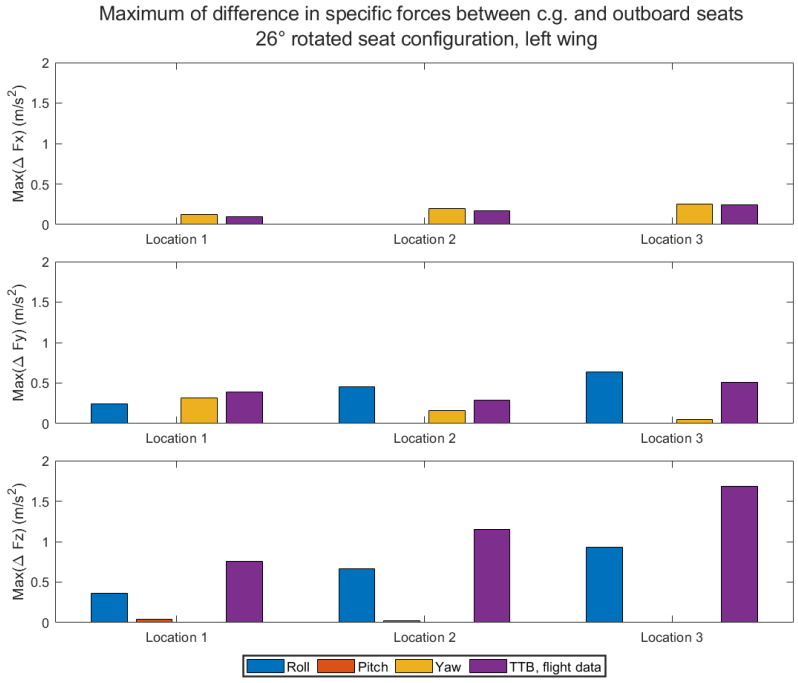

Figure 4.31: Maximum Specific forces differences for the left wing, 26° rotated seat configuration

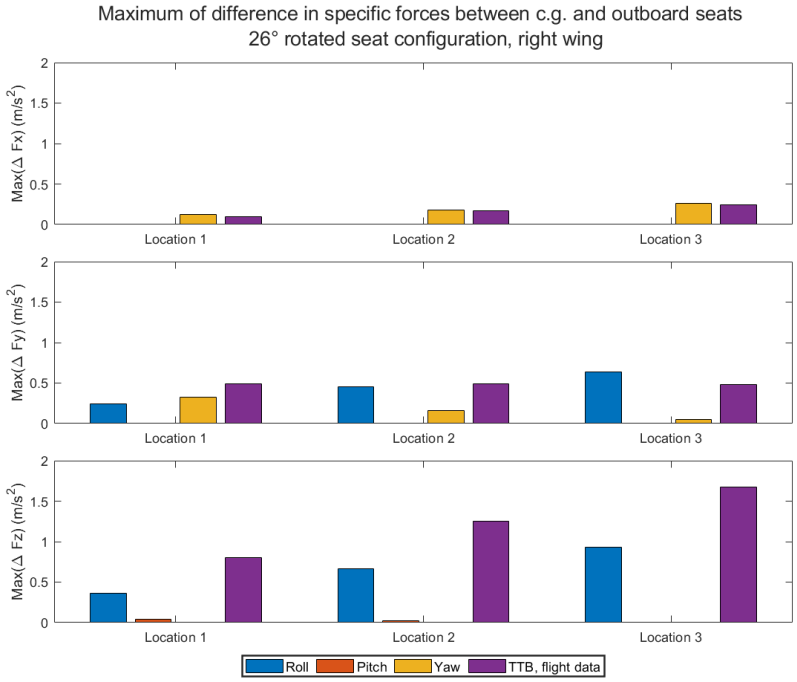

Figure 4.32: Maximum Specific forces differences for the right wing, 26° rotated seat configuration

The largest difference in specific forces between the c.g. and the outboard seats is shown in Figures 4.31 and 4.32. In comparison to F_x and F_y, it can be seen that F_z has the greatest difference with c.g., and this difference increases the further the seat is from the center-line of the aircraft. This difference gets up to 1.5m/s^2 using the flight data of TTB and 1m/s^2 using only the roll phase of the maneuver. The maximum difference for F_x increases marginally as the seats are moved away from the center line; this maximum reaches around 0.1m/s^2 for the farthest seat from the center-line. The maximum difference for F_y is somewhat indifferent for the seats in the different locations in the Flying-V.

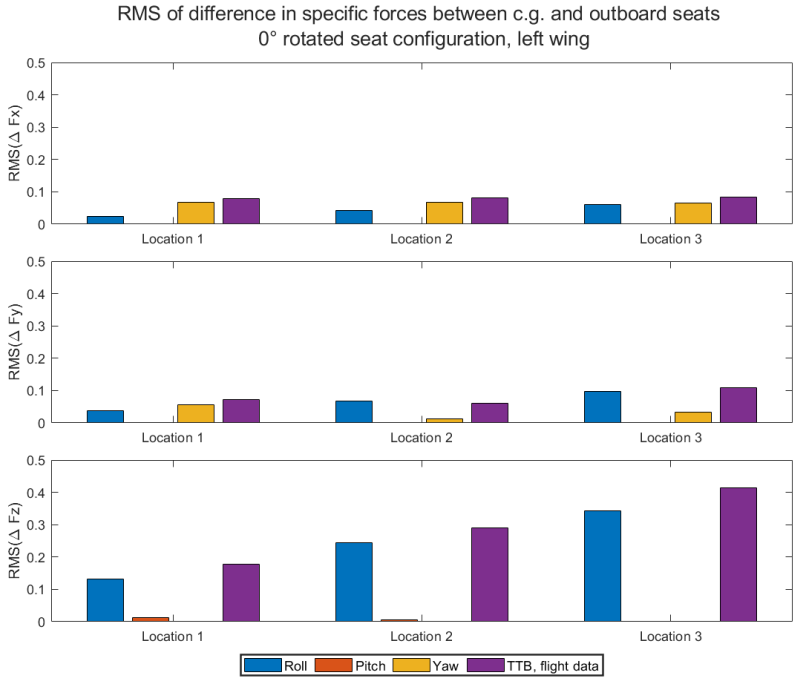

Figure 4.33: RMS Specific forces differences for the left wing, 0° rotated seat configuration

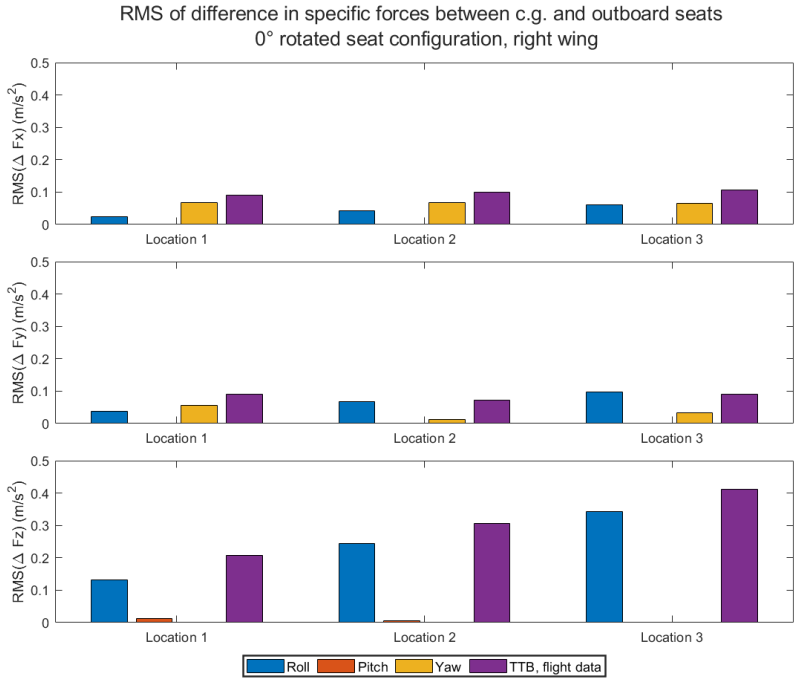

Figure 4.34: RMS Specific forces differences for the right wing, 0° rotated seat configuration

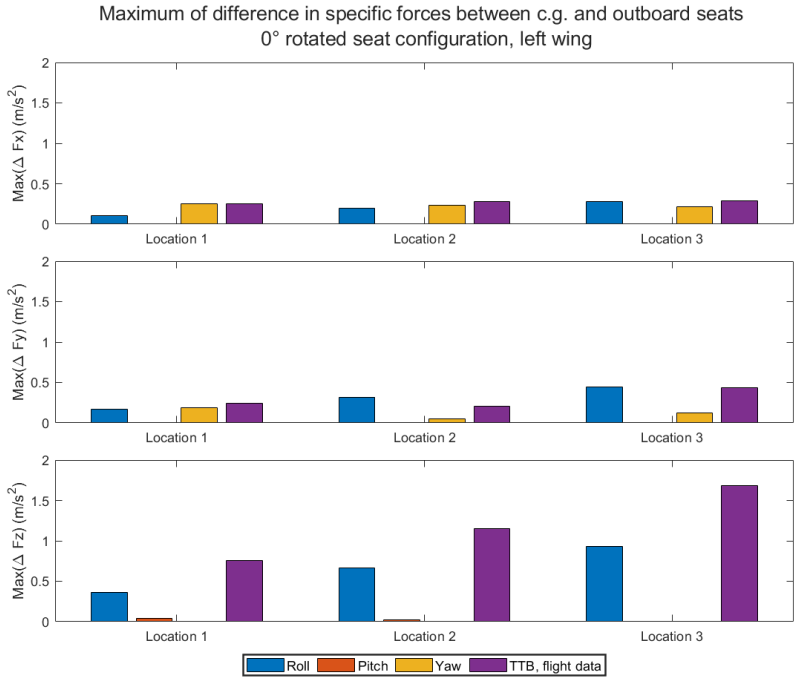

Figure 4.35: Maximum Specific forces differences for the left wing, 0° rotated seat configuration

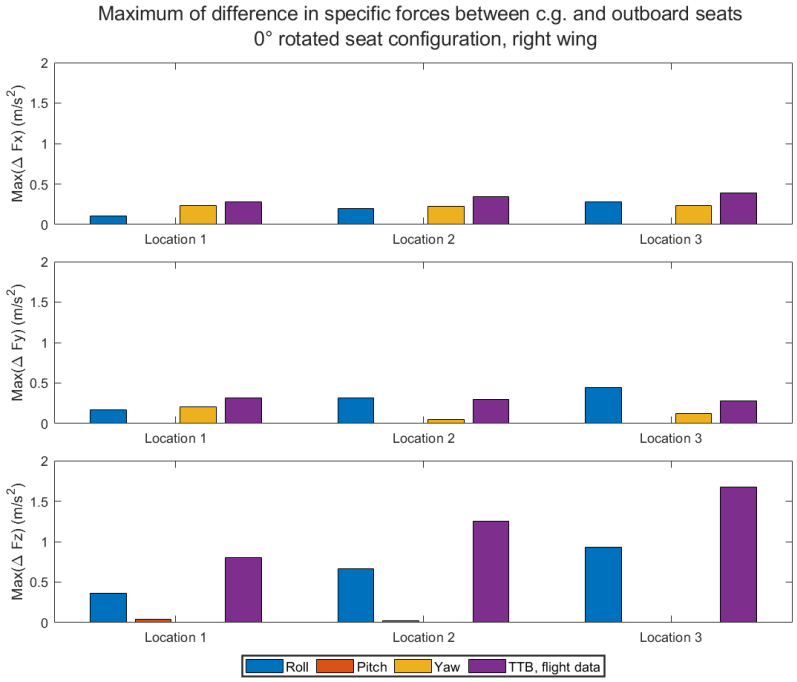

Figure 4.36: Maximum Specific forces differences for the right wing, 0° rotated seat configuration

For a 0° rotated seat layout, Figures 4.33, 4.34, 4.35, and 4.36 display the RMS and maximum difference between center-line and outboard seats. As shown, the contributions of F_x and F_y are different. For F_x and F_y, the roll contribution has changed; the same is true for yaw. Therefore, there is a small increase in F_x and a small decrease in F_y, compared to the 0° rotated seat configuration. However, the total vector for F_x and F_y is still the same. F_z is still the same

4.2. Coordinated Turn Capability Maneuver

Similarly to TTB, CTC's collected data from the pilot-in-the-loop experiment has been filtered to remove the strong peaks of the high-frequency components. Appendix D.1 shows filtering the data across a range of break frequencies. A break frequency of 0.5Hz chosen since it filters out the strong peaks of the high-frequency components and keeps the peaks of the low-frequency components.

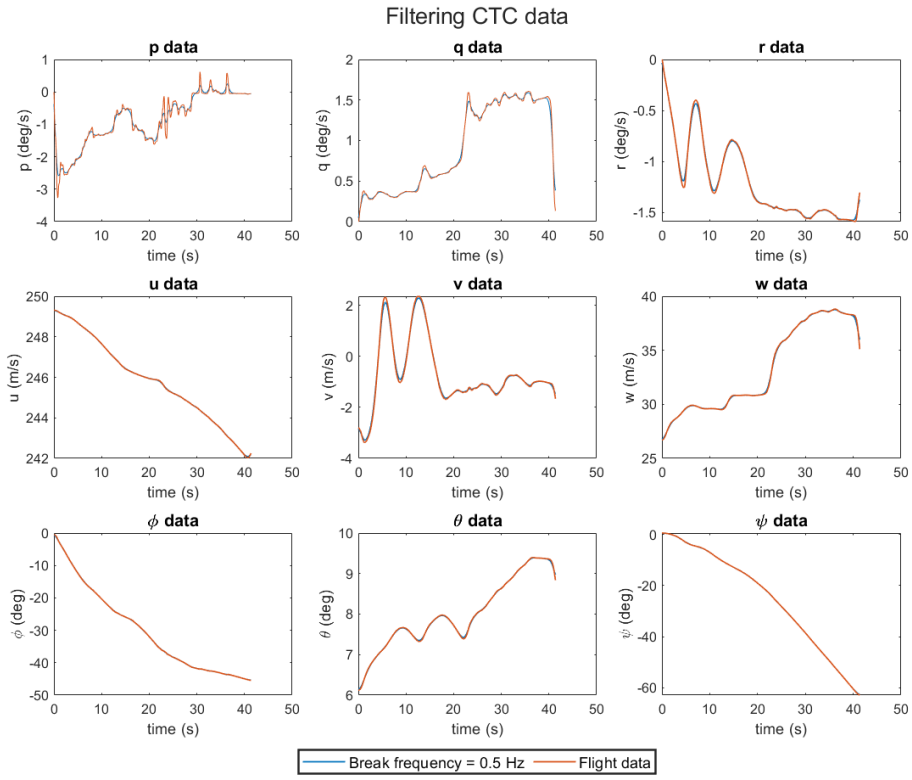

Figure 4.37: Filtering CTC data

Figure 4.37 shows the angular velocities, Euler angles, and body velocities of the CTC maneuver after the data filtering.

4.2.1. Specific forces at the c.g.

The specific forces at the c.g. are calculated using Equation (4.1). The filtered data have been used in this case as well.

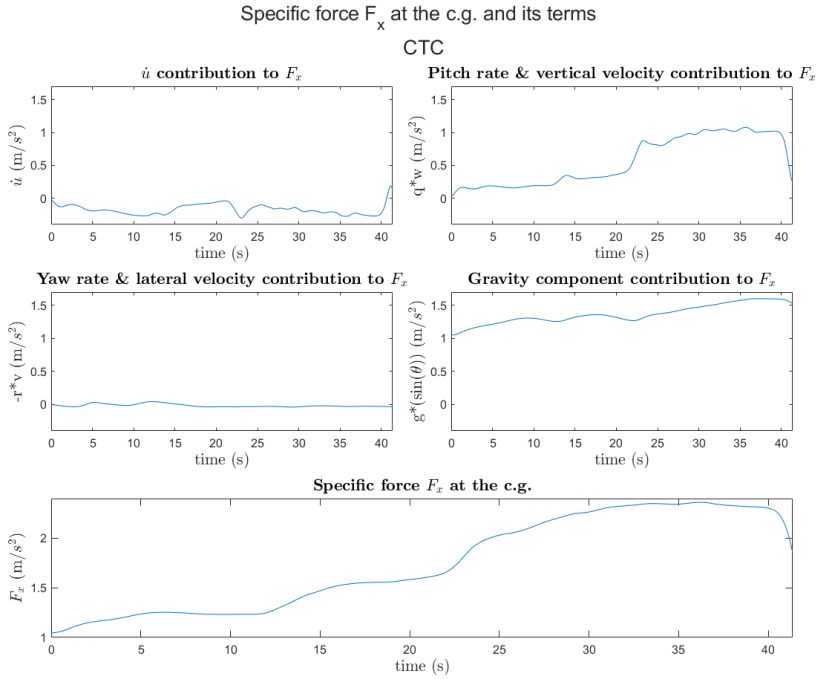

Figure 4.38: Specific force in the longitudinal direction at the c.g. for CTC

Figure 4.38 shows the longitudinal specific force at the c.g.. The F_x is continuously increasing and have a forward longitudinal specific force due to the pitch rate and vertical velocity influence on F_x.

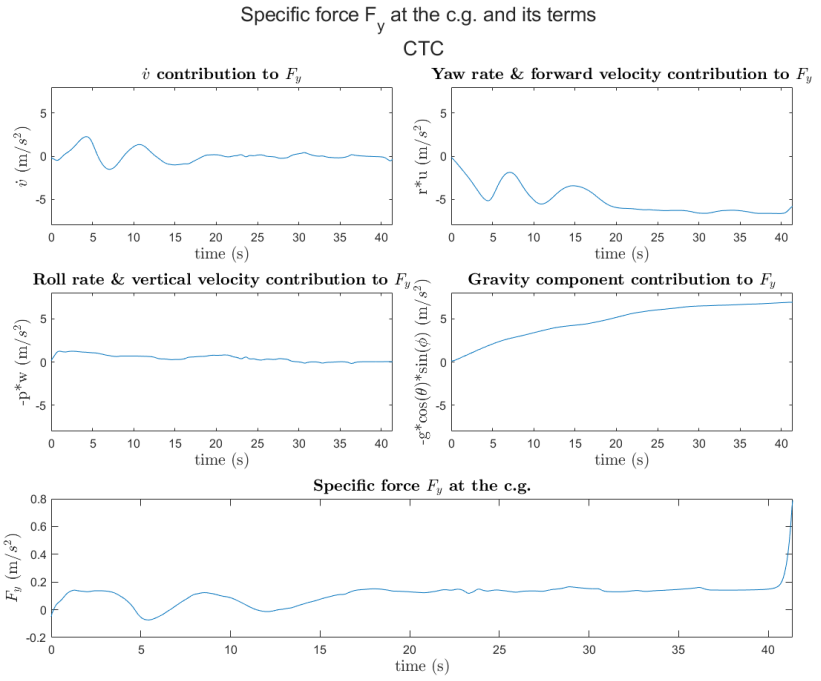

Figure 4.39: Specific force in the lateral direction at the c.g. for CTC

Figure 4.39 shows the lateral specific force at the c.g. The F_y is very small due to the gravity component cancelling most of the yaw rate and forward velocity influence on F_y. It is bounded between 0 - 0.8 m/s^2.

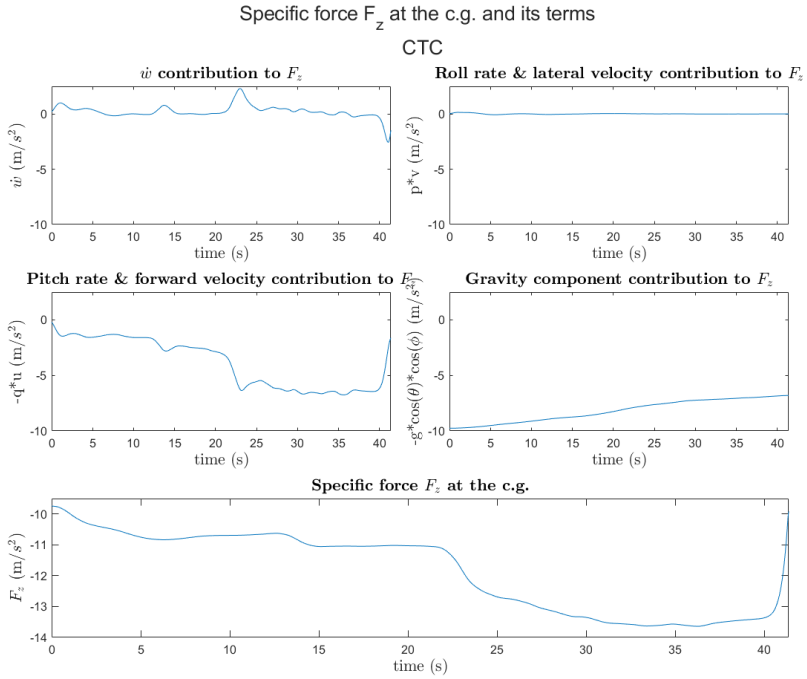

Figure 4.40: Specific force in the vertical direction at the c.g. for CTC

Figure 4.40 shows the vertical specific force at the c.g. The initial value for F_z is around -9.81m/s^2 because of the gravity component. Then there is a decrease in the vertical specific force due to the pitch rate and forward velocity.

4.2.2. 26° rotated Seats

The 26° rotated seat that have been shown in Figure 4.7 are used to calculate the specific forces at the locations that have been specified in Table 4.1. Equations (4.3), (4.4), and (4.5) are used again to transform the specific forces from the c.g. to the chosen locations in the Flying-V.

Specific force F_x Equation (4.7) is used to analyze the terms and their contribution to the longitudinal specific force.

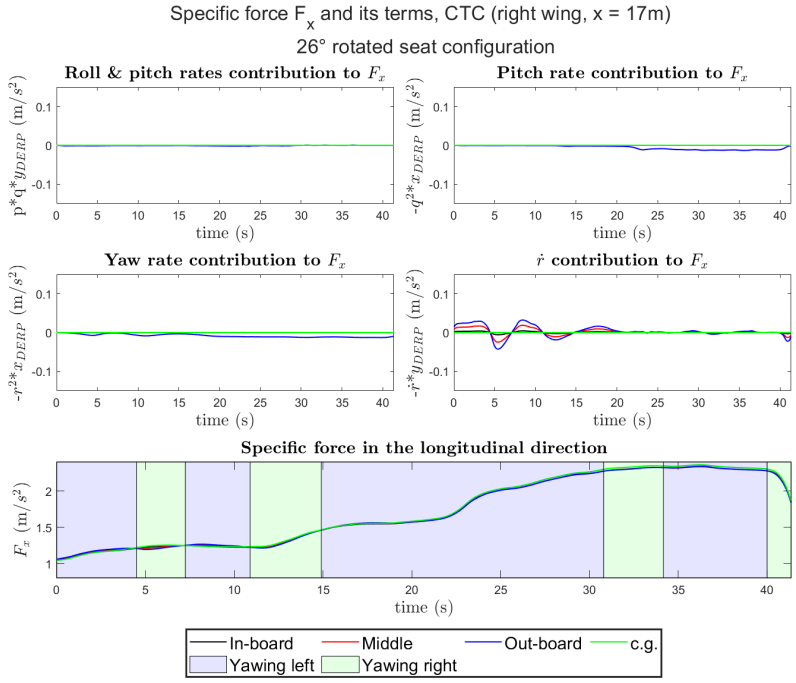

Figure 4.41: Specific force F_x at x = 17m for CTC, right wing, 26° rotated seat configuration

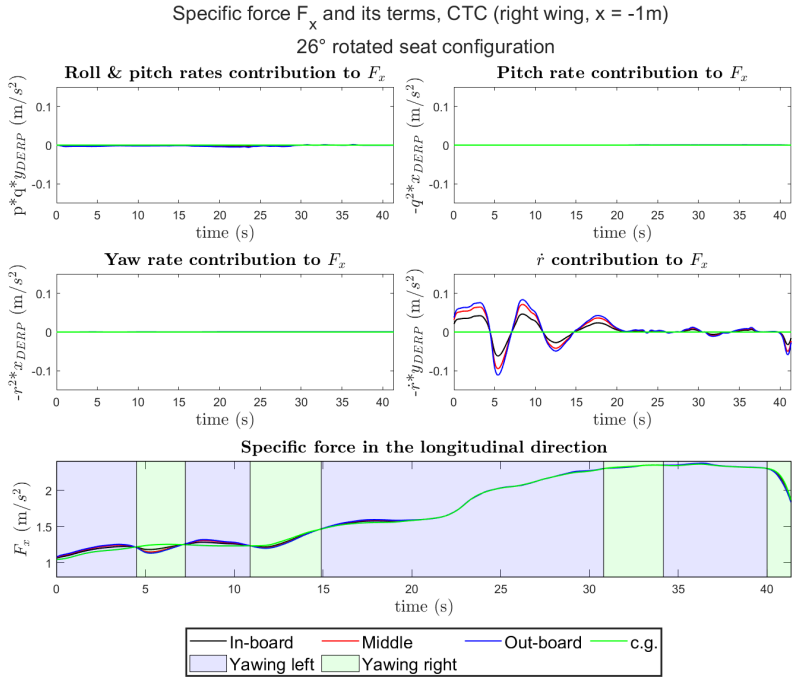

Figure 4.42: Specific force F_x at x = -1m for CTC, right wing, 26° rotated seat configuration

Figures 4.41 and 4.42 show F_x and the contribution of its terms for x = 17m and -1m from the c.g, for the right wing. It can be seen that $\dot{r}$ is the dominant component of the longitudinal specific force. $\dot{r}$ contribution to F_x increases linearly for the out-board locations since they are further away from the center-line , compared to the middle and in-board locations. However, this difference between the seats is only noticeable at the beginning of the maneuver. When the turn becomes steady and there is no acceleration anymore, there is no difference in F_x between the locations anymore.

Specific force F_y In this section, the lateral specific force is calculated for the 26° rotated seat configuration. Calculating and analyzing F_y for the 26° rotated seat configuration requires the use of Equation (4.9).

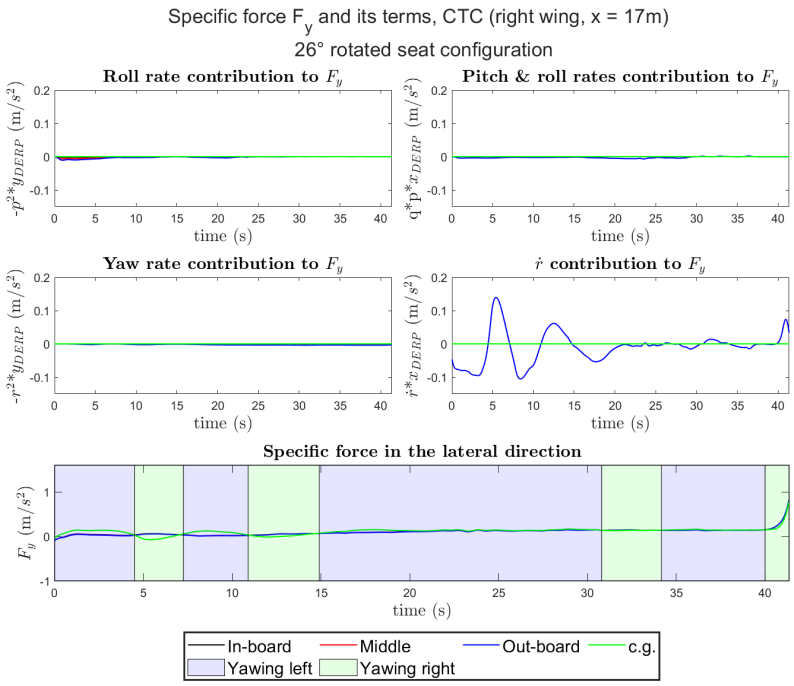

Figure 4.43: Specific force F_y at x = 17m for CTC, right wing, 26° rotated seat configuration

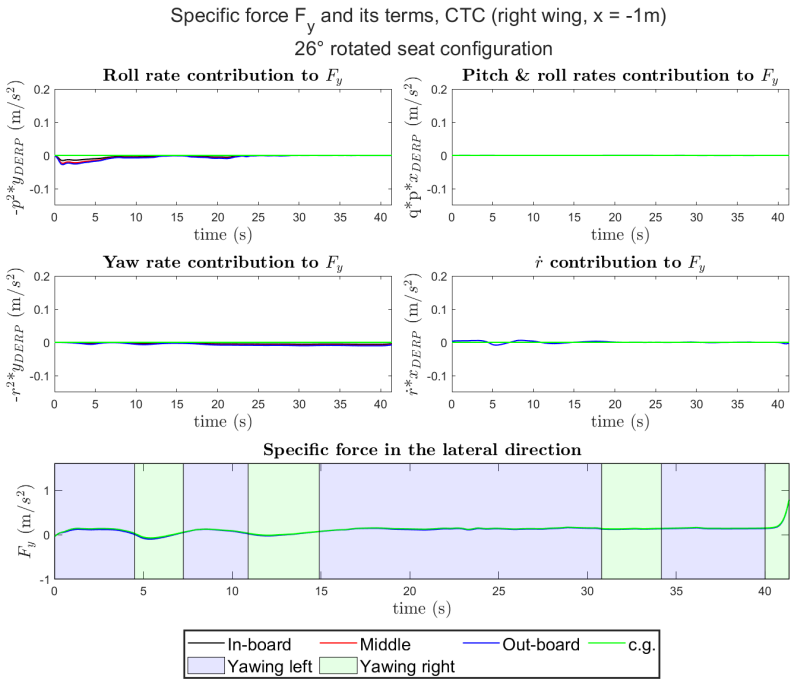

Figure 4.44: Specific force F_y at x = -1m for CTC, right wing, 26° rotated seat configuration

Figures 4.43 and 4.44 show F_y for the most front and most aft of the Flying-V, for the right wing. $\dot{r}$ is the dominant component of the lateral specific force. However, it is the same contribution to F_y for all seats at the same longitudinal location. Moreover, this contribution to F_y gets smaller for the aft locations because the moment arm gets smaller. The contributions to F_y of roll, pitch, and yaw rates are small and

negligible compared to $\dot{r}$ for the front seats. Therefore, there is no difference between seats within the same longitudinal location.

Specific force F_z The vertical specific force is calculated for the 26° rotated seat configuration. Equation (4.11) is used to calculate and analyze the vertical specific force for the 26° rotated seat configuration.

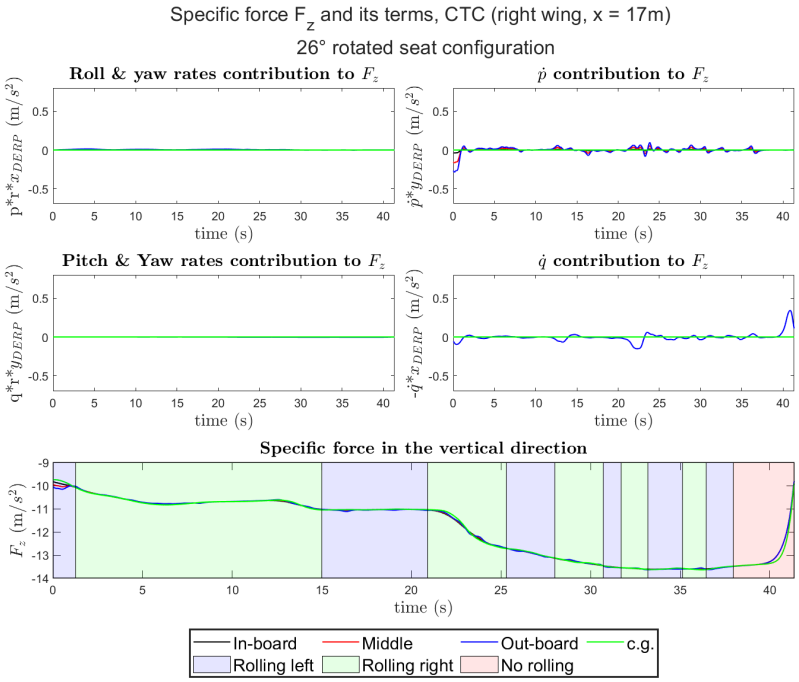

Figure 4.45: Specific force F_z at x = 17m for CTC, right wing, 26° rotated seat configuration

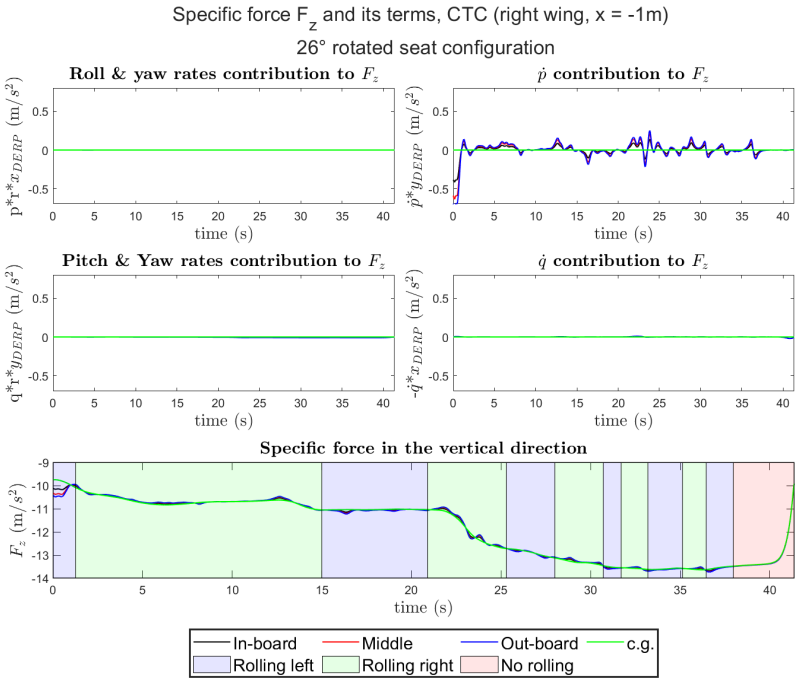

Figure 4.46: Specific force F_z at x = -1m for CTC, right wing, 26° rotated seat configuration

Figures 4.45 and 4.46 show the vertical specific force for both the right wing. $\dot{p}$ is the dominant com-

ponent, and its contribution to F_z increases for the aft locations because they are further away from the center-line. The biggest difference between the seats is at the beginning of the maneuver. After that, the difference between the locations is not noticeable.

4.2.3. 0° rotated Seats

The specific forces have been calculated again for the 0° rotated seat configuration that has been shown in Figure 4.20. Therefore, the rotation matrix (4.12) is applied to the specific forces that have been obtained in Section 4.2.2.

Specific force F_x The longitudinal specific force is calculated and analyzed for the 0° rotated seat configuration in this section of the report.

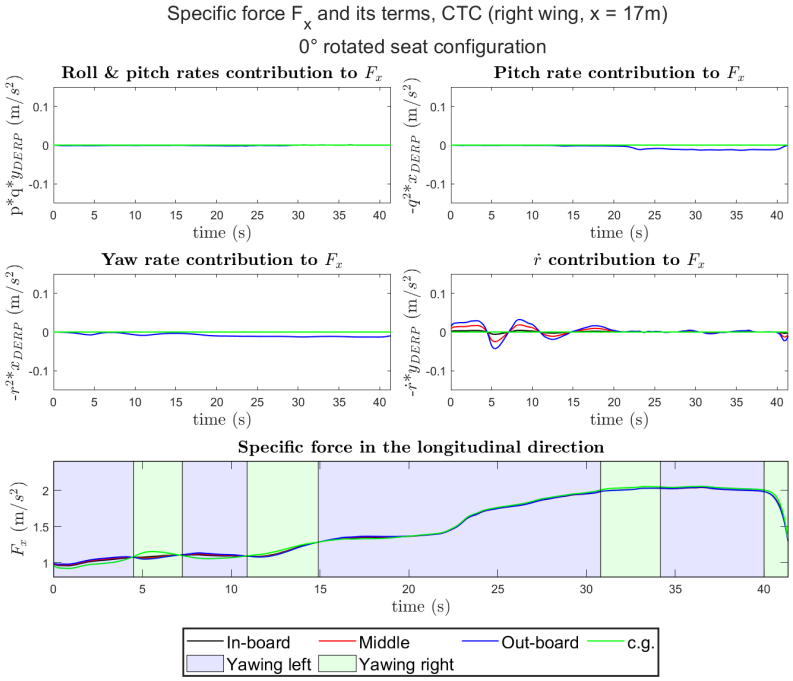

Figure 4.47: Specific force F_x at x = 17m for CTC, right wing, 0° rotated seat configuration

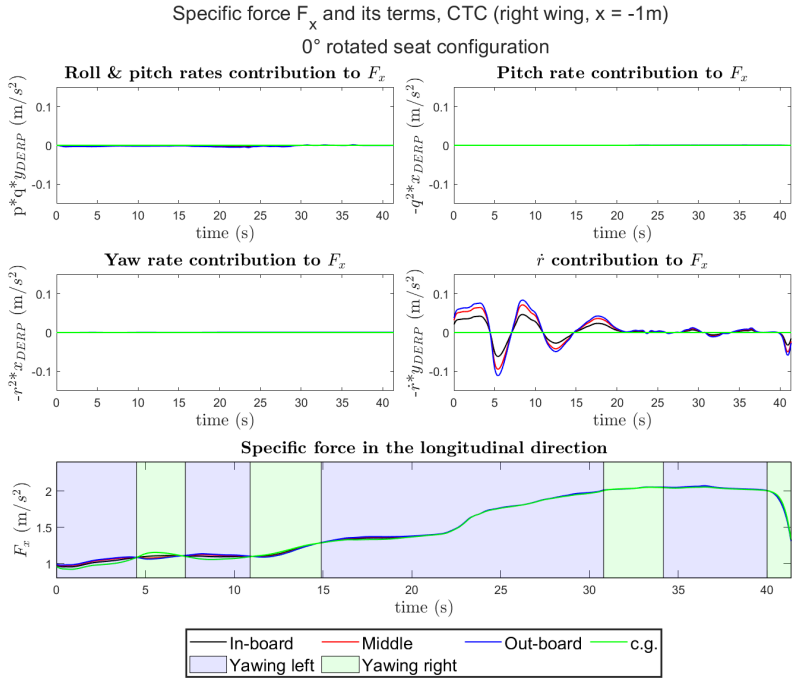

Figure 4.48: Specific force F_x at x = -1m for CTC, right wing, 0° rotated seat configuration

Figures 4.47 and 4.48 show F_x for the 0° rotated seat configuration, for the right wing. The biggest difference between the 26° rotated seat configuration and the 0° rotated seat configuration is that the longitudinal specific force starts at a lower value for the normal seats configuration than for the 0° rotated seats configuration, because of the trimmed pitch angle.

Specific force F_y In this section, the lateral specific is shown for the 0° rotated seat configuration.

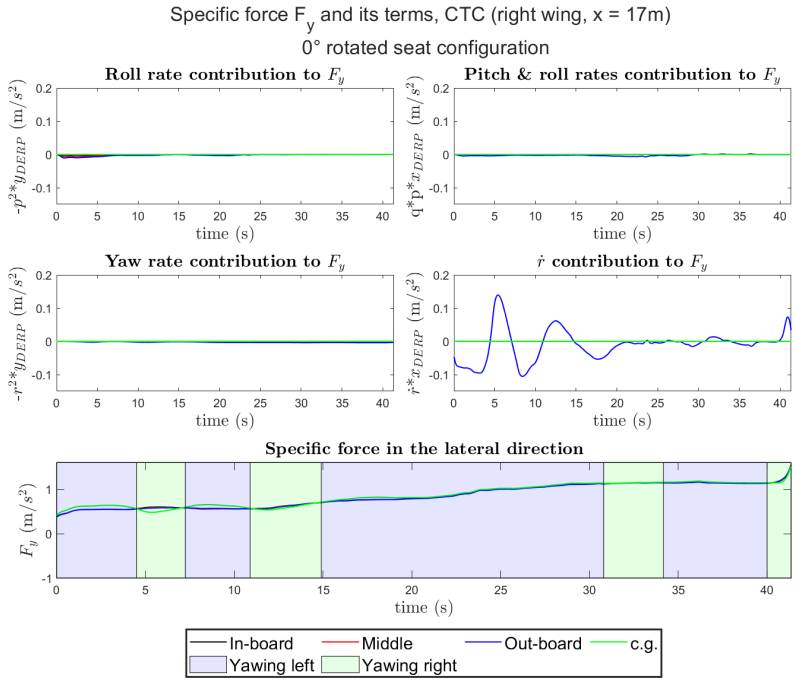

Figure 4.49: Specific force F_y at x = 17m for CTC, right wing, 0° rotated seat configuration

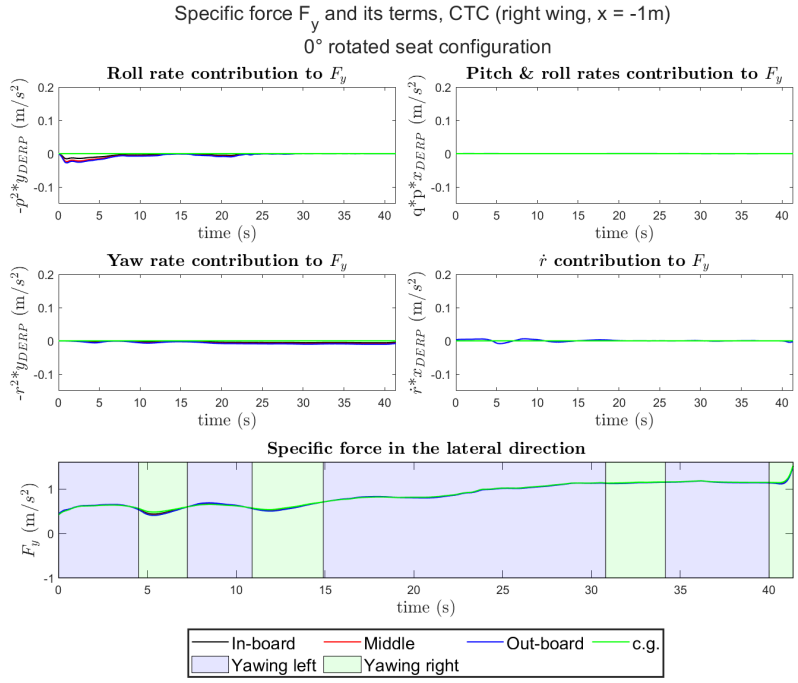

Figure 4.50: Specific force F_y at x = -1m for CTC, right wing, 0° rotated seat configuration

Figures 4.49 and 4.50 show the lateral specific force for the 0° rotated seat configuration, for the right wing. In contrast to the 26° rotated seat configuration, which starts from 0m/s^2, F_y starts from a negative specific force for the left wing and a positive specific force for the right wing, because a fragment of the longitudinal specific force is perceived as lateral specific force, due to the rotation of the seat.

Specific force F_z In this section, the vertical specific force is shown for the 0° rotated seat configuration.

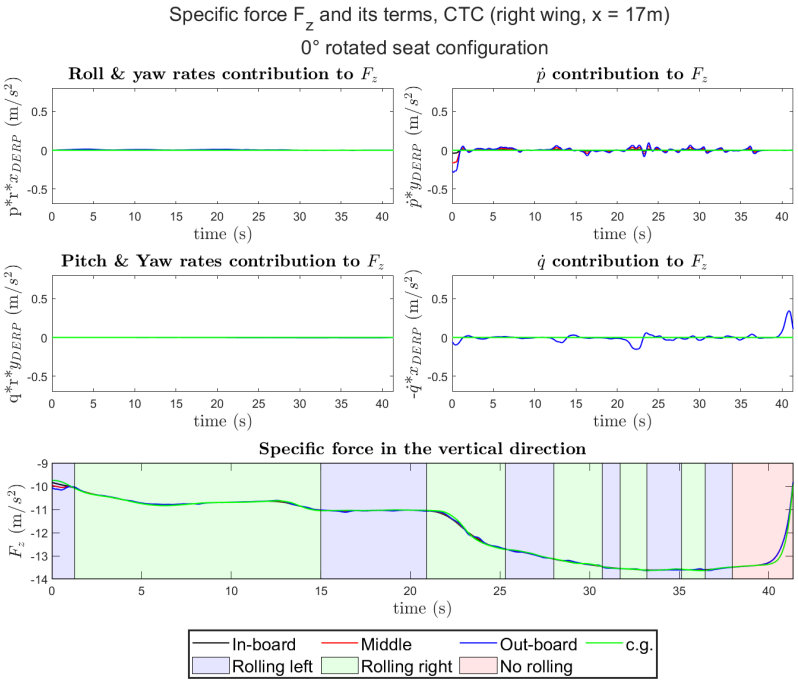

Figure 4.51: Specific force F_z at x = 17m for CTC, right wing, 0° rotated seat configuration

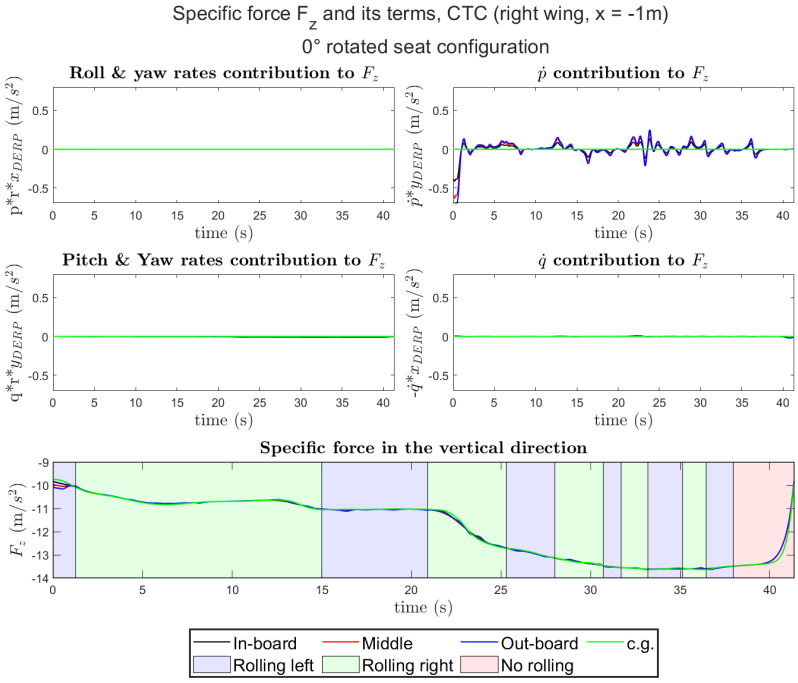

Figure 4.52: Specific force F_z at x = -1m for CTC, right wing, 0° rotated seat configuration

Figures 4.51 and 4.52 show the vertical specific force for the 0° rotated seat configuration, for the right wing. Due to the rotation of the reference frame around the z-axis, there is no difference between the configuration of the seats in their 26° and 0° rotated seat.

4.3. Conclusion

In this chapter, the specific forces were computed for TTB and CTC maneuvers in two different seat arrangements. It was observed that quick maneuvers, such as TTB, resulted in higher variance in specific forces across seat positions compared to slow maneuvers like CTC, which had less rotational acceleration.

For TTB and 26° rotated seat configuration, the longitudinal specific force F_x had yaw acceleration as a dominant component. It has been observed that the yaw acceleration contribution to the F_x gets bigger for the seats at the back because they are farther away from the center-line. The increase reaches 0.2m/s^2. Simple cases were used to validate this result, and findings from the yaw maneuver alone supported it. It has been observed that F_x will be lower in the 0° rotated seat configuration compared to the 26° rotated seat configuration.

The lateral specific force F_y for 26° rotated seat configuration is small, and the biggest difference within the seats occurs when the bank angle is changed from positive to negative. The dominant component is the roll rate, and it increases for the aft seats because they are farther away from the center-line. The increase for the last seat reaches 0.5m/s^2. For the 0° rotated seat configuration, the lateral specific force starts at a higher positive value for the right wing and the same value but negative value for the left wing.

The vertical specific force F_z is the same for both seat configurations. The roll acceleration has been determined to be the primary factor in F_z, and it contributes more the further the seats are from the center-line. The increase can be as high as 2m/s^2, compared to the c.g. position. These findings were verified using the straightforward example of a roll, which produced findings that were equivalent to those attained using flight data. Therefore, the vertical acceleration has the biggest change in specific forces due to sitting further away from the center-line, and will be the focus of further analysis.

The specific forces that have been obtained using the flight data will be used to calculate the conflict for both maneuvers and both seat configurations, with more focus on TTB, since it has shown greater variations in terms of specific forces.

5

Motion Sickness Prediction

In this chapter, the motion sickness model 6DOF-SVC is simulated to predict the motion sickness in the Flying-V during the TTB and CTC maneuvers. Moreover, this analysis will be done on the different seat configurations, including the 0° and 26° rotated seat configurations. Since vertical acceleration has been determined to be dominant in the specific forces, 6DOF-SVC has been chosen over MSOM since it has been used widely in the motion sickness prediction application and proven its reliability in detecting motion sickness in vertical acceleration, as has been discussed in Section 2.2.3 and Table 2.1. Because the conflict's transfer function is independent of acceleration frequency and the peak frequency for lateral acceleration is 0.02Hz, MSOM does not work well in identifying sickness due vertical acceleration. Additionally, it hasn't been used in applications for motion sickness; instead, it was mostly used in aerospace applications for human spatial orientation perception. In addition, the visual part of 6DOF-SVC that has been shown in Figure 2.7 will not be used since it only takes into account the angular visual velocities and does not consider the linear visual velocities. Moreover, it has not been widely used and validated. Therefore, the 6DOF-SVC model that has been shown in Figure 2.6 will be used. The model's parameters are directly taken from [42] and listed in Table 5.1.

The output of the 6DOF-SVC is the MSI. However, this will not be used in the motion sickness analysis of the Flying-V since the flight data only runs for around 60 seconds. Thus, the MSI will not show a big difference between the different locations and seats in the Flying-V. Instead, the three conflict terms of the model (thus, c_{gx}, c_{gy}, and c_{gz}) will be looked at individually, and then the magnitude of the three terms of the conflict will be calculated ($\sqrt{c_{gx}^2 + c_{gy}^2 + c_{gz}^2}$) and a simple integrator on the absolute conflict will be applied. The Motion Sickness (MS) proxy can be seen in Equation (5.1):

$$\mathrm{MS} = \int_0^t |\vec{c}(t)| dt \tag{5.1}$$

As a baseline for comparison for the total conflict, a hypothetical seat is proposed at the c.g. of the Flying-V. This way, it can be distinguished between the sickness that is being caused due to the rotation around the c.g. and the sickness due to sitting offset from the c.g.. Heat-maps will be utilized for comparison, and various colors will be employed. Moreover, Heat-maps are used for the single conflict terms to check how much each conflict makes of the total conflict. To avoid any asymmetry between both wings, the maneuvers are repeated to be symmetrical for both wings.

K_a	K_ω	$K_{\omega c}$	K_{vc}	K_{ac}	$\tau_d\,(s)$	$\tau_a\,(s)$	$b\,(m/s^2)$
0.1	0.8	5	5	1	7	190	0.5

Table 5.1: 6DOF-SVC parameters [42]

5.1. Time to Bank Sickness Simulation

The 6DOF-SVC model will be given the specific forces that were calculated for the TTB maneuver in order to predict motion sickness and conflict terms in the Flying-V. The conflict terms for the three fixed locations listed in Table 4.1 will be reviewed in this chapter. After that, a heat map will be displayed to give a broad

picture of the entire aircraft and explain how the conflict changes depending on where a seat is located. This analysis is carried out for both the rotated and normal seating arrangements.

5.1.1. 26° rotated seat configuration

The 26° rotated seat configuration, which is depicted in Figure 4.7, is the first to be investigated for motion sickness. The conflict terms are compared to the hypothetical seat at the c.g. of the Flying-V.

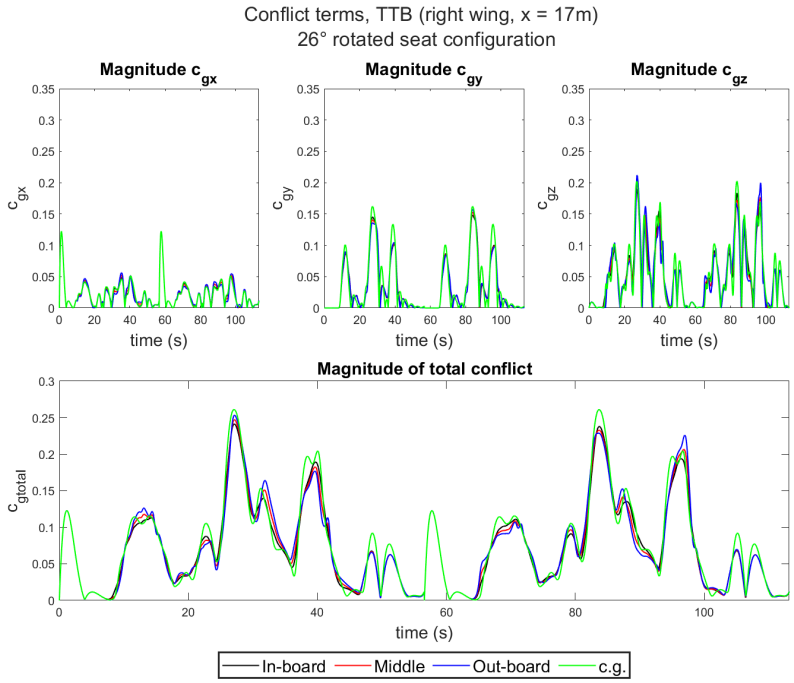

Figure 5.1: Conflict terms at x = 17m for TTB, right wing, 26° rotated seat configuration

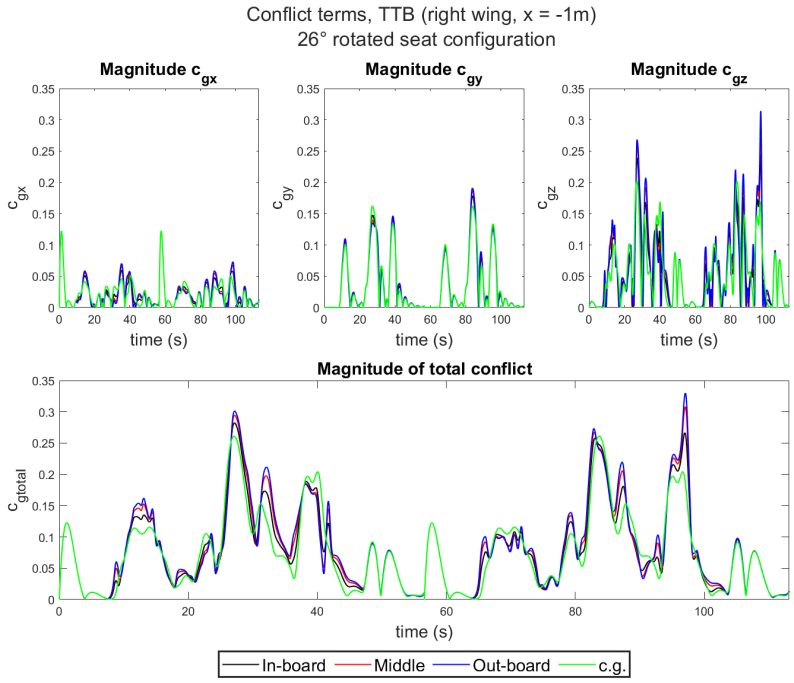

Figure 5.2: Conflict terms at x = -1m for TTB, right wing, 26° rotated seat configuration

Figures 5.1 and 5.2 show the conflict terms (c_{gx}, c_{gy}, c_{gz} and c_{gtotal}) at x = 17m and -1m, for the right wing. It can be seen that the vertical conflict is the highest conflict in the maneuver since the vertical specific force that is experienced in the Flying-V during TTB maneuver is higher than the lateral and longitudinal specific forces, and the vertical specific force increases for the seats that are the farthest away from the center-line. The total conflict at the Flying-V's front where the seats are closest to the center-line, is less than the conflict at the c.g., as can it is shown in Figure 5.1, because $\dot{q}$ is taken into account for the vertical conflict, and it is dominant for the front locations and opposite to $\dot{p}$. Therefore, making the vertical specific forces to be lower than the specific forces at the c.g., which led to lower conflict. The overall conflict rises for the aft positions, where the seats are the furthest from the center-line, and surpasses the conflict at the c.g. position, as can be seen in Figure 5.2. Appendix A shows the MS for a range that covers the whole aircraft. Heat-maps are created to study the development of the motion sickness during TTB for the whole aircraft, in both wings.

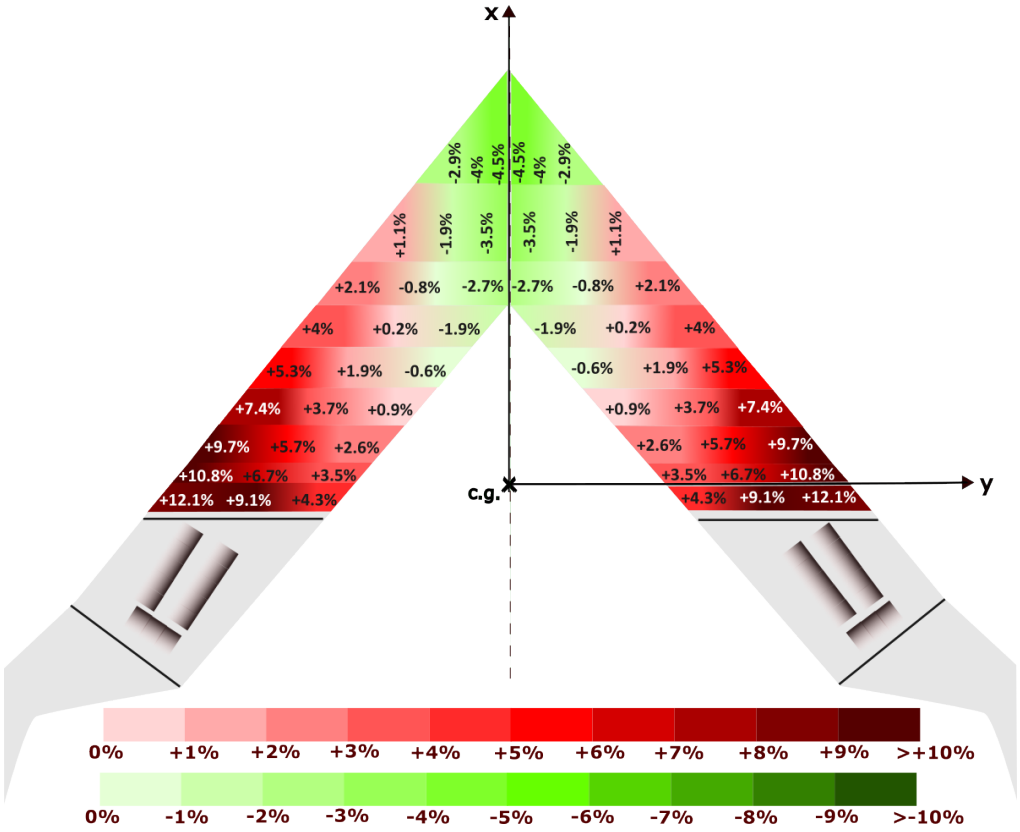

Figure 5.3: Heat-map for total conflict of TTB, 26° rotated seat configuration

Figure 5.3 shows a heat-map for total conflict in the Flying-V to show how the total conflict term is developed across the whole Flying-V geometry, compared to the c.g. position. It is clear that the front locations have a lower conflict compared to the c.g.. The conflict increases the further the seats are from the center-line. It increases up to +12% for both of the wings, compared to the c.g. position. It is noticed that the total conflict in the wings starts to get higher than the conflict at the c.g. at y = 6.5m. Further analysis is done to check which conflict term dominates the total conflict. In order to determine how much each of the conflict terms (c_{gx}, c_{gy}, and c_{gz}) contributes to the overall conflict, heat-maps are created.

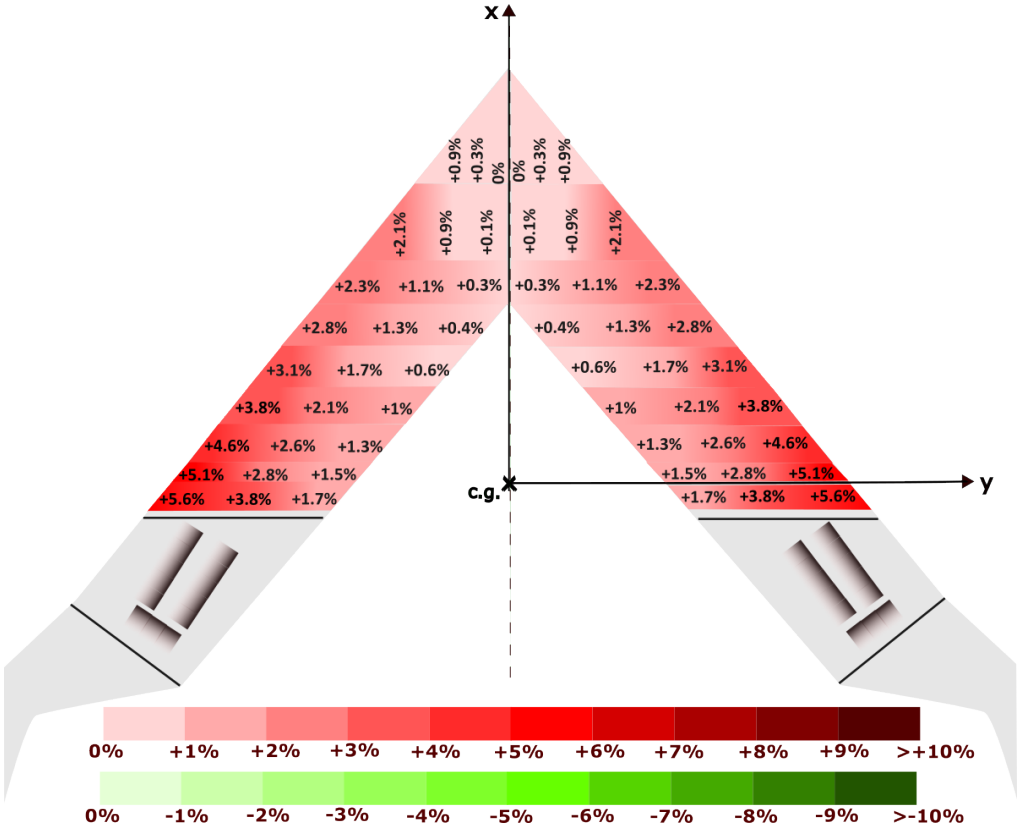

Figure 5.4: Heat-map for c_{gx}, 26° rotated seat configuration

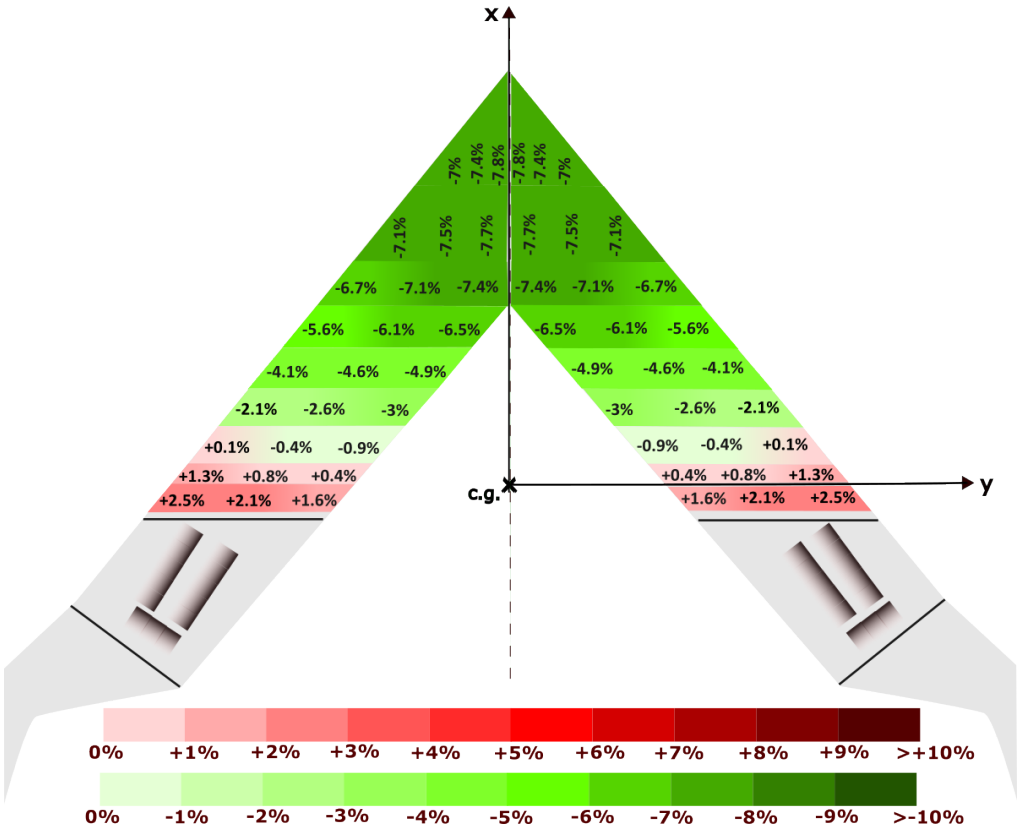

Figure 5.5: Heat-map for c_{gy}, 26° rotated seat configuration

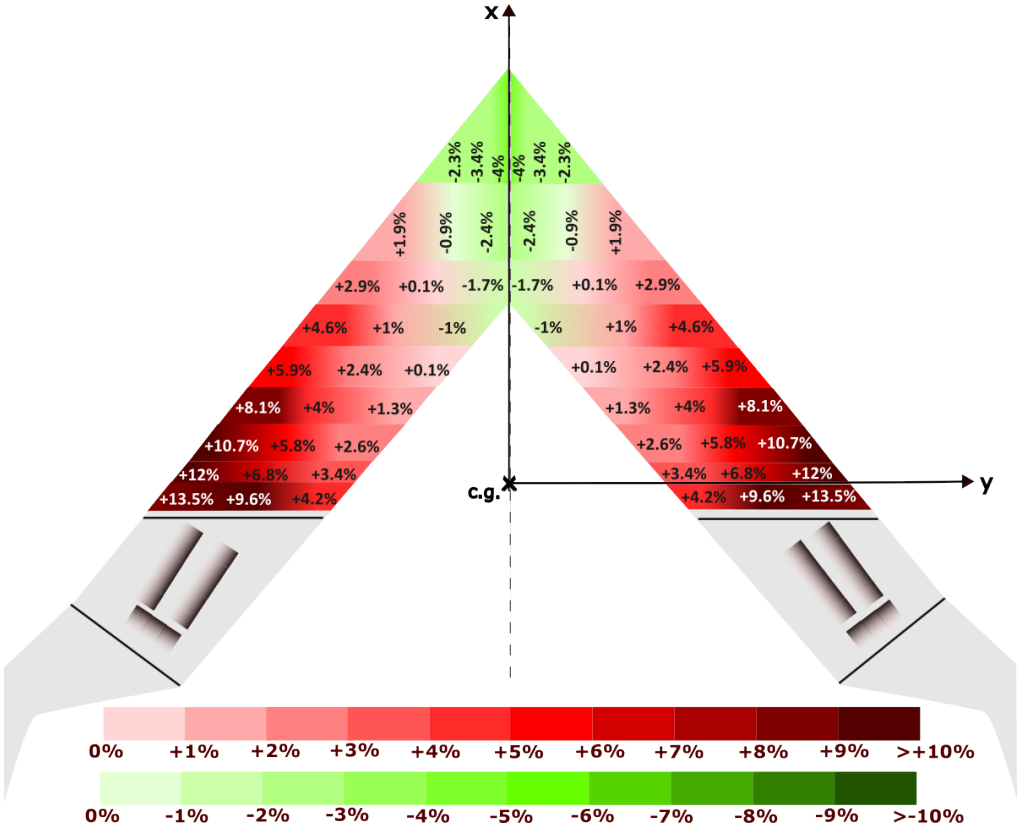

Figure 5.6: Heat-map for c_{gz}, 26° rotated seat configuration

Figure 5.4 depicts the longitudinal conflict and how it is developed compared to the longitudinal conflict at c.g. The lateral conflict compared to the lateral conflict at the c.g. is depicted in Figure 5.5. Figure 5.6 shows the vertical conflict compared to the vertical conflict at the c.g. It can be seen from the total conflict heat-map in Figure 5.3 resembles the vertical conflict heat-map in Figure 5.6, therefore, the highest and most dominant conflict during the maneuver is the vertical conflict, for both wings. The vertical conflict increases up to 13.5% for both wings, which is caused by the roll phase of the maneuver. The lateral conflict is showing a lower conflict for the majority of the aircraft compared to the c.g. position, except for the locations that are behind the c.g., where the conflict in these locations are higher than the conflict at the c.g. The longitudinal conflict is showing an increasing conflict compared to the c.g. position, this increase is up to 5.6% for both wings. It can be seen that the total conflict heat-map in Figure 5.3 resembles the vertical conflict heat-map in Figure 5.6

5.1.2. 0° rotated seat configuration

The 0° rotated seat layout (see Figure 4.20) is the second case to investigate. Therefore, the specific forces that have been calculated in Section 4.1.3 are given as an input to calculate the total conflict across the different locations in the Flying-V.

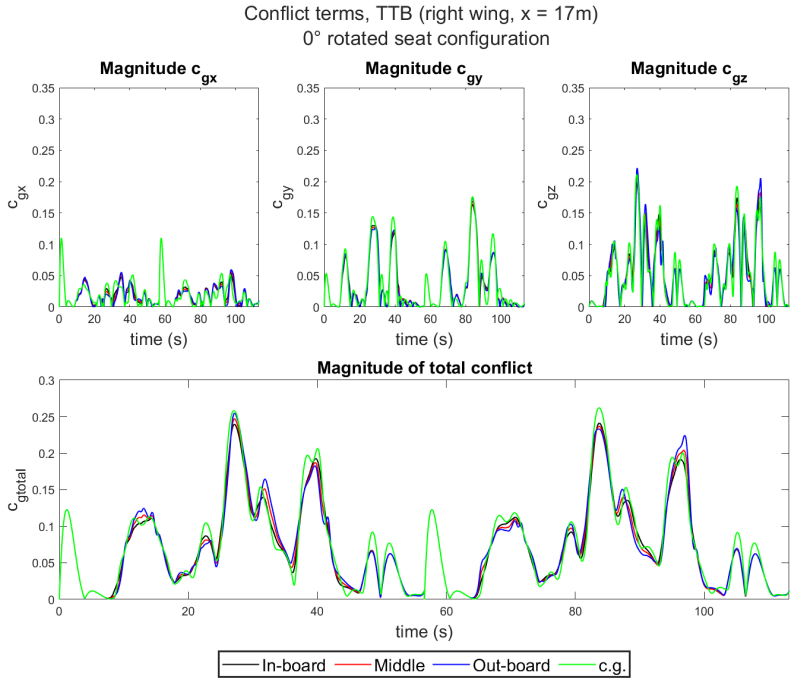

Figure 5.7: Conflict terms at x = 17m for TTB, right wing, 0° rotated seat configuration

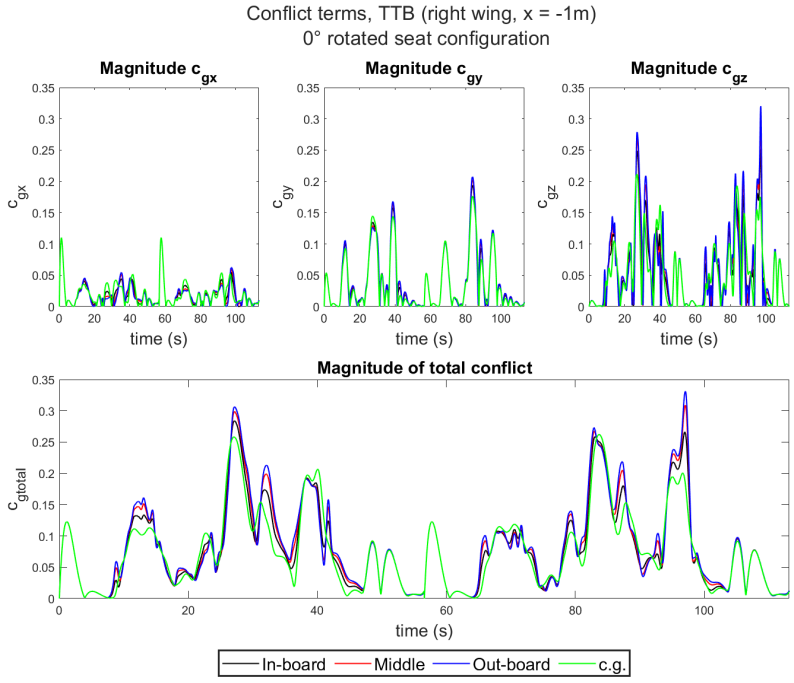

Figure 5.8: Conflict terms at x = -1m for TTB, right wing, 0° rotated seat configuration

Figures 5.7 and 5.8 show the conflict terms across the different locations in the Flying-V, for both wings using the 0° rotated seat configuration. The figures show that conflict terms and the total conflict did not have a noticeable increase or decrease, compared with the 26° rotated seat configuration. Appendix B show the MS for the individual and total conflict terms for the 0° rotated seat configuration. Compared to the 26° rotated seat configuration, the longitudinal conflict has decreased for the 0° rotated seat configuration, because the longitudinal specific force has decreased. This is because a portion of the longitudinal specific force will be felt as a lateral specific force due to the rotation of the seat. As a result, the lateral conflict has

increased for the 0° rotated seat compared to the 26° rotated seat. The vertical conflict has not changed for the 0° rotated seat configuration compared to the 26° rotated seat configuration.

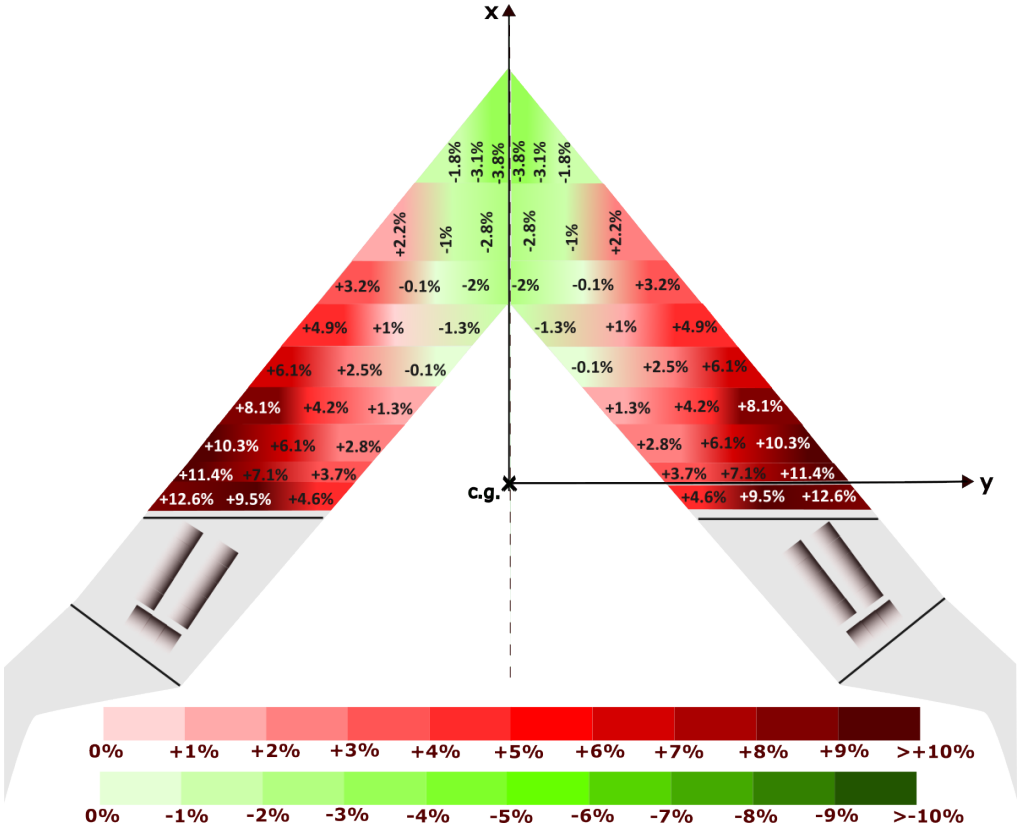

Figure 5.9: Heat-map for TTB, 26° rotated seat configuration

Figure 5.9 shows the heat-map for TTB with the 0° rotated seat configuration. The aft locations have a larger total conflict when compared to the c.g. position than the seats at the front positions, which is similar to the 26° rotated seat configuration. Moreover, the vertical conflict c_{gz} is still the highest conflict in the maneuver. Additionally, the outboard locations have more conflict than the inboard and middle locations with the same longitudinal coordinate. Figures 5.3 and 5.9 when compared, reveal that there is not much more overall conflict for the 0° rotated seat layout than there is for the 26° rotated seat configuration.

5.2. Conclusion

Comparing the motion sickness conflicts that TTB and CTC are going to cause while flying in the Flying-V, it is clear that TTB has a higher conflict and shows greater variations in the results across the different seating locations in the Flying-V. The TTB has showed that it is four times more sickening than the CTC maneuver. The highest and most dominant conflict that is being shown in TTB is the vertical conflict c_{gz}, which increases the further the seats are from the center-line. Comparing the two seat configurations, there was no change in the total conflict or the vertical conflict for either configuration. It does, however, show a small change in c_{gx} and c_{gy}. CTC is showing a smaller conflict compared to the TTB maneuver.

As a result, fast maneuvers with varying acceleration, like TTB, have higher conflict than slow maneuvers that have constant acceleration, like CTC. Moreover, the vertical conflict is the conflict term that dominates the total conflict and that is showing the highest MS values.

6

Experiment Proposal

Motion sickness development in the Flying-V can be identified by motion sickness experiment in SIMONA research simulator. In this chapter, the details of the experiment are being discussed.

6.1. Experiment Set-up

After identifying that the dominant factor causing sickness in the Flying-V is the vertical conflict, which increases as passengers move away from the center of rotation, an experiment has been set up to validate the results of the analysis.

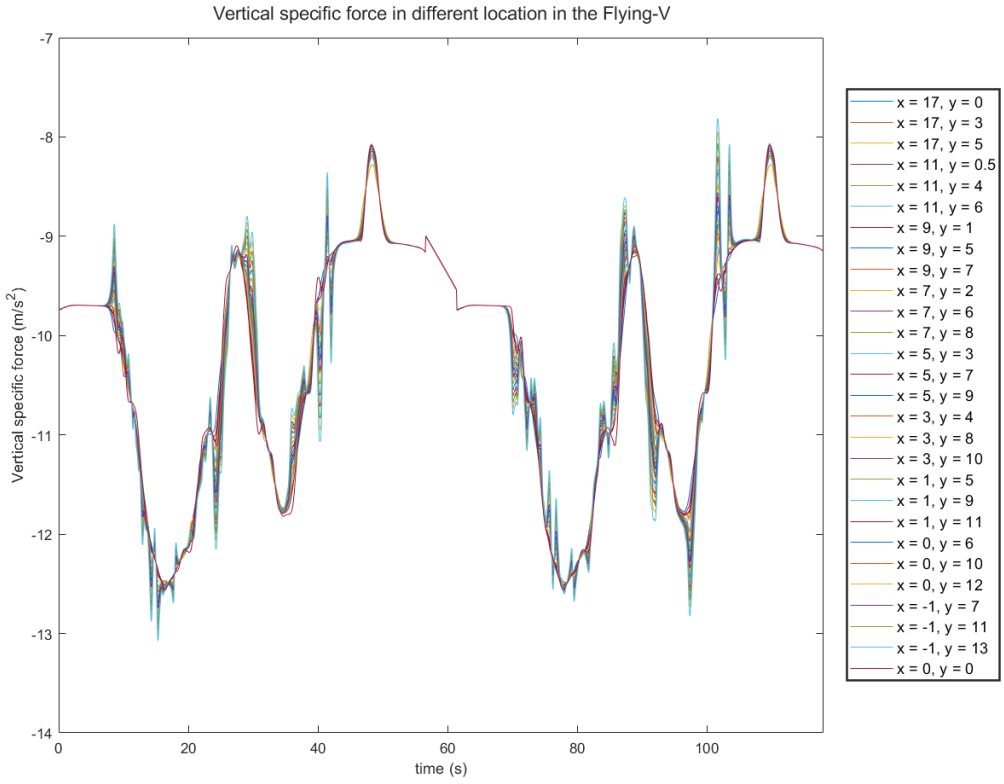

Figure 6.1: Vertical specific force across different locations

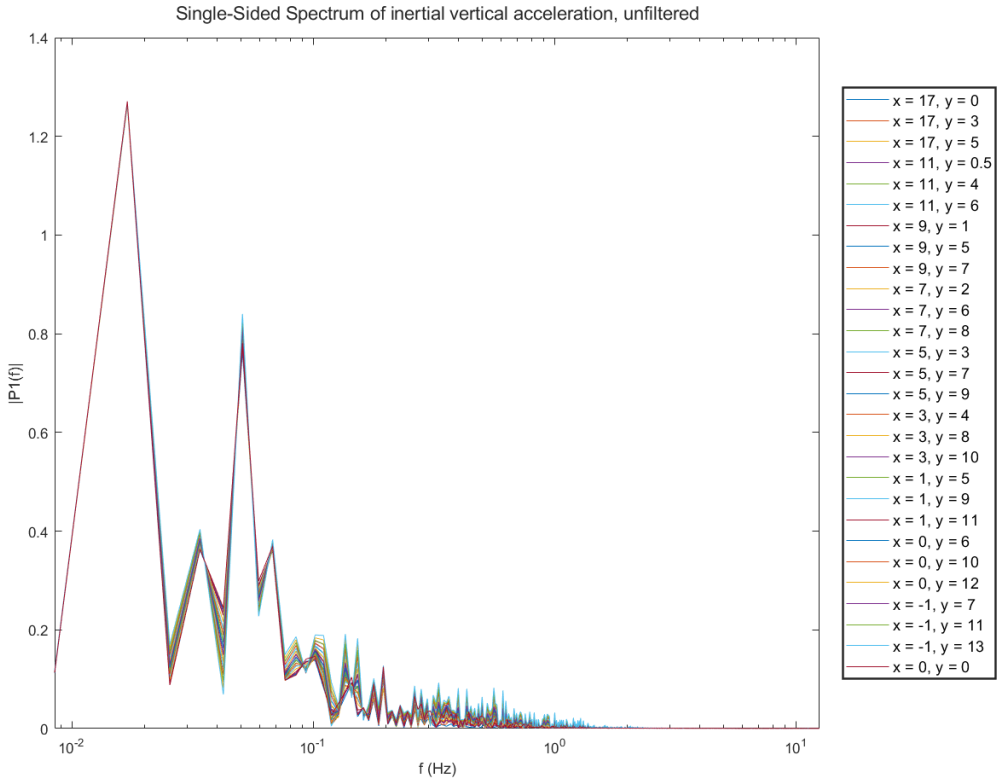

Figure 6.2: FFT of the vertical acceleration

Figure 6.1 presents the vertical specific force and Figure 6.2 presents the corresponding Fast Fourier Transform (FFT) of the vertical acceleration at different positions within the Flying-V, based on the TTB maneuver data. The FFT indicates that the maneuver occurs at a low frequency that cannot be replicated by the simulator. Therefore, simplifications need to be done in order to do an experiment in the simulator.

In the simulator, a roll maneuver will be performed, taking into account the additional vertical acceleration resulting from the roll. The vertical specific force has been calculated as follows:

$$F_z = \dot{p} \cdot y - g \tag{6.1}$$

To ensure the feasibility of the experiment in the simulator, the aerodynamic effects of the maneuver and pitch/yaw will be excluded. The experiment will focus on testing the impact of the sitting offset from the center of rotation, during rolling.

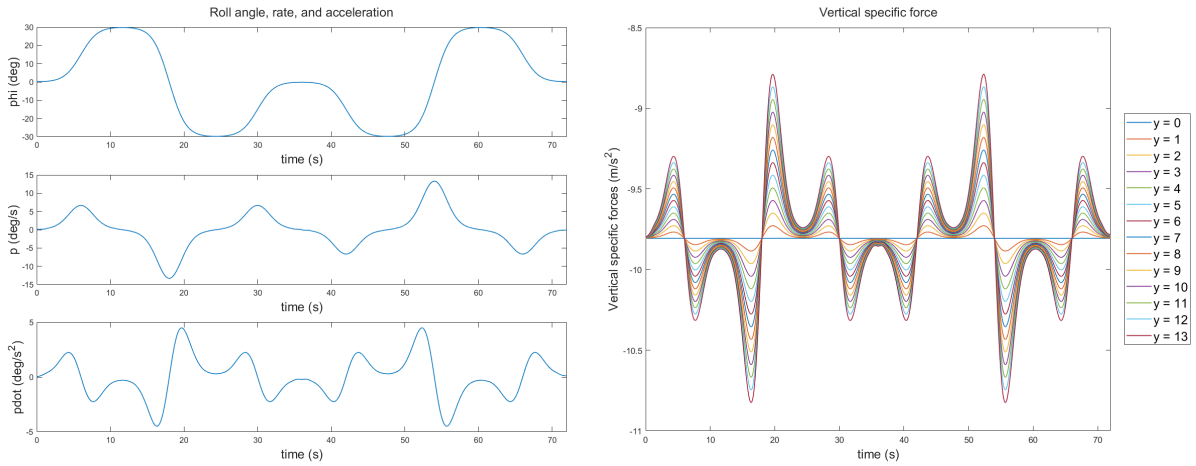

(a) Simplified roll case, unfiltered

(b) Vertical specific force for simplified roll case, unfiltered

Figure 6.3: Unfiltered roll maneuver with its specific forces

Figure 6.3 shows the simplified roll data, that contains the roll angle, roll rate, and $\dot{p}$. Moreover, it illustrates the vertical specific force in the simplified roll scenario. It demonstrates that the vertical specific force increases as the distance from the center of rotation to the seats increases. However, filtering will be applied to the data, to make it feasible in the simulator. A third-order high-pass filter will be utilized instead of a second-order high-pass filter. This is because the third-order filter has a return-to-neutral effect, which allows for a slower return of the cab to its neutral position during steady-state accelerations. However, this comes at the cost of higher phase distortions [59]:

$$H(s) = \frac{k \cdot s^2}{s^2 + 2\zeta\omega_n + s\omega_n^2} \cdot \frac{s}{s + \omega_b} \tag{6.2}$$

Gouverneur's analysis has been done to determine the optimal gain and the natural break-frequency for the motion filter. The third-order filter is applied on the roll and the vertical acceleration. The motion filter parameters have been chosen to prevent excessive filtering of the motion signals:

$$\omega_n = 1[\text{rad/s}] \quad \zeta = 0.7 \quad \omega_b = 0.3[\text{rad/s}] \quad k = 1 \tag{6.3}$$

6.1.1. Experiment conditions

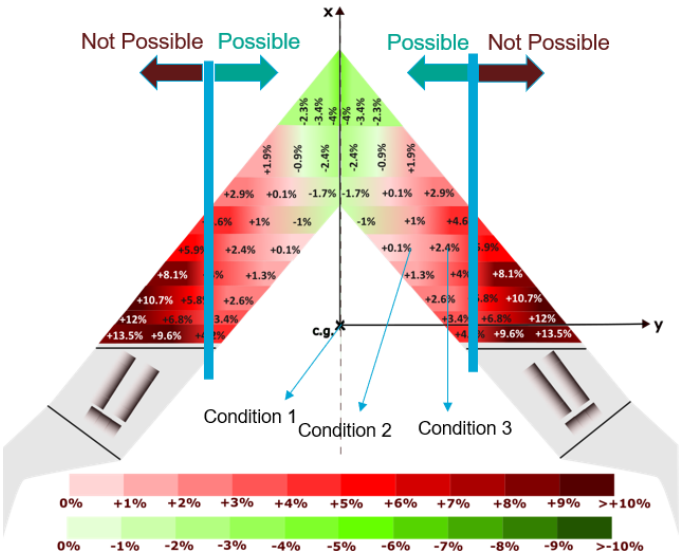

Figure 6.4: Possible locations in the Flying-V

With the current motion filter parameters, the maximum lateral distance that can be done in the Flying-V is up to 7m, see Figure 6.4. To provide more insight into the shape of the relationship between the motion sickness and the locations that are further away from the center of rotation, 3 locations are chosen as conditions:

- Condition 1: y = 0m
- Condition 2: y = 3.5m
- Condition 3: y = 7m

By selecting 3.5m as one of the conditions, the distances between all conditions are made equal. This approach minimizes biases associated with distances from the center of rotation, allowing for a direct comparison of the effects of each condition on motion sickness. In addition, this approach facilitates the identification of trends and patterns in the relationship between motion sickness and distance from the center of rotation.

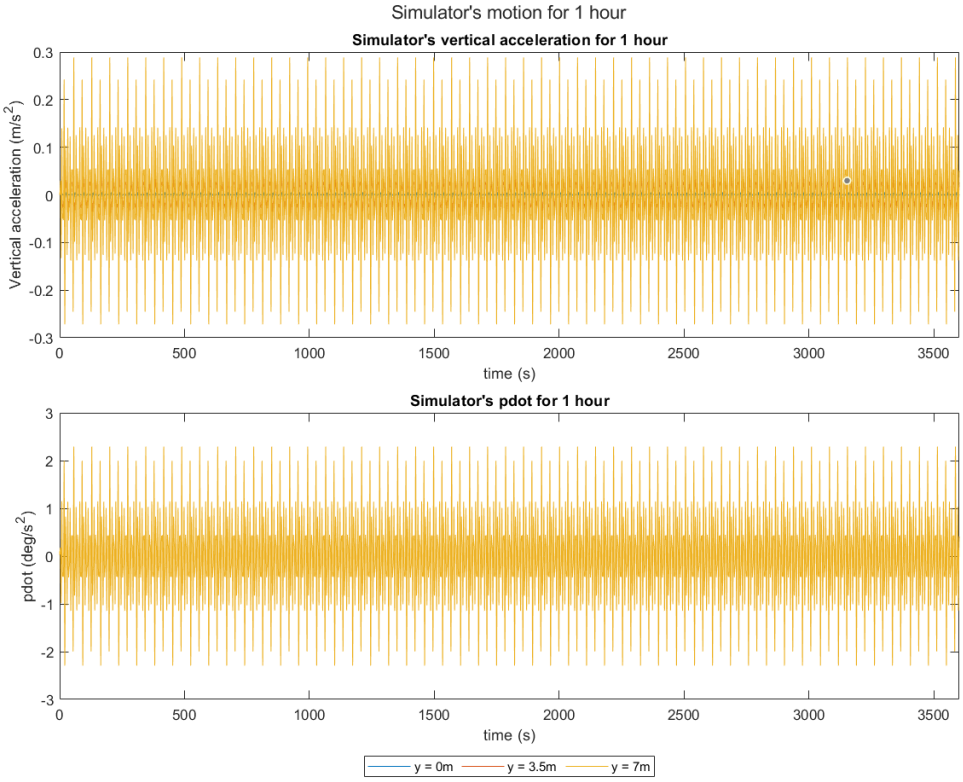

Figure 6.5: Simulator's motion for 1 hour

The first condition involves rolling only, while conditions 2 and 3 include the additional vertical acceleration caused by the rolling. During the experiment, participants will be exposed to the motion stimuli for a duration of one hour. All conditions have the same roll. See Figure 6.5.

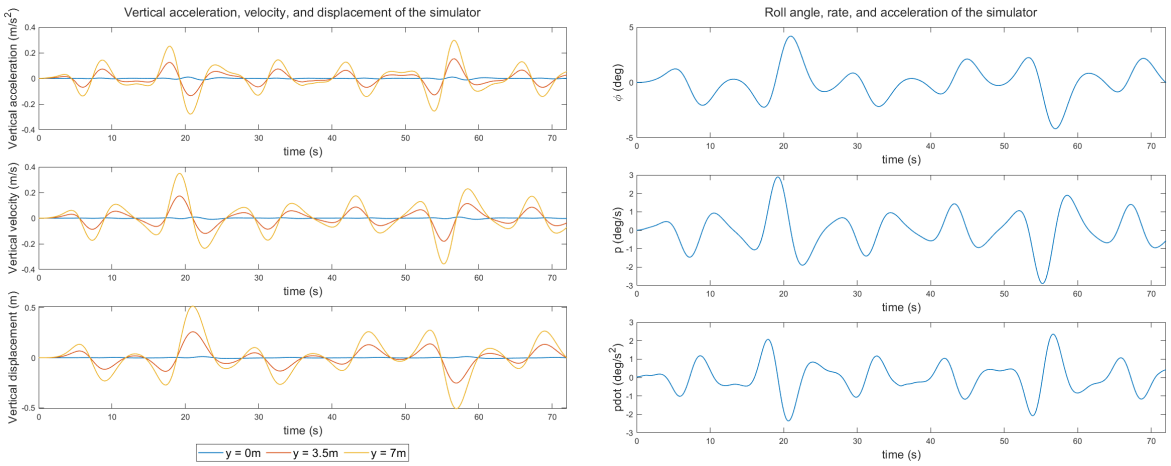

(a) Zoomed-in simulator's vertical motion

(b) Zoomed-in simulator's roll motion

Figure 6.6: Zoomed-in simulator's motion

In Figure 6.6, the difference between the conditions is displayed in terms of heave motion, while the roll motion remains consistent across all conditions. The maximum roll angle produced by the simulator is approximately 4° for all conditions. However, as the distance from the center of rotation increases, there is a noticeable increase in vertical acceleration, velocity, and displacement. The third condition has the highest maximum vertical acceleration produced by the simulator, at around $0.3 m/s^2$, resulting in a displacement of approximately 0.5m in the upward and downward direction

6.1.2. Experiment's expected results

The motion stimuli for all three conditions have been used as an input to the 6DOF-SVC motion sickness model to predict the level of motion sickness induced by each stimulus.

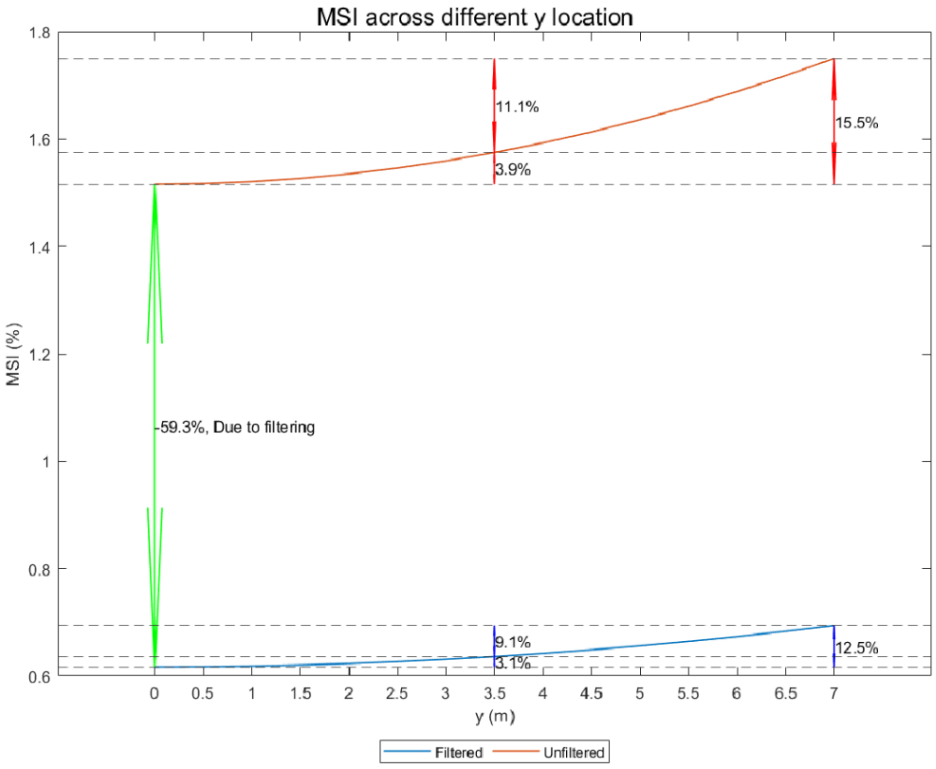

Figure 6.7: Predicted MSI for the unfiltered and filtered motion

Figure 6.7 presents the predicted MSI for both the filtered and unfiltered motion stimuli. The results demonstrate that the severity of motion sickness decreased by approximately 60% due to the implementation of motion filtering. Furthermore, the inclusion of heave motion in conjunction with rolling motion is shown to increase the predicted level of motion sickness. Therefore, an increase in the MSI can be seen from y = 0m to y = 7m. The difference in predicted MSI between the first and second conditions is approximately 3%, while the difference between the second and third conditions is approximately 9%. The difference between the first and third conditions is approximately 12.5%. These results suggest an exponential increase in predicted motion sickness severity as the distance between seats and the center of rotation increases. However, it should be noted that MSI represents the point at which participants reach the vomiting phase. In the actual experiment, participants will provide their MISC score, and the session will be stopped as soon as participants report feeling nauseous, before reaching the vomiting phase. de Winkel et al. [60] have fitted the MISC scores using Steven power law, in a fore-aft oscillation experiment, at a fixed frequency and an increased amplitude in four sessions. Moreover, de Winkel et al. [60] found out that the motion sickness and discomfort increases monotonously with MISC score.

Therefore, the hypotheses that will be tested in the experiment are:

Hypothesis 1

Participants exposed to both roll and heave motion will experience higher level of motion sickness compared to being exposed to roll motion only, as measured by the MISC scores.

Hypothesis 2

As the distance from the center of rotation increases, the MISC values reported by participants will increase.

Hypothesis 3

The relationship between the reported MISC scores and the distance from the center of rotation is assumed to follow an exponential function, such that as the distance increases, the MISC scores will increase exponentially.

Hypothesis 4

As the distance from the center of rotation increases, the severity of motion sickness ratings increase with the MISC scores

6.1.3. Experiment participants

A within-subject experiment is being used as a setup for this experiment. 12 participants are invited to complete and participate in the different conditions in the experiment. One confound in the within-subject experiment is the condition order

Participants	Condition order		
1	C1	C2	C3
2	C2	C3	C1
3	C3	C1	C2
4	C1	C3	C2
5	C2	C1	C3
6	C3	C2	C1
7	C1	C2	C3
8	C2	C3	C1
9	C3	C1	C2
10	C1	C3	C2
11	C2	C1	C3
12	C3	C2	C1

Table 6.1: Condition order for experiment

Table 6.1 shows the condition order. All participants will be invited to participate in all conditions.

6.1.4. Experiment procedure and instructions

Participants will take part in the participants after reading the experiment briefing and signing an informed consent form. The experiment briefing contains information about the background of the research, the purpose of the research, risks of participating, and what does the participation in the research involve. The participants will not be told what are the differences between the conditions that they will experience because doing so could introduce a confound into the experiment. The experiment protocols for the experiment were approved by the Human Research Ethics Committee of TU Delft. The participants will be guided into SIMONA Research Simulator, where they will be exposed to the motion simulation.

Symptom		Rating
No problems		0
Slight discomfort but no specific symptoms		1
Dizziness, warm, headache, stomach awareness, sweating etc.	Vague Some Medium Severe	2 3 4 5
Nausea	Some Medium Severe Retching	6 7 8 9
Vomiting		10

Table 6.2: Misery SCale symptoms and ratings [61]

Participants are required to rate their discomfort on the MISC rating scale (see Table 6.2) by saying out the corresponding number every 30 seconds. The experiment will have 3 separate sessions, each approximately an hour long (maximum). The motion simulation will continue until either the participant has experienced some nausea (MISC level 6), or until an hour has passed.

6.1.5. Apparatus

Figure 6.8: SIMONA Research Simulator

The experiment will be performed in the SIMONA Research Simulator at TU Delft, see Figure 6.8. The simulator's hydraulic 6-DOF hexapod motion system has a maximum displacement of 1.12m, a maximum speed of 0.9m/s, and a maximum acceleration of 13m/s^2 ([62], [63]). The participants will be sitting inside a closed cabin and fastened with a five-point harness. An intercom system is set up to enable two-way communication between the experimenter and the participants.

6.2. Data analysis

The gathered data in the experiment will be used to get more insight on the effects of sitting laterally further away from the center of rotation in the Flying-V. Details about the data analysis are given in this section.

6.2.1. Dependent measures

Two dependent measures will be collected during and after the experiment, which are:

1. The MISC scale's subjective evaluations were found to be the most effective method for estimating the progression of illness over time [15]. The MISC values range from 0 to 10, as can be seen in Table 6.2. However, experiment will be stopped if participant reach MISC value of 7. Participants will be asked to give their MISC value every 30 seconds.
2. Participants will be asked to fill in a motion sickness symptoms checklist after the session is done, to capture how they were feeling during and after exposure to the simulator motion. This checklist contains specific symptoms, and the participants need to choose if the symptoms they felt were (None, some, medium, and severe). This because the MISC do not give a specific rating for a specific symptom.

7

Conclusion

In this chapter, the findings of the literature phase and the outcomes of the analysis phase will be highlighted by answering the research questions.

Research question 1

Which motion sickness model is better suited to predict the motion sickness in the Flying-V?

During the literature review phase, several motion sickness models were considered and compared against each other using a trade-off table. Among these models, two stood out: the 6DOF-SVC and MSOM. The 6DOF-SVC model has been widely used in motion sickness studies and performs well with lateral, vertical, and forward acceleration. On the other hand, the MSOM model has not been used in motion sickness studies but is commonly used in aerospace spatial orientation applications. Although it did not perform well with lateral, vertical, and forward acceleration, it showed better performance with roll, pitch, and yaw. For the motion sickness analysis in the Flying-V, the 6DOF-SVC model was chosen due to its reliability in motion sickness prediction and good performance in vertical acceleration. The 6DOF-SVC model allows the estimated gravity magnitude to vary, which allows for a leakage in the gravito-inertial force to the estimated gravity's magnitude term, resulting in better performance with vertical acceleration than other models that do not permit this.

Research question 2

What visual conditions increase the incidence of motion sickness?

At the beginning of the research, the role of visual conditions in motion sickness was considered, as it is an important factor. It has been observed that consistent visual conditions cause the least sickness, followed by eyes-closed and conflicting situations. While the visual system has been integrated into motion sickness models, these models have not yet been validated for use. As a result, the analysis of motion sickness in the Flying-V does not take into account visual input.

Research question 3

Which component of the motion has the biggest influence on the specific forces?

The analysis of specific forces has been conducted on two maneuvers, namely TTB and CTC. In addition, simple roll, pitch, and yaw cases have been examined to validate the results. The analysis reveals that rolling around the c.g. is the most significant component, as it causes the most significant variations in the vertical specific force between the c.g. position and various locations in the Flying-V. This rolling motion generates additional vertical acceleration that passengers can feel. The magnitude of this acceleration increases with the distance of the seats from the center of rotation.

Research question 4

Which Flying-V's maneuver provides a bigger conflict signals and a higher motion sickness incidence value?

The 6DOF-SVC motion sickness model was used with the specific forces calculated for TTB and CTC maneuvers as inputs. The results showed that TTB induced a conflict three times greater than CTC, indicating that fast maneuvers with changing acceleration are more likely to cause motion sickness compared to slow maneuvers like CTC.

Research question 5

Which seat configuration in the Flying-V causes the most motion sickness?

Two seating configurations were analyzed in this study: the 26° rotated seat configuration and the 0° rotated seat configuration. In the 26° configuration, the seats were parallel to the aircraft's center-line, but rotated 26° relative to the fuselage's longitudinal axis. The 0° configuration, on the other hand, was parallel to the fuselage's longitudinal axis. While there was not a significant difference in terms of the vertical and total conflict between the two configurations, there was a decrease in longitudinal conflict and an increase in lateral conflict for the 0° configuration. This is because a portion of the longitudinal specific force is perceived as lateral specific force in the 0° configuration.

Therefore, rolling around the c.g. is the dominant flight parameter that contribute to motion sickness in the Flying-V. Calculating the specific forces for the TTB maneuver and using them as an input for the 6DOF-SVC to predict the MSI at various locations in the Flying-V. That helped to simplify the TTB maneuver to make the maneuver possible in the simulator and to only focus on the rolling around the c.g.

After finishing the literature and analysis phase, there are still some questions need to be answered in the experiment phase. The research question for the experiment phase is:

Research question 1 - Experiment phase

How does the presence of heave motion affect motion sickness compared to roll motion only, as measured by the MISC scores and symptom severity ratings?

An experiment has been designed to investigate the effects of roll motion and extra vertical acceleration on motion sickness. The experiment will be conducted in the SIMONA Research Simulator and will consist of three different conditions. In condition 1, participants will be exposed to roll motion only. In conditions 2 and 3, participants will experience the extra vertical acceleration caused by the rolling around the c.g., but for farther lateral locations. This will allow studying the impact of sitting with an increasing lateral distance from the center of rotation on motion sickness in the Flying-V. Moreover, this will verify the results obtained from the 6DOF-SVC model to predict the motion sickness in the Flying-V, to achieve the research objective.

References

1. Bertolini, G. & Straimann, D. Moving in a Moving world: A Review on vestibular Motion Sickness. *Frontiers in neurology* **7,** 1–11 (2016).
2. Bos, J., Machinnon, S. & Patterson, A. Motions Sickness Symptoms in a Ship Motion Simulator: Effects of Inside, Outside, and No View. *Aviat Space Environ Med* **76,** 1111–1118 (2005).
3. Reason, J. & Brand, J. *Motion Sickness* (Academic Press, London, 1975).
4. Delft, T. *Flying-V. Flying long distance energy-efficiently* `https://www.tudelft.nl/en/ae/flying-v`.
5. Joosten, S., Stroosma, O., Vos, R. & Mulder, M. Simulator Assessment of the Lateral-Directional Handling Qualities of the Flying-V. *Not published yet* (2022).
6. Claremont, C. The psychology of seasickness. *Psyche* **11,** 86–90 (1931).
7. Reason, J. Motion sickness adaptation: a neural mismatch model. *Journal of the Royal Society of Medicine* **71,** 819–829 (1978).
8. Oman, C. Motion sickness: a synthesis and evaluation of the sensory conflict theory. *Canadian journal of physiology and pharmacology* **68,** 294–303 (1988).
9. Borah, J., Young, L. R. & Curry, R. E. Sensory mechanism modelling. *Air Force Human Resources Laboratory,* 78–83 (1978).
10. Bos, J. & Bles, W. Modelling motion sickness and subjective vertical mismatch detailed for vertical motions. *Brain Research Bulletin* **47,** 537–542 (1998).
11. Mayne, R. A systems concept of the vestibular organs. In: Kornhuber,H. H., ed. Handbook of sensory physiology IV/2: vestibular system. *Springer-Verlag* **6,** 493–580 (1974).
12. Oman, C. M. A heuristic mathemaitcal model for the dynamics of sensory conflict and motion sickness. *Acta oto-laryngologica. Supplementum* **392,** 1–44 (1982).
13. Oman, C. Motion sickness: a synthesis and evaluation of the sensory conflict theory. *Can. J. Physiol. Pharmacol.* **68,** 294–303 (1990).
14. Lewkowicz, R. Modelling Motion Sickness. *Polish Aviation Medicine Society* **22,** 33–42 (2016).
15. Irmak, T. *Understanding and Modelling of Motion Sickness and Its Individual Differences For The Comfortable Control of Automated Vehicles* (Delft, 2022).
16. Kotian, V., Irmak, T., Happee, R., de Winkel, K. & Pool, D. M. Amplitude Dynamics of Motion Sickness. *Frontiers in Systems Neuroscience* **16** (2022).
17. Lawther, A. & Griffin, M. Prediction of the incidence of motion sickness from the magnitude, frequency, and duration of vertical oscillation. *The Journal of the Acoustical society of America* **82** (1987).
18. 6841, B. S. I. B. *Measurement and evaluation of human exposure to the whole-body mechanical vibration and repeated shock* (London, UK, 1987).
19. McCauley, M., Royal, J., Wylie, C., O'Hanlon, J. & Mackie, R. *Motion sickness incidence: Exploratory studies of habituation, pitch and roll, and the refinement of a mathematical model. Technical report* (Human Factors Research Inc., Santa Barbara Research Park, Goleta, California, 1976).
20. Alexander, S., Cotzin, M., Klee, J. & Wend, G. Studies of motion sickness: XVI. The effects upon sickness rates of waves of various frequencies but identical acceleration. *J Exp Psychol. American Psychological Association* **37** (1947).
21. O'Hanlon, J. & McCauley, M. *Motion sickness incidence as a function of the frequency and acceleration of vertical sinusoidal motion* (Goleta, California, 1973).
22. Forstberg, J. *Ride comfort and motion sickness in tilting trains. Human responses to motion environment in train and simulator experiments. Doctoral thesis* (Royal Institute of Technology, 2000).

23. Griffin, M. Physical characteristics of stimuli provoking motion sickness. Motion sickness: significance in aerospace operations and prophylaxis. *AGARD-LS* **3,** 1–32 (1991).
24. Wada, T., Kamiji, N. & Doi, S. A Mathematical model of motion sickness in 6DOF motion and its application to vehicle passengers. *Proc. 2nd Int. Symp. Digital Human Modeling,* 1–6 (2013).
25. Wada, T., Kawano, J., Okafuji, Y., Takamatsu, A. & Makita, M. A Computational Model of Motion Sickness Considering Visual and Vestibular Information. *Frontiers in Systems Neuroscience,* 1758–1763 (2020).
26. Dai, M., Kunin, M., Raphan, T. & Cohen, B. The relation of motion sickness to the spatial–temporal properties of velocity storage. *Exp Brain Res* **151,** 173–189 (2003).
27. Griffin, M. & Howarth, H. Effect of roll oscillation frequency on motion sickness. *Aviation, space, and environmental medicine* **74,** 326–31 (2003).
28. Donohew, B. & Griffin, M. Motion sickness: effect of the frequency of lateral oscillation. *Aviation, space, and environmental medicine* **75,** 649–56 (2004).
29. O'Hanlon, J. & McCauley, M. Motion sickness incidence as a function of the frequency and acceleration of vertical sinusoidal motion. *Aerospace medicine* **45,** 366–9 (1974).
30. Bijveld, M., Bronstein, A., Golding, J. & Gresty, M. Nauseogenicity of offvertical axis rotation vs. equivalent visual motion. *Aviation, space, and environmental medicine* **79,** 661–665 (2008).
31. Cian, C., Ohlmann, T., Ceyte, H., Gresty, M. & Golding, J. Off vertical axis rotation motion sickness and field dependence. *Aviation, space, and environmental medicine* **82,** 959–963 (2011).
32. Griffin, M. & Newman, M. M. Visual field effects on motion sickness in cars. *Aviat Sp. Environ. Med.* **15** (2004).
33. Wada, T. & Yoshida, K. Effect of passenger' active head tilt and opening/closure of eyes on motion sickness in lateral acceleration. *Ergonomics* **59,** 1050–1059 (2016).
34. Newman, M. A Multisensory Observer Model for Human Spatial Orientation Perception. *Massachusetts84.Institute of Technology* (2009).
35. Merfeld, D. & Zupan, L. Neural processing of gravitoinertial cues in humans. III Modeling tilt and translation responses. *Journal of Neurophysiology* **87,** 819–833 (2002).
36. Vingerhoets, R., Ginsbergen, J. V. & Medendorp, W. Verticality perception during off vertical axis rotation. *Journal of Neurophysiology* **97,** 3256–3268 (2007).
37. Braccesi, C. & Cianetti, F. Motion sickness. Part I: development of a model for predicting motion sickness incidence. *Human Factors Modelling and Simulation* **2,** 163–187 (2011).
38. Laurens, J. & Droulez, J. *Probabilistic Reasoning and Decision Making in Sensory-Motor Systems* (Springer, 2008).
39. Laurens, J. & Droulez, J. Bayesian processing of vestibular information. *Biological Cybernetics* **4,** 389–404 (2016).
40. Angelaki, D. Three-dimensional organization of otolith-ocular reflexes in rhesus monkeys. iii. response to translation. *J. Neurophysiol* **80,** 680–695 (1998).
41. Angelaki, D., Merfeld, D. & Hess, B. Low-frequency otolith and semicircular canal interactions after canal inactiviation. *Exp. Brain Res.* **132,** 539–549 (2000).
42. Kamiji, N., Kurata, Y., Wada, T. & Doi, S. Modeling and validation of carsickness mechanism. *SICE Annual Conference* **7,** 1138–1143 (2007).
43. Turan, O., Verveniotis, C. & Khalid, H. Motion sickness onboard ships: Subjective vertical theory and its application to full-scale trials. *Journal of Marine Science and Technology* **14,** 409–416 (2009).
44. Khalid, H., Turan, O. & Bos, J. Theory of a subjective vertical-horizontal conflict physiological motion sickness model for contemporary ships. *Journal of Marine Science and Technology* **16,** 214–225 (2011).
45. Kravets, V., Dixon, J., Ahmed, N. & Clark, T. Compass: Computations for orientation and motion perception in altered sensorimotor states. *Frontiers in Neural Circuits* **15** (2021).
46. Martínez-Val, R. & Schoep, E. Flying Wing Versus Conventional Transport Airplane: The 300 Seat Case. *International Congress Of Aeronautical Sciences* **22,** 113.1–113.12 (2000).
47. Martinez-Val, R. Flying Wings. A New Paradigm for Civil Aviation? *Acta Polytechnica* **47,** 163–187 (2007).

48. Benad, J. The Flying V. A New Aircraft Configuration for Commercial Passenger Transport. *Deutscher Luft- und Raumfahrtkongress* (2015).

49. Faggiano, F. Aerodynamic Design Optimization of a Flying V aircraft. *17th AIAA Aviation Technology, Integration, and Operations Conference* (2017).

50. TU Delft. *The technology behind the Flying-V* `https://www.tudelft.nl/lr/flying-v/technologie`.

51. Oosterom, W. & Vos, R. Conceptual Design of a Flying-V Aircraft Family. *American Institute of Aeronautics and Astronautics Inc. (AIAA),* 1–28 (2022).

52. Van den Bos, E. *CAD specialist at the ASM department of the faculty of Aerospace Engineering* `Through%20email` (2022).

53. Liu, Z., Rotte, T., Anjani, S. & Vink, P. Seat pitch and comfort of a staggered seat configuration. *Work* **68,** S151–S159 (2021).

54. Torelli, R., Stroosma, O., Vos, R. & Mulder, M. Piloted simulator evaluation of low speed handling qualities of the Flying-V. *Not published yet* (2022).

55. Vugts, G., Stroosma, O., Vos, R. & Mulder, M. Simulator Evaluation of Flightpath-oriented Control Allocation for the Flying-V. *Not published yet* (2022).

56. EASA. *Certification Specifications and Acceptable Means of Compliance for Large Aeroplanes* (EASA, 2019).

57. Cappuyns, T. Handling Qualities of a Flying-V configuration. *Master's thesis, TU Delft* (2019).

58. Van Overeem, S., Wang, X. & van Kampen, E. Modelling and Handling Quality Assessment of the Flying-V Aircraft. *AIAA SCITECH 2022 Forum* (2022).

59. Gouverneur, B., Mulder, J., van Passen, M. & Stroosma, O. Optimisation of the SIMONA Research Simulator's Motion Filter Setting for Handling Qualities Experiment. *AIAA Modeling and Simulation Technologies Conference and Exhibit,* 11–14 (2003).

60. De Winkel, K., Irmak, T., Kotian, V., Pool, D. & Happee, R. Relating individual motion sickness levels to subjective discomfort ratings. *Experimental Brain Research,* 1231–1240 (2022).

61. Bos, J., de Vries, S., van Emmerik, M. & Groen, E. The effect of internal and external fields of view on visually induced motion sickness. *Applied ergonomics* **41,** 516–521 (2010).

62. Berkouwer, W., Stroosma, O., van Paassen, R., Mulder, M. & Mulder, J. Measuring the performance of the SIMONA Research Simulator's motion system. *AIAA Modeling and Simulation Technologies Conference,* 1258–1269 (2005).

63. Stroosma, O., van Paassen, R. & Mulder, M. Using the Simona Research Simulator for human-machine interaction research. *AIAA Modeling and Simulation Technologies Conference and Exhibit,* 1–8 (2003).

Part III:

Appendices: Paper

A

Experiment Briefing, Consent Form, and Symptoms Checklist

PARTICIPANT INFORMATION LETTER

Motion Sickness in the Flying-V

Hello,

You have been asked to take part in the Motion Sickness in the Flying-V experiment. The experiment will be performed by Basem Deeb (TU Delft MSc student), under supervision of Daan Pool, Olaf Stroosma, and Rowenna Wijlens. Information regarding the experiment is provided in this letter. If you have any questions about this experiment, or the Flying-V project, don't hesitate to contact the researcher.

Background of the research

The conventional aircraft configuration is converging to its asymptote of maximum performance and efficiency. Thus, an unconventional aircraft layout has emerged, which is the flying wing. TU Delft has made a design of this blended-wing-body, which is called the Flying-V, see Figure 1**.** The design and layout of the Flying-V has promising results as it showed drag reduction of 10% compared to the conventional design with comparable performance requirements. However, if motion sickness will be a problem in the Flying-V is still unknown. Therefore, there is an increasing need to model and predict the motion sickness incidence that passengers will feel during the flight to ensure the passengers' comfort.

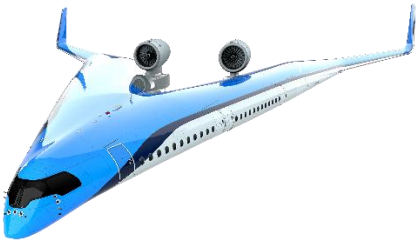

Figure 1 – The Flying-V

Purpose of the research

The goal of this study is to investigate the motion sickness in the Flying-V in a flight simulator experiment. The data will be utilized for scientific studies and/or publications. The researcher will never publish your name in any report or publication.

Risks of participating

The goal of the experiment is to determine how quickly motion sickness is develops in an aircraft like the Flying-V. However, the experiment is setup to ensure that you will never actually become truly motion sick while participating. Nevertheless, you might experience the initial symptoms of motion sickness: feeling warm, a headache, stomach awareness, starting to sweat, and feeling nauseous. Every 30 seconds, you will be prompted to report any motion sickness symptoms using the 11-point Misery Scale (MISC), which can be found in Table 1. The experiment will only be carried out up to a maximum MISC level of 6, which will keep the discomfort to some nausea and prevent the condition from getting worse. In the rare event that sickness develops very quickly, sickbags will be available in the event of a true illness (i.e., vomiting). You will be led outside the simulator when its brough back to a controlled stop, and kept under close observation until the symptoms have subsided. Naturally, participation is voluntary, and you have the right to revoke it at any time.

COVID-19 transmission is a possibility as a result of the (still ongoing) pandemic of the coronavirus. The Control and Simulations section at Aerospace Engineering has established COVID safety guidelines, and these will be followed throughout the experiment in order to reduce this risk. Ventilation will be done in the appropriate places before entry.

Table 1: Misery SCale (MISC)

Symptom		**Rating**
No problems		0
Slight discomfort but no specific symptoms		1
Dizziness, warm, headache, stomach awareness, sweating etc.	Vague Some Medium Severe	2 3 4 5
Nausea	Some Medium Severe Retching	6 7 8 9
Vomiting		10

What does participation in the research involve?

The experiment will take place on the SIMONA Research Simulator at the Faculty of Aerospace Engineering of TU Delft, see Figure 2. You will be seated in the simulator and strapped into the seat using a 5-point safety harness. The simulator lights will be switched off to darken the room.

Figure 2 - SIMONA Research Simulator

You will encounter aircraft motion stimuli throughout the experiment, and you will be required to rate your discomfort on the MISC rating scale (see Table 1) by saying out the corresponding number every 30 seconds. If it differs from the rating you previously gave, you might also decide to give a MISC rating outside the period of 30 seconds. The audio recordings will be converted to text and then will be deleted. The motion stimulation will continue until either you experience moderate nausea (MISC level 6), or until one hour has passed.

This experiment will consist of 3 separate sessions, each approximately 2 hours long (maximum). Each session will be separated by at least 1 day, to prevent habituation.

Procedures for withdrawal from the study

Your participation in this study is fully voluntary, and you are free to end it at any time, including in the middle of the experiment, by telling the researcher using the simulator's built-in microphone. You have the right to ask for personal data access, correction, or deletion. You are not required to provide justification for your choice. To do this, get in touch with the researchers using the details provided in at the end of this document.

Confidentiality of data

It is required to gather and use the following personal information for this investigation: Name, email address, age, gender, including whether you have any vestibular disorders, and voice recordings. We shall take the necessary security precautions to protect your personal information and ensure its confidentiality. This means that your data will be kept in a safe storage environment at TU Delft at all times. Only the researchers will have access to the data. All information will be handled in confidence and kept in a participant-only database. Only on the informed consent form will your name be connected to a participant number. The informed consent form will be kept in a separate, secure location and kept digitally. Your information will remain private in this manner. The only people that know your participant number are the researchers.

The personal data will be retained for linking your participation number to the informed consent, to facilitate the erasure of personal details, if you request. E-mail address will be retained for contacting you until the end of all the experiments.

The findings of this investigation will possibly be reported in upcoming scientific journals. Any publications (master's thesis report, scientific papers, reports) about the study will never include your participant number or name.

Contact Information

If you have any complaints regarding confidentiality of your data, you can contact the Aerospace faculty's data steward, Heather Andrews, via ( ).

Researcher's names, numbers and email addresses:

Basem Deeb:

Daan Pool:

Olaf Stroosma:

Rowenna Wijlens:

Consent Form for Motion Sickness in the Flying-V

Researchers:	**Basem Deeb**
Title of research:	***Motion Sickness in the Flying-V***
Supervisors:	**Daan Pool; Olaf Stroosma; Rowenna Wijlens**

Please tick the appropriate boxes	**Yes**	**No**
Taking part in the study		
I have read and understood the study information or it has been read to me. I have been able to ask questions about the study and my questions have been answered to my satisfaction.	○	○
I consent voluntarily to be a participant in this study and understand that I can refuse to answer questions and I can withdraw from the study at any time, without having to give a reason.	○	○
I understand that taking part in the study involves recording of subjective discomfort levels using audio, which will be transcribed and stored anonymously.	○	○
Risks associated with participating in the study		
I understand that taking part in this study that focuses on motion sickness involves the following risks: limited discomfort, dizziness or nausea. I hereby confirm that I will at all times honestly indicate my experiencing of any of these symptoms to the researchers.	○	○
I understand that taking part in the study involves the very small risk of developing Mal Debarquement syndrome.	○	○
Use of the information in the study		
I understand that the data that I provide will be used for scientific reports and or publications and that the researcher will not identify me by name in any report or publication that will result from this experiment and that my confidentiality as a participant in this study remains secure.	○	○
I understand that personal information collected about me that can identify me, will not be shared beyond the study team.	○	○
Future use and reuse of the information by others		
I give permission for the data, containing the discomfort levels that I provide to be archived so it can be used for future research and learning.	○	○
Safety		
I confirm that the researcher has provided me with detailed safety briefing and operational instructions to guarantee that the experiment can be performed in line with the current TU Delft COVID-19 guidelines and that I have understood these instructions, and that this experiment shall at all times follow the TU Delft guidelines	○	○

I understand that this research study has been reviewed and approved by the TU Delft Human Research Ethics Committee (HREC). I am aware that I can report any problems regarding my participation in the experiment to the researchers using the contact information below. ○ ○

Signatures

_____	_____	_____
Name of participant:	Signature	Date

I have accurately read out the information sheet to the potential participant and, to the best of my ability, ensured that the participant understands to what they are freely consenting.

_____	_____	_____
Researcher name:	Signature	Date

Study contact details for further information:

Basem Deeb

Daan Pool

Motion Sickness Symptoms Checklist
Motion sickness in the Flying-V

Part. no.: _____ (to be filled out by researcher)

Session: _____ (to be filled out by researcher)

Date: _____

This checklist is designed to capture how you were feeling during and right after exposure to the simulator motion. Please tick whether/to which extent you were/are experiencing the symptoms stated below. If appropriate, please also include the number of appearances of these symptoms.

	None	Some	Medium	Severe
General discomfort				
Fatigue				
Headache				
Eyestrain				
Difficulty focusing (eyes)				
Increased salivation				
Decreased salivation				
Sweating				
Hot flashes / Feeling overheated				
Cold flashes / Feeling cold				
Increased heartbeat				
Nausea				
Difficulty concentrating				
Fullness of head				
Blurred vision				
Dizziness (eyes open)				
Dizziness (eyes closed)				
Vertigo				
Faintness				
Awareness of breathing				
Stomach awareness				
Decreased appetite				
Increased appetite				
Burping				

Did you experience any other symptoms not mentioned above?

_____

B

Participants' Symptoms Checklist and MSSQ

B.1. Participant 2

The following question are designed to find out...
Your childhood experience only (before 12 years of age), for each of the following types of transport or entertainment please indicate...
As a **child (before age 12)**, how often you **felt sick or nauseated** (tick circle):

	Not applicable - Never travelled	Never felt sick	Rarely felt sick	Sometimes felt sick	Frequently felt sick
Cars	○	○	○	○	●
Buses or coaches	○	○	○	●	○
Trains	●	○	○	○	○
Aircrafts	●	○	○	○	○
Small boats	●	○	○	○	○
Ships, e.g. channel ferries	●	○	○	○	○
Swings in playgrounds	○	○	○	●	○
Roundabouts in playgrounds	○	○	○	●	○
Roller coasters/funfair rides	○	○	○	○	●

The following question are designed to find out...
Your experience over the last 10 years (approximately), for each of the following types of transport or entertainment please indicate...
Over the last 10 years, how often you **felt sick or nauseated** (tick circle):

	Not applicable - Never traveled	Never felt sick	Rarely felt sick	Sometimes felt sick	Frequently felt sick
Cars	○	○	○	●	○
Buses or coaches	○	○	○	●	○
Trains	○	○	●	○	○
Aircraft	○	○	●	○	○
Small boats	●	○	○	○	○
Ships, e.g. channel ferries	●	○	○	○	○
Swings in playgrounds	○	○	●	○	○
Roundabouts in playgrounds	○	○	●	○	○
Roller coasters/funfair rides	○	○	○	●	○

Figure B.1: MSSQ for Participant 2

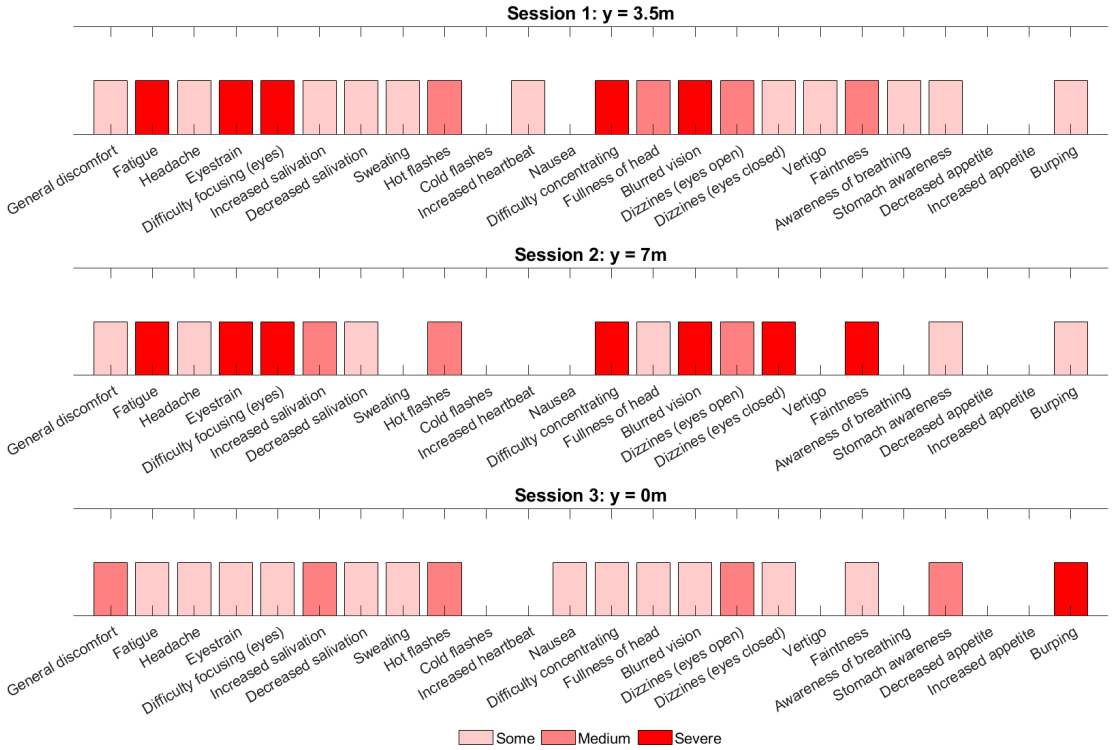

Figure B.2: Symptoms checklist for Participant 2

B.2. Participant 3

The following question are designed to find out...
Your childhood experience only (before 12 years of age), for each of the following types of transport or entertainment please indicate...
As a **child (before age 12)**, how often you **felt sick or nauseated** (tick circle):

	Not applicable - Never travelled	Never felt sick	Rarely felt sick	Sometimes felt sick	Frequently felt sick
Cars	○	○	●	○	○
Buses or coaches	○	●	○	○	○
Trains	○	●	○	○	○
Aircrafts	○	○	●	○	○
Small boats	○	○	●	○	○
Ships, e.g. channel ferries	●	○	○	○	○
Swings in playgrounds	○	●	○	○	○
Roundabouts in playgrounds	○	○	●	○	○
Roller coasters/funfair rides	○	○	○	○	●

The following question are designed to find out...
Your experience over the last 10 years (approximately), for each of the following types of transport or entertainment please indicate...
Over the last 10 years, how often you **felt sick or nauseated** (tick circle):

	Not applicable - Never traveled	Never felt sick	Rarely felt sick	Sometimes felt sick	Frequently felt sick
Cars	○	○	●	○	○
Buses or coaches	○	●	○	○	○
Trains	○	●	○	○	○
Aircraft	○	●	○	○	○
Small boats	○	○	●	○	○
Ships, e.g. channel ferries	●	○	○	○	○
Swings in playgrounds	○	●	○	○	○
Roundabouts in playgrounds	○	○	●	○	○
Roller coasters/funfair rides	○	○	●	○	○

Figure B.3: MSSQ for Participant 3

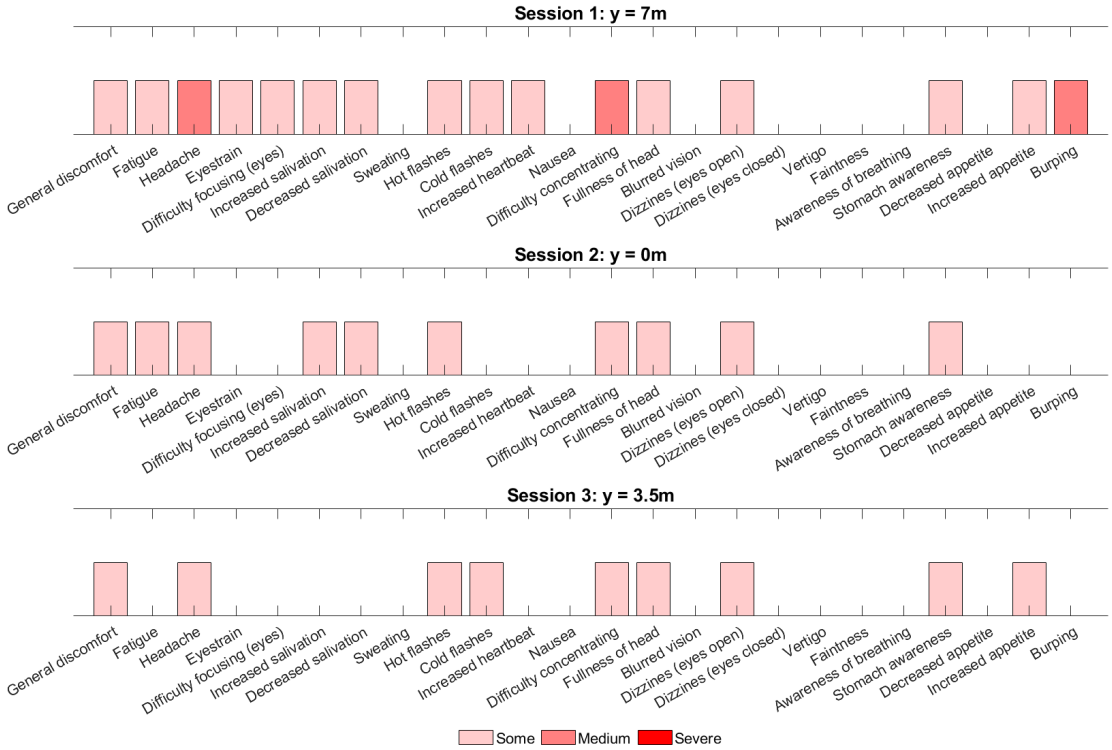

Figure B.4: Symptoms checklist for Participant 3

B.3. Participant 4

The following question are designed to find out...
Your childhood experience only (before 12 years of age), for each of the following types of transport or entertainment please indicate...
As a **child (before age 12)**, how often you **felt sick or nauseated** (tick circle):

	Not applicable - Never travelled	Never felt sick	Rarely felt sick	Sometimes felt sick	Frequently felt sick
Cars	○	○	○	●	○
Buses or coaches	○	○	○	●	○
Trains	○	●	○	○	○
Aircrafts	○	○	●	○	○
Small boats	○	○	●	○	○
Ships, e.g. channel ferries	○	○	●	○	○
Swings in playgrounds	○	●	○	○	○
Roundabouts in playgrounds	○	●	○	○	○
Roller coasters/funfair rides	○	○	○	●	○

The following question are designed to find out...
Your experience over the last 10 years (approximately), for each of the following types of transport or entertainment please indicate...
Over the last 10 years, how often you **felt sick or nauseated** (tick circle):

	Not applicable - Never traveled	Never felt sick	Rarely felt sick	Sometimes felt sick	Frequently felt sick
Cars	○	●	○	○	○
Buses or coaches	○	○	●	○	○
Trains	○	●	○	○	○
Aircraft	○	●	○	○	○
Small boats	○	●	○	○	○
Ships, e.g. channel ferries	○	○	●	○	○
Swings in playgrounds	○	●	○	○	○
Roundabouts in playgrounds	○	●	○	○	○
Roller coasters/funfair rides	○	●	○	○	○

Figure B.5: MSSQ for Participant 4

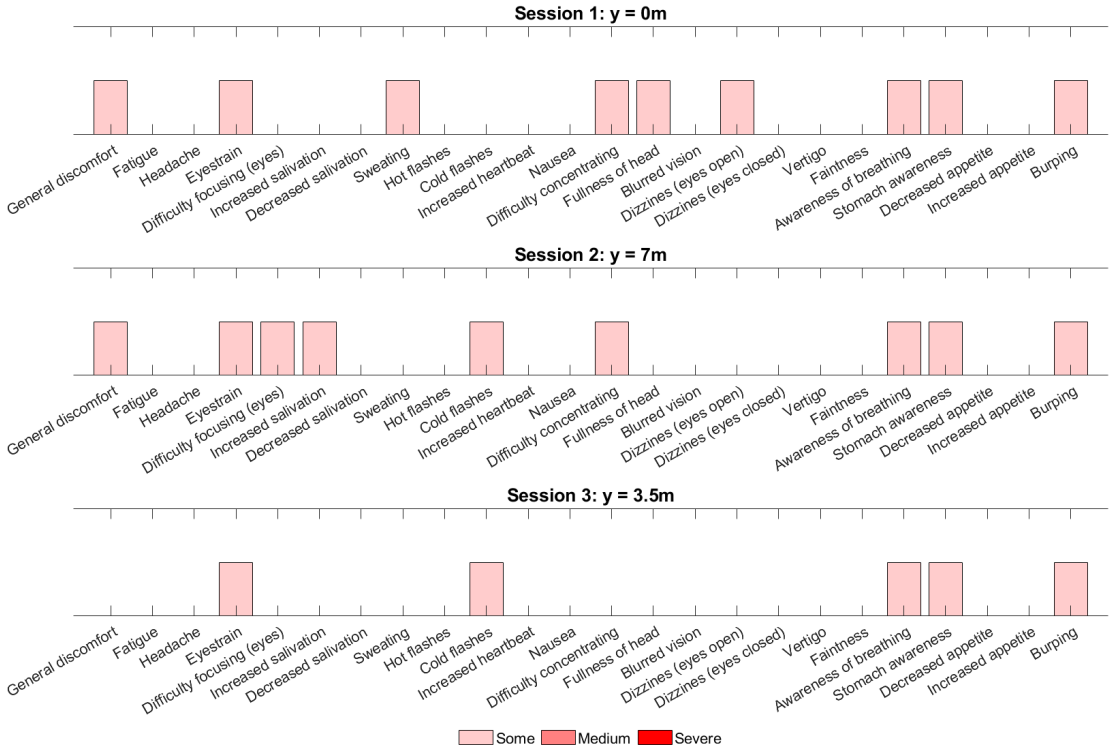

Figure B.6: Symptoms checklist for Participant 4

B.4. Participant 5

The following question are designed to find out...
Your childhood experience only (before 12 years of age), for each of the following types of transport or entertainment please indicate...
As a **child (before age 12)**, how often you **felt sick or nauseated** (tick circle):

	Not applicable - Never travelled	Never felt sick	Rarely felt sick	Sometimes felt sick	Frequently felt sick
Cars	○	○	●	○	○
Buses or coaches	○	○	●	○	○
Trains	○	○	●	○	○
Aircrafts	○	○	●	○	○
Small boats	○	○	●	○	○
Ships, e.g. channel ferries	○	○	○	●	○
Swings in playgrounds	○	○	○	●	○
Roundabouts in playgrounds	○	○	●	○	○
Roller coasters/funfair rides	○	●	○	○	○

The following question are designed to find out...
Your experience over the last 10 years (approximately), for each of the following types of transport or entertainment please indicate...
Over the last 10 years, how often you **felt sick or nauseated** (tick circle):

	Not applicable - Never traveled	Never felt sick	Rarely felt sick	Sometimes felt sick	Frequently felt sick
Cars	○	○	●	○	○
Buses or coaches	○	○	●	○	○
Trains	○	○	○	○	●
Aircraft	○	○	●	○	○
Small boats	○	○	●	○	○
Ships, e.g. channel ferries	○	○	○	●	○
Swings in playgrounds	○	○	●	○	○
Roundabouts in playgrounds	○	●	○	○	○
Roller coasters/funfair rides	○	●	○	○	○

Figure B.7: MSSQ for Participant 5

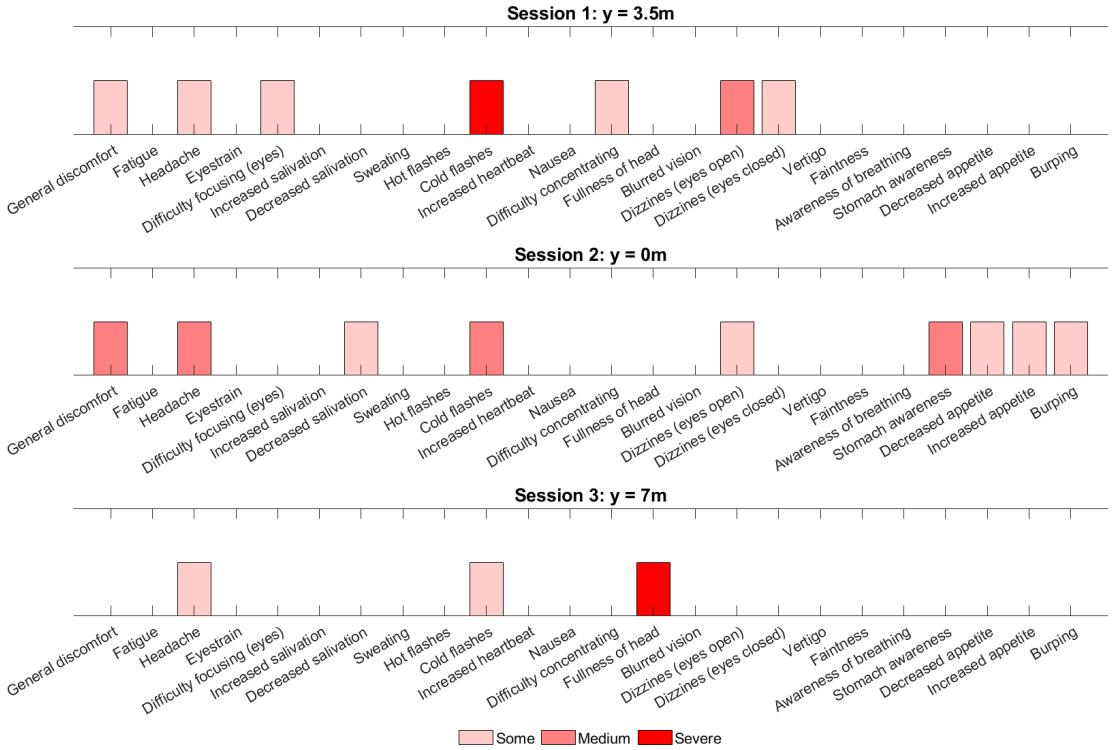

Figure B.8: Symptoms checklist for Participant 5

B.5. Participant 6

The following question are designed to find out...
Your childhood experience only (before 12 years of age), for each of the following types of transport or entertainment please indicate...
As a **child (before age 12)**, how often you **felt sick or nauseated** (tick circle):

	Not applicable - Never travelled	Never felt sick	Rarely felt sick	Sometimes felt sick	Frequently felt sick
Cars	○	○	○	●	○
Buses or coaches	○	○	○	●	○
Trains	○	○	○	●	○
Aircrafts	○	○	○	●	○
Small boats	○	○	●	○	○
Ships, e.g. channel ferries	○	○	●	○	○
Swings in playgrounds	○	○	●	○	○
Roundabouts in playgrounds	○	○	●	○	○
Roller coasters/funfair rides	○	○	●	○	○

The following question are designed to find out...
Your experience over the last 10 years (approximately), for each of the following types o transport or entertainment please indicate...
Over the last 10 years, how often you **felt sick or nauseated** (tick circle):

	Not applicable - Never traveled	Never felt sick	Rarely felt sick	Sometimes felt sick	Frequently felt sick
Cars	○	○	○	●	○
Buses or coaches	○	○	○	●	○
Trains	○	○	○	●	○
Aircraft	○	○	●	○	○
Small boats	○	○	●	○	○
Ships, e.g. channel ferries	○	○	○	●	○
Swings in playgrounds	○	○	○	●	○
Roundabouts in playgrounds	○	○	○	○	●
Roller coasters/funfair rides	○	○	○	●	○

Figure B.9: MSSQ for Participant 6

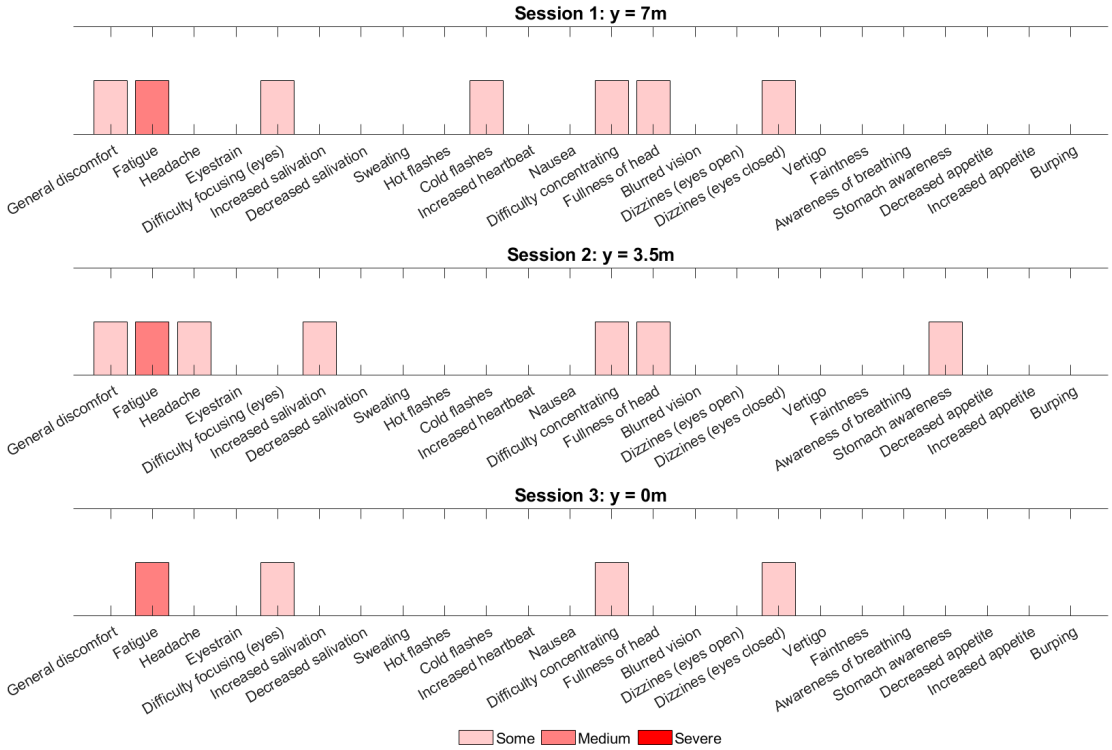

Figure B.10: Symptoms checklist for Participant 6

B.6. Participant 7

The following question are designed to find out...
Your childhood experience only (before 12 years of age), for each of the following types of transport or entertainment please indicate...
As a **child (before age 12)**, how often you **felt sick or nauseated** (tick circle):

	Not applicable - Never travelled	Never felt sick	Rarely felt sick	Sometimes felt sick	Frequently felt sick
Cars	●	○	○	○	○
Buses or coaches	●	○	○	○	○
Trains	○	○	●	○	○
Aircrafts	○	○	●	○	○
Small boats	○	○	●	○	○
Ships, e.g. channel ferries	●	○	○	○	○
Swings in playgrounds	●	○	○	○	○
Roundabouts in playgrounds	●	○	○	○	○
Roller coasters/funfair rides	○	○	●	○	○

The following question are designed to find out...
Your experience over the last 10 years (approximately), for each of the following types of transport or entertainment please indicate...
Over the last 10 years, how often you **felt sick or nauseated** (tick circle):

	Not applicable - Never traveled	Never felt sick	Rarely felt sick	Sometimes felt sick	Frequently felt sick
Cars	●	○	○	○	○
Buses or coaches	●	○	○	○	○
Trains	○	○	○	●	○
Aircraft	○	○	○	●	○
Small boats	○	○	●	○	○
Ships, e.g. channel ferries	●	○	○	○	○
Swings in playgrounds	●	○	○	○	○
Roundabouts in playgrounds	●	○	○	○	○
Roller coasters/funfair rides	●	○	○	○	○

Figure B.11: MSSQ for Participant 7

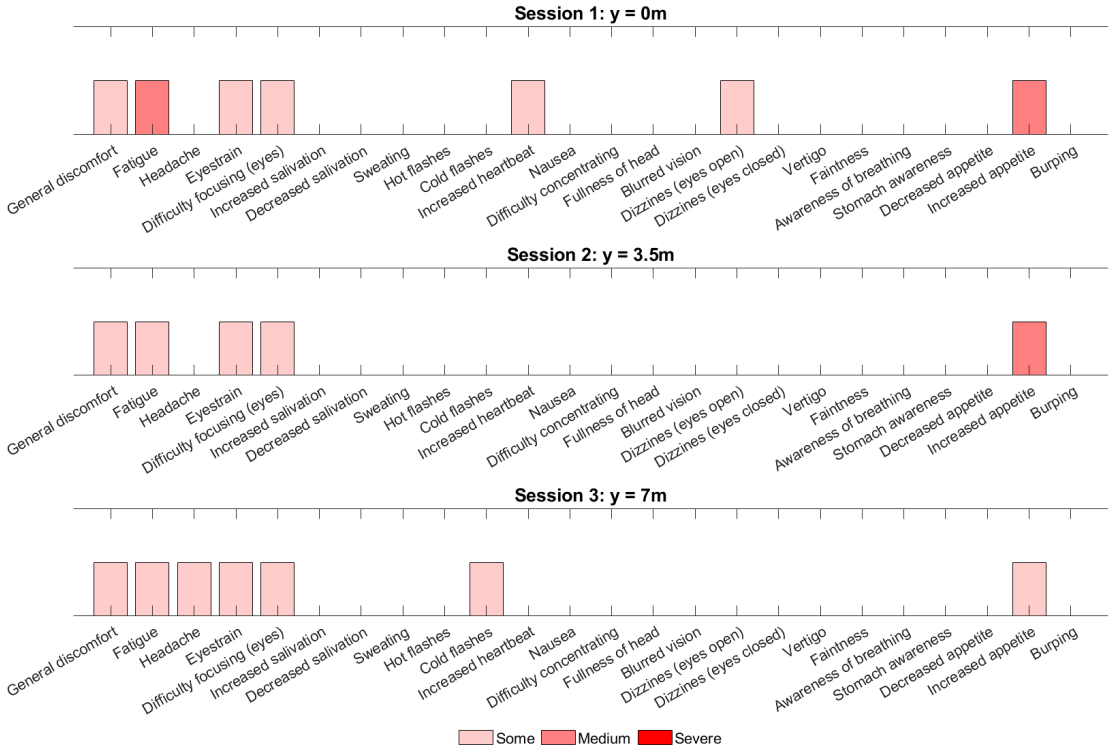

Figure B.12: Symptoms checklist for Participant 7

B.7. Participant 8

The following question are designed to find out...
Your childhood experience only (before 12 years of age), for each of the following types of transport or entertainment please indicate...
As a **child (before age 12)**, how often you **felt sick or nauseated** (tick circle):

	Not applicable - Never travelled	Never felt sick	Rarely felt sick	Sometimes felt sick	Frequently felt sick
Cars	●	○	○	○	○
Buses or coaches	●	○	○	○	○
Trains	●	○	○	○	○
Aircrafts	●	○	○	○	○
Small boats	○	○	●	○	○
Ships, e.g. channel ferries	●	○	○	○	○
Swings in playgrounds	●	○	○	○	○
Roundabouts in playgrounds	○	○	●	○	○
Roller coasters/funfair rides	●	○	○	○	○

The following question are designed to find out...
Your experience over the last 10 years (approximately), for each of the following types of transport or entertainment please indicate...
Over the last 10 years, how often you **felt sick or nauseated** (tick circle):

	Not applicable - Never traveled	Never felt sick	Rarely felt sick	Sometimes felt sick	Frequently felt sick
Cars	●	○	○	○	○
Buses or coaches	●	○	○	○	○
Trains	○	○	●	○	○
Aircraft	○	○	●	○	○
Small boats	○	○	●	○	○
Ships, e.g. channel ferries	●	○	○	○	○
Swings in playgrounds	●	○	○	○	○
Roundabouts in playgrounds	●	○	○	○	○
Roller coasters/funfair rides	●	○	○	○	○

Figure B.13: MSSQ for Participant 8

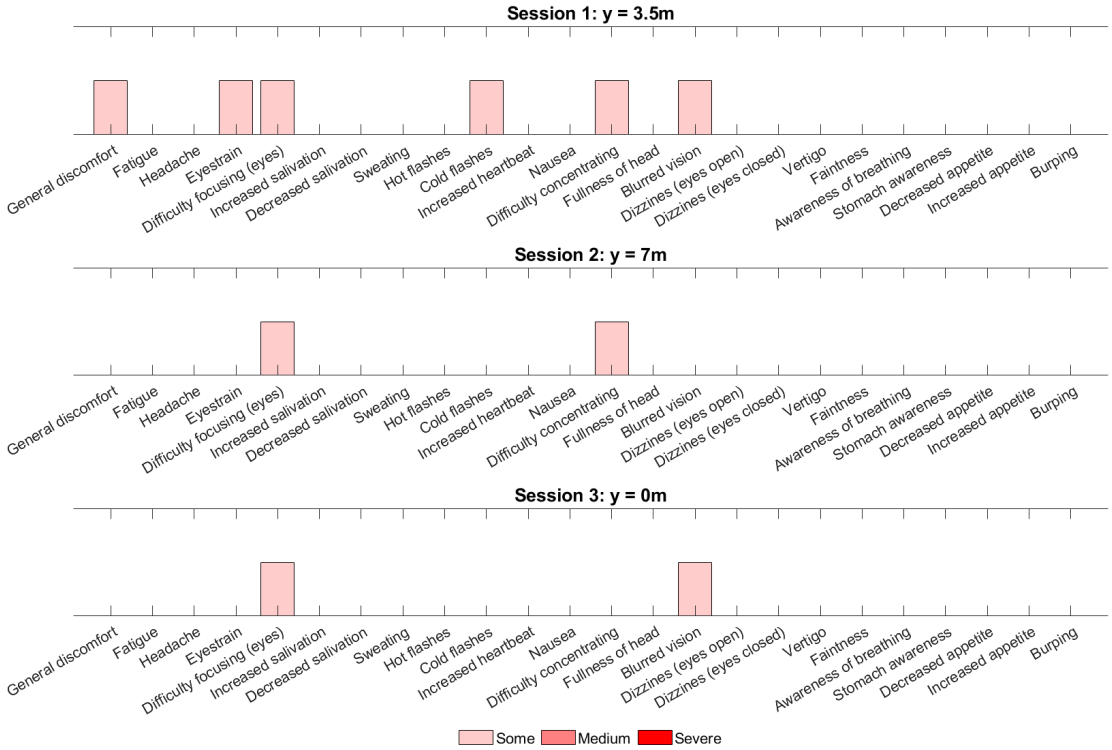

Figure B.14: Symptoms checklist for Participant 8

B.8. Participant 9

The following question are designed to find out...
Your childhood experience only (before 12 years of age), for each of the following types of transport or entertainment please indicate...
As a **child (before age 12)**, how often you **felt sick or nauseated** (tick circle):

	Not applicable - Never travelled	Never felt sick	Rarely felt sick	Sometimes felt sick	Frequently felt sick
Cars	○	○	○	○	●
Buses or coaches	○	○	○	●	○
Trains	○	●	○	○	○
Aircrafts	○	○	●	○	○
Small boats	○	○	○	○	●
Ships, e.g. channel ferries	○	○	●	○	○
Swings in playgrounds	○	○	○	○	●
Roundabouts in playgrounds	○	○	○	○	●
Roller coasters/funfair rides	●	○	○	○	○

The following question are designed to find out...
Your experience over the last 10 years (approximately), for each of the following types of transport or entertainment please indicate...
Over the last 10 years, how often you **felt sick or nauseated** (tick circle):

	Not applicable - Never traveled	Never felt sick	Rarely felt sick	Sometimes felt sick	Frequently felt sick
Cars	○	○	○	●	○
Buses or coaches	○	○	●	○	○
Trains	○	●	○	○	○
Aircraft	○	●	○	○	○
Small boats	○	○	●	○	○
Ships, e.g. channel ferries	○	●	○	○	○
Swings in playgrounds	○	○	○	●	○
Roundabouts in playgrounds	●	○	○	○	○
Roller coasters/funfair rides	○	●	○	○	○

Figure B.15: MSSQ for Participant 9

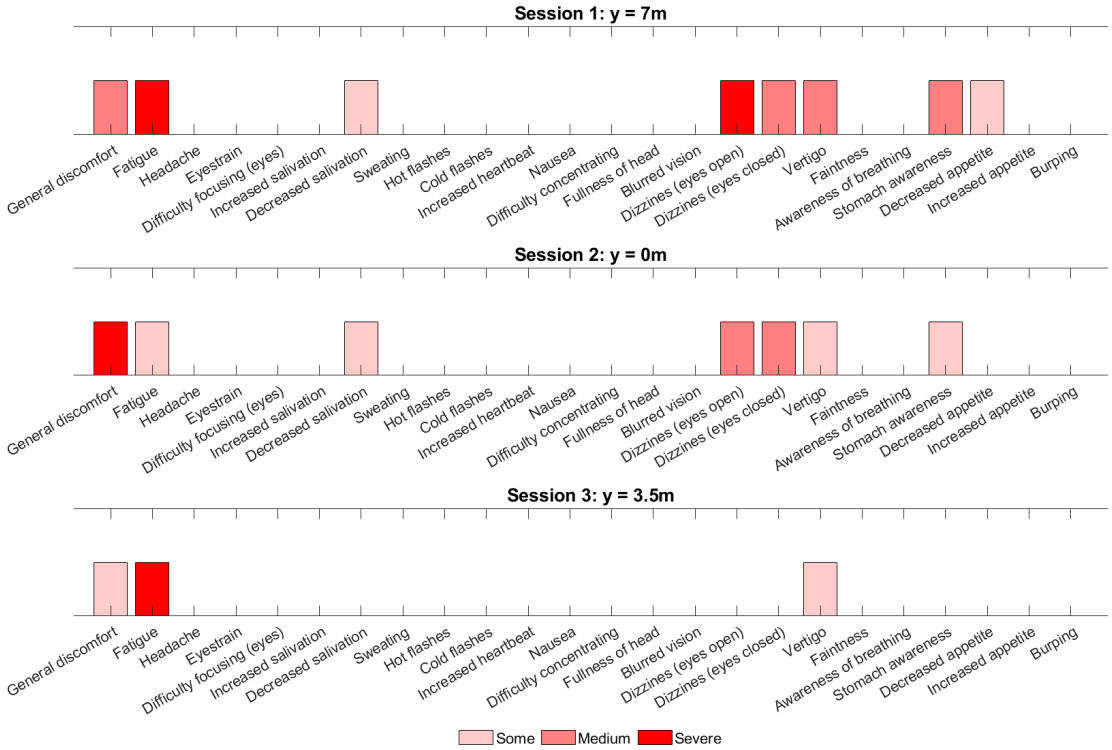

Figure B.16: Symptoms checklist for Participant 9

B.9. Participant 10

The following question are designed to find out...
Your childhood experience only (before 12 years of age), for each of the following types of transport or entertainment please indicate...
As a **child (before age 12)**, how often you **felt sick or nauseated** (tick circle):

	Not applicable - Never travelled	Never felt sick	Rarely felt sick	Sometimes felt sick	Frequently felt sick
Cars	○	○	○	●	○
Buses or coaches	○	○	○	●	○
Trains	●	○	○	○	○
Aircrafts	○	○	●	○	○
Small boats	○	●	○	○	○
Ships, e.g. channel ferries	○	●	○	○	○
Swings in playgrounds	○	●	○	○	○
Roundabouts in playgrounds	○	●	○	○	○
Roller coasters/funfair rides	○	○	●	○	○

The following question are designed to find out...
Your experience over the last 10 years (approximately), for each of the following types of transport or entertainment please indicate...
Over the last 10 years, how often you **felt sick or nauseated** (tick circle):

	Not applicable - Never traveled	Never felt sick	Rarely felt sick	Sometimes felt sick	Frequently felt sick
Cars	○	○	○	●	○
Buses or coaches	○	○	○	●	○
Trains	○	●	○	○	○
Aircraft	○	●	○	○	○
Small boats	○	○	●	○	○
Ships, e.g. channel ferries	○	○	●	○	○
Swings in playgrounds	○	●	○	○	○
Roundabouts in playgrounds	○	●	○	○	○
Roller coasters/funfair rides	○	○	●	○	○

Figure B.17: MSSQ for Participant 10

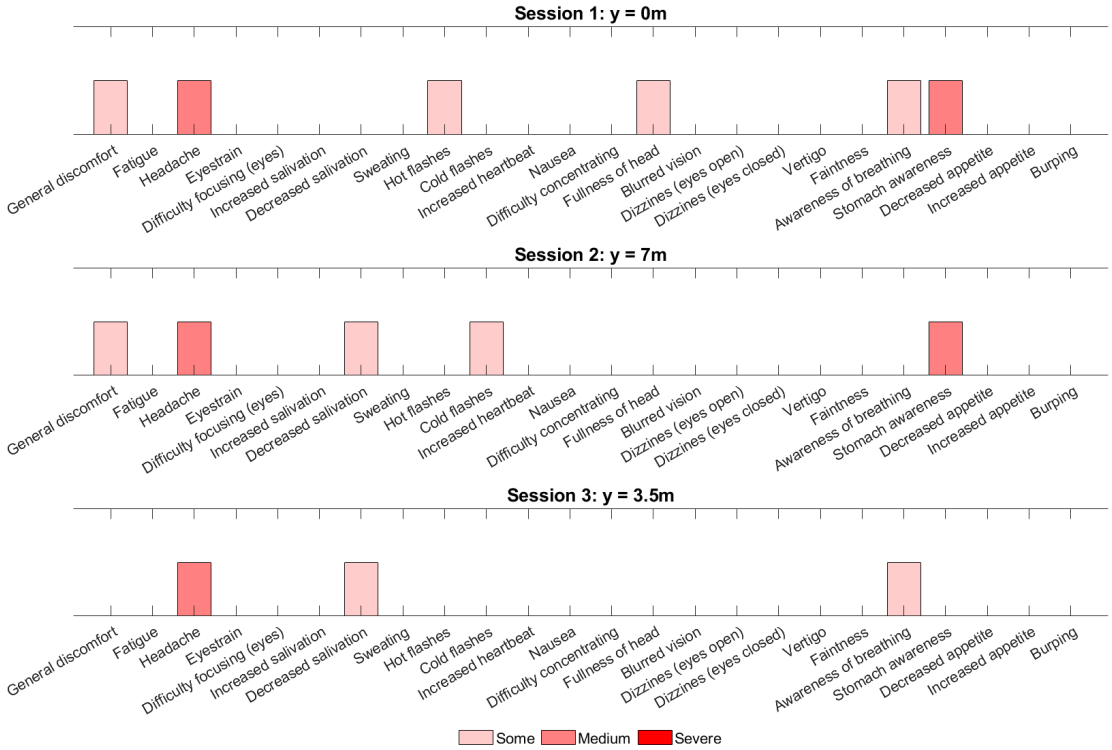

Figure B.18: Symptoms checklist for Participant 10

B.10. Participant 11

The following question are designed to find out...
Your childhood experience only (before 12 years of age), for each of the following types of transport or entertainment please indicate...
As a **child (before age 12)**, how often you **felt sick or nauseated** (tick circle):

	Not applicable - Never travelled	Never felt sick	Rarely felt sick	Sometimes felt sick	Frequently felt sick
Cars	○	○	●	○	○
Buses or coaches	○	○	●	○	○
Trains	○	○	●	○	○
Aircrafts	○	○	●	○	○
Small boats	○	●	○	○	○
Ships, e.g. channel ferries	○	●	○	○	○
Swings in playgrounds	○	○	●	○	○
Roundabouts in playgrounds	○	●	○	○	○
Roller coasters/funfair rides	○	●	○	○	○

The following question are designed to find out...
Your experience over the last 10 years (approximately), for each of the following types of transport or entertainment please indicate...
Over the last 10 years, how often you **felt sick or nauseated** (tick circle):

	Not applicable - Never traveled	Never felt sick	Rarely felt sick	Sometimes felt sick	Frequently felt sick
Cars	○	○	●	○	○
Buses or coaches	○	○	●	○	○
Trains	○	○	●	○	○
Aircraft	○	●	○	○	○
Small boats	○	●	○	○	○
Ships, e.g. channel ferries	○	●	○	○	○
Swings in playgrounds	○	●	○	○	○
Roundabouts in playgrounds	○	●	○	○	○
Roller coasters/funfair rides	○	●	○	○	○

Figure B.19: MSSQ for Participant 11

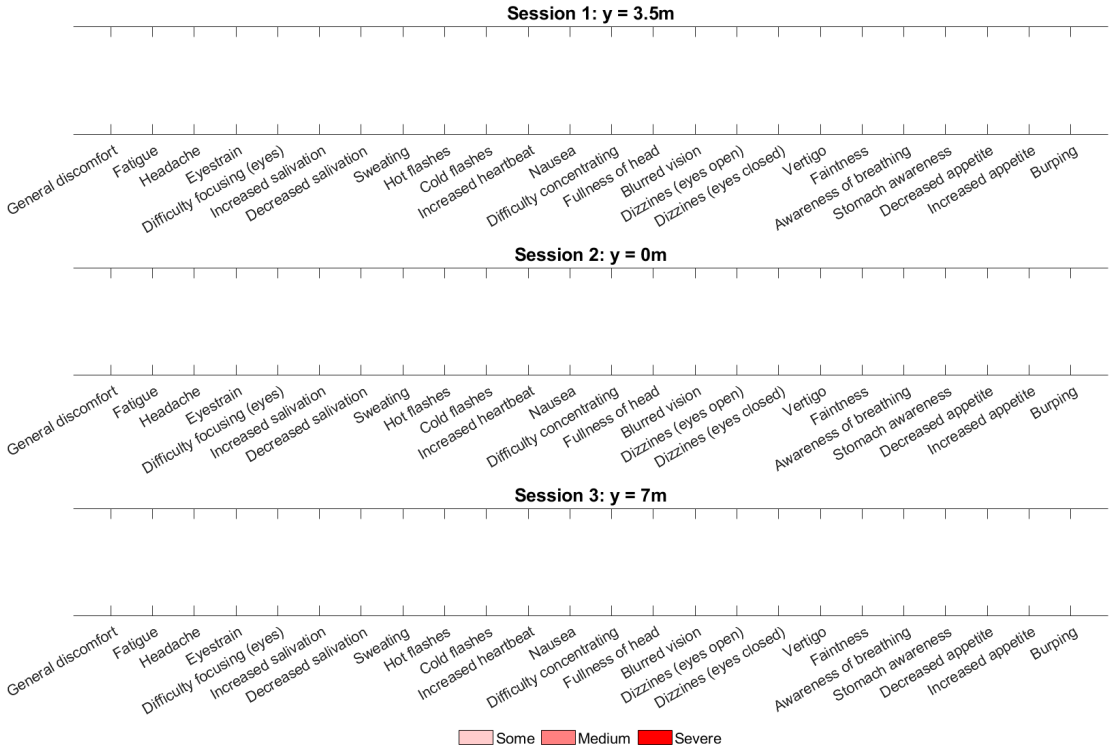

Figure B.20: Symptoms checklist for Participant 11

B.11. Participant 12

The following question are designed to find out...
Your childhood experience only (before 12 years of age), for each of the following types of transport or entertainment please indicate...
As a **child (before age 12)**, how often you **felt sick or nauseated** (tick circle):

	Not applicable - Never travelled	Never felt sick	Rarely felt sick	Sometimes felt sick	Frequently felt sick
Cars	○	○	○	●	○
Buses or coaches	○	○	○	●	○
Trains	○	○	●	○	○
Aircrafts	○	○	●	○	○
Small boats	○	○	●	○	○
Ships, e.g. channel ferries	○	●	○	○	○
Swings in playgrounds	○	●	○	○	○
Roundabouts in playgrounds	○	●	○	○	○
Roller coasters/funfair rides	○	●	○	○	○

The following question are designed to find out...
Your experience over the last 10 years (approximately), for each of the following types of transport or entertainment please indicate...
Over the last 10 years, how often you **felt sick or nauseated** (tick circle):

	Not applicable - Never traveled	Never felt sick	Rarely felt sick	Sometimes felt sick	Frequently felt sick
Cars	○	○	●	○	○
Buses or coaches	○	○	●	○	○
Trains	○	○	●	○	○
Aircraft	○	○	●	○	○
Small boats	○	●	○	○	○
Ships, e.g. channel ferries	○	●	○	○	○
Swings in playgrounds	○	●	○	○	○
Roundabouts in playgrounds	○	●	○	○	○
Roller coasters/funfair rides	○	●	○	○	○

Figure B.21: MSSQ for Participant 12

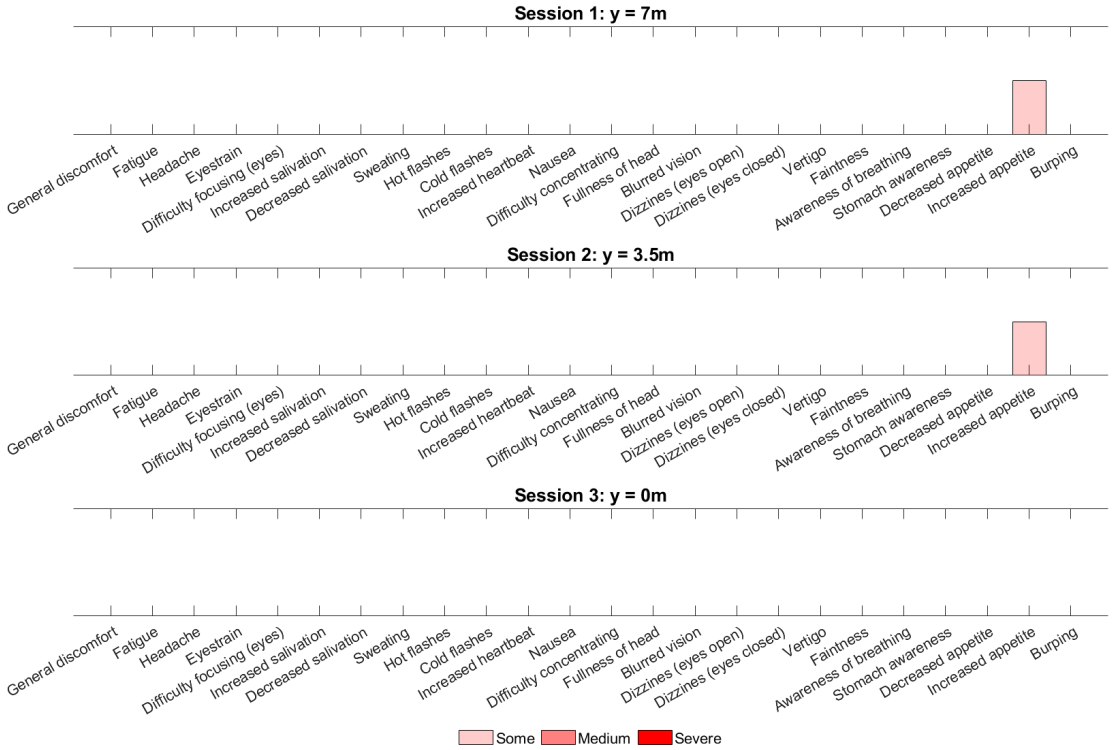

Figure B.22: Symptoms checklist for Participant 12

B.12. Participant 13

The following question are designed to find out...
Your childhood experience only (before 12 years of age), for each of the following types of transport or entertainment please indicate...
As a **child (before age 12)**, how often you **felt sick or nauseated** (tick circle):

	Not applicable - Never travelled	Never felt sick	Rarely felt sick	Sometimes felt sick	Frequently felt sick
Cars	○	○	○	●	○
Buses or coaches	○	○	○	●	○
Trains	○	○	●	○	○
Aircrafts	○	○	●	○	○
Small boats	○	○	●	○	○
Ships, e.g. channel ferries	○	○	●	○	○
Swings in playgrounds	○	○	●	○	○
Roundabouts in playgrounds	○	○	●	○	○
Roller coasters/funfair rides	○	○	●	○	○

The following question are designed to find out...
Your experience over the last 10 years (approximately), for each of the following types of transport or entertainment please indicate...
Over the last 10 years, how often you **felt sick or nauseated** (tick circle):

	Not applicable - Never traveled	Never felt sick	Rarely felt sick	Sometimes felt sick	Frequently felt sick
Cars	○	○	○	●	○
Buses or coaches	○	○	○	●	○
Trains	○	○	○	●	○
Aircraft	○	○	●	○	○
Small boats	○	○	●	○	○
Ships, e.g. channel ferries	○	○	●	○	○
Swings in playgrounds	○	○	●	○	○
Roundabouts in playgrounds	○	○	●	○	○
Roller coasters/funfair rides	○	●	○	○	○

Figure B.23: MSSQ for Participant 13

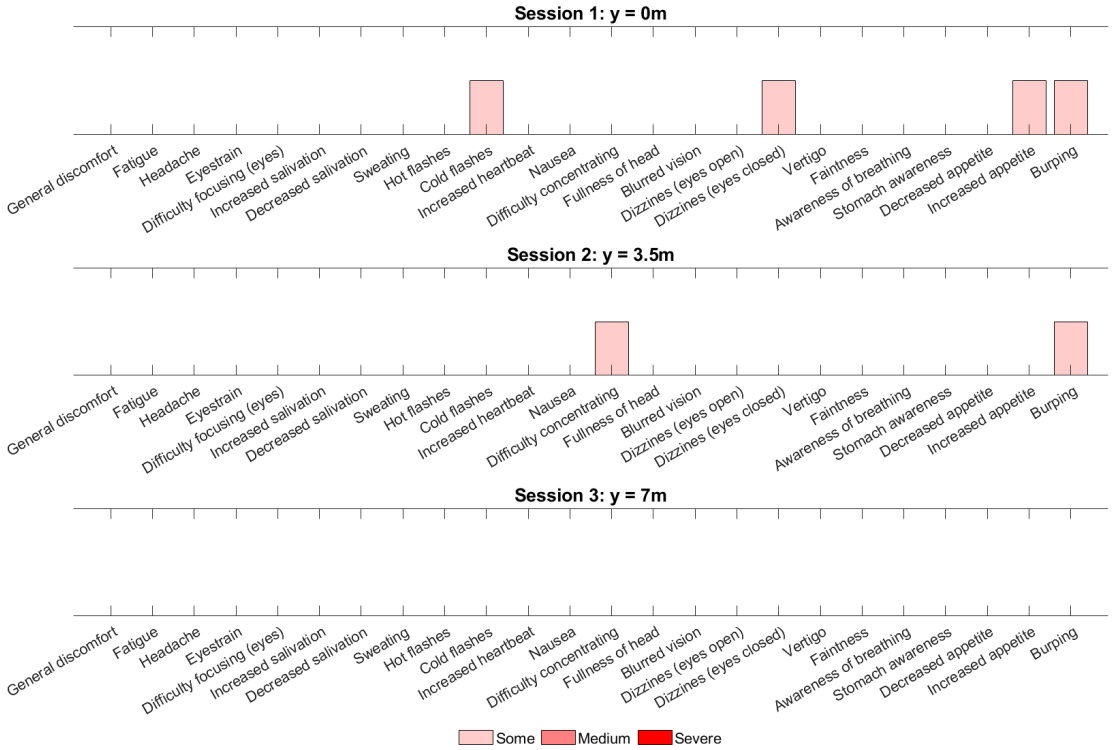

Figure B.24: Symptoms checklist for Participant 13

Part IV:

Appendices: Preliminary Report

NOTE:

This part has already been graded under AE4020

C

Time-to-Bank maneuver's additional figures

C.1. Data Filtering for TTB

In this section, the flight data that has been collected from the pilot-in-the-loop experiments are filtered in order to erase the effect of the high spikes of the data. The figures show that the data have been filtered for a range of break frequency.

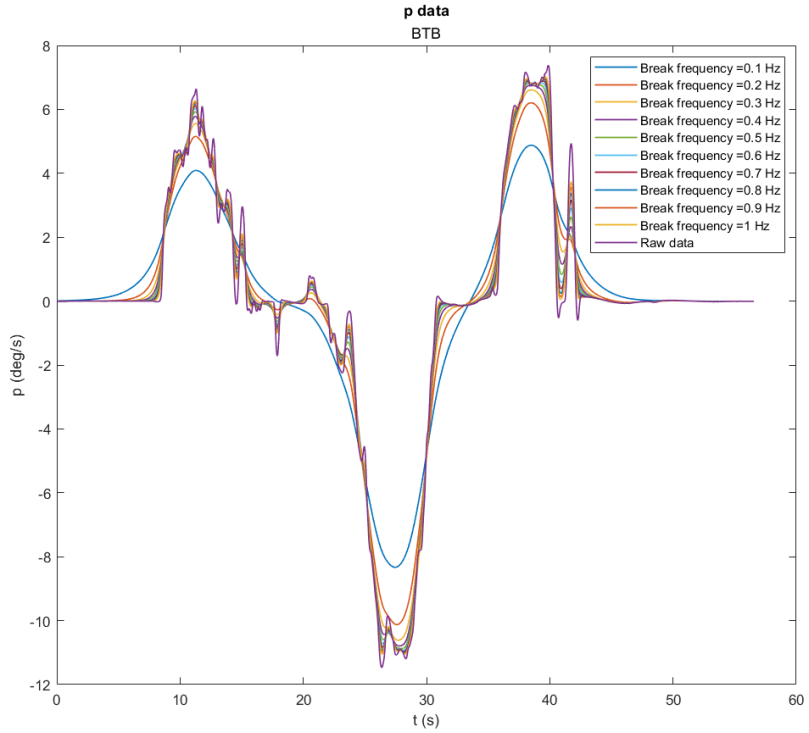

Figure C.1: Roll rate (p) flight data with multiple break frequency

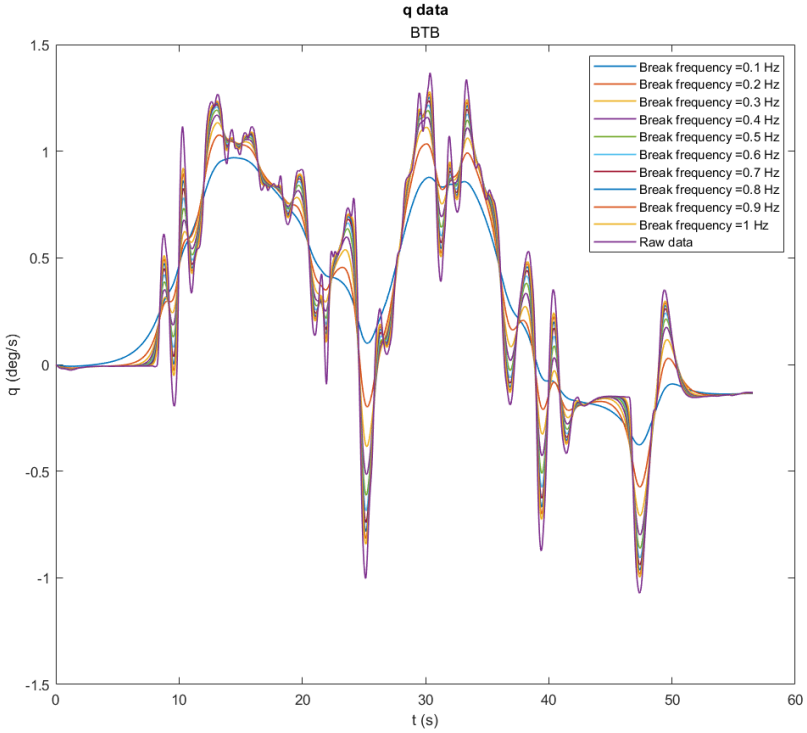

Figure C.2: Pitch rate (q) flight data with multiple break frequency

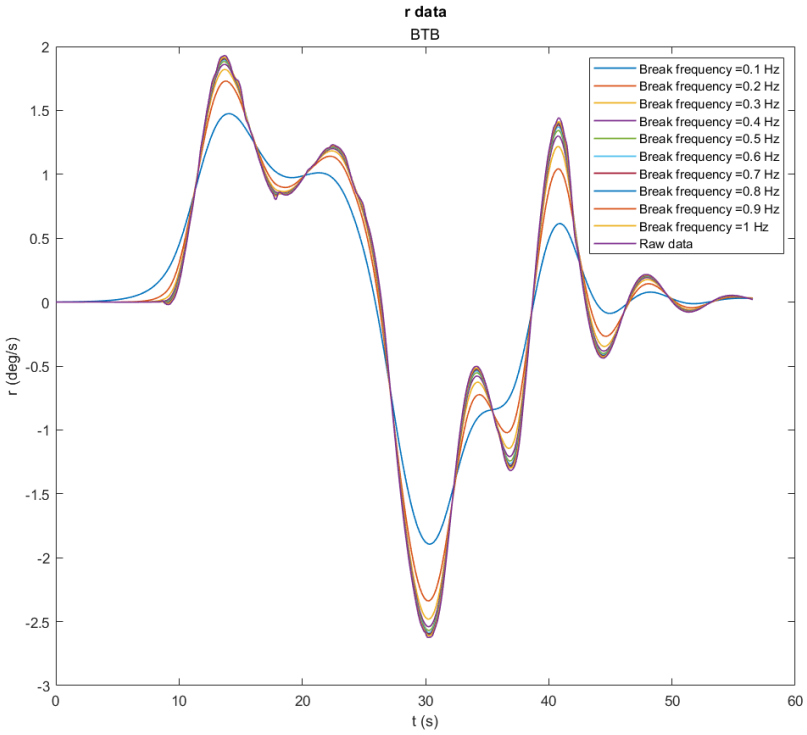

Figure C.3: Yaw rate (r) flight data with multiple break frequency

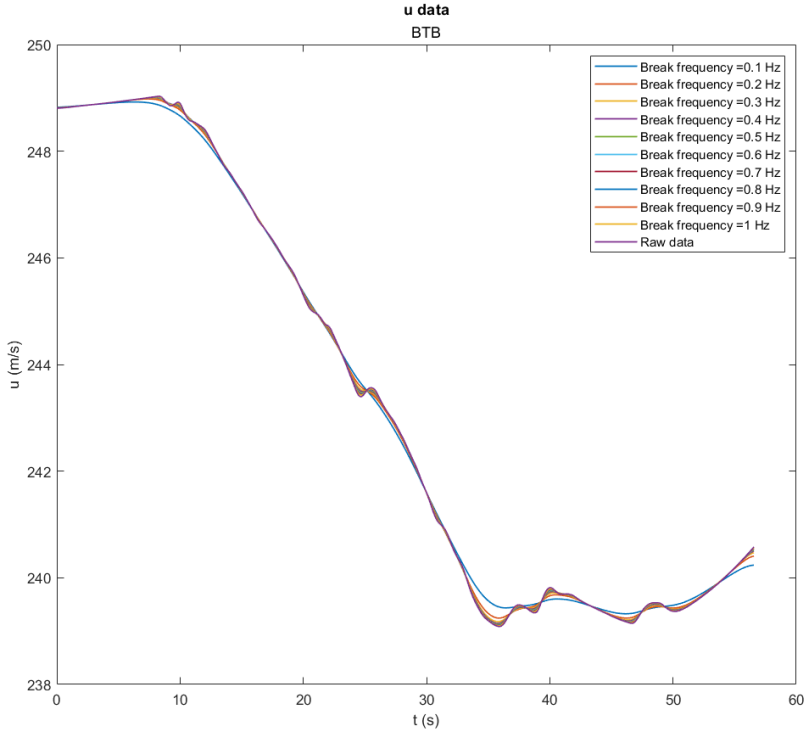

Figure C.4: Forward velocity (u) flight data with multiple break frequency

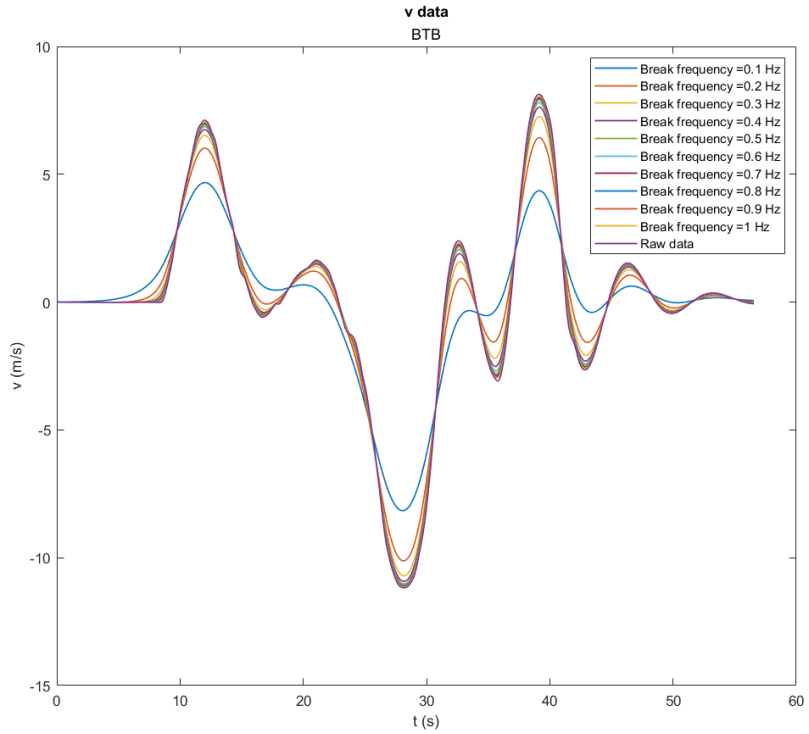

Figure C.5: Lateral velocity (v) flight data with multiple break frequency

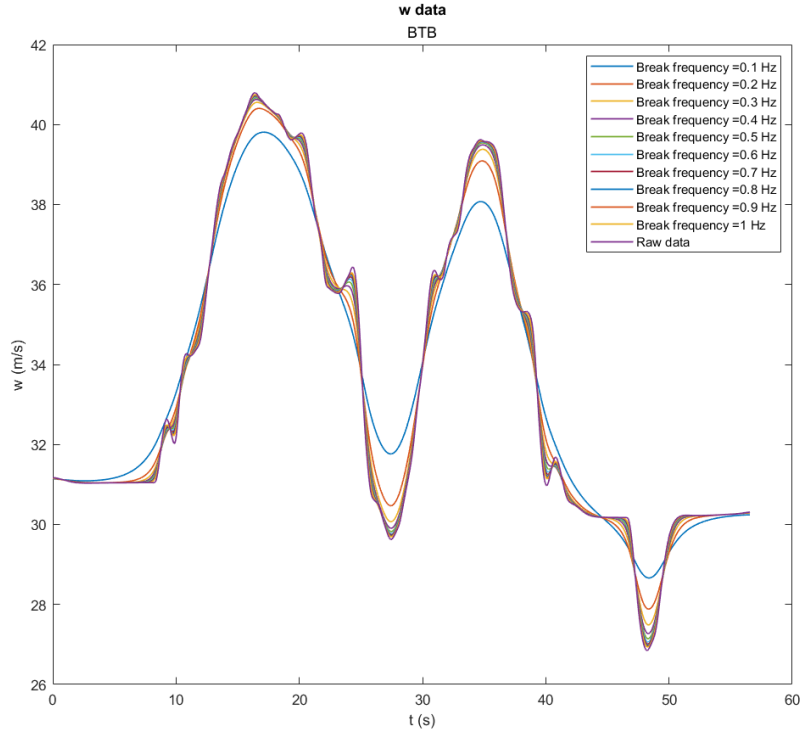

Figure C.6: Vertical velocity (w) flight data with multiple break frequency

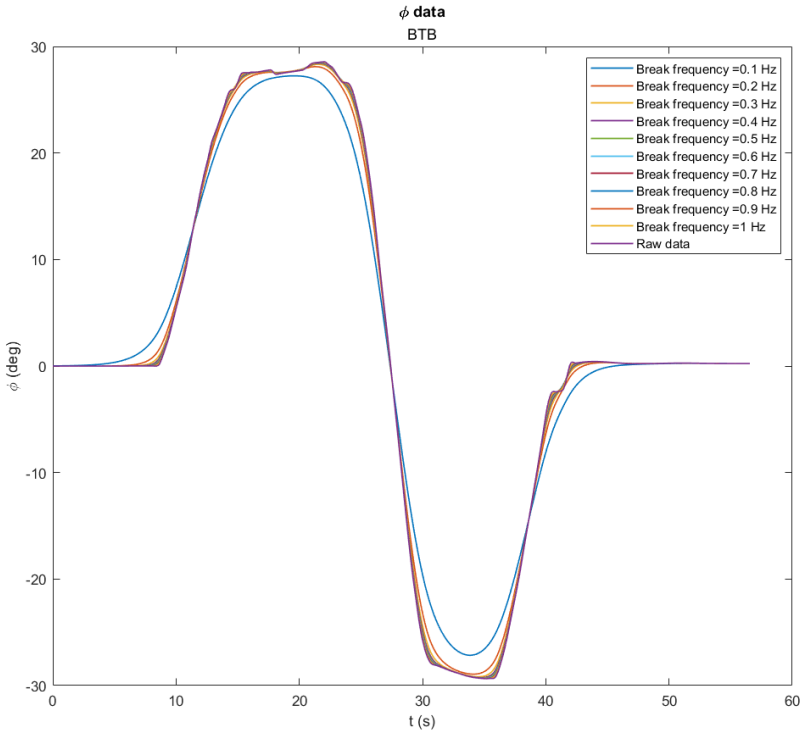

Figure C.7: Roll angle (ϕ) flight data with multiple break frequency

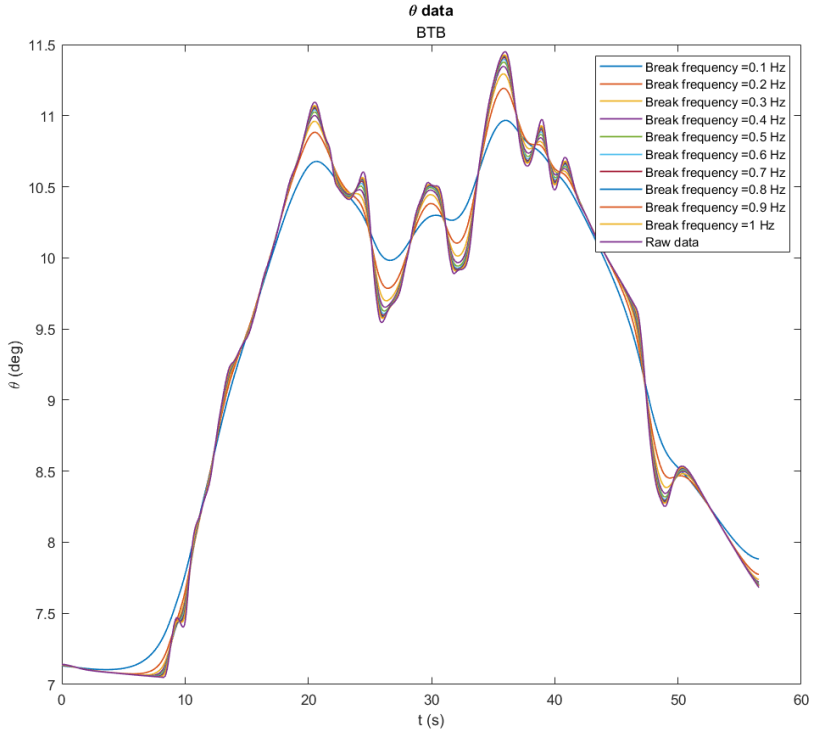

Figure C.8: Pitch angle (θ) flight data with multiple break frequency

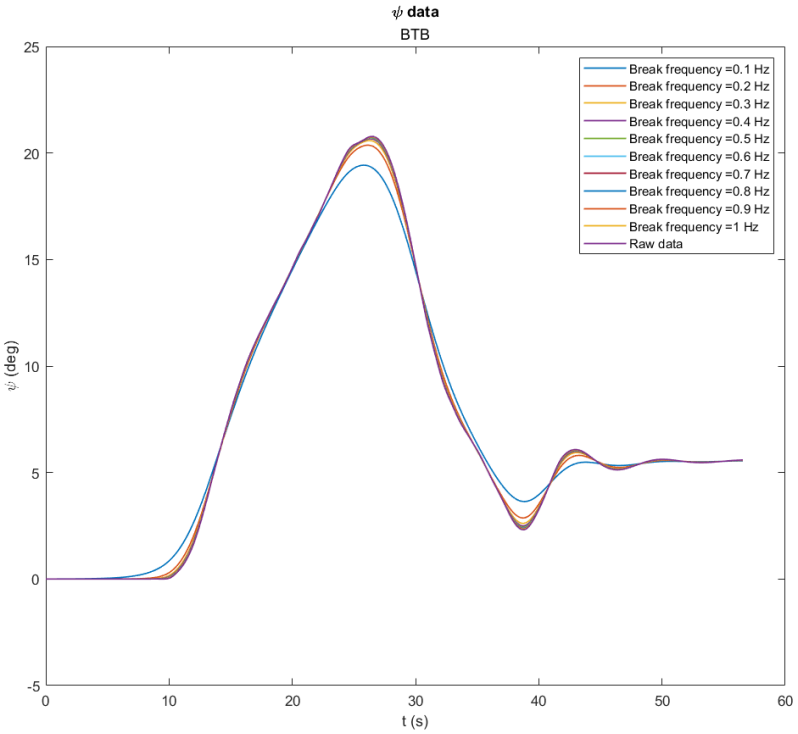

Figure C.9: Yaw angle (ψ) flight data with multiple break frequency

C.2. Specific forces, left wing

The specific forces calculation for the left wing and both seat configuration are shown in this section.

A. 26° rotated seat configuration

The specific forces using 26° rotated seat configuration at x = 17m, and -1m are shown below.

x = 17m

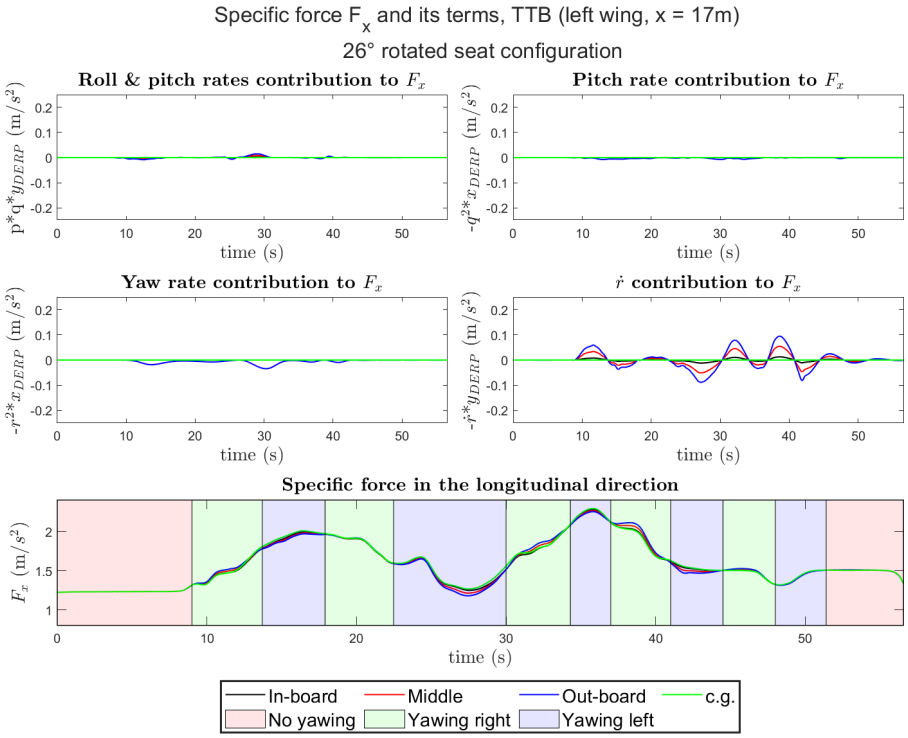

Figure C.10: Specific force F_x at x = 17m, left wing, 26° rotated seat configuration

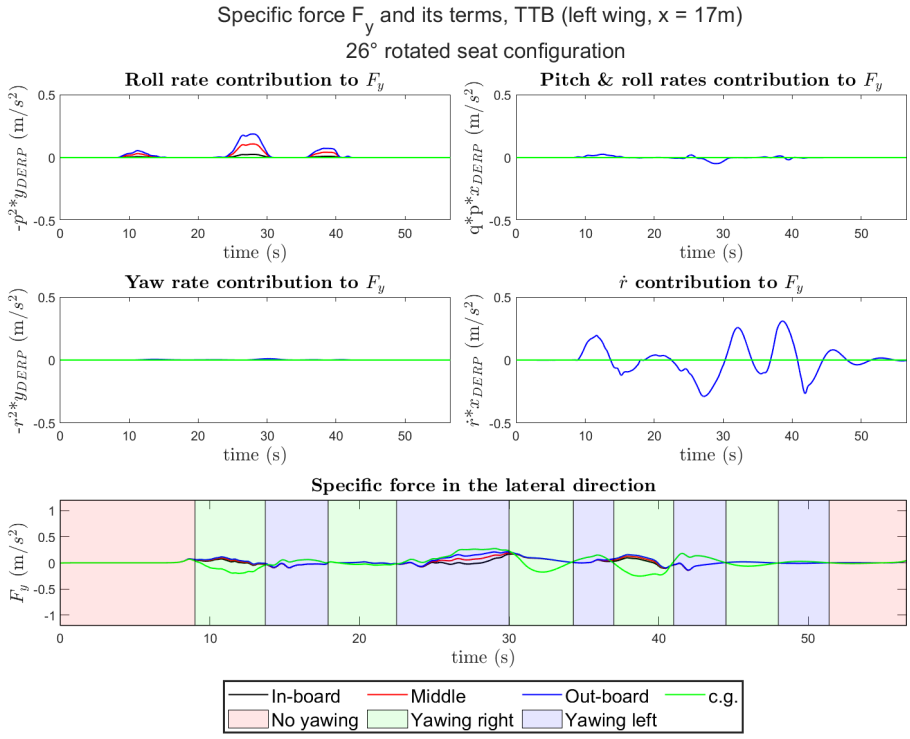

Figure C.11: Specific force F_y at x = 17m, left wing, 26° rotated seat configuration

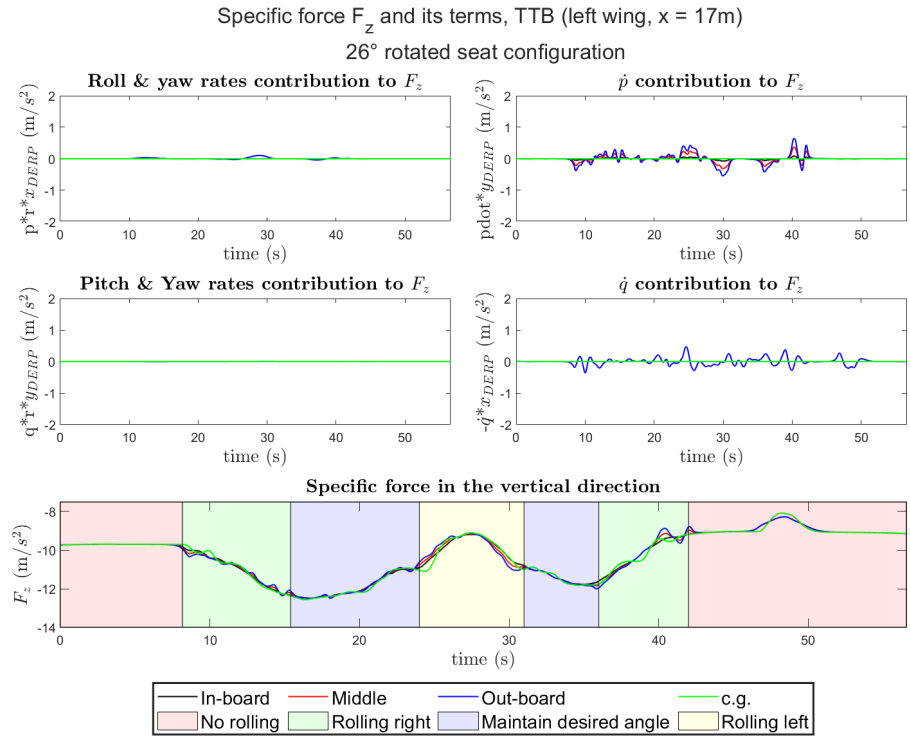

Figure C.12: Specific force F_z at x = 17m, left wing, 26° rotated seat configuration

x = -1m

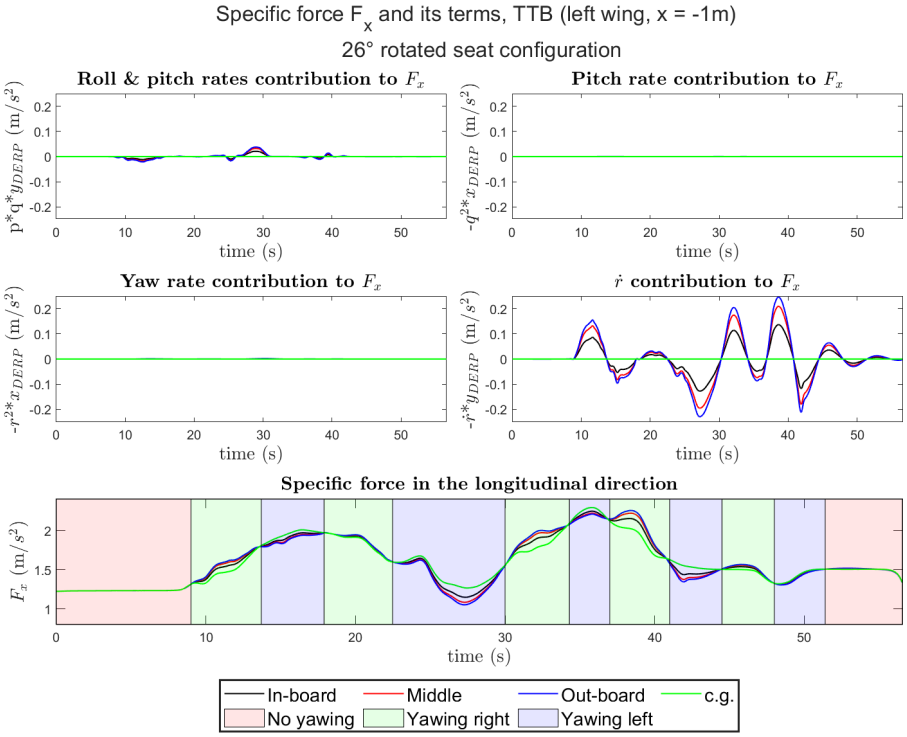

Figure C.13: Specific force F_x at x = -1m, left wing, 26° rotated seat configuration

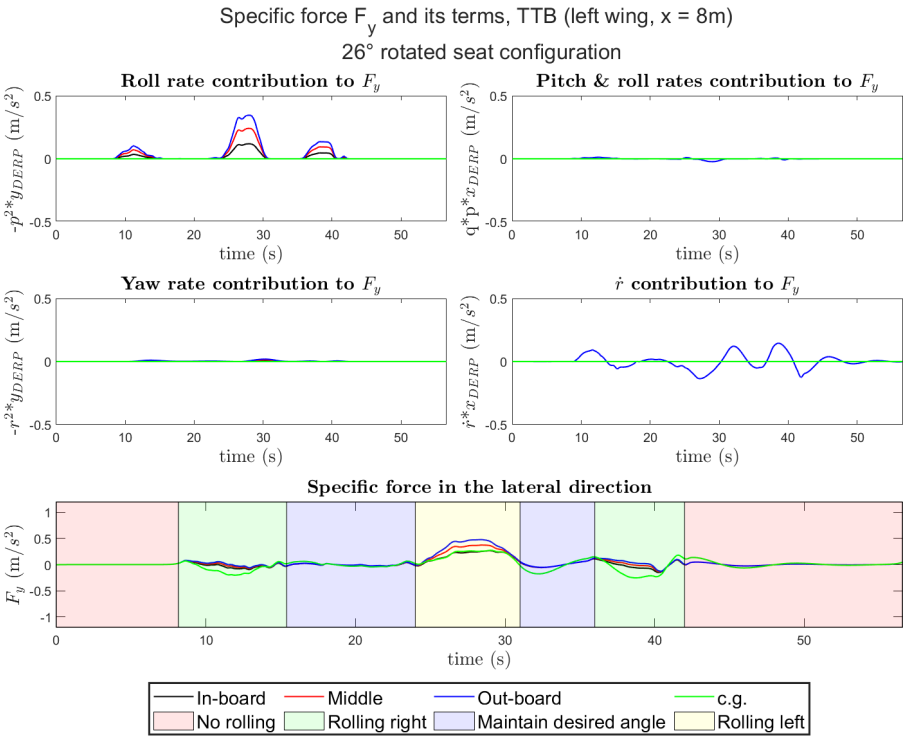

Figure C.14: Specific force F_y at x = -1m, left wing, 26° rotated seat configuration

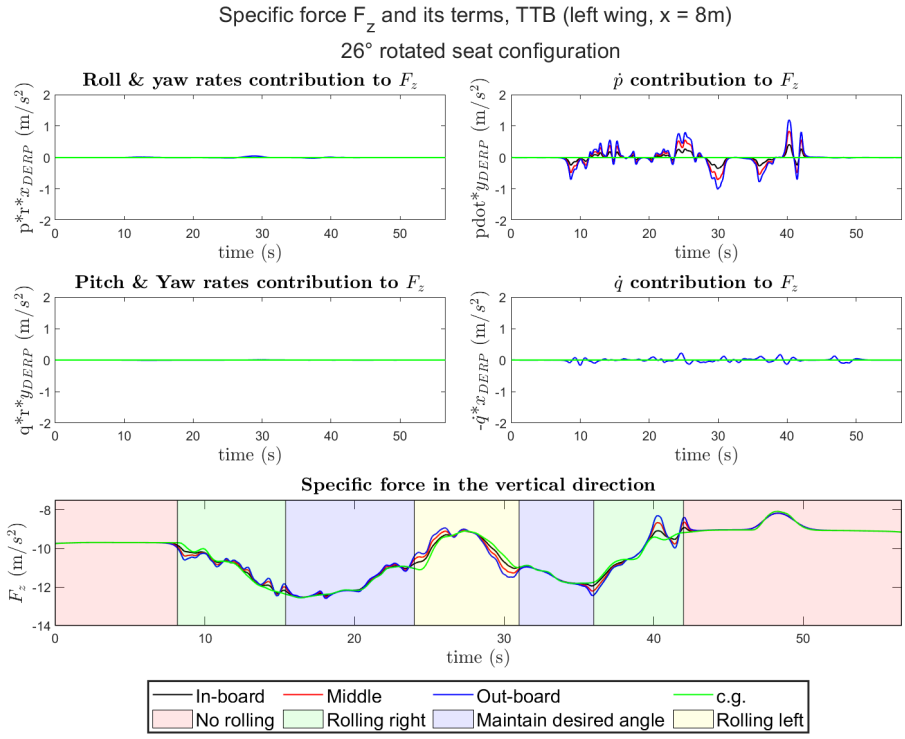

Figure C.15: Specific force F_z at x = -1m, left wing, 26° rotated seat configuration

B. 0° rotated seat configuration

The specific forces using 0° rotated seat configuration at x = 17m, and -1m are shown below.

x = 17m

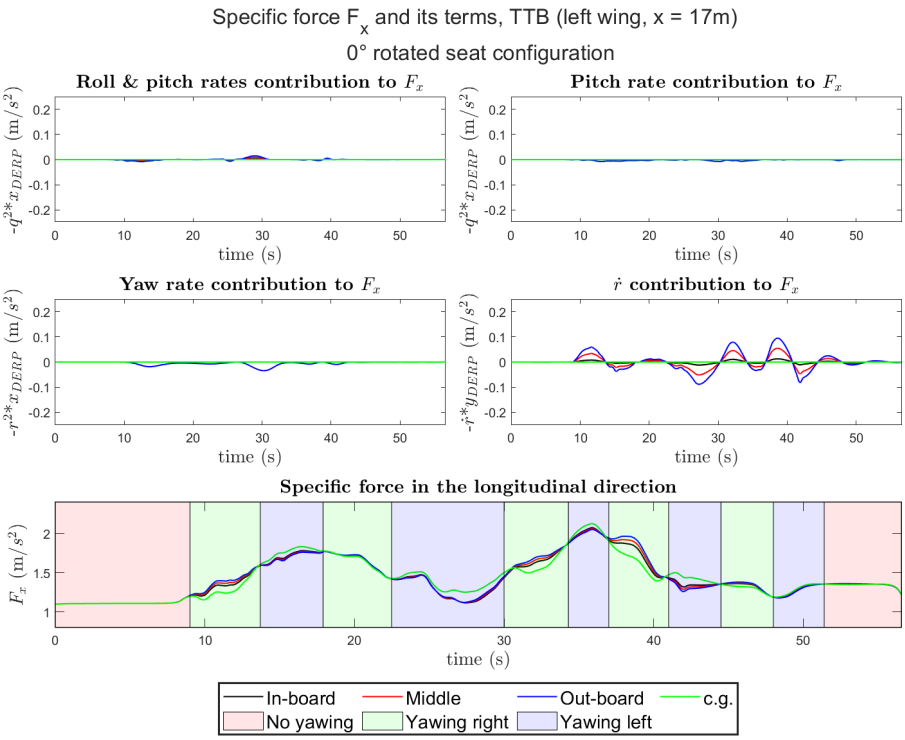

Figure C.16: Specific force F_x at x = 17m, left wing, 0° rotated seat configuration

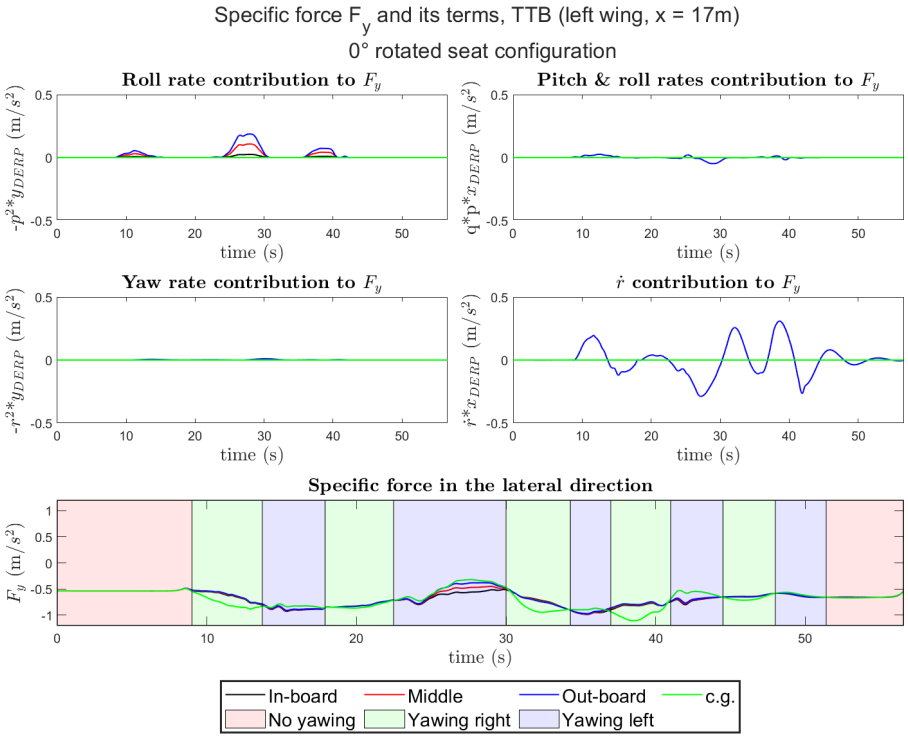

Figure C.17: Specific force F_y at x = 17m, left wing, 0° rotated seat configuration

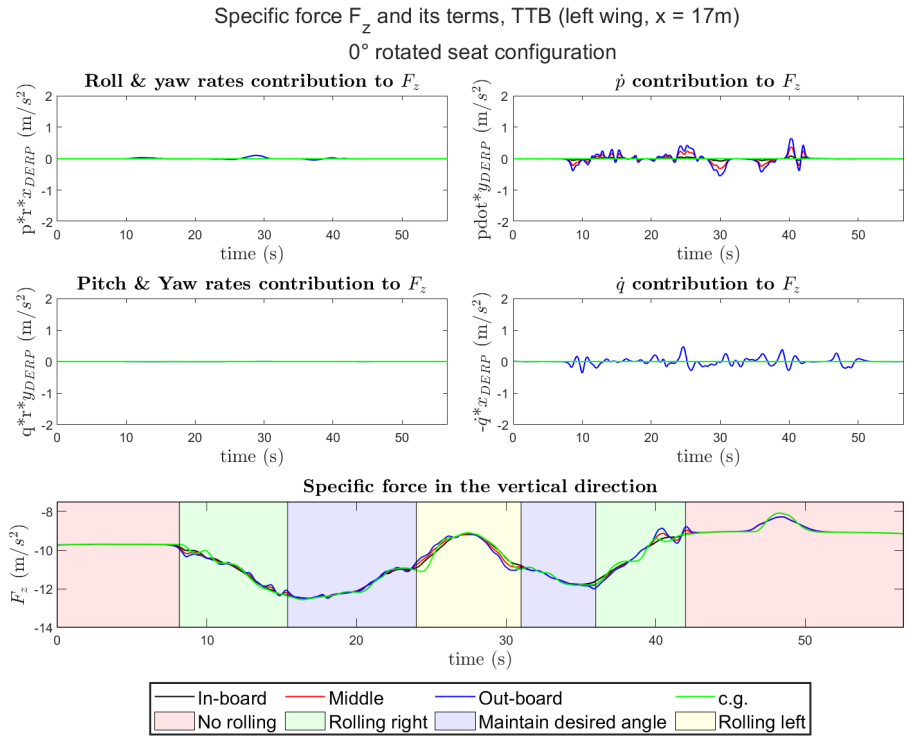

Figure C.18: Specific force F_z at x = 17m, left wing, 0° rotated seat configuration

x = -1m

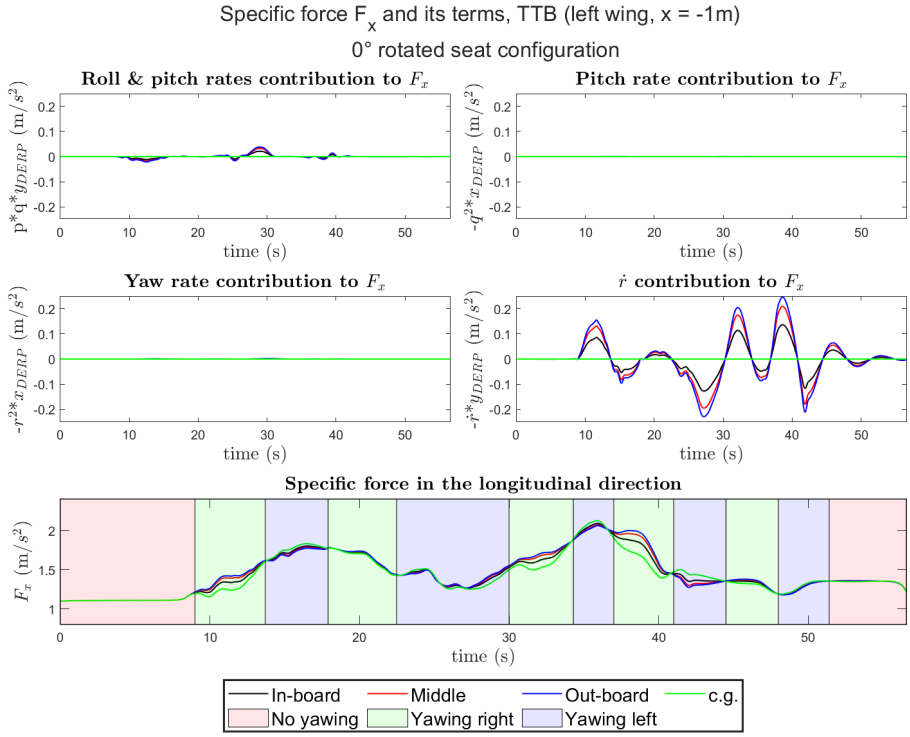

Figure C.19: Specific force F_x at x = -1m, left wing, 0° rotated seat configuration

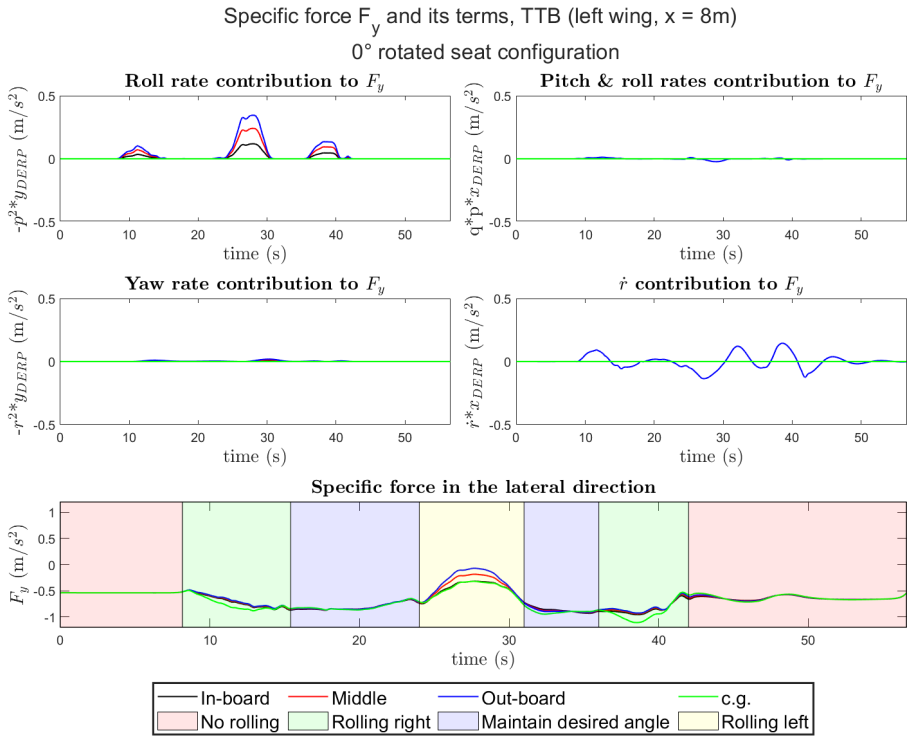

Figure C.20: Specific force F_y at x = -1m, left wing, 0° rotated seat configuration

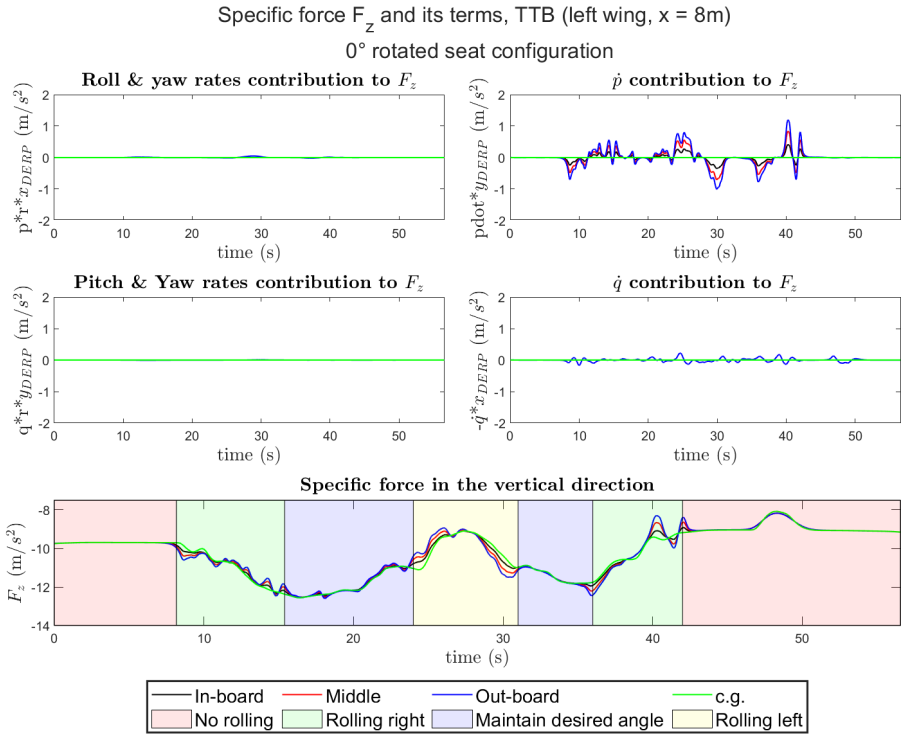

Figure C.21: Specific force F_z at x = -1m, left wing, 0° rotated seat configuration

C.3. Conflict terms tables

In this section, the conflict terms for a bigger range in the Flying-V are shown for TTB, using 26° and 0° rotated seat configurations.

A. 26° rotated seat configuration

		Right wing			
		MS(c_{gx})	**MS(c_{gy})**	**MS(c_{gz})**	**MS($c_{g\text{total}}$)**
x = **17m**	**In-board**	2.4765	3.6517	5.8167	8.1917
	Middle	2.4833	3.6542	5.8480	8.2357
	Out-board	2.4984	3.6593	5.9147	8.3327
x = **11m**	**In-board**	2.4792	3.5930	5.9113	8.2821
	Middle	2.4982	3.6000	5.9997	8.4156
	Out-board	2.5294	3.6141	6.1683	8.6722
x = **9m**	**In-board**	2.4831	3.6045	5.9546	8.3480
	Middle	2.5050	3.6147	6.0638	8.5121
	Out-board	2.5347	3.6317	6.2301	8.7657
x = **7m**	**In-board**	2.4859	3.6408	5.9976	8.4196
	Middle	2.5094	3.6536	6.1166	8.6009
	Out-board	2.5462	3.6761	6.3350	8.9213
x = **5m**	**In-board**	2.4927	3.7020	6.0613	8.5295
	Middle	2.5189	3.7148	6.2009	8.7410
	Out-board	2.5531	3.7341	6.4130	9.0355
x = **3m**	**In-board**	2.5006	3.7772	6.1324	8.6572
	Middle	2.5290	3.7907	6.2964	8.8967
	Out-board	2.5699	3.8098	6.5495	9.2164
x = **1m**	**In-board**	2.5094	3.8619	6.2161	8.8009
	Middle	2.5400	3.8763	6.4070	9.0670
	Out-board	2.5917	3.8958	6.7023	9.4104
x = **0m**	**In-board**	2.5140	3.9069	6.2619	8.8783
	Middle	2.5458	3.9218	6.4705	9.1572
	Out-board	2.6036	3.9415	6.7853	9.5120
x = **-1m**	**In-board**	2.5189	3.9536	6.3097	8.9593
	Middle	2.5696	3.9749	6.6377	9.3646
	Out-board	2.6161	3.9888	6.8717	9.6164
	c.g.	2.4767	3.8924	6.0562	8.5820

Table C.1: Conflict terms for the right wing

		Left wing			
		MS(c_{gx})	**MS(c_{gy})**	**MS(c_{gz})**	**MS($c_{g\text{total}}$)**
x = **17m**	**In-board**	2.4765	3.6517	5.8167	8.1917
	Middle	2.4833	3.6542	5.8480	8.2357
	Out-board	2.4985	3.6593	5.9147	8.3327
x = **11m**	**In-board**	2.4792	3.5930	5.9113	8.2821
	Middle	2.4983	3.6000	5.9997	8.4156
	Out-board	2.5294	3.6141	6.1683	8.6723
x = **9m**	**In-board**	2.4831	3.6045	5.9546	8.3480
	Middle	2.5050	3.6147	6.0638	8.5122
	Out-board	2.5347	3.6317	6.2301	8.7658
x = **7m**	**In-board**	2.4859	3.6408	5.9976	8.4196
	Middle	2.5094	3.6536	6.1166	8.6009
	Out-board	2.5463	3.6761	6.3350	8.9214
x = **5m**	**In-board**	2.4927	3.7020	6.0613	8.5295
	Middle	2.5189	3.7148	6.2009	8.7410
	Out-board	2.5531	3.7341	6.4130	9.0356
x = **3m**	**In-board**	2.5006	3.7772	6.1324	8.6572
	Middle	2.5291	3.7907	6.2964	8.8968
	Out-board	2.5699	3.8098	6.5495	9.2165
x = **1m**	**In-board**	2.5094	3.8619	6.2161	8.8009
	Middle	2.5400	3.8763	6.4070	9.0670
	Out-board	2.5917	3.8958	6.7023	9.4105
x = **0m**	**In-board**	2.5140	3.9069	6.2619	8.8783
	Middle	2.5459	3.9218	6.4705	9.1572
	Out-board	2.6037	3.9415	6.7853	9.5120
x = **-1m**	**In-board**	2.5189	3.9536	6.3097	8.9593
	Middle	2.5697	3.9749	6.6377	9.3646
	Out-board	2.6161	3.9888	6.8717	9.6165
	c.g.	2.4767	3.8924	6.0562	8.5820

Table C.2: Conflict terms for the left wing

B. 0° rotated seat configuration

		Right wing			
		MS(c_{gx})	**MS(c_{gy})**	**MS(c_{gz})**	**MS($c_{g\text{total}}$)**
x = **17m**	**In-board**	2.2872	3.8632	5.8264	8.1427
	Middle	2.2815	3.8578	5.8614	8.2015
	Out-board	2.2820	3.8560	5.9310	8.3123
x = **11m**	**In-board**	2.2644	3.8500	5.9214	8.2331
	Middle	2.2550	3.8637	6.0138	8.3796
	Out-board	2.2588	3.8893	6.1875	8.6517
x = **9m**	**In-board**	2.2556	3.8703	5.9648	8.2940
	Middle	2.2463	3.8936	6.0784	8.4707
	Out-board	2.2493	3.9242	6.2501	8.7368
x = **7m**	**In-board**	2.2493	3.9009	6.0077	8.3575
	Middle	2.2380	3.9305	6.1314	8.5501
	Out-board	2.2418	3.9748	6.3570	8.8840
x = **5m**	**In-board**	2.2395	3.9449	6.0720	8.4590
	Middle	2.2293	3.9821	6.2146	8.6807
	Out-board	2.2325	4.0255	6.4374	8.9863
x = **3m**	**In-board**	2.2298	3.9983	6.1435	8.5762
	Middle	2.2208	4.0412	6.3121	8.8254
	Out-board	2.2252	4.0886	6.5773	9.1558
x = **1m**	**In-board**	2.2203	4.0589	6.2251	8.7077
	Middle	2.2124	4.1062	6.4260	8.9832
	Out-board	2.2181	4.1610	6.7334	9.3374
x = **0m**	**In-board**	2.2156	4.0912	6.2707	8.7786
	Middle	2.2083	4.1425	6.4913	9.0668
	Out-board	2.2147	4.2001	6.8179	9.4323
x = **-1m**	**In-board**	2.2110	4.1259	6.3193	8.8527
	Middle	2.2052	4.2001	6.6636	9.2710
	Out-board	2.2113	4.2405	6.9055	9.5300
	c.g.	2.3010	3.9958	6.0586	8.4673

Table C.3: Conflict terms for the right wing

		Left wing			
		MS(c_{gx})	**MS(c_{gy})**	**MS(c_{gz})**	**MS($c_{g\text{total}}$)**
x = 17m	**In-board**	2.2871	3.8632	5.8264	8.1427
	Middle	2.2814	3.8579	5.8614	8.2015
	Out-board	2.2820	3.8561	5.9310	8.3123
x = 11m	**In-board**	2.2643	3.8501	5.9214	8.2330
	Middle	2.2550	3.8638	6.0138	8.3796
	Out-board	2.2588	3.8894	6.1875	8.6517
x = 9m	**In-board**	2.2556	3.8704	5.9648	8.2940
	Middle	2.2463	3.8937	6.0784	8.4707
	Out-board	2.2493	3.9243	6.2501	8.7368
x = 7m	**In-board**	2.2493	3.9010	6.0077	8.3575
	Middle	2.2380	3.9306	6.1314	8.5501
	Out-board	2.2418	3.9749	6.3570	8.8840
x = 5m	**In-board**	2.2394	3.9450	6.0720	8.4590
	Middle	2.2293	3.9821	6.2146	8.6807
	Out-board	2.2325	4.0256	6.4374	8.9863
x = 3m	**In-board**	2.2298	3.9984	6.1435	8.5762
	Middle	2.2207	4.0413	6.3121	8.8254
	Out-board	2.2252	4.0887	6.5773	9.1559
x = 1m	**In-board**	2.2202	4.0590	6.2251	8.7077
	Middle	2.2124	4.1063	6.4260	8.9832
	Out-board	2.2181	4.1611	6.7334	9.3374
x = 0m	**In-board**	2.2156	4.0913	6.2707	8.7786
	Middle	2.2083	4.1426	6.4913	9.0668
	Out-board	2.2147	4.2002	6.8179	9.4324
x = -1m	**In-board**	2.2110	4.1260	6.3193	8.8527
	Middle	2.2052	4.2002	6.6636	9.2710
	Out-board	2.2113	4.2406	6.9055	9.5300
	c.g.	2.3009	3.9958	6.0586	8.4673

Table C.4: Conflict terms for the left wing

D

Coordinated Turn Capability maneuver's additional figures

D.1. Data Filtering for CTC

In this section, the flight data that has been collected from the pilot-in-the-loop experiments are filtered in order to erase the effect of the high spikes of the data. The figures show that the data have been filtered for a range of break frequency

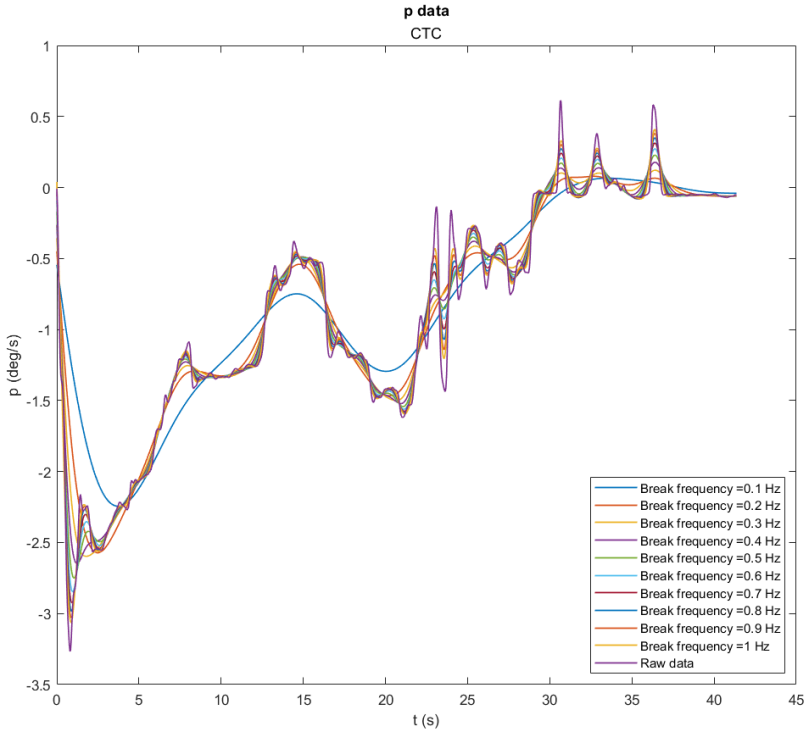

Figure D.1: Roll rate (p) flight data with multiple break frequency

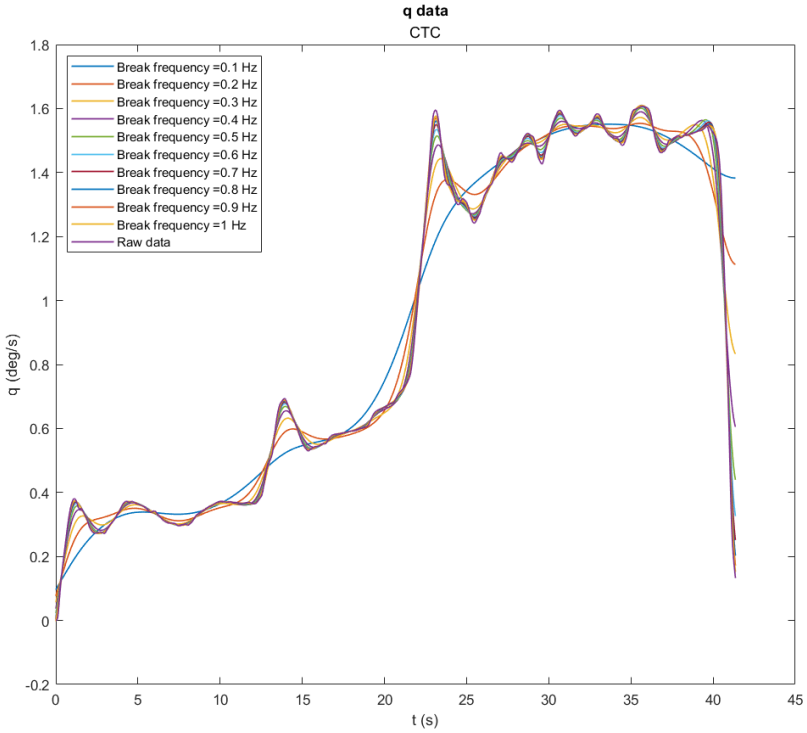

Figure D.2: Pitch rate (q) flight data with multiple break frequency

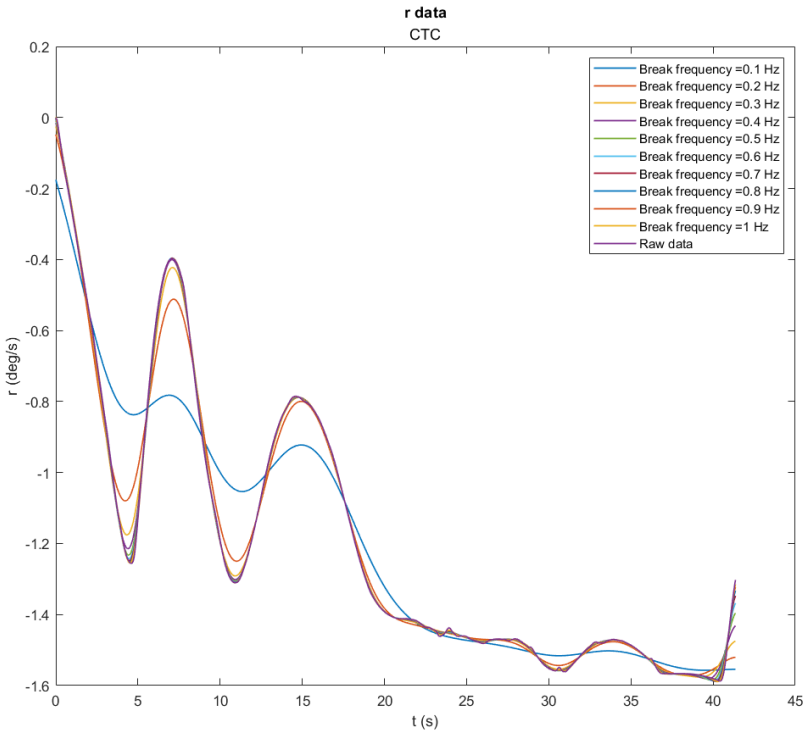

Figure D.3: Yaw rate (r) flight data with multiple break frequency

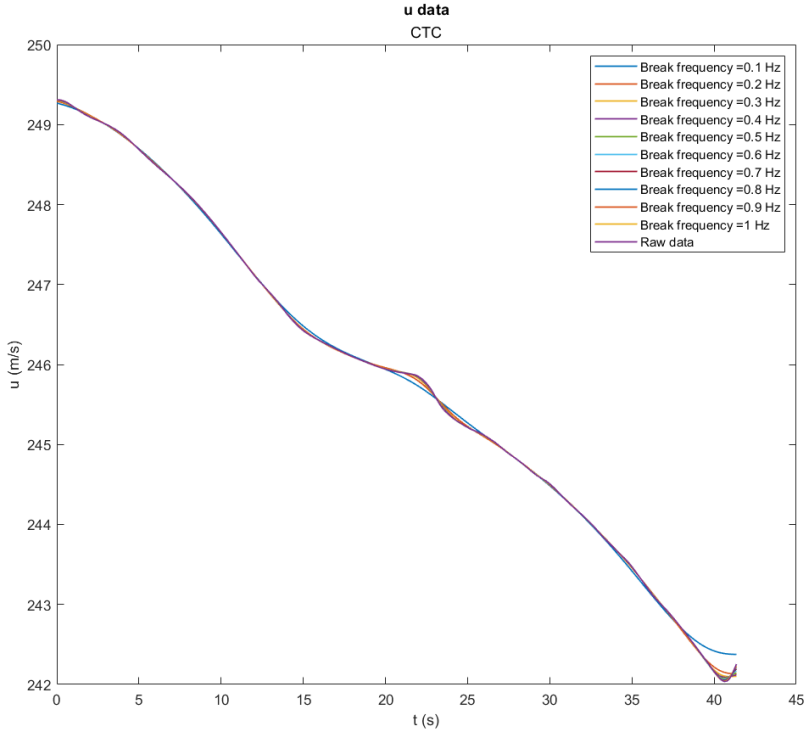

Figure D.4: Forward velocity (u) flight data with multiple break frequency

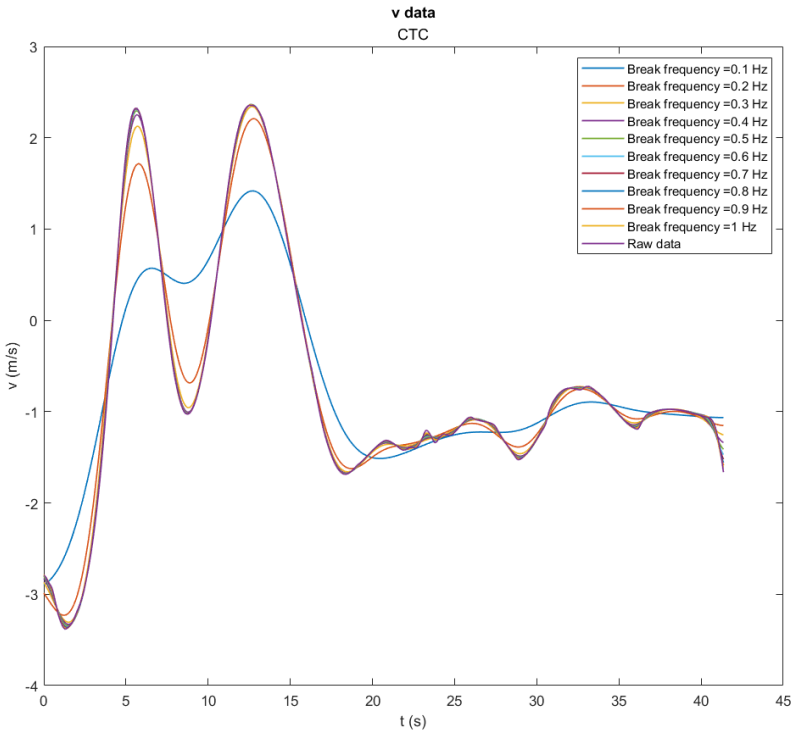

Figure D.5: Lateral velocity (v) flight data with multiple break frequency

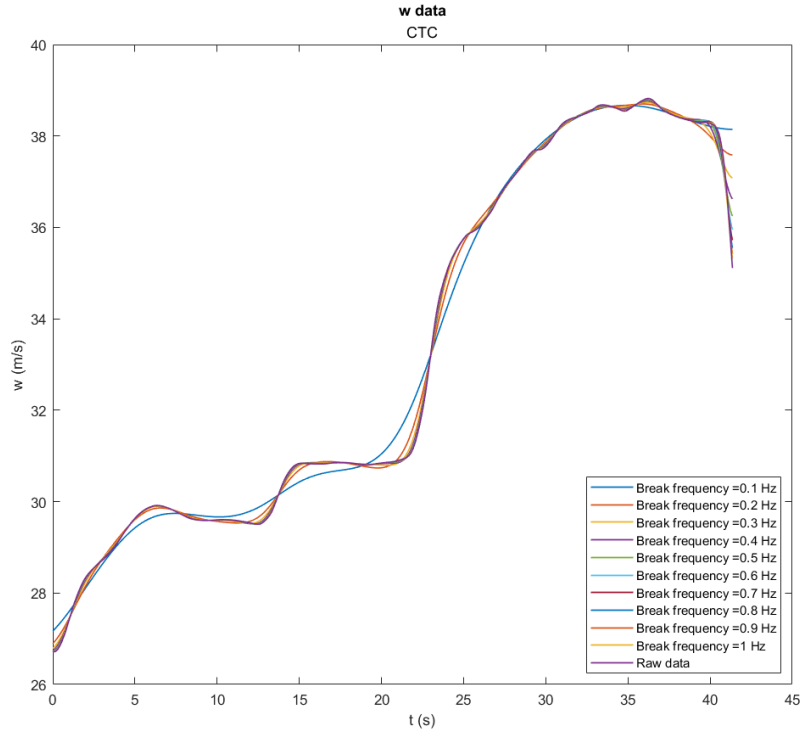

Figure D.6: Vertical velocity (w) flight data with multiple break frequency

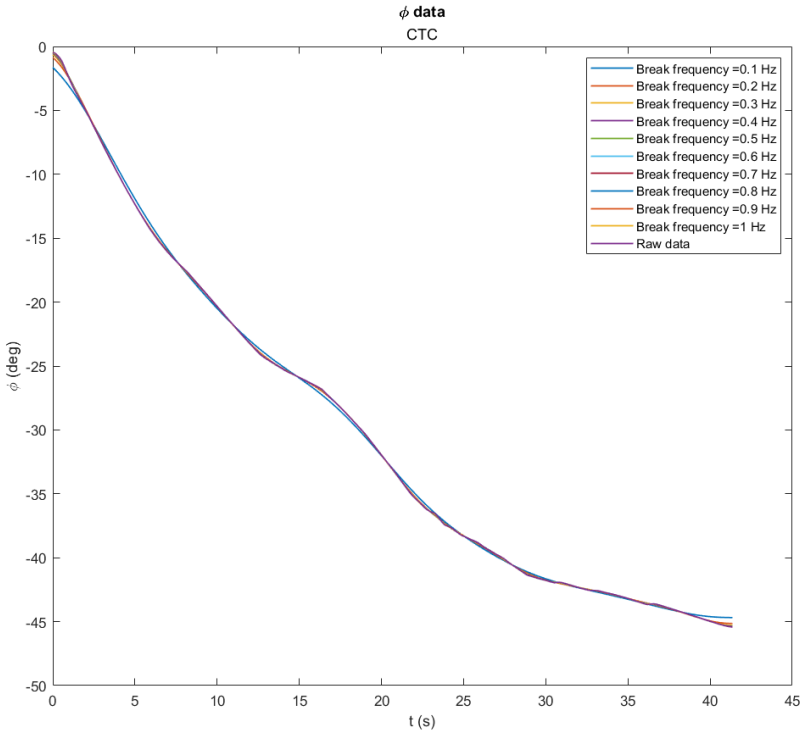

Figure D.7: Roll angle (ϕ) flight data with multiple break frequency

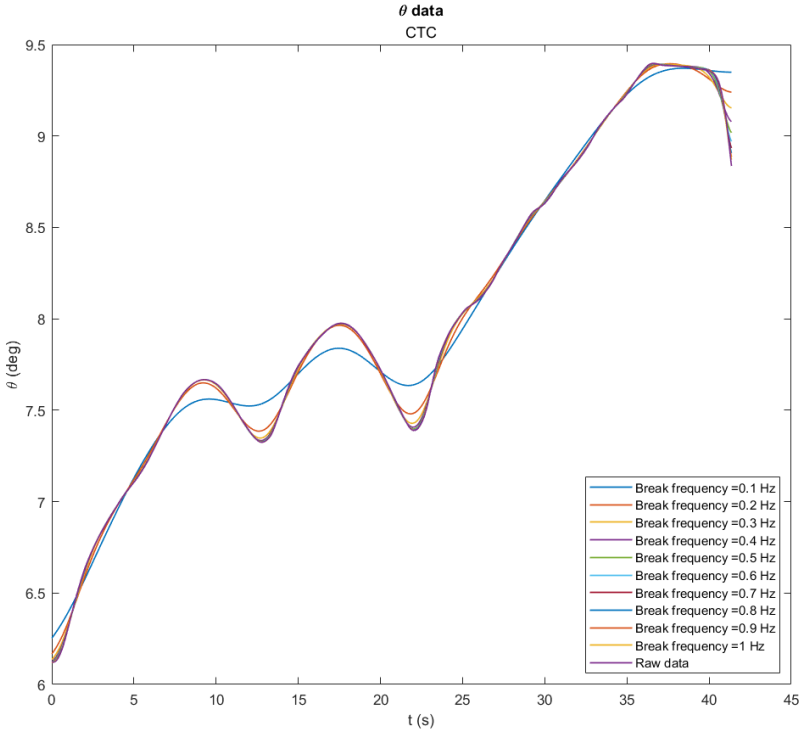

Figure D.8: Pitch angle (θ) flight data with multiple break frequency

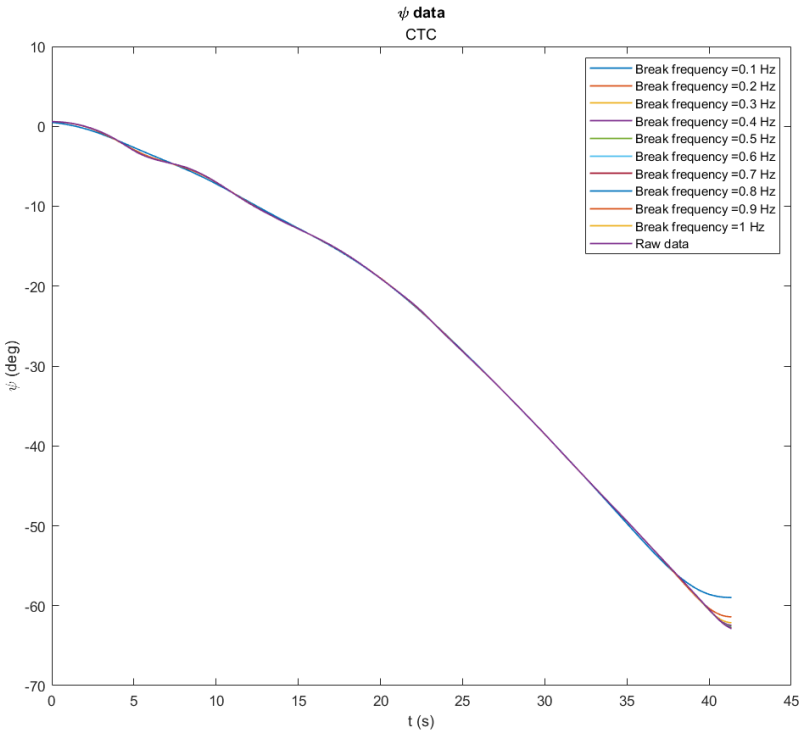

Figure D.9: Yaw angle (ψ) flight data with multiple break frequency

D.2. Specific forces, left wing

The specific forces calculation for the left wing and both seat configuration are shown in this section.

A. 26° rotated seat configuration

The specific forces using 26◦ rotated seat configuration at x = 17m, and -1m are shown below.

x = 17m

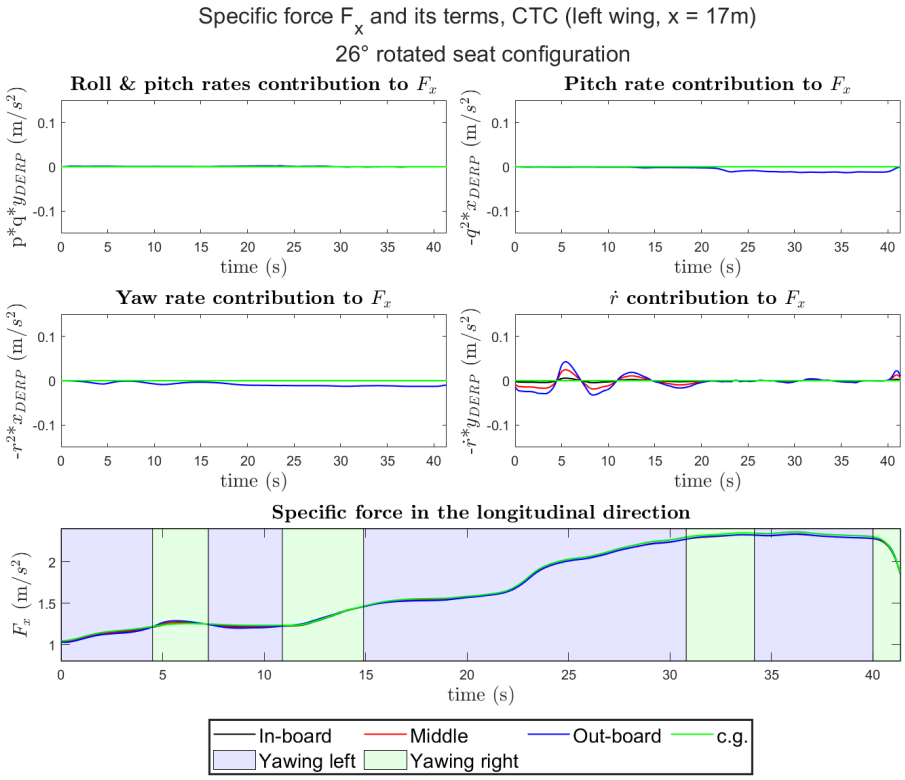

Figure D.10: Specific force F_x at x = 17m, left wing, 26° rotated seat configuration

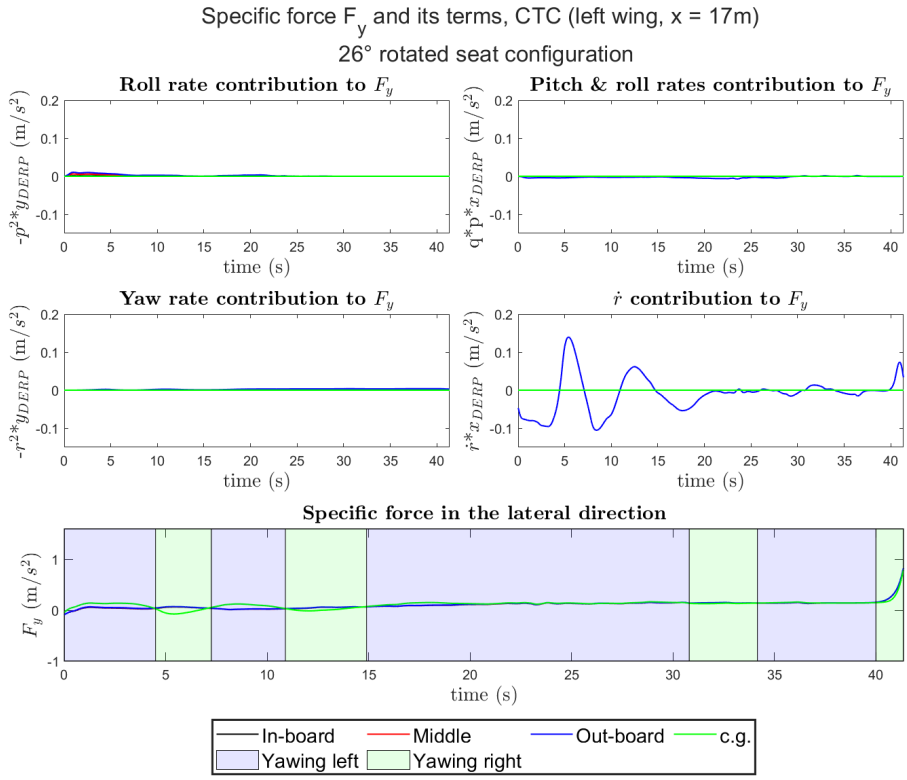

Figure D.11: Specific force F_y at x = 17m, left wing, 26° rotated seat configuration

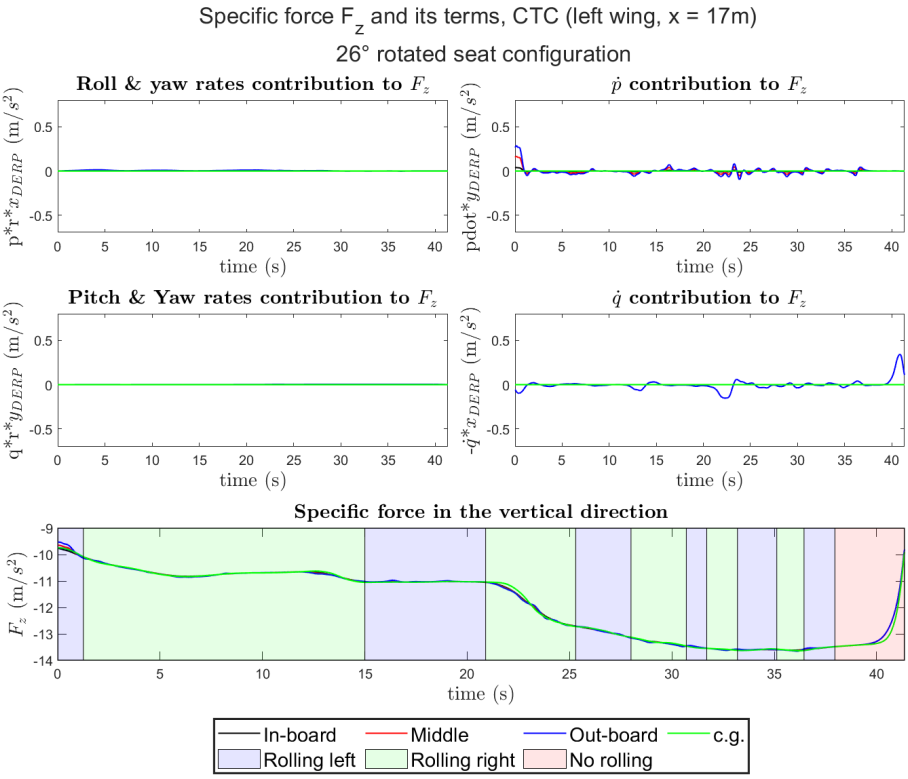

Figure D.12: Specific force F_z at x = 17m, left wing, 26° rotated seat configuration

x = -1m

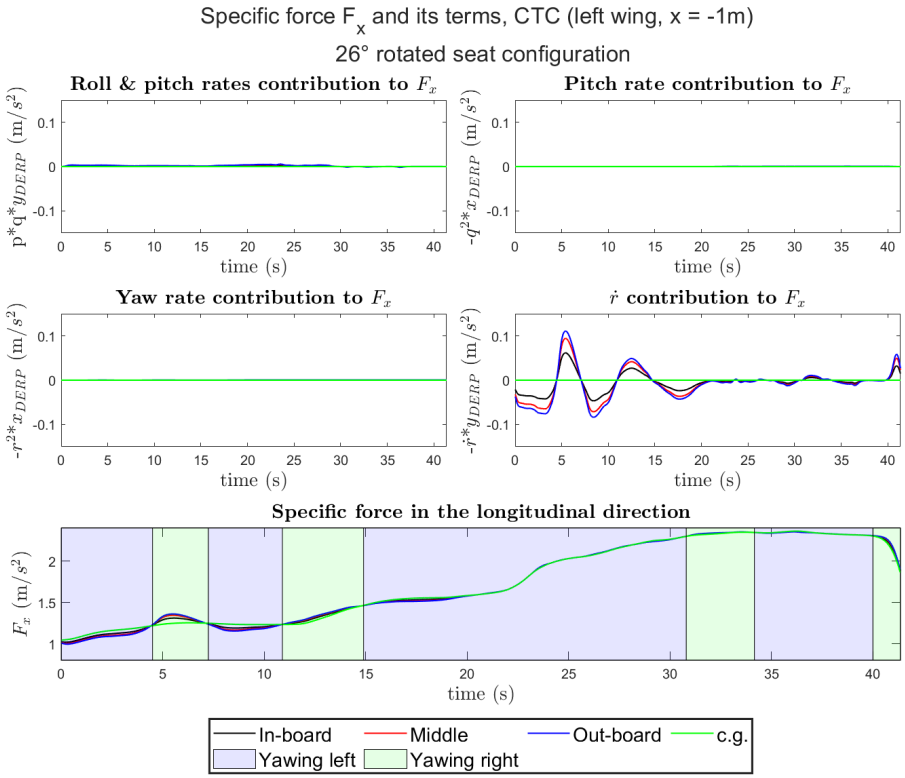

Figure D.13: Specific force F_x at x = -1m, left wing, 26° rotated seat configuration

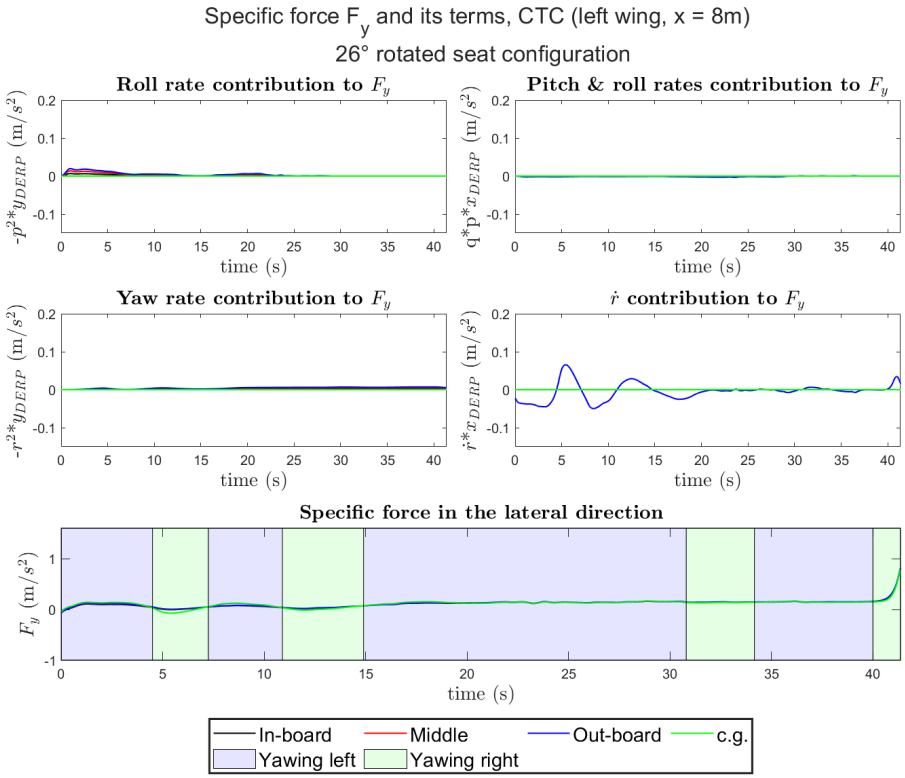

Figure D.14: Specific force F_y at x = -1m, left wing, 26° rotated seat configuration

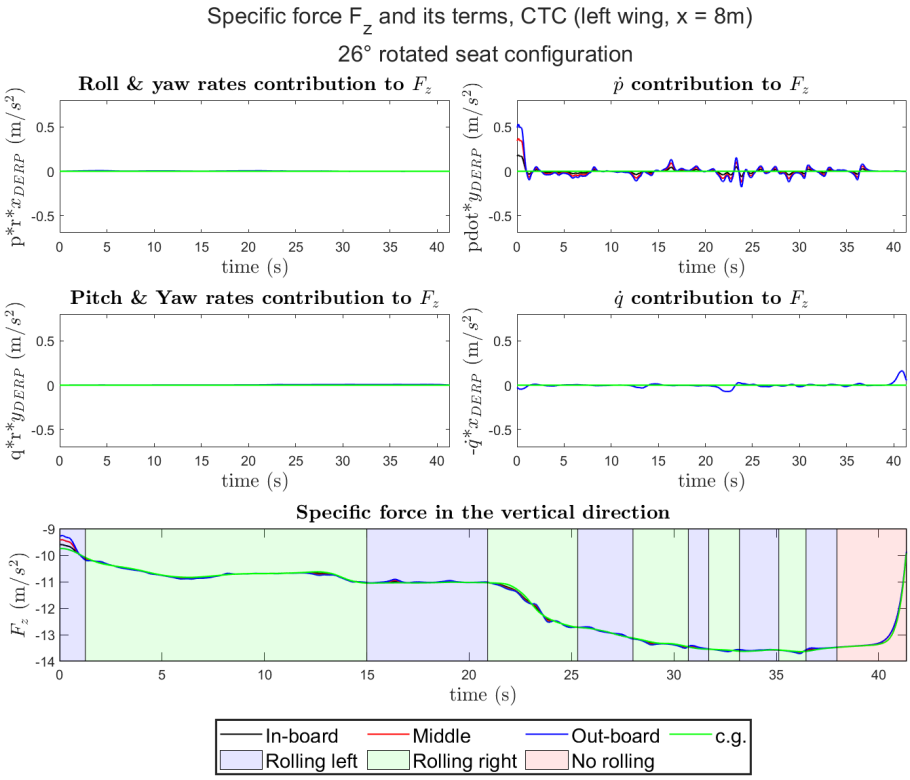

Figure D.15: Specific force F_z at x = -1m, left wing, 26° rotated seat configuration

B. 0° rotated seat configuration

The specific forces using 0◦ rotated seat configuration at x = 17m, and -1m are shown below.

x = 17m

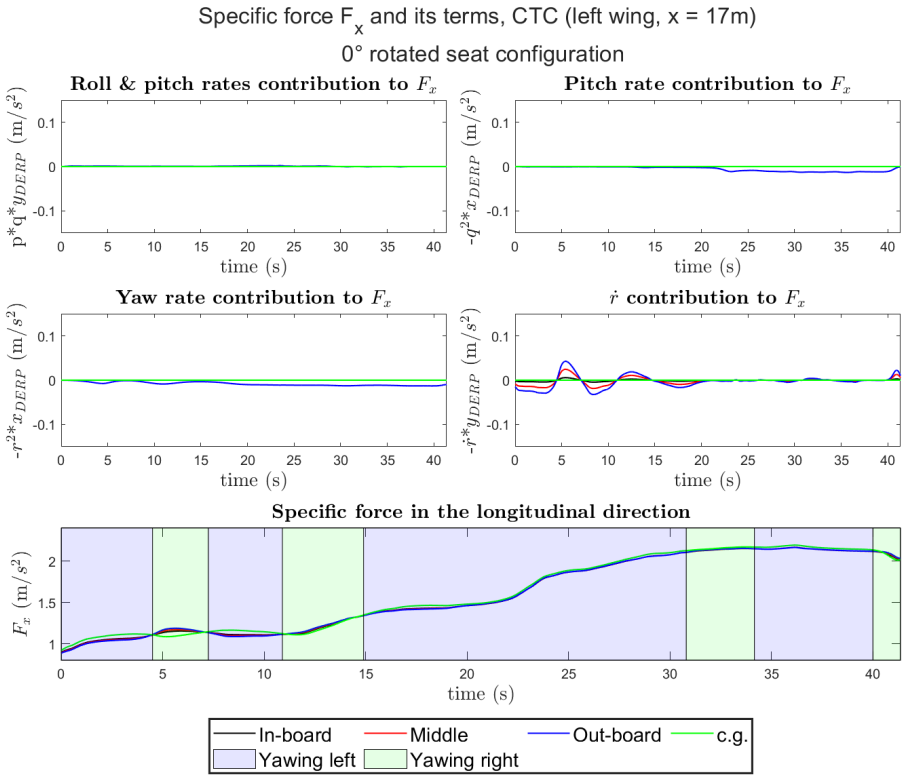

Figure D.16: Specific force F_x at x = 17m, left wing, 0° rotated seat configuration

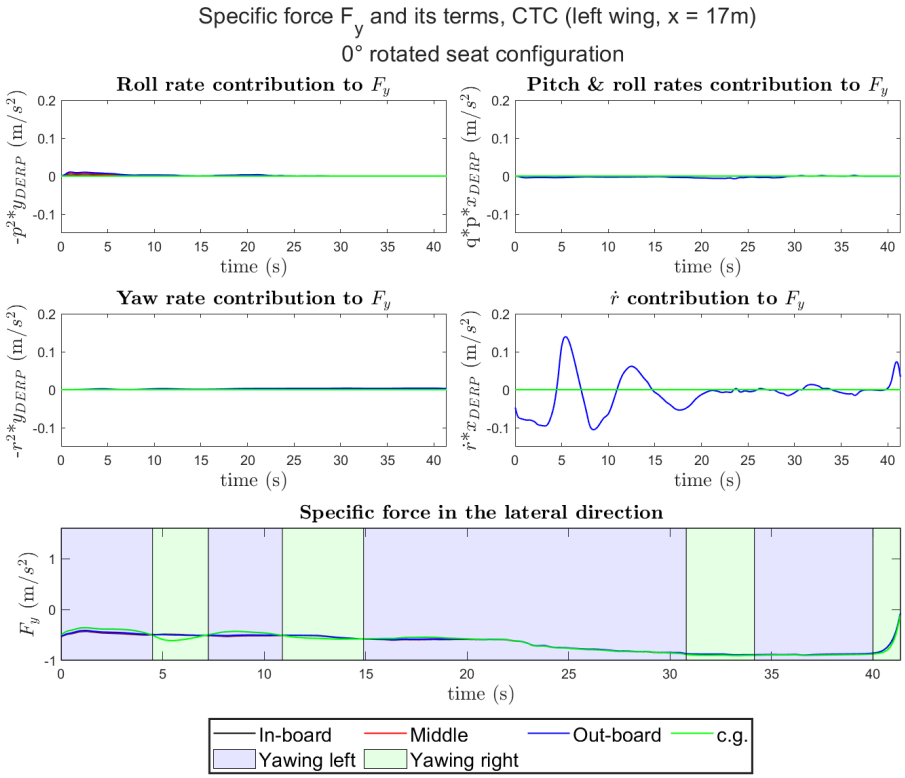

Figure D.17: Specific force F_y at x = 17m, left wing, 0° rotated seat configuration

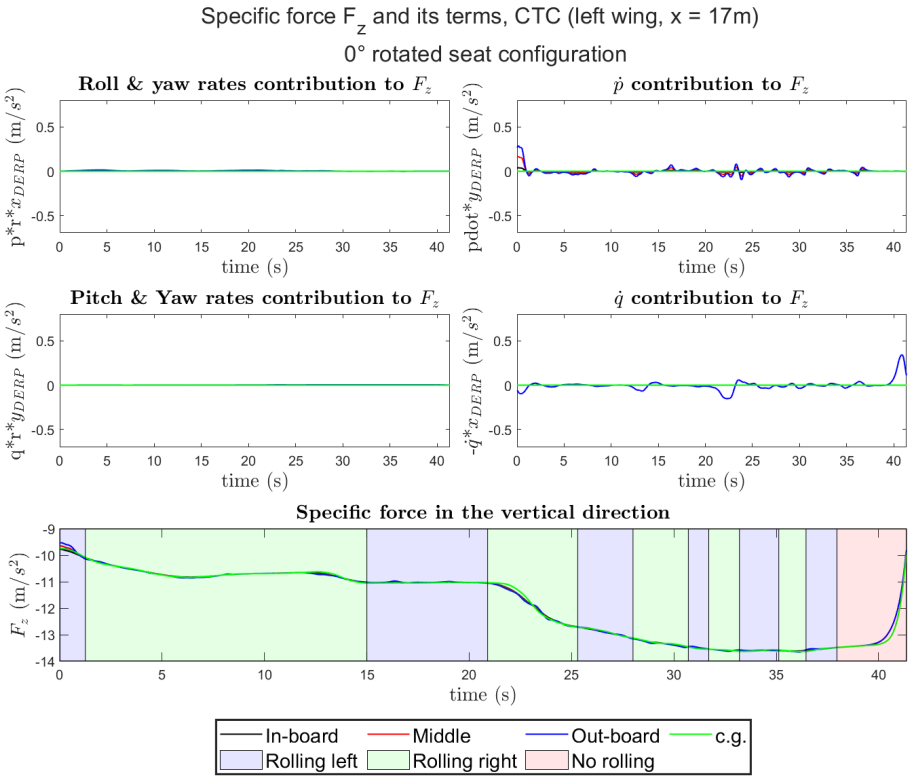

Figure D.18: Specific force F_z at x = 17m, left wing, 0° rotated seat configuration

x = -1m

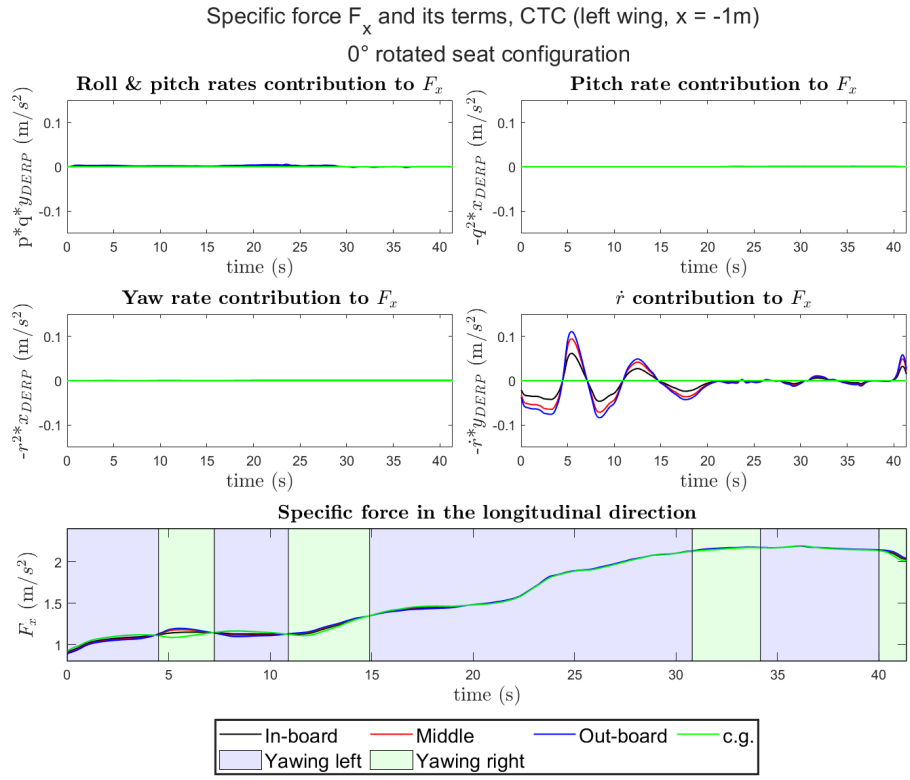

Figure D.19: Specific force F_x at x = -1m, left wing, 0° rotated seat configuration

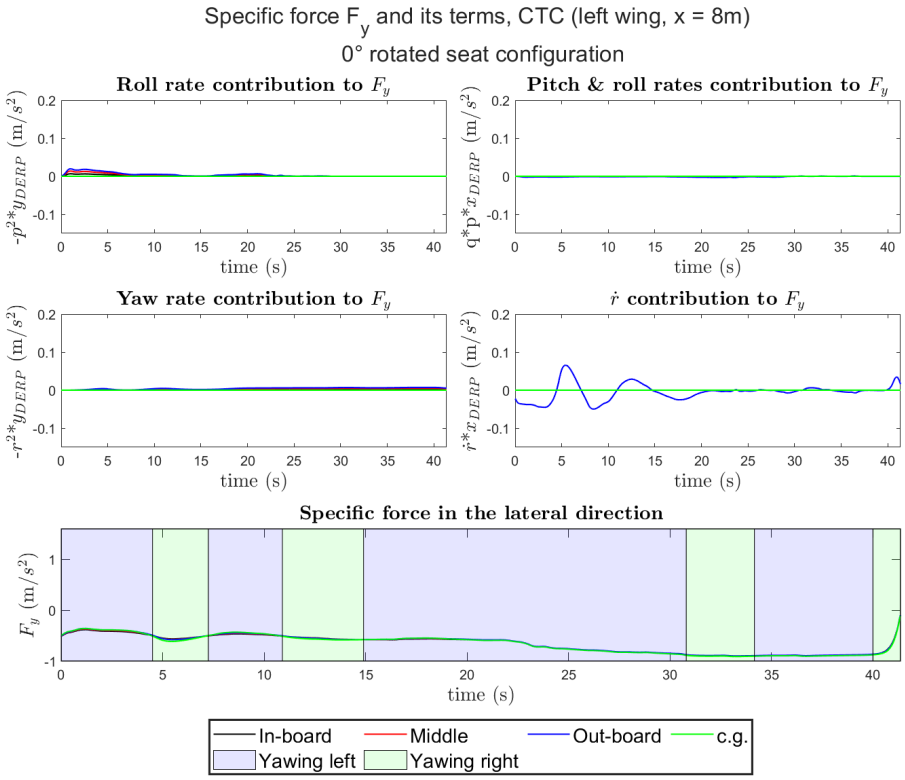

Figure D.20: Specific force F_y at x = -1m, left wing, 0° rotated seat configuration

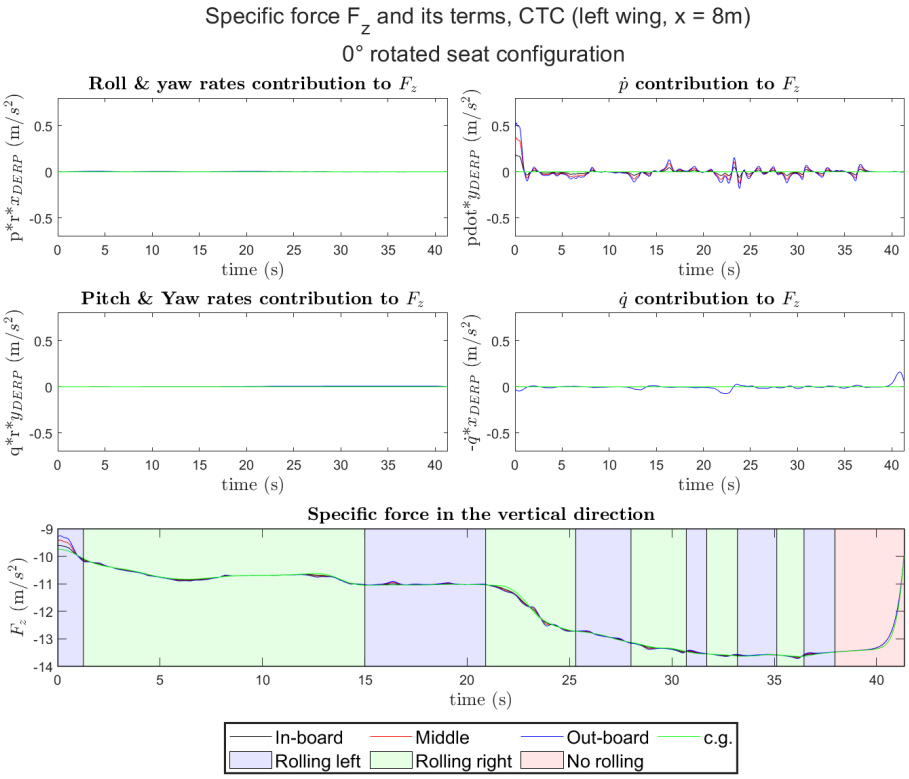

Figure D.21: Specific force F_z at x = -1m, left wing, 0° rotated seat configuration

D.3. Coordinated Turn Capability Sickness Simulation

The second maneuver to investigate the sickness is the CTC. The 6DOF-SVC model will be given the specific forces that have been calculated for the 0° and 26° rotated seat configurations. Moreover, a heat-map will be displayed to understand how the motion sickness developed in the Flying-V during this maneuver.

A. 26° rotated seat configuration

The 26° rotated seat that have been shown in Figure 4.7 are the first to be analyzed. Therefore, the specific forces that have been calculated in Section 4.2.2 is provided to the motion sickness model to predict the conflict terms

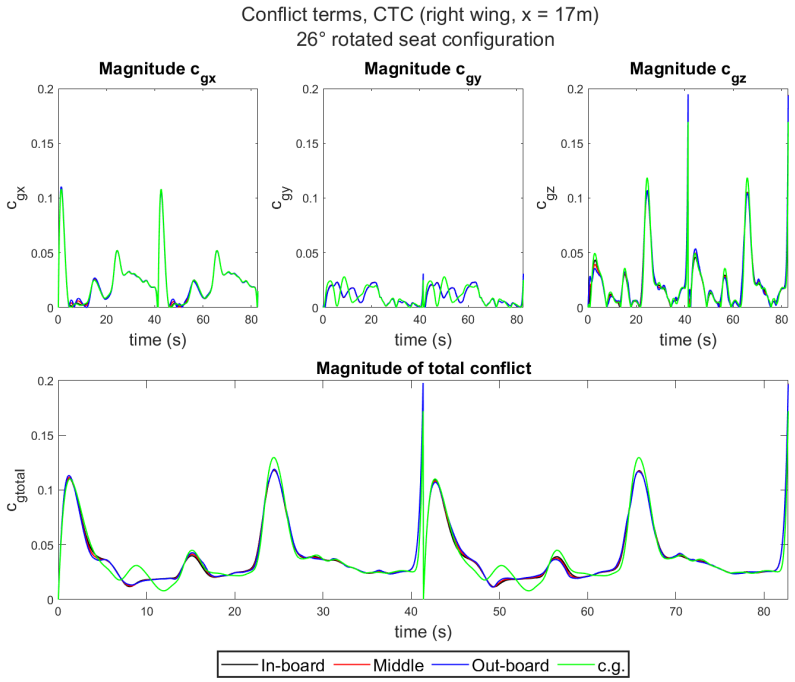

Figure D.22: Conflict terms at x = 17m for CTC, right wing, 26° rotated seat configuration

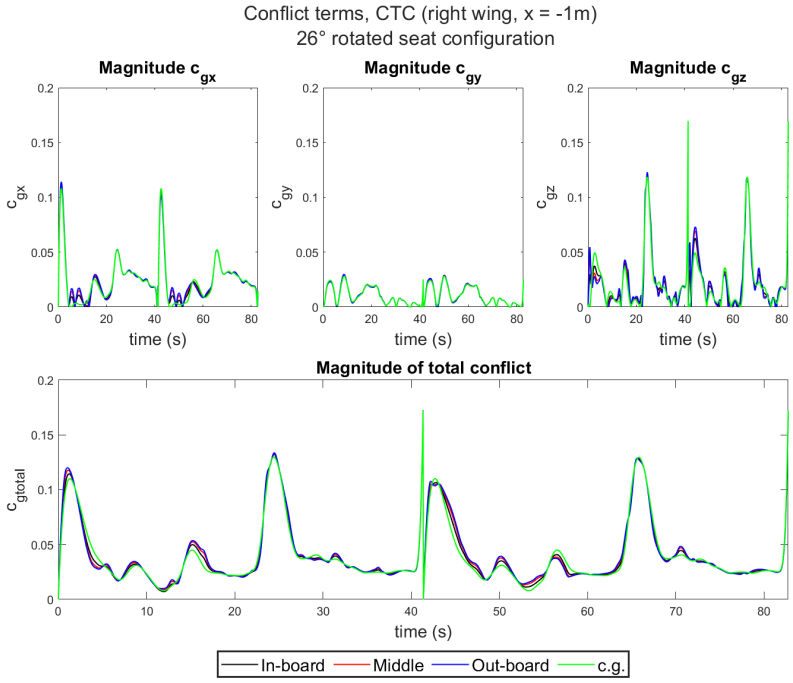

Figure D.23: Conflict terms at x = -1m for CTC, right wing, 26° rotated seat configuration

Figures D.22 and D.23 show the conflict terms for the CTC for the 26° rotated seat layout. As can be observed, there are not significant differences in the conflicts (c_{gx}, c_{gy}, and c_{gz}) between the seats at the various locations and with the c.g. position. Appendix A shows the MS of the conflict terms for both wings.

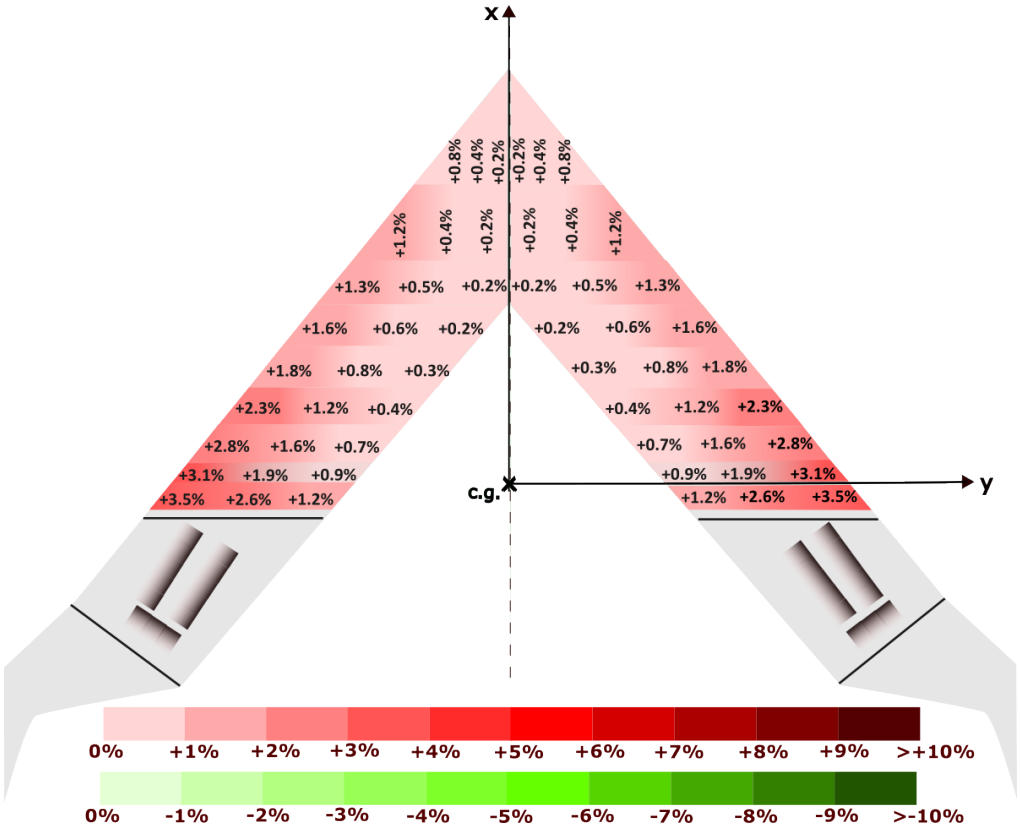

Figure D.24: Heat-map for CTC, 26° rotated seat configuration

Figure D.24 displays the heat-map for CTC, for 26° rotated seat configuration. The small conflicts that have been shown in Figures D.22 and D.23 have resulted in a small total conflict, compared to the TTB maneuver. Consequently, there is just a slight variance in the increase in conflict between the seats and the c.g. position. The MS of the overall conflict increases by up to 3.5% for both wings.

B. 0° rotated seat configuration

The 0° rotated seat layout (see Figure 4.20) is the second case to investigate for the CTC maneuver. Therefore, the specific forces that have been calculated in Section 4.2.3 are given as an input to calculate the total conflict across the different locations in the Flying-V.

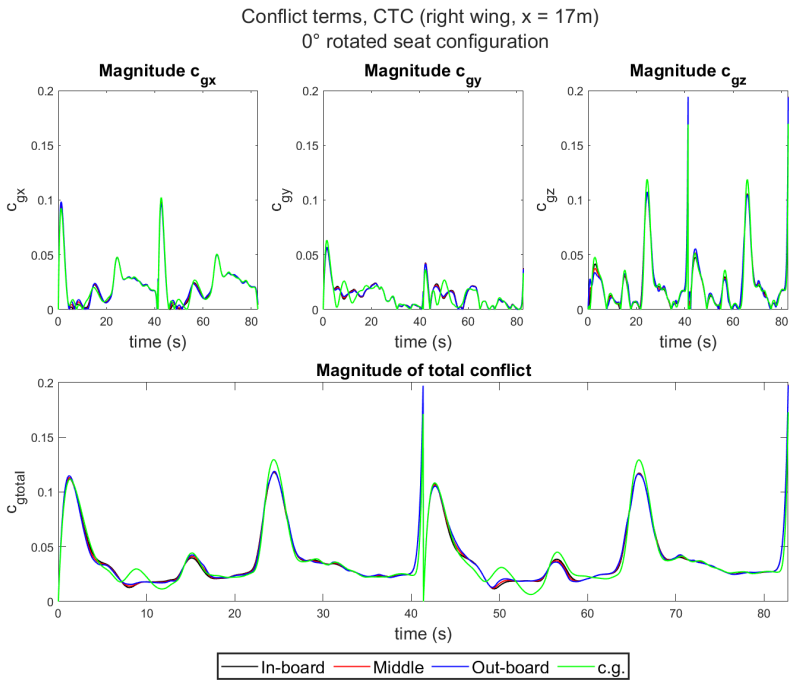

Figure D.25: Conflict terms at x = 17m for CTC, right wing, 0° rotated seat configuration

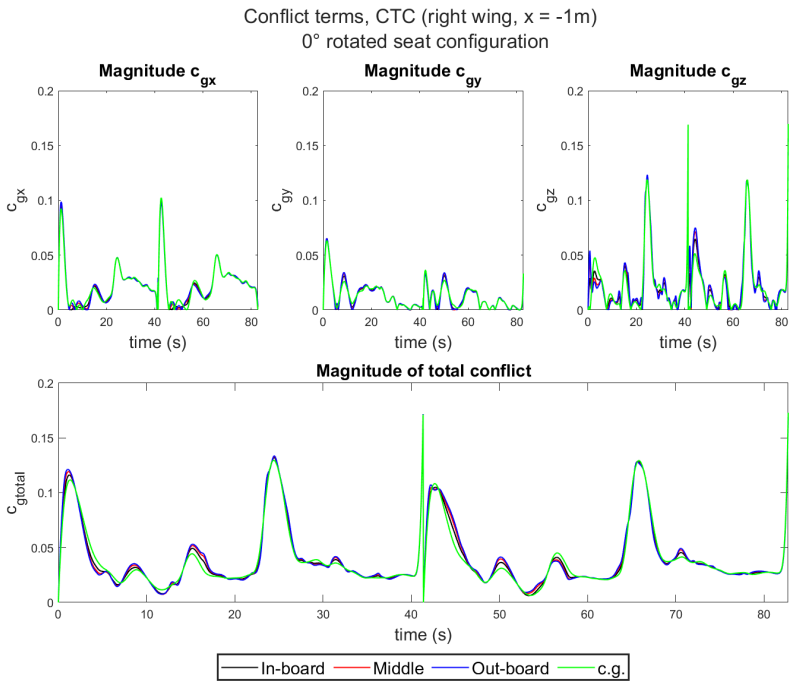

Figure D.26: Conflict terms at x = -1m for CTC, right wing, 0° rotated seat configuration

The conflict plots for the most aft and front locations in the Flying-V are shown in Figures D.25 and D.26. Not much change has happened in terms of conflict compared to the 26° rotated seat configuration. A table for the right and left wings for the evolution of the conflict across the entire geometry of the Flying-V is shown in Appendix B.

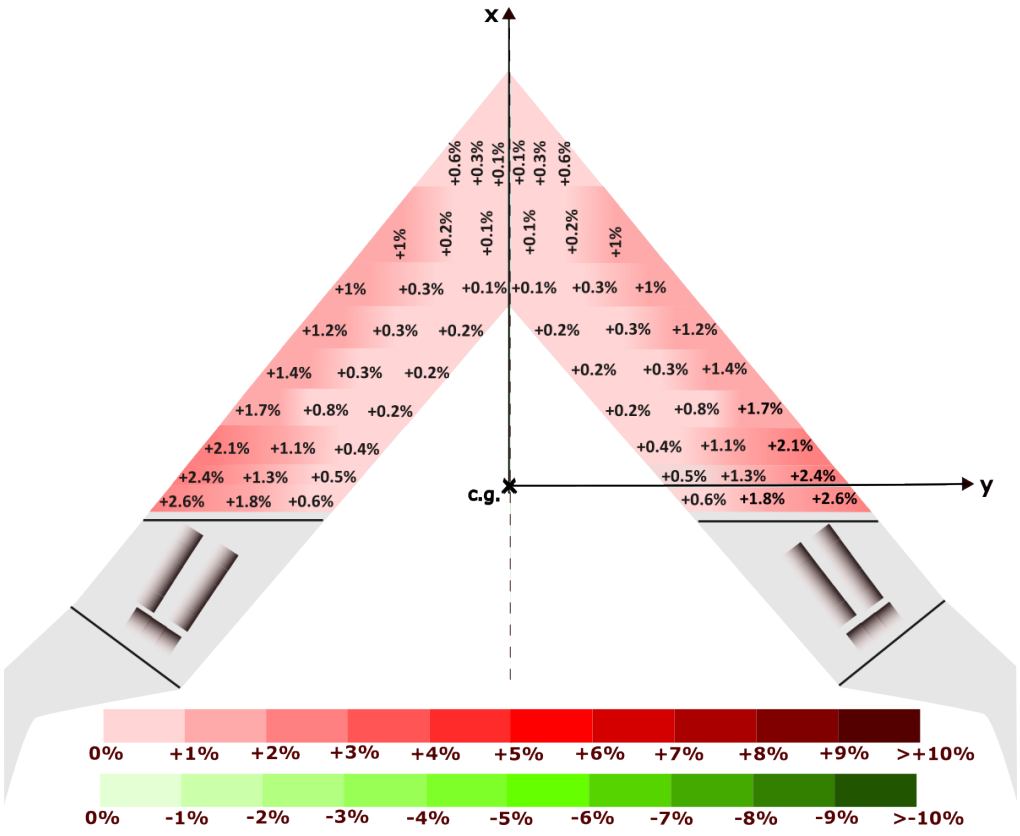

Figure D.27: Heat-map for CTC, 0° rotated seats configuration

The heat-map for the CTC's 0° rotated seat layout is shown in Figure D.27. A comparison of the Figures D.27 and D.24 shows that the increase in the MS for both wings is still up to 2.6%.

D.4. Conflict terms tables

In this section, the conflict terms for a bigger range in the Flying-V are shown for CTC, using 26° and 0° rotated seat configurations.

A. 26° rotated seat configuration

		Right wing			
		MS(c_{gx})	**MS(c_{gy})**	**MS(c_{gz})**	**MS($c_{g\text{total}}$)**
x = **17m**	**In-board**	1.9506	0.8622	1.8865	3.2853
	Middle	1.9594	0.8622	1.8973	3.2907
	Out-board	1.9758	0.8622	1.9130	3.3021
x = **11m**	**In-board**	1.9570	0.8590	1.8870	3.2751
	Middle	1.9782	0.8590	1.9086	3.2888
	Out-board	2.0102	0.8590	1.9379	3.3162
x = **9m**	**In-board**	1.9626	0.8583	1.8908	3.2756
	Middle	1.9859	0.8583	1.9142	3.2923
	Out-board	2.0162	0.8583	1.9425	3.3194
x = **7m**	**In-board**	1.9668	0.8578	1.8932	3.2767
	Middle	1.9914	0.8578	1.9179	3.2953
	Out-board	2.0278	0.8578	1.9530	3.3300
x = **5m**	**In-board**	1.9751	0.8574	1.9002	3.2822
	Middle	2.0020	0.8574	1.9273	3.3044
	Out-board	2.0340	0.8574	1.9587	3.3368
x = **3m**	**In-board**	1.9839	0.8572	1.9083	3.2903
	Middle	2.0131	0.8572	1.9377	3.3161
	Out-board	2.0458	0.8572	1.9706	3.3518
x = **1m**	**In-board**	1.9936	0.8570	1.9178	3.3012
	Middle	2.0245	0.8570	1.9489	3.3305
	Out-board	2.0579	0.8570	1.9842	3.3695
x = **0m**	**In-board**	1.9989	0.8570	1.9230	3.3077
	Middle	2.0303	0.8570	1.9547	3.3388
	Out-board	2.0640	0.8570	1.9914	3.3793
x = **-1m**	**In-board**	2.0042	0.8575	1.9283	3.3149
	Middle	2.0473	0.8577	1.9724	3.3607
	Out-board	2.0701	0.8578	1.9987	3.3897
	c.g.	1.9562	0.8570	1.8730	3.2767

Table D.1: Conflict terms for the right wing

		Left wing			
		MS(c_{gx})	**MS(c_{gy})**	**MS(c_{gz})**	**MS($c_{g\text{total}}$)**
x = 17m	**In-board**	1.9506	0.8622	1.8864	3.2853
	Middle	1.9594	0.8622	1.8973	3.2907
	Out-board	1.9757	0.8622	1.9129	3.3021
x = 11m	**In-board**	1.9570	0.8590	1.8870	3.2751
	Middle	1.9782	0.8590	1.9085	3.2888
	Out-board	2.0101	0.8590	1.9379	3.3162
x = 9m	**In-board**	1.9625	0.8583	1.8908	3.2756
	Middle	1.9858	0.8583	1.9141	3.2922
	Out-board	2.0161	0.8583	1.9425	3.3194
x = 7m	**In-board**	1.9668	0.8578	1.8932	3.2767
	Middle	1.9913	0.8578	1.9179	3.2953
	Out-board	2.0277	0.8578	1.9529	3.3299
x = 5m	**In-board**	1.9751	0.8574	1.9001	3.2822
	Middle	2.0019	0.8574	1.9273	3.3044
	Out-board	2.0339	0.8574	1.9586	3.3367
x = 3m	**In-board**	1.9839	0.8571	1.9083	3.2902
	Middle	2.0130	0.8572	1.9377	3.3160
	Out-board	2.0457	0.8572	1.9705	3.3517
x = 1m	**In-board**	1.9935	0.8570	1.9178	3.3011
	Middle	2.0244	0.8570	1.9488	3.3305
	Out-board	2.0577	0.8570	1.9841	3.3694
x = 0m	**In-board**	1.9988	0.8570	1.9229	3.3076
	Middle	2.0302	0.8570	1.9546	3.3387
	Out-board	2.0638	0.8570	1.9913	3.3792
x = -1m	**In-board**	2.0041	0.8575	1.9283	3.3149
	Middle	2.0471	0.8577	1.9723	3.3607
	Out-board	2.0699	0.8578	1.9987	3.3897
	c.g.	1.9562	0.8570	1.8730	3.2767

Table D.2: Conflict terms for the left wing

B. 0° rotated seat configuration

		Right wing			
		MS(c_{gx})	**MS(c_{gy})**	**MS(c_{gz})**	**MS($c_{g\text{total}}$)**
x = **17m**	**In-board**	1.8668	0.9993	1.8908	3.2561
	Middle	1.8794	0.9963	1.9019	3.2614
	Out-board	1.8970	0.9935	1.9179	3.2723
x = **11m**	**In-board**	1.8664	0.9858	1.8914	3.2471
	Middle	1.8775	0.9828	1.9136	3.2583
	Out-board	1.9033	0.9799	1.9438	3.2828
x = **9m**	**In-board**	1.8670	0.9821	1.8954	3.2470
	Middle	1.8773	0.9797	1.9195	3.2604
	Out-board	1.8999	0.9773	1.9486	3.2843
x = **7m**	**In-board**	1.8677	0.9794	1.8979	3.2474
	Middle	1.8754	0.9771	1.9234	3.2619
	Out-board	1.9011	0.9744	1.9592	3.2921
x = **5m**	**In-board**	1.8685	0.9764	1.9052	3.2508
	Middle	1.8765	0.9742	1.9328	3.2683
	Out-board	1.8979	0.9719	1.9650	3.2963
x = **3m**	**In-board**	1.8693	0.9736	1.9136	3.2561
	Middle	1.8776	0.9714	1.9433	3.2767
	Out-board	1.8992	0.9692	1.9772	3.3076
x = **1m**	**In-board**	1.8701	0.9708	1.9231	3.2635
	Middle	1.8787	0.9687	1.9547	3.2871
	Out-board	1.9004	0.9666	1.9908	3.3209
x = **0m**	**In-board**	1.8705	0.9694	1.9283	3.2679
	Middle	1.8793	0.9674	1.9606	3.2931
	Out-board	1.9010	0.9654	1.9981	3.3283
x = **-1m**	**In-board**	1.8709	0.9681	1.9337	3.2729
	Middle	1.8865	0.9656	1.9786	3.3107
	Out-board	1.9017	0.9655	2.0057	3.3362
	c.g.	1.9041	0.9745	1.8773	3.2516

Table D.3: Conflict terms for the right wing

		Left wing			
		MS(c_{gx})	**MS(c_{gy})**	**MS(c_{gz})**	**MS($c_{g\text{total}}$)**
x = **17m**	**In-board**	1.8664	0.9997	1.8908	3.2561
	Middle	1.8790	0.9967	1.9019	3.2614
	Out-board	1.8966	0.9939	1.9179	3.2723
x = **11m**	**In-board**	1.8659	0.9862	1.8914	3.2471
	Middle	1.8770	0.9831	1.9136	3.2583
	Out-board	1.9028	0.9803	1.9437	3.2827
x = **9m**	**In-board**	1.8665	0.9825	1.8954	3.2470
	Middle	1.8768	0.9800	1.9195	3.2604
	Out-board	1.8994	0.9777	1.9485	3.2842
x = **7m**	**In-board**	1.8673	0.9798	1.8979	3.2474
	Middle	1.8749	0.9774	1.9234	3.2619
	Out-board	1.9006	0.9748	1.9592	3.2921
x = **5m**	**In-board**	1.8680	0.9768	1.9052	3.2508
	Middle	1.8760	0.9745	1.9328	3.2683
	Out-board	1.8975	0.9723	1.9650	3.2962
x = **3m**	**In-board**	1.8688	0.9739	1.9136	3.2561
	Middle	1.8771	0.9718	1.9433	3.2767
	Out-board	1.8987	0.9696	1.9771	3.3075
x = **1m**	**In-board**	1.8696	0.9712	1.9231	3.2635
	Middle	1.8782	0.9691	1.9546	3.2870
	Out-board	1.8999	0.9670	1.9907	3.3208
x = **0m**	**In-board**	1.8700	0.9698	1.9283	3.2679
	Middle	1.8788	0.9677	1.9606	3.2930
	Out-board	1.9005	0.9658	1.9980	3.3282
x = **-1m**	**In-board**	1.8704	0.9685	1.9337	3.2729
	Middle	1.8860	0.9660	1.9786	3.3107
	Out-board	1.9011	0.9659	2.0057	3.3362
	c.g.	1.9036	0.9749	1.8773	3.2516

Table D.4: Conflict terms for the left wing